GEOLOGICA ULTRAIECTINA

Mededelingen van de
Faculteit Aardwetenschappen
Universiteit Utrecht

No. 111

CHANGES IN THE EARTH'S ROTATION BY TECTONICS

GRAVITO-ELASTODYNAMICS

BERT VERMEERSEN

GEOLOGICA ULTRAIECTINA

Mededelingen van de
Faculteit Aardwetenschappen
Universiteit Utrecht

No. 111

CHANGES IN THE EARTH'S ROTATION BY TECTONICS

GRAVITO-ELASTODYNAMICS

BERT VERMEERSEN

CIP-GEGEVENS KONINKLIJKE BIBLIOTHEEK, DEN HAAG

Vermeersen, Lambertus Ludovicus Angela

Changes in the earth's rotation by tectonics :
gravito-elastodynamics / Lambertus Ludovicus Angela
Vermeersen. - Utrecht : Faculteit Aardwetenschappen der
Universiteit Utrecht. - (Geologica Ultraiectina, ISSN
0072-1026 ; no. 111)
Proefschrift Universiteit Utrecht. - Met lit. opg. - Met
samenvatting in het Nederlands.
ISBN 90-71577-65-1
Trefw.: aardrotatie / tektoniek / gravito-elastodynamica.

Changes in the Earth's Rotation by Tectonics
Gravito-elastodynamics

Veranderingen in de Rotatie van de Aarde
door Tektoniek
Gravito-elastodynamica

(met een samenvatting in het Nederlands)

PROEFSCHRIFT

TER VERKRIJGING VAN DE GRAAD VAN DOCTOR
AAN DE UNIVERSITEIT UTRECHT,
OP GEZAG VAN DE RECTOR MAGNIFICUS PROF. DR J.A. VAN GINKEL,
INGEVOLGE HET BESLUIT VAN HET COLLEGE VAN DEKANEN
IN HET OPENBAAR TE VERDEDIGEN OP
MAANDAG 8 NOVEMBER 1993 DES NAMIDDAGS TE 2.30 UUR

DOOR

LAMBERTUS LUDOVICUS ANGELA VERMEERSEN

GEBOREN OP 25 AUGUSTUS 1961 TE CLINGE

PROMOTOR: PROF. DR N.J. VLAAR

The research described in this thesis was carried out at the:

Department of Geophysics
Institute of Earth Sciences
Utrecht University
Budapestlaan 4
3584 CD Utrecht
The Netherlands

Daer dedic Ysingrijn bi mi
Up dat huus clemmen boven.
Ic seide, ic wilde hem gheloven,
Wildi crupen in die valdore
Dat hire soude vinden vore
Van vetten hoenren sijn ghevouch.
Ter valdore ghinc hi ende louch,
Ende croep daer in met vare
Ende began tasten harentare.
Hi taste ende als hi niet en vant,
Sprac hi: 'Neve hets hier bewant
Te bezorghen; ic ne vinder niet.'
Ic sprac: 'Oem wats u ghesciet?
Cruupter een lettel bet in!
Men moet wel pijnen om gewin.
Ic hebse wech diere saten voren.'

Van den vos Reynaerde

Aan mijn moeder
Ter nagedachtenis aan mijn vader en Bert Vermeersen (1949-1960)

Contents

Chapter 1

INTRODUCTION AND SUMMARY ____ 11

Chapter 2

THE VARIABLE ROTATION OF THE EARTH ____ 17
Abstract ____ 17
Observations ____ 17
Rotational changes for a rigid Earth ____ 21
Some historical notes ____ 25
Continental drift ____ 28
Post-glacial rebound ____ 31
Contemporary changes in the ice - water distribution ____ 32
References ____ 34

Chapter 3

PRESENT-DAY CHANGES IN THE EARTH'S ROTATION
BY TECTONIC MOVEMENTS, PART 1 ____ 39
Abstract ____ 39
Introduction ____ 40
Isostatic uplift of a continental plateau ____ 40
Non-isostatic uplift ____ 48
Two-layer model for the rotational forcings ____ 51
Tectonic mechanisms ____ 55
Erosion ____ 56
Foundering flexure ____ 58
Slab detachment and delamination ____ 58
Subhorizontal subduction and underplating ____ 60
Epeirogenic movements and denudation ____ 62
Displacements of the center of mass of the Earth ____ 72

Antipodal symmetric and anti-symmetric geoid shifts ____ 78
Conclusions ____ 80
References ____ 80

Chapter 4

PRESENT-DAY CHANGES IN THE EARTH'S ROTATION BY TECTONIC MOVEMENTS, PART 2 ____ 85
Abstract ____ 85
Introduction ____ 86
Normal mode model ____ 89
Uplift histories ____ 95
Changes in J_2 ____ 99
Surface density of finite spherical and delta surface loads ____ 100
Heaviside uplift ____ 103
Linear uplift ____ 105
Exponential uplift ____ 106
Polar wander ____ 110
Heaviside uplift ____ 118
Linear uplift ____ 124
Exponential uplift ____ 128
Conclusions ____ 133
Acknowledgments ____ 134
References ____ 134

Chapter 5

LONG-TERM CHANGES IN ROTATION BY CHANGES IN OCEANIC SPREADING RATES AND SUBDUCTION ____ 137
Abstract ____ 137
Introduction ____ 138
Increase in spreading activity ____ 141
Case I ____ 146
Case II ____ 156
Case III ____ 164
Conclusions ____ 173

References 174

Chapter 6

THE GRAVITO-ELASTODYNAMICS OF A PRE-STRESSED ELASTIC EARTH 179
Abstract 179
Introduction 180
Initial finite stresses and the finite strain problem 181
The hydrostatic case 182
The general case 184
Normal modes 190
Unified scheme 193
Conclusions 195
References 196
Appendix: Measures of stress 197

Samenvatting (Summary in Dutch) 202

Dankbetuiging / Acknowledgments 205

Curriculum Vitae 207

If I told you what it takes
to reach the highest high,
You'd laugh and say 'nothing's that simple'
But you've been told many times before
Messiahs pointed to the door
And no one had the guts to leave the temple!

Tommy - The Who

CHAPTER 1

INTRODUCTION AND SUMMARY

The rotation of the Earth is not regular. It changes on virtually every timescale we know in both position of the rotation axis and rotation rate. Even in our daily lives we sometimes experience the consequences of such changes, such as the second that is subtracted or added to clocks at the beginning of a new year. Although this second is not much more than a curiosity for most of us, the rotational changes it implies can influence our lives in a more fundamental sense. There are indications that the emergence of the great ice ages some two million years ago was triggered by a gradual shift of the rotation axis over the Earth's surface, combined with wandering of the continents and associated changes in ocean currents. The geological record shows that times during which there was wide-spread glaciation have been followed by times during which virtually no glaciation occurred, and vice versa, several times. The fact that we are currently living in an interglacial period of a 100,000 year glaciation cycle is also attributable to changes in the position of the rotation axis. Changes in insolation resulting from the periodic rotational changes due to the gravitational interaction between the Earth and the other members of the solar system trigger the onset and decay of the large polar ice sheets. This so-called Milankovitch cycle is responsible for the relatively mild climates we have now, instead of the severe glacial circumstances that governed the planet some 10,000 years ago. Rather than worrying about foregoing temperatures, we are troubled by an enhancement of the greenhouse effect and concomitant sea-level changes by fossil fuel combustion.

The causes of these rotation changes are as diverse as the timescales on which the changes in rotation take place. Grossly, they can be divided into two categories: astronomical and geological. The effects they induce differ mainly in the way the rotation axis shifts. Extra-terrestrial causes generally induce shifts of the rotation axis with respect to the distant stars, but not with respect to the Earth's surface. Terrestrial causes generally induce shifts of the rotation axis with respect to the Earth's surface, but not with respect to the distant stars. For an observer in outer space it looks in this latter case as though the Earth were shifting as a rigid unit underneath its rotation axis, which remains fixed in position with respect to him. For an Earth-

bound observer, however, the polar axis seems to wander with respect to a fixed point on the ground.
Some of the driving mechanisms are established with high certainty, of others we know little at the moment or virtually nothing, like the Chandler wobble. Two of the signatures for which the driving mechanisms are thought to be known are the present-day secular shift in the direction of Canada (that is, on the northern hemisphere) with a magnitude of some 10 meters per 100 years, and the satellite-derived non-tidal secular change in the second degree harmonic of the gravitational potential field. Basically all theories which have been published during the last decade relate both these signatures exclusively to post-glacial rebound and recent changes in the ice - water distribution over the Earth's surface. The main theme of this thesis is that this is not correct. It is shown that also various tectonic processes are contributing to these changes in rotation and gravitational potential field.

The secular shift of the rotation axis is not due to the continental drift of the particular plate through which it pierces on the northern or southern hemisphere, which would be called 'Apparent Polar Wander' (APW), but is supposed to reflect a true wander with respect to the mantle. It is therefore called 'True Polar Wander' (TPW). The question which emerges immediately from this 'with respect to the mantle' statement is how one can determine the mantle reference frame. For long-term TPW, the so-called 'hotspot reference frame' is usually taken for this fixed reference frame. Hotspots are places on the Earth's surface that show an enhanced heat flow and huge basalt outpourings. They are generally thought to be the heads of rising mantle plumes originating at the core - mantle boundary, although diverse opinions about this question exist. The hotspots are reported to be fairly stable in position with respect to one another in time: relative velocities are a factor 10 smaller than the velocities of the moving plates.
Whenever the Earth becomes more elliptical or more spherical, a satellite will experience a changing gravitational field. If the rotation rate of the Earth decelerates, the planet reacts to the diminished centrifugal force by effectively transporting mass away from the equator so that the Earth becomes more spherical. The most important effect of such a change on a satellite orbiting above the Earth is that the places where it crosses the equator, called the nodes, are not equidistant anymore. The nodes will be progressively closer to each other as time proceeds. Such a deceleration of the nodes has been measured by laser satellite ranging to a few dedicated satellites. It turned out that after the deceleration of the rotation rate of the Earth due to tidal interaction with the Moon was removed from the data, residual deceleration remained.
To get some idea about the mass displacements necessary to induce a significant

contribution to the present-day TPW and non-tidal deceleration of the Earth: the total Pleistocene ice that melted away some 10,000 years ago had a mass of about 10^{19} kilograms. As post-glacial rebound takes on the order of 10,000 years to relax to this vanished load, a value of about 10^{15} kilograms per year must be displaced to have a significant influence. Of course, the efficiency of the forcing depends also on a number of other parameters, like the positions on the globe. A value of 10^{15} kilograms per year gives a proper order of magnitude, however. In table 1.1 a few typical mass displacements are listed.

Mass displacement	kg/year
Impact of cosmic dust on Earth: 50 tons per day	2×10^{7}
Yearly oil production	2.6×10^{12}
Yearly natural gas production	1.3×10^{12}
Yearly coal production	3.7×10^{12}
Yearly total ore production	$< 10^{12}$
Sea-level rise of 2 mm per year	7×10^{14}
Contemporary ice mass changes	10^{14-15}

Table 1.1. Typical yearly mass displacements.

The yearly oil, natural gas, coal and ore production rates are based on *The Global 2000 Report to The President, Volume 2,* published by Blue Angel Inc., Charlottesville, USA, 1981. According to this report, the production rate of oil in 1976 was 21.7 billion barrels of 159 liter (p. 190), of natural gas 50 tera cubic feet (p. 191), and the consumption rate of coal 3.7 billion tons (p. 193), while the upper limit of the world ore production in 1977 is derived from table 12-7 on page 219 of the report. The figures on cosmic dust, sea-level rise and ice mass changes are

canonical values (e.g. for the contemporaneous melting rates of the 31 largest mountain glaciers, M.F. Meier in *Science, 226,* 1418-1421, 1984, gives a value of ice discharge of 661.0 km^3 per year).
Transporting the total world population of about 5 billion human beings times a mean weight of 50 kilograms would result in a total mass being transported of 2.5×10^{11} kilograms. Even in the most favorable situation it is clear from this figure and table 1.1 that human induced activities (or perhaps one should say *direct* human induced activities) and cosmic impacts are not effective in inducing TPW.

In chapter 2 a survey is given of the variations in the Earth's rotation. The formulations for the rotational changes for a rigid Earth are presented, followed by a historical overview of the theories on the driving mechanisms of the secular drift of the polar axis. A study at the end of the 1970's on continental drift as being the responsible forcing is re-examined, as this study has led to the conclusion that post-glacial rebound and recent ice - water redistributions constitute the driving mechanisms. The assumption that the shifting columns in the continental drift model are in isostatic equilibrium turns out the be the most critical one, and forms the key for the models exposed in chapter 3.
In chapter 3 it is shown that also tectonic movements can be effective mechanisms in inducing the observed changes. The tectonic changes must result in fast vertical movements taking place under non-isostatic conditions to become effective. Examples of such mechanisms are the formation of mountains and plateaus, the detachment of subducting slabs, the foundering of oceanic basins, and all kinds of processes that can accompany these, such as erosion and sedimentation, underplating after subhorizontal subduction, and delamination. These non-isostatic fast movements might also result in a shift of the center of mass of the Earth by which an antipodal antisymmetric shift of the sea-level is associated. In regions that were glaciated some 10,000 years ago, the free surface is presently rebounding to restore isostasy. It is commonly assumed that this process takes place by passive mantle relaxation, uninhibited by any lithospheric stress field. The upper part of models that simulate the relaxation in studies on post-glacial rebound is usually taken as effectively elastic. Internal deformation, which is important in the models on the tectonic mechanisms employed in chapter 3, is not taken into account in these studies. Contrary to post-glacial rebound, the processes described in this thesis can be effective on timescales of up to a few million years, as the forcing mechanisms can keep the mantle from relaxing on timescales of post-glacial rebound in a compressive stress regime.
In chapter 4 the effects of the readjustment of the equatorial bulge are incorporated in the models. A redistribution of mass generally induces a torque on the equatorial

bulge. Because the Earth is a deformable planet, the equatorial bulge will react to this torque by shifting in the lateral direction. In fact, the shifts determined in chapter 3 would result in an angle between the rotation axis and the plane of the equatorial bulge which is not 90 degrees if the bulge would not shift over the Earth's surface. The shift of the equatorial bulge only stops when the region that deviates from isostasy (assuming that it would be the only region on the planet which deviates from isostasy) is either at one of the poles or at the equator, so this adjustment of the equatorial bulge makes it possible that large degrees of polar wander are feasible, which would not be the case for a rigid planet. At the same time, the region that deviates from isostasy strives to restore isostasy, resulting in a complicated interplay between load relaxation (the direct effect) and tidal relaxation (the induced shift). When complete isostasy has been reached by load relaxation, the shift of the equatorial bulge stops. The amount and speeds of the shifts are not only dependent on the loads, however. Also the rheological properties of the mantle are important. A lower mantle or transition zone that has a high viscosity can greatly reduce the rates at which the equatorial bulge shifts by its gravitational interaction with the upper layers. In the normal mode model, which is used in chapter 4 to determine the complex gravitational interaction between the visco-elastically flowing mantle layers and the load, it is assumed that the rheological properties of the mantle can be adequately described by a linear Maxwell model. In order to study the consequences of a possible 'hard' transition zone, the mantle is divided into three layers, each having uniform rheological properties. Although a normal mode analysis is not the proper technique to model the direct effects of the loads because it is unable to deal with the crucially important lateral variations, it can be used to establish lower limits to the induced effects. For the tidal relaxation it is a good technique, however, as we are only dealing with the largest length scale of the Earth in this case. The results show that for a 10% Airy overcompensated root of the Himalayas and Tibetan Plateau, a linear uplift model leads for a lower mantle viscosity which is 10 times the upper mantle viscosity to the same polar wander rates as are presently observed. For values of the lower mantle to upper mantle viscosity ratio which are small, the polar wander rates are very sensitive to the viscosity of the transition zone.

In chapter 5 the long-term changes in the Earth's rotation are studied. The long-term TPW can be derived from paleomagnetic observations. Some recent studies attribute the mechanism behind long-term TPW to changes in subduction. In this chapter the accompanying changes in bathymetry and induced sea-level changes are examined after their effectiveness, and it is shown that for a convecting mantle these changes must be taken into account whenever they are dynamically supported by the deeper mantle layers. Recent studies on long-term TPW from numerical

convection experiments, which deal automatically with the rising material as a forcing function as well, do not take the lithospheric and hydrospheric forcings into account. Also the induced shifts of the equatorial bulge are not modeled in the present numerical simulations. As is shown in chapter 4, a viscosity contrast of more than a factor 10 between the lower mantle and the layers above it can greatly reduce any polar wander rate, making the neglect of the influence of the equatorial bulge in these numerical models questionable. The influence of the long-term changes in bathymetry and sea-levels on the length of day are shown to be negligible.

In chapter 6 a general description is presented for the gravito-elastodynamics of a planet that has arbitrarily large stresses. This chapter is not directly related to the main part of this thesis. In chapter 6 it is demonstrated that by means of a Lagrangian, the equation of motion and its associated boundary and continuity conditions can be derived by the Variational Principle in different kinds of coordinate systems (Eulerian, Lagrangian) and with different kinds of stress measures (Cauchy, Piola-Kirchhoff). The reason for looking for such a general description emerged from different opinions in the literature about the incorporation of pre-stress terms in the equations of motions. The deviatoric, especially, gave rise to opposing points of views, leading to incompatible formulations of the basic equations of linearized gravito-elastodynamics. It is shown in this chapter that the concept of pre-stress does not lead to violations of the law of conservation of angular momentum upon implementing it in the equations of motions. This violation has been claimed by advocates who regard pre-stress as a mathematical concept rather than as a physical concept. It is also shown that in an Eulerian coordinate system the derived equations of motion lead to a complete set of normal modes. This has been demonstrated previously in a Lagrangian coordinate system but not explicitly in Eulerian coordinates.

CHAPTER 2

THE VARIABLE ROTATION OF THE EARTH

Abstract

A survey is given of the measured variations in position of the rotation axis, the changes in the length of the day and the second degree zonal harmonic of the geoid. The expressions for the determination of polar shift and change in length of day are derived for a rigid planet. The long history of studies on the secular polar drift is outlined, in which theories on polar ice caps and solid Earth deformations as the driving mechanism repeatedly replaced one another. At the end of the 1970's it was found that continental drift could not explain the observed drift. This resulted in theories of post-glacial rebound as the driving mechanism in the early 80's, followed by contemporary redistributions of water and ice as an additional mechanism in the second half of the 80's. In this chapter a critical review is given of the assumptions in the models which let to discard continental drift as a viable mechanism for inducing the observed polar shift. The assumption that the shifting columns are in isostatic equilibrium turns out to be most critical one.

Observations

By the 19th century it was already recognized that the rotation of the Earth is not regular. Both the rate of rotation and the position of the rotation axis were shown to be variable. Nowadays we know that these changes occur on all timescales: from shorter than a day until geological scales of hundreds of millions of years.
The changes in the position of the rotation axis can be divided into two categories:

those in which the position of the axis changes with respect to the distant stars but not with respect to the Earth's surface, and vice versa. For the latter category it looks to a hypothetical observer in space as though the Earth shifts underneath its rotation axis as a solid unit while the rotation axis itself remains fixed, while for an observer on Earth it looks as though the rotation axis is wandering over the Earth's surface. Displacements of the axis of rotation with respect to the 'fixed' stars (changes in which the whole planet is moving rigidly as one unit) are mainly due to external forces, notably the gravitational interactions between the Earth and the Sun, the Moon and the other planets of the solar system. The astronomically well-known precession and nutation are examples of this. The external forces exert a net torque on the equatorial flattening of the Earth, as a consequence of which the rotation axis will spin. The most important periods are about 26,000 years (precession) and 18.6 years (nutation).

Displacements of the axis of rotation with respect to a fixed position on the Earth's surface are mainly due to mass displacements in the interior of the Earth and in the hydro- and atmosphere. These mass displacements will generally induce changes in the moments and products of inertia. As the Earth is a deformable medium, the rotation axis will re-adjust itself to the new situation by shifting over the surface. The rotation axis does not change its position with respect to the stars as during these mass displacements the angular momentum of the Earth is conserved.

Apart from the tidal interactions, there are a number of possible mechanisms responsible for the observed changes, like growth and decay of ice sheets, changes in sea-level, ocean currents, winds and changes in the pressure distribution of the atmosphere, seasonal changes, earthquakes, tectonic plate movements, changes in convection of the mantle and core, and interactions between the core and mantle. Each of these mechanisms operate on specific timescales and this is reflected in the timescales on which the rotation of the Earth changes. Table 2.1 gives a gross indication of the observed present-day variations in position of the polar axis. The observed changes in the position of the rotation axis with respect to the Earth's surface, generally termed polar wander, consist of two kinds of movements: cyclic and linear. The cyclic motions consist mainly of two periods. The annual wobble is mainly caused by the seasonally varying zonal winds. The cause of the Chandler wobble is still unknown, although a lot of research has been done on this (e.g. Runcorn et al., 1988). This periodic movement, which is essentially the free precession of the Earth, was predicted by Euler in the 18th century but not observed until the end of the 19th century. Euler had predicted that the period of this wobble should be about 10 months. S.C. Chandler, an American salesman and amateur astronomer, discovered a periodic movement in 1891, but with a period of 14 months. Only a year after this discovery, Newcomb showed that the discrepancy between

type	magnitude	presumed causes
annual wobble	5 meters per year	changes in atmospheric pressure
Chandler wobble	10 meters per 14 months	basically unknown (earthquakes, El Nino)
secular drift	1 meter per 10 years	post-glacial rebound, contemporary ice-water redistributions

Table 2.1. Variations in the position of the rotation axis.

the two periods is due to the fact that the Earth is not a rigid body. Deformations of the solid Earth, ocean currents and currents inside the outer core result in a lengthening of 4 months (Smith and Dahlen, 1981).
The contemporary secular drift has been determined by astrometric observations. Dickman (1977) comes to the conclusion by examining International Latitude Service (ILS) data covering a 75 year timespan, that the rotation pole is compatible with a drift of 0.003" per year toward 76°W, and is not an observational artifact of continental drift moving the ILS stations.

The observed changes in the length of day, with the mechanisms that are thought to be responsible, are indicated in table 2.2. Short-time fluctuations are very well explained by changes in the pressure distribution over the globe and zonal winds (Lambeck, 1980a). Changes on timescales of a few tens of years, the decade fluctuations, are attributable to the exchange of angular momentum between the fluid outer core and the lower mantle. They are strongly correlated with changes in the magnetic field strength (Le Mouël et al., 1992). The long-term variation is mainly due to tidal exchange of angular momentum between the Earth and the Moon and to a somewhat lesser degree between the Earth and the Sun. The secular decrease of the rotation velocity is due to the fact that the Earth is rotating faster around its axis than the Moon is revolving around the Earth, and because the Earth is not per-

timescale	magnitude	presumed causes
daily	milliseconds	atmosphere and tides
annual	milliseconds	seasons
decades	10 milliseconds	core-mantle coupling
hundreds of years and longer	2 milliseconds per 100 years	tidal interaction between Earth and Moon/Sun post-glacial rebound

Table 2.2. Variations in the length of the day.

fectly elastic. As a result, the line Earth - Moon does not coincide exactly with the line between the center of the Earth and the place on the surface that shows the maximum tidal height. This gives a net torque, which brakes the Earth's rotation rate and accelerates the Moon in its orbit around the Earth. As the Earth rotates with a progressively slower rate, the centrifugal force diminishes. As a consequence, the ellipticity of the Earth decreases. This in turn implies that the second degree zonal harmonic of the gravitational field, J_2, becomes smaller as time proceeds. This negative value for the time derivative $\dot{J}_2$ results in a deceleration in the succession of points where a satellite crosses the equator (the nodes). This deceleration in the accompanying line of nodes (the line which joins the nodal point with the center of mass of the Earth) as the line of nodes progresses along the equator can be measured by means of tracking the positions of artificial satellites. These satellites are spheres with laser reflecting mirrors on their surfaces. In order to reduce perturbing effects such as the solar wind, the satellite must be as small and as heavy as possible. Since 1975 three satellites have been sent into space for this purpose. Two of these have resulted in long enough time series to determine changes in J_2, viz. STARLETTE (diameter 25 cm, mass 50 kg) and LAGEOS I (diameter 60 cm, mass 400 kg). From laser ranging data that measure the precession of the orbital node of the LAGEOS I satellite, the parameter $\dot{J}_2$ has been determined by Yoder et al. (1983) and Rubincam (1984). They found values of about -3×10^{-11}

per year. The deduced values from LAGEOS I satellite laser ranging observations differ from one another, however, although both groups used approximately the same data set, covering the years 1976 – 1981: Yoder et al. find a value of $\dot{J}_2 = (-3.5 \pm 0.3) \times 10^{-11}$ yr^{-1}, from a $5\frac{1}{2}$ year time span of observations, while Rubincam finds a value of $\dot{J}_2 = (-2.6 \pm 0.6) \times 10^{-11}$ yr^{-1} from a 5 year time span. It is not clear where the difference between the two figures comes from. A more recent value is given by Cheng et al. (1989): they deduce a value of $\dot{J}_2 = (-2.5 \pm 0.3) \times 10^{-11}$ yr^{-1} from a 3 year time span (1983 – 1985) of STARLETTE observations. The most recent value (May 1993) derived from LAGEOS I observations is $\dot{J}_2 = -2.9 \times 10^{-11}$ yr^{-1} (Eanes et al., 1993). It will be assumed in this thesis that $\dot{J}_2 = -3 \times 10^{-11}$ yr^{-1}.

Rotational changes for a rigid Earth

If $\vec{L}$ denotes torque, $\vec{H}$ angular momentum and $\vec{\omega}$ angular velocity, then in a reference frame co-rotating with the Earth, Euler's dynamical equation reads (cf. Munk and MacDonald, 1960, p. 9 and 38, and Lambeck, 1980b, p. 30)

$$\frac{d\vec{H}}{dt} + \vec{\omega} \times \vec{H} = \vec{L} \tag{2.1}$$

with

$$\vec{H} = \int \rho \vec{r} \times (\vec{\omega} \times \vec{r}) dV = \int \rho (r^2 \vec{\omega} - (\vec{r} \cdot \vec{\omega}) \vec{r}) dV \tag{2.2}$$

or

$$\vec{H} = \mathbf{I} \cdot \vec{\omega} \quad \text{with} \quad I_{ij} = \int \rho (r_k r_k \delta_{ij} - r_i r_j) dV \tag{2.3}$$

representing the components of the inertia tensor **I**, with δ_{ij} being the Kronecker delta function.
This results in the Liouville equation

$$\frac{d}{dt} (\mathbf{I} \cdot \vec{\omega}) + \vec{\omega} \times (\mathbf{I} \cdot \vec{\omega}) = \vec{L} \tag{2.4}$$

In the general case **I** is time dependent because mass displacements and motion, $\vec{u}$,

can occur with respect to the axis $\vec{r}$. Therefore $\vec{H}(t)$ is rewritten as

$$\vec{H}(t) = \mathbf{I}(t) \cdot \vec{\omega} + \vec{h}(t) \tag{2.5}$$

in which

$$\vec{h}(t) = (h_1, h_2, h_3)^T = \int \rho \vec{r} \times \vec{u} dV \tag{2.6}$$

leading to the so-called 'Liouville equation'

$$\frac{d}{dt}\left(\mathbf{I}(t) \cdot \vec{\omega} + \vec{h}(t)\right) + \vec{\omega} \times \left(\mathbf{I}(t) \cdot \vec{\omega} + \vec{h}(t)\right) = \vec{L} \tag{2.7}$$

If Ω denotes the mean angular velocity of the Earth, then the components of $\vec{\omega}$ can be expressed in the dimensionless quantities m_i as

$$\vec{\omega} = \Omega\,(m_1, m_2, 1 + m_3)^T \tag{2.8}$$

The quantities m_i are small whenever the deviations from the axis of rotation are small.

Assuming that $\vec{h}$ and the changes in $\mathbf{I}$ are small the inertia tensor can be written as

$$\mathbf{I} = \begin{pmatrix} A + \Delta I_{11}(t) & \Delta I_{12}(t) & \Delta I_{13}(t) \\ \Delta I_{21}(t) & A + \Delta I_{22}(t) & \Delta I_{23}(t) \\ \Delta I_{31}(t) & \Delta I_{32}(t) & C + \Delta I_{33}(t) \end{pmatrix} \tag{2.9}$$

in which A and C denote the moments of inertia for an equatorial principal axis and the polar principal axis respectively.

It then follows that

$$\mathbf{I} \cdot \vec{\omega} = \begin{pmatrix} (A + \Delta I_{11})\omega_1 + \Delta I_{12}\omega_2 + \Delta I_{13}\omega_3 \\ \Delta I_{21}\omega_1 + (A + \Delta I_{22})\omega_2 + \Delta I_{23}\omega_3 \\ \Delta I_{31}\omega_1 + \Delta I_{32}\omega_2 + (C + \Delta I_{33})\omega_3 \end{pmatrix} \approx \begin{pmatrix} Am_1\Omega + \Delta I_{13}\Omega \\ Am_2\Omega + \Delta I_{23}\Omega \\ C\Omega + Cm_3\Omega + \Delta I_{33}\Omega \end{pmatrix} \tag{2.10}$$

so

$$\vec{\omega} \times (\mathbf{I} \cdot \vec{\omega} + \vec{h}) \approx \begin{pmatrix} Cm_2\Omega^2 - Am_2\Omega^2 - \Delta I_{23}\Omega - h_2\Omega \\ Am_1\Omega^2 + \Delta I_{13}\Omega + h_1\Omega - Cm_1\Omega^2 \\ 0 \end{pmatrix} \tag{2.11}$$

resulting, with $\vec{L} = (L_1, L_2, L_3)^T$, in

$$\begin{cases} A\Omega\dot{m}_1 + (C-A)\Omega^2 m_2 = -\Omega\Delta\dot{I}_{13} + \Omega\Delta I_{23} + \Omega h_2 - \dot{h}_1 + L_1 \\ A\Omega\dot{m}_2 - (C-A)\Omega^2 m_1 = -\Omega\Delta\dot{I}_{23} - \Omega\Delta I_{13} - \Omega h_1 - \dot{h}_2 + L_2 \\ C\Omega^2\dot{m}_3 = -\Omega^2\Delta\dot{I}_{33} - \Omega\dot{h}_3 + \Omega L_3 \end{cases} \tag{2.13}$$

With the Chandler wobble frequency

$$\sigma_r \equiv [(C-A)/A]\Omega \tag{2.14}$$

this can be written as

$$\begin{cases} \dfrac{\dot{m}_1}{\sigma_r} + m_2 = \phi_2 \\ \dfrac{\dot{m}_2}{\sigma_r} - m_1 = -\phi_1 \\ \dot{m}_3 = \dot{\phi}_3 \end{cases} \tag{2.15}$$

in which

$$\begin{cases} \phi_1 = \dfrac{1}{(C-A)\Omega^2}\left(\Omega^2\Delta I_{13} + \Omega\Delta\dot{I}_{23} + \Omega h_1 + \dot{h}_2 - L_2\right) \\ \phi_2 = \dfrac{1}{(C-A)\Omega^2}\left(\Omega^2\Delta I_{23} - \Omega\Delta\dot{I}_{13} + \Omega h_2 - \dot{h}_1 + L_1\right) \\ \phi_3 = \dfrac{1}{C\Omega^2}\left(-\Omega^2\Delta I_{33} - \Omega h_3 + \Omega\int_0^t L_3 dt'\right) \end{cases} \tag{2.16}$$

are the dimensionless load excitation functions.
If we only consider mass displacements – neglecting influences of relative motions ($\vec{h}$, $\dot{\vec{h}}$, $\Delta\dot{I} = 0$) – in the absence of external torques ($\vec{L} = 0$), then these excitation functions from loading reduce for polar wander to the complex excitation function

$$\Phi_L \equiv \phi_1 + i\phi_2 = \frac{\Delta I_{13}}{C-A} + i\frac{\Delta I_{23}}{C-A} \tag{2.17}$$

As in a deformable Earth there are no stable reference frames in the strict sense, it is necessary to define such a reference system in a practical way. For short-term polar wander it is convenient to take the geographical frame as reference frame. It could be defined as the mean position of a number of fixed points in stable continental areas.

For long-term true polar wander the choice of a reference frame becomes more complicated, as the whole mantle can change its configuration. Usually, the hotspot reference frame is taken as the frame in which the mean mantle material is stable. The relative velocities between the hotspots are generally found to be a factor of one tenth smaller than the relative plate velocities (e.g. Duncan and Richards, 1991).
m_1 and m_2 now give the resultant polar shift in radians: m_1 in the x-direction which is chosen to be in the equatorial plane from the center of the Earth towards the Greenwich meridian, and m_2 in the y-direction which is chosen to be in the equatorial plane from the center of the Earth towards 90 degrees East longitude.
m_3 gives the change in the length of day in radians per sidereal day. To express it in seconds one must multiply by 86,164 s.

With this and the polar shift in complex notation $\mathbf{m} \equiv m_1 + im_2$, the linearized Liouville equation for polar wander becomes

$$i\frac{\dot{\mathbf{m}}}{\sigma_r} + \mathbf{m} = \Phi_L \tag{2.18}$$

For loadings which change with much smaller frequencies than σ_r, this linearization of the Liouville equation leads ultimately to

$$m_1 = \frac{\Delta I_{xz}}{C - A} \quad \text{rad} \qquad x - \text{component of polar shift} \tag{2.19}$$

$$m_2 = \frac{\Delta I_{yz}}{C - A} \quad \text{rad} \qquad y - \text{component of polar shift} \tag{2.20}$$

$$m_3 = \frac{\Delta I_{zz}}{C} \cdot 86164 \text{ s} \qquad \text{change in length of day} \tag{2.21}$$

From (2.19) and (2.20) it is clear that the equatorial flattening is of great importance to the amount of polar shift. If there were no equatorial flattening, implying C = A, the shift would become infinite. Munk and MacDonald (1960, p. 57) relate how at the end of the nineteenth century the United States government was very interested in a proposal by the 'North Polar Practical Association' to fire a projectile of 180,000 tons from 45° latitude in order to displace the pole by 23°. The association had neglected the equatorial flattening, however, in their calculations on what projectile is needed to adjust the equatorial bulge with the orbital plane of the Earth around the Sun.
Another important issue is that (2.19) and (2.20) do not take into account a shift in the equatorial bulge. This implies that (2.19) and (2.20) give only the 'polar wander' for a rigid planet. If the rotation axis were to coincide with the axis perpendic-

ular to the plane of the equatorial flattening before a mass change occurs, then after the mass change (2.19) and (2.20) would give the new position of the rotation axis that coincides with the axis of maximum moment of inertia. This new position would not be perpendicular to the plane of the equatorial flattening whenever the perturbing mass is not on the poles or the equator. On a deformable planet, the equatorial bulge will strive to adjust itself by shifting until the perturbing mass is either at the equator (in the case of an excess mass) or at one of the poles (in the case of a deficiency in mass). This process allows, in principle, for polar wander magnitudes that can greatly exceed the amounts derived from (2.19) and (2.20). The additional formulations to take the deformation of the equatorial bulge into account, which are rather complicated, will be set out in chapter 4.

Some historical notes

Studies after the secular polar drift and its causes have a long history. Much of this can be found in the book by Munk and MacDonald (1960), which has become the classical work on Earth rotation theories of the pre-continental drift era.

Already in the beginning of this century, by analyzing data from the ILS, the pole was found to shift. Values were found of 0.0062" per year in the direction 90°W by Lambert (1922) from observations during the years 1900-1917, and 0.0047" per year in the direction 42°W by Wanach (1927) from observations during the years 1900-1926.

Milankovitch (1934) and Kuiper (1943) relate the secular shift to the difference in the distance between the center of mass of the Earth and the center of mass of a column of oceanic lithosphere, and the center of mass of the Earth and the center of mass of a column of continental lithosphere. It is assumed that both columns are in isostatic equilibrium. Because of this difference, a net torque – dubbed the Eötvös force – is exerted on the lithosphere (the 'sial-layer'). This sial-layer is envisioned to float as one single rigid unit on the mantle (the 'sima-layer') by means of a 'plastic' layer between them. The torque will displace the sial-layer until its axis of maximum moment of inertia adjusts with the polar axis.

Whereas Milankovitch and Kuiper modeled horizontal movements of the lithosphere being in isostatic equilibrium, in Munk and Revelle (1952, paragraph 4) the effects of vertical movements of the Earth's crust are modeled by cutting the

Earth's surface into 21 blocks, each block thus having about the area of North-America. The blocks are allowed to move up and down randomly under the constriction that as much mass goes up as goes down at all times. As upper limits to the rate of vertical movement they take a few centimeters per several decades. As the mean latitude and longitude of the rising and sinking blocks generally do not coincide, a polar wander can be triggered of a few meters in 60 years. This would be about the right order of magnitude of the observed value.

Like Milankovitch and Kuiper, it is Munk's (1958) opinion too that the distribution of continents and oceans is the main determinant for retrieving the moments and products of inertia. If this would indeed be the case, according to him the axis of maximum moment of inertia would be some 400 miles southwest of Hawaii. He acknowledges, however, that if the isostatic balance of a crustal mass column is not precise, this will result in an order of magnitude greater effect on polar wander. For such an 'intriguing possibility', as he calls it, he suggests erosion of continental matter and sedimentation on the sea floor. Munk calculates what the amount of uncompensated erosion of the continents would have to be to place the axis of maximum moment of inertia alongside the present-day rotation axis and finds a value of 28 meters. The induced gravity anomalies of about -4.5 mgals would not be in conflict with observed magnitudes. He doubts, however, whether the Earth is capable of maintaining such 'large' deviations from isostasy.

Another interesting aspect of Munk's article is that he points to the Himalayas and the Andes as being the main sources for the continental contribution to the products of inertia. According to him, no reasonable ice cap can balance the torque exerted by continents, discarding a hypothesis made by Gold (1955) that the polar ocean could provide a trap for the rotation axis. Gold had tried to explain the difference between the assumed position of the maximum moment of inertia near Hawaii and the present-day position of the rotation axis as follows: suppose that at a time when there is no wide-spread glaciation the rotation axis pierces through an ocean, coinciding with the axis of maximum moment of inertia. At a certain time, great ice ages commence. The ice that is formed on the continents drive the rotation axis in such a way that it follows the changed maximum moment of inertia by the formed ice. The rotation axis will move on until it has reached a continent: if the continent reaches the pole, ice will settle down on it, thereby changing the axis of maximum moment of inertia in such a way that the drift of the rotation axis is first stopped and then reverses its direction away from the continent. In such a way the continents could 'trap' the rotation axis during ice ages under the condition that ice and water are the determining agents for the moments of inertia during such times. Although he does not support this with explicit derivations, Gold (1955, p. 528) mentions that if a continent of the size of South America were 'suddenly' (which might

be a period of up to 100,000 years) raised by 30 meters, the rotation axis of the Earth would be displaced at a rate of one degree per thousand years by the 'plastic' shift of the equatorial bulge (the shift for the case of a rigid Earth would only be of the order of one hundredth of a degree). It is important to note, however, that Gold assumes that the damping of the Chandler wobble takes place in the mantle, and consequently assumes also that the characteristic flow time constant for polar wander would be around 10 years. Indeed, during the late forties and fifties sensational articles appeared in newspapers and magazines in which the public was told that catastrophic turn-overs of the Earth's polar axis might be possible. It was even speculated at that time that the sudden appearance of ice-ages could be due to this, explaining why mammoths could be found in arctic ice as if they were captured by surprise and instantaneously were frozen in. This idea seems to have been originally contrived by an electrical engineer, Hugh A. Brown, in 1911 (Hapgood, 1958, p. 15; and Muir Wood, 1985, p. 114). He attributed the fact that frozen mammoths had been found with the stereotyped 'buttercups still clenched between their teeth' to changes in Antarctic ice volume. According to him, it was possible that the Earth might capsize by this process. In 1946 he founded the 'Global Stabilisation Organisation' to prevent such a sudden catastrophic event. Even the detonation of nuclear explosives were put forward to halt a possibly devastating turnover.

A very inviscid mantle would be in sharp disagreement with the mantle viscosities of the order of 10^{21} Pa · s derived from post-glacial rebound studies, however (Haskell, 1935; and Vening-Meinesz, 1937). Indeed, Munk (1958) comments that it is probably not correct to derive the mantle viscosity from the dissipation rate of the Chandler wobble.

Dicke (1966, p. 129), discards vertical continental movements as an effective mechanism for inducing rotational changes. In his subsection on 'Continental Unrest' he states that an upper limit of the rate of rise or fall of a whole continent is 0.2 mm/yr, as this would result in a vertical displacement of 2 kilometers after a period of 10 million years has elapsed. If all the continents participated 'independently', this would result in a change of $\dot{J}_2 = -0.35 \times 10^{-11}$ yr^{-1}. As the vertical movements are at least partially isostatically compensated (according to Dicke, the induced free air gravity anomaly of 200 mgals is at least a factor 20 too high), he proposes a 'safe' upper limit for $\dot{J}_2$ of one tenth of this figure, resulting in $\dot{J}_2 = -0.035 \times 10^{-11}$ yr^{-1}, which is orders of magnitude too low indeed. Twenty-five years of tectonophysical and geodetical studies later we know, however, that uplift rates of more than one order of magnitude larger have been reported for several regions unrelated to post-glacial rebound, while free-air gravity anomalies exceed 100 mgals in several parts of the world.

Continental drift

Dickman (1979) assumes that the main contribution from the changing positions of the ten major lithospheric plates during the last Myr to changes in the Earth's inertia tensor stems from the difference in density structure between oceanic and continental regions. As a plate moves, continental and oceanic lithosphere is effectively interchanged between the continental margins at the leading and trailing edges of the continent (figure 2.1).

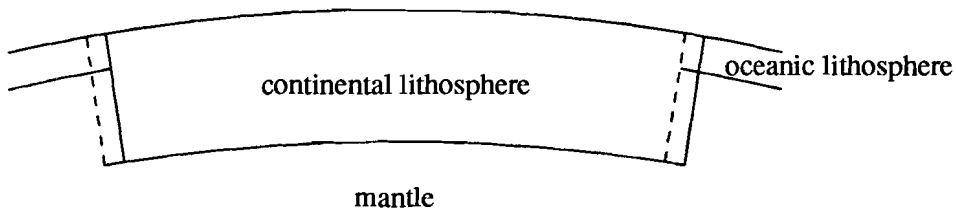

Figure 2.1 Continental drift.

The oceanic crust is modeled as a three-layer water/sediment/intermediate composition crust column extending to 11 kilometers depth, the continental crust as a one-layer intermediate composition crust column extending to 34.6 kilometers depth; both columns being placed upon a uniform peridotite mantle. The continental margins are assumed to coincide with the 500-fathom bathymetric contour. The plate velocities are taken from the AM1 model of Minster et al. (1974), which gives the velocities with respect to the hot-spot reference frame.
The combined effect of the moving plates on polar wander and non-tidal acceleration, without taking the deformation of the equatorial bulge into account, can be determined from a linearization of the Liouville equation.
The mass displacements of the moving plates make **I** time dependent. The changes in the components of the inertia tensor follow from (2.3) as

$$\Delta I_{ij} = \int_V (r^2\delta_{ij} - r_i r_j)\Delta\rho dV \qquad (2.22)$$

in which $\Delta\rho(r, t)$ is the change in density contrast.
Assuming that the dependence of ρ on r has the form of Heaviside functions (as is the case here) and as the infinitesimal volume element dV is proportional to r^2dr, it

is clear that the change in the inertia tensor is approximately proportional to the fourth power of the radius.

The result of the calculations is that after 1 Myr the plates induce a net polar shift of 0.63 arcseconds in the direction – 36.0 degrees east longitude, while the net change in the length of day is – 0.75 milliseconds. The observed rate of polar wander is about 1 degree per Myr in the direction 76 degrees west longitude (Dickman, 1977), while the non-tidal change in the length of day amounts about 4 seconds if it is assumed that the value $\dot{J}_2 = -2.5 \times 10^{-11}$ yr^{-1} persisted for the last one million years.

So the rate of polar wander induced by lithospheric plate motions appears to be more than three orders of magnitude too low to account for the observed value, while the direction is not in accordance with the observations either.

Dickman has performed a number of sensitivity analyses of the various assumptions in his models in order to find out whether they might have resulted in an order of magnitude too low estimation. Two of these that might have a considerable effect are episodic instead of continuous plate motion (the plates might have moved much faster during the last 75 years than during the longer timescale to which the AM1 model applies) and partial decoupling of the lithosphere from the mantle (in this case the induced changes in rotation are only partially mediated to the mantle). For both of these cases, the upper bounds he derives are still at least one order of magnitude too low to account for the observed values.

Although Dickman established that continental drift is several orders of magnitude too low to account for the observed present-day true polar wander, he acknowledges that in his work there are some major sources of uncertainty, the most important being the assumption of isostasy:

1. Airy isostasy

In calculating the effects of plate motions during the last 1 Myr Dickman assumes Airy isostasy for the crust for both columns. In oceanic regions Pratt isostasy seems to be more appropriate, however. As the compensation depth for Pratt isostasy lies at the bottom of the lithosphere, in contrast with Airy isostasy where compensation is assumed to occur at the Moho, it is necessary to consider density differences between a continental column and an oceanic column in the whole lithosphere instead of only in the crust.

If in Dickman's model a column of oceanic lithosphere is replaced by continental lithosphere the density changes as a function of depth below sea-level as:

$$0 - 5 \text{ km} \qquad \Delta\rho = 1.82 \times 10^3 \text{ kg} \cdot \text{m}^{-3}$$

$$5 - 6 \text{ km} \qquad \Delta\rho = 0.82 \times 10^3 \text{ kg} \cdot \text{m}^{-3}$$

$$11 - 34.6 \text{ km} \qquad \Delta\rho = -0.42 \times 10^3 \text{ kg} \cdot \text{m}^{-3}$$

It is clear that changing the density columns changes the moments of inertia in a linear fashion (the radius of the columns is not changed). This means that replacing the Airy isostatic oceanic column by one which is in Pratt isostasy and extending the oceanic and lithospheric columns down to a depth of 150 kilometers does only change the polar shift by a factor which scales as the newly adopted density differences to the density differences Dickman has used. It is obvious that even in extreme cases this cannot lower the factor 5000 which plate motions lack in explaining the observed true polar wander down to unity.

2. Departures from isostasy
A greater uncertainty concerns the question whether the columns are really in isostatic equilibrium. Especially at active continental margins, where oceanic lithosphere subducts below continental lithosphere, strong gravity and geoid anomalies indicate this assumption not to be correct.

3. Topography
A further uncertainty arises from the fact that the continental column does not rise above sea-level, so there is no topography in Dickman's calculations. Contributions from topographic features, such as the Himalayas and mid-ocean ridges are acknowledged by Dickman as only secondary effects because the leading and trailing edges are relatively close.
The same reasoning can be applied for the implementation of topography as in the case of extending the columns downwards and using Pratt isostasy for the oceanic lithosphere: the continental column could be extended by e.g. 1 kilometer above sea-level. Instead of replacing continental material by oceanic material, 1 kilometer height of continental material is now replaced by air. So it is clear that introducing a topography at the continental margins gives no substantial contribution to lowering the factor 5000 either.

From the three additional sources of uncertainty given above only departures from isostasy remain. It is clear that purely lateral displacements of lithospheric columns are not capable of explaining the observed present-day true polar wander and non-tidal acceleration.
The most important contributions of lithospheric and upper mantle forcings to present-day changes in the rotation figure of the Earth appear to be those associated with large departures from isostasy. This has made glacial loading and unloading

the prime candidate for causing the observed present-day true polar wander and non-tidal acceleration.

Post-glacial rebound

Changes in the ice sheet volumes and sea-levels during the great ice ages were fast enough to induce large departures from isostasy. It is estimated that in each of the great ice ages the massive ice sheets contained about 10^{19} kg ice which lead to a global sea level rise of approximately 100 meters in interglacial times (Peltier, 1982). This means that about 1 part in 1,000,000 of the entire mass of the Earth shifted over considerable distances along the surface of the planet, thereby inducing movement of mantle material. Such large changes in mass distribution in a geologically very recent past have unequivocal influence on the rotation of the Earth, both on the position of the rotation axis with respect to the surface and on the rate of rotation.

After Dickman's work (1979), Nakiboglu and Lambeck (1980) and Sabadini and Peltier (1981) indeed found that the visco-elastic response of the Earth to Pleistocene deglaciation is capable of explaining both direction and magnitude of present-day polar wander. Also the satellite-derived non-tidal change in J_2 seemed to be explainable by the process of post-glacial rebound (Peltier, 1983). Further investigations by Sabadini et al. (1982, 1984), Yuen et al. (1982, 1985), and Wu and Peltier (1984) seemed to confirm the hypothesis that post-glacial rebound explains both rotational signatures. These authors use the rotational data to derive a radial viscosity profile for the mantle by modeling the mantle as a visco-elastic linear Maxwell body. The models have in common that the observed data are related to basically two unknown quantities: the loading history of the ice sheet complexes and the radial viscosity profile of the mantle. Although large uncertainties remain, it is believed that the loading history is the best known of the two, hence the loading history is dealt with as an input function and the viscosity profile consequently as the modeling parameter. In these models, the mantle is divided into an upper and a lower part, each having specific values for the rheological parameters. It was found from the polar wander studies that the viscosity of the lower mantle would be $1 - 10$ times larger than the upper mantle viscosity. From the studies on $\dot{J}_2$, two classes of solutions for the lower mantle viscosity were found: one in agreement

with the values found from the studies on polar wander, and one with a few orders of magnitude larger viscosity. The reason for the emergence of two classes of solutions from the $\dot{J}_2$ models may be attributed to the fact that we are living some 5,000 years after the Pleistocene ice masses have melted away. In the case of a lower mantle viscosity of a few times the upper mantle viscosity most of the rebound has been completed, resulting in slow vertical movement rates, while in the case of a lower mantle viscosity of a few orders more than the upper mantle viscosity the same vertical movement rates occur because relaxation is slow. The great difference between the two classes of solutions is that in the small lower/upper mantle viscosity contrast cases isostasy has nearly been obtained, while in the large viscosity contrast cases the deviations from isostasy are still large today. As a relatively small viscosity contrast of not more than one order of magnitude was found to be more compatible with the values derived from other studies (geoid anomaly studies, relative sea-level studies), the upper branch solutions representing a high lower mantle viscosity were usually discarded.
Later studies by Spada et al. (1991, 1992) include the transition zone as a separate third layer between the shallow upper and lower mantle in order to study the effects of a hypothetical high viscosity of this layer due to the garnet component (Karato, 1989).

Contemporary changes in the ice - water distribution

Although at present we are in an interglacial period of the Milankovitch cycle, there is still ongoing activity in ice melting and ice buildup. These present-day glacial forcings also have their influence on the rotation of the Earth. Over the last 100 years the global sea-level may have been rising by 10 – 20 cm (e.g. Lambeck, 1988, p. 115). These values have a large uncertainty because they are deduced from tidal gauge records which have a poor geographical distribution and do not discriminate between redistribution of ocean water and a true increase of ocean water volume. To explain this contemporary rise several causes with various relative contributions have been suggested.
Lambeck and Nakiboglu (1984) attribute 30% to 50% to crustal rebound from Pleistocene glacial forcings, while the rest is mainly due to melting from mountain glaciers and thermal expansion of ocean water. Meier (1984) finds that one third to

one half is due to temperate latitude glacier melting and attributes the rest to ocean warming. The Greenland and Antarctic ice sheets are excluded because the first seemed to be close to equilibrium, while the latter was assumed to subtract water from the oceans rather than to discharge meltwater. Recent satellite altimetry measurements indicate that the Greenland ice sheet has been growing since 1970 at rates of a few tens of centimeters per year (Zwally et al., 1989). Peltier and Tushingham (1989) find that filtering the Pleistocene post-glacial rebound component from the tide gauge data results in a present sea-level rise of 2.4 ± 0.9 mm/yr, from which no more than a fourth comes from ocean warming.

Temperate latitude mountain glaciers have a typical mass which is only one thousandth of the former Pleistocene Laurentian ice sheet, while their rate of melting is only 5% of the last glacial maximum (Gasperini et al., 1986). Nevertheless, the effects they induce could be as important as the effects from the Pleistocene ice sheets because the forcings are recent in contrast with the Pleistocene glacial forcings, making considerations of the transient rheological responses of the Earth important. Several studies on the effects of recent glacial forcings to the polar motion and non-tidal acceleration of the Earth's rotation axis have been made since Yoder and Ivins (1985) suggested the possible influence of contemporary ice mass changes on rotation (Gasperini et al., 1986; Yuen et al., 1987; Sabadini et al., 1988; Peltier, 1988; Trupin et al., 1992; Trupin, 1993; and Mitrovica and Peltier, 1993).

Yoder and Ivins (1985) used the estimates of Meier (1984) for the melting rates of temperate latitude glaciers and found a value for $\dot{J}_2$ of 3.5×10^{-11} yr^{-1}. This value can only be reconciled with the satellite-observed value if other mechanisms, like post-glacial rebound, are responsible for a large negative contribution to $\dot{J}_2$. As for the present-day melting effect upon the polar motion they find the value from their models, 0.0017" per year toward 160°E, not to be incompatible with the observed drift of 0.003" per year toward 76°W. Hence the contemporary ice disintegration of the glaciers is not likely to be the main cause of the observed drift.

Whereas Yoder and Ivins (1985) used a one-layer mantle model in which they applied the Maxwell rheological model, Gasperini et al. (1986) have studied the effects of recent glacial discharges and a possible growth of the Antarctic ice sheet for Maxwell and Burger's body rheologies in a one-layer and a two-layer mantle model. In order to model the forcing function of each glacier they assume that the glaciers have grown to a maximum mass by the year 1400 A.D., being the product of the present-day melting rate and a characteristic time scale representing glacial dynamics of 200 years (1200 – 1400 A.D.). They further assume the glaciers remain constant from 1400 A.D. till 1900 A.D. and begin melting in 1900 A.D. at a linear rate until the whole glacier is diminished in 2100 A.D. The rise of the global sea-level due to melting of the glaciers induces a decrease of the spin-rate, or an in-

crease of J_2 (opposite to the effects of Pleistocene ice sheet melting). Especially for the two-layer mantle models with a high viscosity contrast between the lower and upper mantle the contribution from glaciers is found to be a significant fraction (up to 33%) of the observed value. The Antarctic ice sheet is modeled as growing with rates of equivalent changes in global sea-level of -0.6 mm/yr and -0.2 mm/yr. Recent research indicates, however, that the Antarctic ice has been accumulating with an enhanced rate since the late 1960's. Morgan et al. (1991) estimate that the equivalent lowering of the sea-level amounts to 1.0 – 1.2 mm/yr, which illustrates the great uncertainties in modeling the loads. The changes in the Antarctic ice sheet complex also appear to have a considerable influence on the $\dot{J}_2$-value for a high steady-state viscosity contrast (it even could account for the whole observed value), but now with the same sign as that due to Pleistocene ice sheet melting. The recent glacial forcings do not have a considerable influence on polar wander because Alaska and the Himalayas, where two of the largest glaciers are located, act in discordance as a consequence of their geographical locations (but in concordance with respect to variations of J_2), whereas Antarctica is situated near the rotational axis.

Both post-glacial rebound and present-day ice-water redistributions, notably Meier's (1984) glacier discharges, the Antarctic and Greenland ice sheets, and the contemporary sea-level rise, are included in the study on the changes in the zonal geoid harmonics by Mitrovica and Peltier (1993).

References

Cheng, M.K., R.J. Eanes, C.K. Shum, B.E. Schutz, and B.D. Tapley, Temporal variations in low degree zonal harmonics from Starlette orbit analysis, *Geophys. Res. Lett., 16,* 393-396, 1989.

Dicke, R.H., The secular acceleration of the Earth's rotation and cosmology, in *The Earth-Moon System,* edited by B.G. Marsden and A.G.W. Cameron, 98-164, Plenum Press, New York, 1966.

Dickman, S.R., Secular trend on the Earth's rotation pole: Consideration of motion of the latitude observations, *Geophys. J. R. astron. Soc., 51,* 229-244, 1977.

Dickman, S.R., Continental drift and true polar wandering, *Geophys. J. R. astron. Soc., 57,* 41-50, 1979.

Duncan, R.A., and M.A. Richards, Hotspots, mantle plumes, flood basalts, and true polar wander, *Rev. Geophys., 29*, 31-50, 1991.

Eanes, R.J., M.M. Watkins, and B.D. Tapley, On the use of LAGEOS-1 and LAGEOS-2 for the determination of zonal harmonic variations, *Annales Geophysicae, 11(1)*, C109, 1993.

Gasperini, P., R. Sabadini, and D.A. Yuen, Excitation of the Earth's rotational axis by recent glacial discharges, *Geophys. Res. Lett., 13*, 533-536, 1986.

Gold, T., Instability of the Earth's axis of rotation, *Nature, 175*, 526-529, 1955.

Hapgood, C.H., (in collaboration with J.H. Campbell and with a foreword by Albert Einstein), *Earth's Shifting Crust*, 438 pp., Pantheon Books Inc., New York, 1958.

Haskell, N.A., Motion of a viscous fluid under a surface load, *Physics, 6*, 265-269, 1935.

Karato, S., Plasticity-crystal structure systematics in dense oxides and its implications for the creep strength of the Earth's deep interior: A preliminary result, *Phys. Earth Planet. Inter., 55*, 234-240, 1989.

Kuiper, H., *Poolbewegingen Tengevolge van Poolvluchtkracht*, PhD-thesis Utrecht University, 87 pp., N.V. Noord-Hollandsche Uitgevers Maatschappij, Amsterdam, 1943.

Lambeck, K., Changes in length-of-day and atmospheric circulation, *Nature, 286*, 104-105, 1980a.

Lambeck, K., *The Earth's Variable Rotation: Geophysical Causes and Consequences*, 449 pp., Cambridge University Press, New York, 1980b.

Lambeck, K., *Geophysical Geodesy: The Slow Deformations of The Earth*, 718 pp., Oxford University Press, Oxford, 1988.

Lambeck, K., and S.M. Nakiboglu, Recent global changes in sealevel, *Geophys. Res. Lett., 11*, 959-961, 1984.

Lambert, W.D., The interpretation of apparent changes in mean latitude and the International Latitude Stations, *Astron. J., 904*, 1922.

Le Mouël, J.-L., V. Courtillot, and D. Jault, Changes in Earth rotation rate, *Nature, 355*, 26-27, 1992.

Meier, M.F., Contribution of small glaciers to global sea level, *Science, 226*, 1418-1421, 1984.

Milankovitch, M., Der Mechanismus der Polverlagerungen und die daraus sich ergebenden Polbahnkurven, *Gerlands Beitr. z. Geoph., 42* 70-97, 1934.

Minster, J.B., T.H. Jordan, P. Molnar, and E. Haines, Numerical modeling of instantaneous plate tectonics, *Geophys. J. R. astron. Soc., 36*, 541-576, 1974.

Mitrovica, J.X., and W.R. Peltier, Present-day secular variations in the zonal harmonics of Earth's geopotential, *J. Geophys. Res., 98*, 4509-4526, 1993.

Morgan, V.I., I.D. Goodwin, D.M. Etheridge, and C.W. Wookey, Evidence from Antarctic ice cores for recent increases in snow accumulation, *Nature, 354,* 58-60, 1991.

Muir Wood, R., *The Dark Side of The Earth,* 246 pp., Allen & Unwin, London, 1985.

Munk, W., Remarks concerning the present position of the pole, *Geophysica, 6,* 335-355, 1958.

Munk, W., and R. Revelle, On the geophysical interpretation of irregularities in the rotation of the earth, *Monthly Notices, Roy. astron. Soc., Geophys. Supplement, 6,* 331-347, 1952.

Munk, W.H., and G.J.F. MacDonald, *The Rotation of The Earth: A Geophysical Discussion,* 323 pp., Cambridge University Press, Cambridge, England, 1960.

Nakiboglu, S.M., and K. Lambeck, Deglaciation effects on the rotation of the Earth, *Geophys. J. R. astron. Soc., 62,* 49-58, 1980.

Peltier, W.R., Dynamics of the Ice Age Earth, in *Advances in Geophysics, 24,* edited by B. Saltzman, 1-146, Academic Press, New York, 1982.

Peltier, W.R., Constraint on deep mantle viscosity from Lageos acceleration data, *Nature, 304,* 434-436, 1983.

Peltier, W.R., Global sea level and Earth rotation, *Science, 240,* 895-901, 1988.

Peltier, W.R., and A.M. Tushingham, Global sea level rise and the Greenhouse Effect: might they be connected?, *Science, 244,* 806-810, 1989.

Rubincam, D.P., Postglacial rebound observed by LAGEOS and the effective viscosity of the lower mantle, *J. Geophys. Res., 89,* 1077-1087, 1984.

Runcorn, S.K., G.A. Wilkins, E. Groten, H. Lenhardt, J. Campbell, R. Hide, B.F. Chao, A. Souriau, J. Hinderer, H. Legros, J.-L. Le Mouël, and M. Feissel, The excitation of the Chandler wobble, *Surveys in Geophysics, 9,* 419-449, 1988.

Sabadini, R., and W.R. Peltier, Pleistocene deglaciation and the Earth's rotation: implications for mantle viscosity, *Geophys. J. R. astron. Soc., 66,* 553-578, 1981.

Sabadini, R., D.A. Yuen, and E. Boschi, Polar wandering and the forced responses of a rotating, multilayered viscoelastic planet, *J. Geophys. Res., 87,* 2885-2903, 1982.

Sabadini, R., D.A. Yuen, and E. Boschi, A comparison of the complete and truncated versions of the polar wander equations, *J. Geophys. Res., 89,* 7609-7620, 1984.

Sabadini, R., D.A. Yuen, and P. Gasperini, Mantle rheology and satellite signatures from present-day glacial forcings, *J. Geophys. Res., 93,* 437-447, 1988.

Smith, M.L., and F.A. Dahlen, The period and Q of the Chandler wobble, *Geophys. J. R. astron. Soc., 64,* 223-281, 1981.

Spada, G., R. Sabadini, and D.A. Yuen, Viscoelastic responses of a hard transition zone: Effects on postglacial uplifts and rotational signatures, *Earth Planet. Sc. Lett., 105,* 453-462, 1991.

Spada, G., R. Sabadini, D.A. Yuen, and Y. Ricard, Effects on post-glacial rebound from the hard rheology in the transition zone, *Geophys. J. Int., 109,* 683-700, 1992.

Trupin, A.S., Effects of polar ice on the Earth's rotation and gravitational potential, *Geophys. J. Int., 113,* 273-283, 1993.

Trupin, A.S., Meier, M.F., and Wahr, J.M., Effect of melting glaciers on the Earth's rotation and gravitational field: 1965-1984, *Geophys. J. Int., 108,* 1-15, 1992.

Vening-Meinesz, F.A., The determination of the Earth's plasticity from the post-glacial uplift of Scandinavia; Isostatic adjustment, *Proc. Kon. Ned. Akad. Wetensch., 40,* 654-662, 1937.

Wanach, B., Eine fortschreitende Lagenänderung der Erdachse, *Zeitschrift Geophysik, 3,* 102, 1927.

Wu, P., and W.R. Peltier, Pleistocene deglaciation and the Earth's rotation: A new analysis, *Geophys. J. R. astron. Soc., 76,* 753-791, 1984.

Yoder, C.F., and E.R. Ivins, Changes in Earth's gravity field from Pleistocene deglaciation and present-day glacial melting, *EOS Trans. AGU, 66,* 245, 1985.

Yoder, C.F., J.G. Williams, J.O. Dickey, B.E. Schutz, R.J. Eanes, and B.D. Tapley, Secular variation of Earth's gravitational harmonic J_2 coefficient from LAGEOS and nontidal acceleration of Earth rotation, *Nature, 303,* 757-762, 1983.

Yuen, D.A., R. Sabadini, and E.V. Boschi, Viscosity of the lower mantle as inferred from rotational data, *J. Geophys. Res., 87,* 10745-10762, 1982.

Yuen, D.A., and R. Sabadini, Viscosity stratification of the lower mantle as inferred by the $\dot{J}_2$ observation, *Annales Geophysicae, 3,* 647-654, 1985.

Yuen, D.A., P. Gasperini, R. Sabadini, and E. Boschi, Azimuthal dependence in the gravity field induced by recent and past cryospheric forcings, *Geophys. Res. Lett., 14,* 812-815, 1987.

Zwally, H.J., A.C. Brenner, J.A. Major, R.A. Bindschadler, and J.G. Marsh, Growth of Greenland ice sheet: measurement, *Science, 246,* 1587-1589, 1989.

CHAPTER 3

PRESENT-DAY CHANGES IN THE EARTH'S ROTATION BY TECTONIC MOVEMENTS, PART 1 †

Abstract

Present-day true polar wander and the secular non-tidal acceleration of the Earth are usually attributed to post-glacial rebound. In the models that relate this rebound to changes in rotation, the mantle is assumed to relax passively to the melted ice-loads. The lithosphere is usually modeled as a highly viscous upper layer in these models, having viscosities which exceed mantle viscosities by several orders of magnitude.

We propose that lithospheric processes unrelated to post-glacial rebound and taking place under non-isostatic conditions are also able to induce non-negligible influences on the Earth's rotation. Examples of such processes are mountain building and erosion, foundering flexure of oceanic basins and lithospheric snapbacking resulting from detachment of subducting slabs. Lithospheric and crustal rheologies and intraplate-stresses are the dominant factors in these mechanisms, contrary to the mantle rheologies which are assumed to dominate the process of post-glacial rebound. The departures from isostasy can be maintained for timescales exceeding the time it takes mantle viscosities to restore isostasy by post-glacial rebound because the lithospheric forcings are sometimes still operative, and because of the rheological state of the Earth's outer layers which result in large relaxation times. This is in contrast to post-glacial rebound, where the forcings (the melting of the Pleistocene ice-sheets) have surmised some 10,000 years ago.

The proposed tectonic forcings can also influence the position of the center of mass

---

† Parts of this chapter were originally published as: L.L.A. Vermeersen and N.J. Vlaar, Changes in the Earth's rotation by tectonic movements, *Geophys. Res. Lett., 20,* 81-84 and 1107-1109, 1993.

of the Earth. It is shown that the figures of this induced shift by our models can be comparable in magnitude to those found from modeling contemporary ice – water redistributions.

Introduction

As was shown in chapter 2, Dickman (1979) has outlined that continental drift under isostatic conditions is not effective as a forcing for changing the Earth's rotation, and that consequently a non-isostatic process like post-glacial rebound (Nakiboglu and Lambeck, 1980, and Sabadini and Peltier, 1981) was found to be extremely effective. In studies after the relation between post-glacial rebound and changes in rotation, the rapid melting of the Pleistocene ice-sheets and the consequent increase in eustatic sea-level were modeled as a redistribution of loads on an elastic lithosphere. The mantle was assumed to adjust itself to the new situation by viscously flowing from underneath oceanic areas towards the formerly glaciated areas. In the radially stratified rheological models, the core was assumed to be inviscid, while the mantle was assumed to behave as a linear visco-elastic medium having different viscosities for the upper and the lower mantle.
Not only areas which were formerly glaciated show uplift or subsidence nowadays, however. In several tectonically active regions in the world vertical movements have been reported of several millimeters per year for relatively large areas and even up to 20 – 30 millimeters per year at some places. In most of these cases the uplifts and subsidences are clearly not related to post-glacial rebound.

Isostatic uplift of a continental plateau

Radial displacements taking place under isostatic conditions are not effective in inducing polar wander and non-tidal acceleration, although a large part of the interior of the plates is now at stake instead of swifting small lithospheric columns at the

borders of the continents. In this section this is explicitly shown for uplift taking place under Airy or Pratt isostatic conditions.

To investigate the influence of radial lithospheric mass displacements under isostatic conditions on the position of the rotation axis and the rotation rate of the Earth, consider a simple model in which a continental plateau rises by its own thermal expansion. We assume that the plateau receives an excess heat, causing a rise of the plateau by thermal expansion of the lithospheric material.

Consider such a plateau having a thickness of L meters and a uniform density of ρ kilograms per cubic meter before thermal expansion. After thermal expansion, which is assumed to be taken up in the radial direction only, the plateau has risen to a height of h meters, while the density of the plateau has fallen with an amount of $\Delta\rho$ to a value of ρ^* kilograms per cubic meter. The compensation depth does not change its position (Pratt isostatic condition).

Then

$$\rho^* = \rho + \Delta\rho = \rho(1 - \alpha\Delta T) \tag{3.1}$$

in which ΔT denotes the increase in temperature and α the thermal expansion coefficient. If R denotes the radius of the Earth, then the change of density as a function of the distance r to the center of the Earth can be written as

$$\Delta\rho = -\alpha\rho\Delta T \qquad R - L \le r \le R \tag{3.2a}$$

$$\Delta\rho = \rho(1 - \alpha\Delta T) \qquad R \le r \le R + h \tag{3.2b}$$

The condition that mass must be conserved can be written as

$$\rho(R^3 - (R - L)^3) = \rho^*((R + h)^3 - (R - L)^3)$$

As $h \ll L \ll R$, this can be approximated by

$$\frac{\rho^*}{\rho} = \frac{R^3 - (R - L)^3}{(R + h)^3 - (R - L)^3} \approx \frac{LR - L^2}{(L + h)R - h^2} = \frac{1}{1 + \dfrac{R}{R - L} \cdot \dfrac{h}{L}} \tag{3.3}$$

From (3.1) and (3.3) it follows that the elevation h with respect to the original column thickness L amounts

$$\frac{h}{L} \approx \left(\frac{\rho}{\rho^*} - 1\right)\left(1 - \frac{L}{R}\right) = \frac{\alpha\Delta T}{1 - \alpha\Delta T}\left(1 - \frac{L}{R}\right) \approx$$

$$\approx \alpha\Delta T(1+\alpha\Delta T)\left(1-\frac{L}{R}\right) \approx \alpha\Delta T\left(1+\alpha\Delta T-\frac{L}{R}\right) \tag{3.4}$$

If the modeled area extends quadrilateral between co-latitudes θ_1 and θ_2 and longitudes ϕ_1 and ϕ_2, then the induced changes in the products of inertia, neglecting displacements of the equatorial bulge, follow from (2.22) as

$$\Delta I_{xz} = \alpha\rho\Delta T \int_{R-L}^{R}\int_{\phi_1}^{\phi_2}\int_{\theta_1}^{\theta_2} r^4 \sin^2\theta\cos\theta\cos\phi\, d\theta\, d\phi\, dr$$

$$- \rho(1-\alpha\Delta T)\int_{R}^{R+h}\int_{\phi_1}^{\phi_2}\int_{\theta_1}^{\theta_2} r^4 \sin^2\theta\cos\theta\cos\phi\, d\theta\, d\phi\, dr =$$

$$= \left(\alpha\rho\Delta T\left[\int_{R-L}^{R} r^4 dr + \int_{R}^{R+h} r^4 dr\right] - \rho\int_{R}^{R+h} r^4 dr\right) \cdot$$

$$\cdot \int_{\phi_1}^{\phi_2}\cos\phi\, d\phi \int_{\theta_1}^{\theta_2}\sin^2\theta\cos\theta\, d\theta =$$

$$= \alpha\rho\Delta T\left(\left[\frac{1}{5}R^5 - \frac{1}{5}(R-L)^5 + \frac{1}{5}(R+h)^5 - \frac{1}{5}R^5\right]\right.$$

$$\left. - \rho\left[\frac{1}{5}(R+h)^5 - \frac{1}{5}R^5\right]\right)\left(\sin\phi_2 - \sin\phi_1\right)\left(\frac{1}{3}\sin^3\theta_2 - \frac{1}{3}\sin^3\theta_1\right)$$

As $h \ll L \ll R$, using (3.4) the radial dependence can be approximated by

$$\alpha\rho\Delta T\left(\frac{1}{5}R^5 - \frac{1}{5}(R-L)^5 + \frac{1}{5}(R+h)^5 - \frac{1}{5}R^5\right) - \rho\left(\frac{1}{5}(R+h)^5 - \frac{1}{5}R^5\right) \approx$$

$$\approx \alpha\rho\Delta T\left(LR^4 - 2L^2R^3 + hR^4\right) - \rho hR^4 \approx$$

$$\approx \alpha\rho\Delta T\left(LR^4 - 2L^2R^3 + \alpha\Delta TLR^4 - LR^4 - \alpha\Delta TLR^4 + L^2R^3\right) \approx$$

$$\approx -\alpha\rho\Delta TL^2R^3$$

So

$$\Delta I_{xz} \approx -\frac{\alpha\rho\Delta TL^2R^3}{3}(\sin\phi_2 - \sin\phi_1)(\sin^3\theta_2 - \sin^3\theta_1) \tag{3.5}$$

In the same way ΔI_{yz} can be calculated, resulting in

$$\Delta I_{yz} \approx \frac{\alpha\rho\Delta T L^2 R^3}{3}(\cos\phi_2 - \cos\phi_1)(\sin^3\theta_2 - \sin^3\theta_1) \tag{3.6}$$

(3.5) and (3.6) in (2.19) and (2.20) gives the amount of polar shift (if no account is made of shifts of the equatorial bulge) in radians:

$$\left(\frac{\Delta I_{xz}}{C-A}, \frac{\Delta I_{yz}}{C-A}\right) \approx$$

$$\approx -\frac{\alpha\rho\Delta T L^2 R^3}{3(C-A)}(\sin^3\theta_2 - \sin^3\theta_1)(\sin\phi_2 - \sin\phi_1, -\cos\phi_2 + \cos\phi_1) \tag{3.7}$$

in the direction

$$\Phi = \arctan\frac{\Delta I_{yz}}{\Delta I_{xz}} = -\arctan\frac{\cos\phi_2 - \cos\phi_1}{\sin\phi_2 - \sin\phi_1} \qquad \text{east longitude} \tag{3.8}$$

Isostasy is the reason why the polar shift induced by the thermal uplift of a plateau is proportional to the third power instead of the fourth power in R. The thermal uplift as it is modeled here is subject to Pratt isostasy: the effect of the increased length of the column is diminished by a lowering of the density of the whole column.

As an example, a rough estimate of the effect of the rise of the Colorado Plateau on polar shift, assuming that the model of thermal expansion applies to its epeirogeny, can be obtained using the following numbers

$$\alpha = 3.2 \times 10^{-5}\ \mathrm{K}^{-1}$$

$$\Delta T = 300\ \mathrm{K}$$

$$L = 150\ \mathrm{km}$$

$$R = 6370\ \mathrm{km}$$

$$\rho = 3 \times 10^3\ \mathrm{kg \cdot m^{-3}}$$

$$A = 8.0131 \times 10^{37}\ \mathrm{kg \cdot m^2}$$

$$C = 8.0394 \times 10^{37}\ \mathrm{kg \cdot m^2}$$

$$\theta_1 = 50^\circ \qquad \theta_2 = 56^\circ$$

$$\phi_1 = 247^\circ \qquad \phi_2 = 253^\circ$$

For these numbers, (3.4) results in an uplift of 1400 meters. The amount of polar

shift given by (3.7) is $(0.19'', 0.52'')$ or $(6, 16)$ meters (1 radian is equivalent to $206,265''$). Using (3.8) this gives a shift of $\sqrt{36+256} \approx 17$ meters in the direction 70° east longitude. This is away from the Colorado Plateau, so the second order effect (the first order being equal to zero because of isostasy) of the thermal expansion induces a polar drift in the same direction the first order effect would have had.

The increase in the length of day is given by (2.21), with (3.2) and (3.4), as

$$\Delta I_{zz} \approx \alpha\rho\Delta T L^2 R^3 \int_{\phi_1}^{\phi_2} d\phi \int_{\theta_1}^{\theta_2} \sin^3\theta d\theta =$$

$$= -\frac{\alpha\rho\Delta T L^2 R^3}{3}(\phi_2 - \phi_1)\Big(3(\cos\theta_2 - \cos\theta_1) - (\cos^3\theta_2 - \cos^3\theta_1)\Big) \qquad (3.9)$$

This results in a total lengthening with 1 millisecond, which is orders of magnitude smaller compared with a lengthening of 4 seconds, resulting from a persistence of a value of $\dot{J}_2 = -2.5 \times 10^{-11}$ yr^{-1} for one million years.

Another way of modeling the effect of the rise of a plateau or mountain is to invoke a compensating root at the bottom of the lithosphere under the uplifted region. In fact, this Airy isostatic model may be even more appropriate for the Colorado Plateau, as heat diffusion from a source below the plateau upwards through the lithosphere is a far too slow process to induce the proposed thermal expansion (although magma intrusion may soften this difficulty): assuming that the plateau is only heated from below, a rough estimation of the time it takes the excess heat to reach the surface by conduction is $L^2/\kappa \approx 100$ Myr, where $\kappa \approx 10^{-6}$ m$^2 \cdot$ s^{-1} is the thermal diffusivity and L the thickness of the plateau.
Assume that the plateau has a height of h meters after the rise has completed and a uniform density of ρ_L kilograms per cubic meter. The root which is formed below the lithosphere has replaced mantle material with a density ρ_m by lithospheric material with a density ρ_L. The lithosphere before uplift has a thickness L, while the root has a thickness h^*.
Then the effective density change $\Delta\rho(r)$ can be written as

$$\Delta\rho = \rho_L \qquad R \le r \le R + h \qquad (3.11a)$$

$$\Delta\rho = -(\rho_m - \rho_L) \qquad R - L \le r \le R - L - h^* \qquad (3.11b)$$

The Airy isostatic condition, taken into account the curvature of the Earth, is

$$(\rho_m - \rho_L)(R - L)^2 h^* = \rho_L R^2 h$$

or

$$h^* = \frac{\rho_L}{\rho_m - \rho_L}\left(\frac{R}{R-L}\right)^2 h \tag{3.12}$$

With (3.11) the changes in the moments and products of inertia can be calculated:

$$\Delta I_{xz} = -\rho_L \int_R^{R+h}\int_{\phi_1}^{\phi_2}\int_{\theta_1}^{\theta_2} r^4 \sin^2\theta \cos\theta \cos\phi \, d\theta \, d\phi \, dr$$

$$+ (\rho_m - \rho_L) \int_{R-L-h^*}^{R-L}\int_{\phi_1}^{\phi_2}\int_{\theta_1}^{\theta_2} r^4 \sin^2\theta \cos\theta \cos\phi \, d\theta \, d\phi \, dr =$$

$$= \left(-\rho_L \int_R^{R+h} r^4 dr + (\rho_m - \rho_L) \int_{R-L-h^*}^{R-L} r^4 dr \right) \int_{\phi_1}^{\phi_2} \cos\phi \, d\phi \int_{\theta_1}^{\theta_2} \sin^2\theta \cos\theta \, d\theta =$$

$$= \left(-\rho_L \left[\frac{1}{5}(R+h)^5 - \frac{1}{5}R^5 \right] + (\rho_m - \rho_L)\left[\frac{1}{5}(R-L)^5 - \frac{1}{5}(R-L-h^*)^5 \right] \right) \cdot$$

$$\cdot \left(\sin\phi_2 - \sin\phi_1 \right)\left(\frac{1}{3}\sin^3\theta_2 - \frac{1}{3}\sin^3\theta_1 \right)$$

With (3.12), the radial dependence can be approximated by

$$-\rho_L\left[\frac{1}{5}(R+h)^5 - \frac{1}{5}R^5\right] + (\rho_m - \rho_L)\left[\frac{1}{5}(R-L)^5 - \frac{1}{5}(R-L-h^*)^5\right] \approx$$

$$\approx -\rho_L(hR^4 + 2h^2R^3)$$

$$+ (\rho_m - \rho_L)\left(\frac{\rho_L}{\rho_m - \rho_L} h(R-L)^2R^2 - 2\left(\frac{\rho_L}{\rho_m - \rho_L}\right)h^2 \frac{R^4}{R-L} \right) \approx$$

$$\approx -\rho_L(hR^4 + 2h^2R^3) + \rho_L hR^4 - 2\rho_L hLR^3 - 2\frac{\rho_L^2}{\rho_m - \rho_L} h^2R^3 =$$

$$= -2\rho_L\left(\frac{\rho_m}{\rho_m - \rho_L} h + L \right) hR^3$$

Again, isostasy cancels the fourth power radial dependence.
So

$$\Delta I_{xz} \approx -\frac{2}{3}\rho_L\left(\frac{\rho_m}{\rho_m - \rho_L} h + L \right) hR^3(\sin\phi_2 - \sin\phi_1)(\sin^3\theta_2 - \sin^3\theta_1) \tag{3.13}$$

In the same way ΔI_{yz} can be calculated, resulting in

$$\Delta I_{yz} \approx \frac{2}{3}\rho_L\left(\frac{\rho_m}{\rho_m - \rho_L}h + L\right)hR^3(\cos\phi_2 - \cos\phi_1)(\sin^3\theta_2 - \sin^3\theta_1) \qquad (3.14)$$

(3.13) and (3.14) result in an amount of polar shift for a rigid Earth of

$$\left(\frac{\Delta I_{xz}}{C-A}, \frac{\Delta I_{yz}}{C-A}\right) \approx -\frac{2}{3}\rho_L\left(\frac{\rho_m}{\rho_m - \rho_L}h + L\right)hR^3(\sin^3\theta_2 - \sin^3\theta_1) \cdot$$
$$\cdot (\sin\phi_2 - \sin\phi_1\ , -\cos\phi_2 + \cos\phi_1)$$

radians in the direction

$$\Phi = \arctan\frac{\Delta I_{yz}}{\Delta I_{xz}} = -\arctan\frac{\cos\phi_2 - \cos\phi_1}{\sin\phi_2 - \sin\phi_1} \qquad \text{east longitude} \qquad (3.15)$$

A rough estimation of the effect of the elevation of the Colorado Plateau on polar shift by this model can be obtained using the following numbers

$$h = 2 \text{ km}$$
$$L = 150 \text{ km}$$
$$R = 6370 \text{ km}$$
$$\rho_L = 2.9 \times 10^3 \text{ kg} \cdot \text{m}^{-3}$$
$$\rho_m = 3.3 \times 10^3 \text{ kg} \cdot \text{m}^{-3}$$
$$A = 8.0131 \times 10^{37} \text{ kg} \cdot \text{m}^2$$
$$C = 8.0394 \times 10^{37} \text{ kg} \cdot \text{m}^2$$
$$\theta_1 = 50^\circ \qquad \theta_2 = 56^\circ$$
$$\phi_1 = 247^\circ \qquad \phi_2 = 253^\circ$$

Using (3.12), these figures result in a root of 15 kilometers depth. The induced polar shift is about 50 meters in the direction 70° east longitude, which is the same order of magnitude as the shift induced by the thermal expansion model.
The total increase in the length of day, given by (2.21), with

$$\Delta I_{zz} \approx -\frac{2}{3}\rho_L\left(\frac{\rho_m}{\rho_m - \rho_L}h + L\right)hR^3(\phi_2 - \phi_1) \cdot$$
$$\cdot \left(3(\cos\theta_2 - \cos\theta_1) - (\cos^3\theta_2 - \cos^3\theta_1)\right) \qquad (3.16)$$

is about 3 milliseconds, which is again a far too small number compared to the ob-

servations.

It appears that this isostatic model, like the thermal expansion model, does not lead to substantial changes in the position of the rotation axis or rate of rotation. The rise of the Colorado Plateau would result in a polar shift of a few tens of meters (neglecting the re-adjustment of the equatorial bulge). Paleomagnetic data indicate polar wander rates which have been more than a factor of one thousand times larger: Besse and Courtillot (1991) e.g. give a value of 0.6° per million years for the last 10 Myr. Although this effect is too small to be detectable in paleomagnetic records, it is interesting to note that the rise of the Colorado Plateau on its own induces a polar shift which is of the same order of magnitude as that induced by continental drift during the last million years: Dickman found that 1 Myr of continental drift induces a polar shift with a magnitude of about 0.6 arcseconds, or about 20 meters, and a shortening of the length of day by about 3/4 of a millisecond, while the rise of the Colorado Plateau would induce a total amount of a few milliseconds. This stresses the point that especially radial displacements have a strong, although not sufficient, influence on polar wander.

Of course, this simple model and comparison is crude and differs in a number of respects from the real situation. For instance, the rise of the Colorado Plateau was not accomplished in 1 Myr. Lucchitta (1979) states that the plateau has been uplifted at least 880 m with respect to sea level since 5.5 Myr ago, but on the other hand there are strong indications that a much larger part of the western United States has been uplifted (Unruh, 1991).

One must also bear in mind that the figures given for the lithospheric thickness and the temperature increase over the whole lithospheric column are upper limits, making the calculated polar shift an over-estimation (Thompson and Zoback, 1979, give an estimated value of approximately 80 kilometers with a 40 kilometers thick crust).

On the other hand, no density changes resulting from chemical or phase-change boundaries have been considered. These effects might be important as they can give a contribution to the polar wander which is proportional to the fourth power of the radius. If one could contrive a model in which the raise of the lithospheric column is accomplished without a decrease of the density in the column, then the effect would be substantially larger (in fact, the simple isostatic models can not account for the whole figure of plateau uplift, as the mean elevation of the Colorado Plateau is about 2 kilometers above sea-level; excess uplift might be accomplished by e.g. eclogite – gabbro conversion and partial melting as Thompson and Zoback indicate). Then the raise of the plateau with an amount h would induce

$$\Delta I_{xz} = -\rho_L \int_R^{R+h} r^4 dr \int_{\phi_1}^{\phi_2} \cos\phi \, d\phi \int_{\theta_1}^{\theta_2} \sin^2\theta \cos\theta \, d\theta \tag{3.17}$$

and

$$\Delta I_{yz} = -\rho_L \int_R^{R+h} r^4 dr \int_{\phi_1}^{\phi_2} \sin\phi \, d\phi \int_{\theta_1}^{\theta_2} \sin^2\theta \cos\theta \, d\theta \tag{3.18}$$

which, as now in the case of the thermal expansion model according to (3.4) h can be approximated by $h \approx \alpha\Delta TL$, would result in a polar shift of

$$\left(\frac{\Delta I_{xz}}{C-A}, \frac{\Delta I_{yz}}{C-A}\right) \approx -\frac{\alpha\rho\Delta TLR^4}{3(C-A)} (\sin^3\theta_2 - \sin^3\theta_1) \cdot \cdot (\sin\phi_2 - \sin\phi_1, -\cos\phi_2 + \cos\phi_1) \tag{3.19}$$

being a factor $R/L \approx 40$ larger than in the isostatic case (compare (3.7)), resulting in a polar shift of up to a few kilometers. In fact, this is one of the main reasons why glacial loadings and unloadings are so effective in changing the Earth's rotation axis.

Non-isostatic uplift

Mountain building in fold and thrust belts is a process in which deviations from isostasy are usually observed. Sedimentary rocks now found in mountainous areas, must have been deposited in marine environments. They indicate that in the first stages of the process a crustal root is formed in a compressive stress regime by the convergence of two lithospheric plates. Only at a later stage uplift sets in and the crust rises above sea-level. Intra- and interplate stresses are responsible for forming and maintaining the deviations from Airy isostasy.

Whereas oceanic lithosphere is a rather smooth continuum with only small internal deformation (except flexure), continental lithosphere is a far more complex assemblage of compositional and structural heterogeneities. General flow properties of continental crust and lithosphere are hard to assess, as small changes in e.g. volatile elements content and geotherm can have large consequences for the crustal and

lithospheric rheologies. Gasperini et al. (1990) take in their study on the effects of lateral viscosity variations on post-glacial rebound a value for the viscosity of crust and lithosphere of about 50 times the canonical mantle viscosity of 10^{21} Pa · s, but these values can easily be orders of magnitude larger for specific areas.

Strong crust and lithosphere in a compressive stress regime can inhibit flow to restore isostasy greatly. Such a situation promotes the chances of formation and maintenance of the transient process in which deviations from isostasy occur, which subsequently may result in the process of uplift.

Seismological and gravitational studies can supply additional information concerning existing deviations from isostasy for various regions. For the Himalayas, seismic observations clearly indicate that the Moho is downwarped to a much greater depth than the topography could explain if the area would be in Airy isostasy. Kaila's (1981) deep seismic sounding observations show that the Moho exceeds even depths of 60 kilometers beneath the Great Himalayas Range.

The indication that a light crustal root in this young orogenic region overcompensates the topography by a large amount, can be sustained by the observed gravity anomalies over this region.

Departures from isostasy, which have been shown to be of paramount importance in causing measurable changes in the Earth's rotation, can not be derived by any direct method. Instead, they must be deduced from a combination of gravity measurements (gravity anomalies, geoid anomalies) and density models.

The various anomalies do not lead to unique models for the departures from isostasy. Free air gravity anomalies come closest to indicate whether a region is in hydrostatic equilibrium or not, but only when the region is laterally rather large in comparison with the crustal depth and if it is rather smooth. A young orogen with its rugged topography, such as the Alps, does not conform to this condition, in contrast with a continental plateau as the Colorado Plateau. If such a smooth elevated region as a plateau is in Airy isostatic equilibrium, then the excess gravity from the top of the plateau overcompensates the diminished gravity from the root a little, causing the free air gravity anomaly to be slightly positive in the inner parts of the plateau area. This effect is due to the fact that the root is farther away from the surface than the part of the plateau above sea-level. Towards the edges of the plateau the free air gravity anomaly rises, sharply turning negative at the edge, smoothly running to zero as a function of the distance away from the plateau. This 'edge effect' is simply due to the larger wavelength of the gravity anomaly caused by the mass of the root with respect to the wavelength of the gravity anomaly caused by the mass of the part of the plateau above sea-level, again due to the fact that the root is farther away from the surface than the part of the plateau above sea-level. This is also the reason why a mountainous region is generally not well suited to derive isostatic anomalies

from measured free air gravity anomalies.
A nice example of such a complicated situation is provided by the Himalayas. Whereas plate tectonic models, sustained by seismic studies, indicate that the root of the crust in this young orogenic region overcompensates the topography by a large amount, free air gravity anomaly maps show strong positive values for the central regions of the mountains, at some places even reaching 200 mgals. Only at the southern borders, where the Indo-Ganga-Brahmaputra basin is situated, the maps show a sharp turning of the large positive values into negative values. Basavaiah et al. (1991) discuss the confusion to which these seemingly contrasting data have led and show that the large positive values can be reconciled with an isostatically overcompensated root model by taking the mean value of all the anomalies over the Himalaya and basin region. The 'edge effects' dominate the anomalies here: one cannot attribute the positive anomalies over the mountain areas to the mountains and the negative anomalies to the basin solely.
So, departures from (Airy) isostasy inside an extended continental plateau can be expected whenever the free air gravity anomalies are found to be large, while for more complex areas the simple density model of assigning specific densities to crustal material and to mantle material must be replaced by a more elaborate density model, e.g. based on seismic observations. It then becomes more difficult to determine unambiguously whether a region is in isostatic equilibrium or not, however.
Another way of inferring the departures from isostasy is by means of the Bouguer gravity anomaly. For the above mentioned case of an extended continental plateau, the Bouguer gravity anomaly is simply equal to the gravity anomaly induced by the low-density root. One can get an impression of the amount of departure from isostasy by calculating what Bouguer anomaly the root of the plateau would induce when the root fully compensates the elevated topography of the plateau. The difference between the calculated anomaly and the observed anomaly then gives the isostatic anomaly. Lyon-Caen and Molnar (1985) have performed such an analysis for four profiles across the western Himalaya and the Ganga Basin. Quantitatively they arrive at the same conclusions as Basavaiah et al.: the deviations from local isostatic equilibrium are such that they indicate a larger crustal root underneath the Great Himalayas than the topography would allow for the region being in Airy isostatic equilibrium.
Although there are a lot of uncertainties and ambiguities in the models, it seems safe to conclude that there are indeed deviations from isostasy in at least some of the regions that experience large vertical movements. Assuming that the lithosphere moves up as a solid unit, the net mass changes associated with the upwards buoyancing are confined to two layers: at the top, air is replaced by lithosphere if

the surface is a subaerial one, while at the bottom of the lithosphere mantle material replaces lithospheric material. This leads us to a two-layer model for the vertical movements taking place under non-isostatic conditions (figure 3.1).

Two-layer model for the rotational forcings

Changes in the moment of inertia tensor **I** by a mass redistribution $\Delta\rho dV$, in which $\Delta\rho$ is the change in density of an infinitesimal volume element dV, are given in Cartesian components $\vec{r} = (x, y, z)$ by (2.22). The coordinates x and y are again in the equatorial plane, with x in the direction of the Greenwich meridian and y 90 degrees to the east, while z is in the north direction. The excitation functions from which the polar shift is to be derived, are given by the components ΔI_{xz} and ΔI_{yz} for the polar shift in the x-direction and y-direction respectively.
If ρ_L denotes the density of the lithosphere with a thickness L and ρ_m the density of the mantle, then the change in the product of inertia ΔI_{xz} due to uplift of the upper part of the lithosphere with its top originally at r = R is equal to

$$\Delta I_{xz} = -\rho_L \int_R^{R+\Delta h} r^4 dr \int_{\phi_1}^{\phi_2} \cos\phi \, d\phi \int_{\theta_1}^{\theta_2} \sin^2\theta \cos\theta \, d\theta \qquad (3.20)$$

in which R denotes the mean radius of the Earth, Δh the amount of uplift, and θ_1, θ_2, ϕ_1 and ϕ_2 the edges in spherical coordinates of the quadrilateral modeled areas in which the uplift takes place (θ and ϕ denote co-latitude and longitude respectively).
The change due to the lower part, where lithosphere is replaced by mantle material with the same amount of uplift Δh, is equal to

$$\Delta I_{xz} = -(\rho_m - \rho_L) \int_{R-L}^{R-L+\Delta h} r^4 dr \int_{\phi_1}^{\phi_2} \cos\phi \, d\phi \int_{\theta_1}^{\theta_2} \sin^2\theta \cos\theta \, d\theta \qquad (3.21)$$

The resulting change in the product of inertia ΔI_{xz} is given by (3.20) + (3.21). Evaluation of the integrals with $\Delta h \ll R$ and $L \ll R$ leads to

$$\Delta I_{xz} \approx -\frac{1}{3} \rho_m \Delta h R^4 (\sin\phi_2 - \sin\phi_1)(\sin^3\theta_2 - \sin^3\theta_1) \qquad (3.22)$$

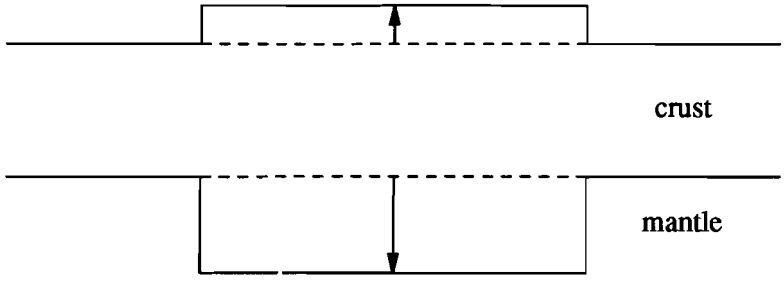

AIRY ISOSTATIC UPLIFT

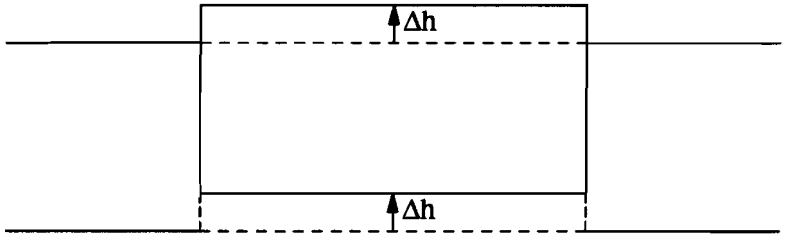

NON - ISOSTATIC UPLIFT

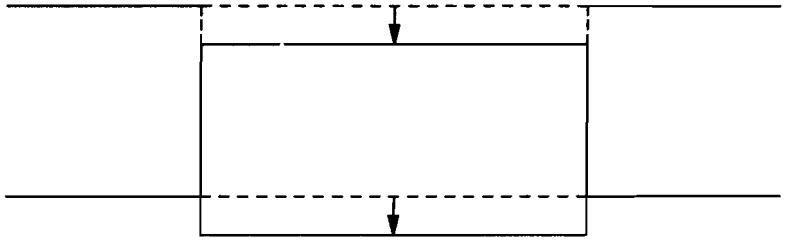

NON - ISOSTATIC SUBSIDENCE

Figure 3.1. Cartoon showing the difference in mass changes between isostatic and non-isostatic uplift. In the top picture, the increase in mass of the upper column is equal to the decrease in mass of the lower column. This cancels the first order effect on the changes in rotation. Such a model would apply to mountain building if topography and root would be formed at the same time. In the middle picture, both the upper and lower layer experience an increase in mass by the uplift dh. Such a model applies to uplift of a mountainous area with a larger light root than the topography can compensate for isostatic equilibrium, or uplift of the upper part of a detached slab. The first order effect on the changes in rotation is retained in this model. In the case of non-isostatic subsidence of a foundering flexure, the arrows in the picture reverse sign. This is illustrated in the bottom picture. In the case of isostatically uncompensated erosion, only the top layer changes in density.

In the same way, the change in the product of inertia ΔI_{yz} can be determined, resulting in

$$\Delta I_{yz} \approx \frac{1}{3}\rho_m \Delta h R^4 (\cos\phi_2 - \cos\phi_1)(\sin^3\theta_2 - \sin^3\theta_1) \qquad (3.23)$$

To illustrate the effectiveness of the non-isostatic tectonic uplift: a hypothetical quadrilateral region situated between 70 degrees and 95 degrees longitude and 55 degrees and 63 degrees co-latitude, which could serve as a crude estimate for the extent of the Himalayan and Tibetan plateau region, which is uplifted by 5 millimeters per year induces changes in I_{xz} and I_{yz} of about -10^{26} kg · m^2 per year and -8×10^{26} kg · m^2 per year respectively. This is equivalent with a shift of the rotational axis with a magnitude (cf. (2.19) and (2.20)) of $\sqrt{\Delta I_{xz}^2 + \Delta I_{yz}^2}/(C - A)$, with $C - A = 2.63 \times 10^{35}$ kg · m^2, resulting in about 2 centimeters on the Earth's surface in the direction 97.5 degrees west longitude (cf. (3.8)). For a comparison: as mentioned in chapter 2, the observed present-day shift of the rotational axis is about 10 centimeters per year in the direction 76 degrees west longitude (Dickman, 1977), so the uplift of this block would account for about a fifth of the magnitude of the observed value.

The uplift has also its effect on the second degree harmonic of the gravitational potential field J_2. The total change in the second zonal harmonic of the gravitational potential ΔJ_2 can be determined in the following way.

If R denotes the mean radius of the Earth, in a spherical harmonic expansion of the gravity potential field V for $r > R$

$$V(r,\theta,\phi) = \frac{GM}{r}\sum_{n=0}^{\infty}\sum_{m=0}^{n}\left(\frac{R}{r}\right)^n (C_{nm}\cos m\phi + S_{nm}\sin m\phi)\, P_{nm}(\cos\theta) \qquad (3.24)$$

with G the gravitational constant, $M = 6 \cdot 10^{24}$ kg the total mass of the Earth and P_{nm} the associated Legendre polynomials of degree n and order m, which can derived from Rodrigues formula (e.g. Butkov, 1968, p. 375)

$$P_{nm}(x) = \frac{(1-x^2)^{m/2}}{2^n n!} \frac{d^{n+m}}{dx^{n+m}} (x^2-1)^n \qquad (0 \le m \le n) \tag{3.25}$$

The Stokes coefficients C_{nm} and S_{nm} read (e.g. Lambeck, 1988, p. 11)

$$C_{nm} = \frac{2-\delta_{0m}}{MR^n} \frac{(n-m)!}{(n+m)!} \int_E \rho r^n P_{nm}(\cos\theta) \cos m\phi \, dV \tag{3.26a}$$

and

$$S_{nm} = \frac{2-\delta_{0m}}{MR^n} \frac{(n-m)!}{(n+m)!} \int_E \rho r^n P_{nm}(\cos\theta) \sin m\phi \, dV \tag{3.26b}$$

in which ρ denotes the density and E the entire volume of the Earth.
So

$$C_{20} = \frac{1}{MR^2} \int_E \rho r^2 \left(\frac{3}{2} \cos^2\theta - \frac{1}{2} \right) dV$$

As $\cos\theta = z/r$, C_{20} can be rewritten as

$$C_{20} = \frac{1}{MR^2} \int_E \rho \left(z^2 - \frac{1}{2}x^2 - \frac{1}{2}y^2 \right) dV$$

or, according to (2.3),

$$C_{20} = -\frac{I_{zz} - \frac{1}{2}I_{xx} - \frac{1}{2}I_{yy}}{MR^2}$$

As $J_2 \equiv -C_{20}$, this results in

$$J_2 = \frac{3I_{zz} - \mathrm{Tr}\, \mathbf{I}}{2MR^2} \tag{3.27}$$

in which Tr **I** is the trace of the inertia tensor, and consequently

$$\Delta J_2 = \frac{3\Delta I_{zz} - \Delta \mathrm{Tr}\, \mathbf{I}}{2MR^2} \tag{3.28}$$

with, using (2.22),

$$\Delta \mathrm{Tr}\, \mathbf{I} = 2 \int_E r^2 \, \Delta\rho \mathrm{d}V \tag{3.29}$$

Again using (2.22) this results in

$$\Delta J_2 \approx - \frac{\rho_m \Delta h R^2}{2M} (\phi_2 - \phi_1) \left(\cos\theta_2 - \cos\theta_1 - (\cos^3\theta_2 - \cos^3\theta_1) \right) \tag{3.30}$$

For the hypothetical quadrilateral region this would result in a value of $\Delta J_2 \approx 10^{-12}$ per year. When the same region would be situated at the equator (between 85 degrees and 95 degrees co-latitude), the effect would be maximal with a value of $\Delta J_2 \approx 4 \times 10^{-12}$ per year. This would be about 15 per cent of the observed non-tidal value in magnitude of $\Delta J_2 \approx -3 \times 10^{-11}$ per year.

Of course, the uplifted material must be replaced by material from elsewhere in order to conserve mass. It is often not clear where this material comes from, however, but generally these areas are likely to be more diffuse which promotes the chances for isostatic relaxation on time-scales of post-glacial rebound for them, in contrast to the case under consideration where relaxation takes place on a much larger timescale. Thus, the compensating areas will generally only play a marginal role in diminishing the effects on rotation, and conservation of mass-requirements are not relevant in this context. In chapter 4 this will be shown explicitly.

Tectonic mechanisms

Other examples of vertical movements taking place under non-isostatic conditions are flexure of oceanic basins caused by lithospheric stresses under sedimentary loads, as proposed by Cloetingh et al. (1985) to explain third and higher order Vail sea-level curves, detachment of a subducting slab, such as seems to be presently taking place beneath the New Hebrides (Barazangi et al., 1973) and in the Mediterranean area (Spakman et al., 1988), subhorizontal subduction, resulting in underplating (Vlaar, 1983), and delamination of the lithosphere (Bird, 1978).
Basically, in all these models non-isostatically induced vertical movements lead to density changes at the top and at the bottom of the lithosphere which act in concordance in changing the Earth's rotation, as illustrated in figure 3.1.

Erosion

Apart from the compressive plate tectonic forces, in later stages of mountain formation erosion can enhance the departures from isostasy whenever the erosion rates are larger than the induced uplift rates due to the light mountain root. Whereas erosion on itself could cause departures from isostasy in an initially isostatic region, such a situation of erosion enhancing existing deviations from isostatic equilibrium in mountainous areas can cause a permanent state of mass deficit in the root uncompensated by the topography. This can be the case if the rheologies of the lithosphere and the crust result in relaxation times which are large compared to the erosion rates. Such might happen, for example, by the following scenario: suppose a block with a high and rough topography is situated between blocks with a low and smoother topography, then erosion will be very effective on the elevated block. If the block has lateral dimensions which are smaller than or comparable to the depth of the crust or the lithosphere, the only way to restore isostasy is by upwards slipping along the edges with the surrounding ones. A complicated morphology of the blocks and the high viscosity of the upper crust and the lithosphere in combination with the compressive intraplate stress field may strongly inhibit such movements. For blocks with lateral dimensions larger than the depth of crust or lithosphere, partial relaxation might be accomplished, but it is likely that especially near the edges of the elevated block this relaxation will be far from complete.

Although the erosional products are usually deposited at a place not far away from the region where they originate, erosion can still be an effective mechanism for inducing changes in rotation because sedimentary deposition probably has a negligible effect on the Earth's rotation as demonstrated in the following.

In the case of the Himalayas, the erosional products are deposited in the Bay of Bengal. Whereas the place where they originated is favorable for inducing deviations from isostasy, the oceanic area on which the deposition takes place is rather large and uniform. The conditions are favorable here for isostatic mantle relaxation on timescales of post-glacial rebound. Apart from this, the erosional products end up below sea-level instead of sub-aerial which diminishes the change in density. The resulting increase in sea-level is distributed more uniformly over the world's oceans which diminishes any effect on the rotation of Earth greatly. Hence we infer an asymmetry concerning the effects of erosion and sedimentation of material in effectiveness on changing rotation.

It is often not clear which of the mechanisms is responsible for the vertical motions in orogenic regions. For the present-day uplift of the Himalayas, for example, both rebound in response to enhanced erosion rates as well as active uplift by the ongoing continent-continent collision have been proposed.

Assume that from the top of an elevated terrain a height Δh is eroded away and that this happens so fast that the lithosphere is not able to rebound isostatically instantaneously. Just as is the case in the melting of the ice sheet, where the increase in eustatic sea-level by the melt water must be incorporated in the models in order to obtain a closed hydrological cycle, the deposition of the erosion products ought to be taken into account (e.g. a large part of the erosional products of the Himalayas is alluvially deposited in the Bay of Bengal). As a first approximation, however, we neglect the contributions of the deposition of the erosional products to the changes in the rotational figures. The erosional products end up usually in submarine areas where they replace water instead of air. The resultant variations in sea-level are not confined to the region of deposition but are more uniformly distributed over the globe, which diminishes any effect on the rotation. Furthermore, the erosional products are often distributed over larger areas than the areas where they originated from, whereby these areas are often situated in tectonically less active regions (again, the Himalayas and the Bay of Bengal serve as an example here). The implication is that in general the conditions for restoring isostasy are more favorable for regions where erosional products are deposited than for the regions where they came from.

Neglecting the deposition of the erosional products, the change in the product of inertia I_{xz} follows from (3.20) by

$$\Delta I_{xz} \approx \frac{1}{3}\rho_L \Delta h R^4 (\sin\phi_2 - \sin\phi_1)(\sin^3\theta_2 - \sin^3\theta_1) \tag{3.31}$$

while for ΔI_{yz} the result is

$$\Delta I_{yz} \approx -\frac{1}{3}\rho_L \Delta h R^4 (\cos\phi_2 - \cos\phi_1)(\sin^3\theta_2 - \sin^3\theta_1) \tag{3.32}$$

Substituting (3.31) and (3.32) in (2.19) and (2.20) leads to a polar shift of

$$\left(\frac{\Delta I_{xz}}{C-A}, \frac{\Delta I_{yz}}{C-A}\right) \approx \frac{\rho_L \Delta h R^4}{3(C-A)}(\sin^3\theta_2 - \sin^3\theta_1) \cdot \cdot (\sin\phi_2 - \sin\phi_1, -\cos\phi_2 + \cos\phi_1) \tag{3.33}$$

This amount is ρ_L/ρ_m times the two-layer non-isostatic uplift of the former section, while the direction of the shift is opposite to it. Also the change in J_2 turns out to determinable by such a simple rescaling of (3.30), resulting in

$$\Delta J_2 \approx -\frac{\rho_L \Delta h R^2}{2M}(\phi_2 - \phi_1)\left(\cos\theta_2 - \cos\theta_1 - (\cos^3\theta_2 - \cos^3\theta_1)\right) \tag{3.34}$$

Table 3.1 gives a gross estimate of the minimum area needed to induce a substantial contribution to the observed non-tidal $\dot{J}_2$ figure of about 3×10^{-11} yr^{-1}. If the

top 2 kilometers of a plateau or mountain area is eroded isostatically uncompensated in a time Δt, then the second column of this table gives the approximate minimum surface area for regions around the equator (where the effect is largest) to induce a value of $\dot{J}_2 = 10^{-11}\ yr^{-1}$. The last column of table 3.1 gives the erosion rate under the assumption that the erosion process is linear in time. This latter column can also be read as the contemporary erosion rate prevailing under the same conditions that were assumed. It is clear from this table that, if erosion is indeed effective under the condition that the isostatic rebound of the lithosphere cannot accommodate the denudation of its roof, the areas do not need to be unrealistically large to have a considerable influence on changes in J_2. Relaxing the condition that no rebound takes places at all would lead to larger minimum areas to induce the same changes, however, so the figures of table 3.1 must be read as upper limits the areas can induce. Roughly, the minimum area is proportional to the amount of relaxation.

Foundering flexure

If it is assumed that in the case of a foundering flexure the thickness of the lithosphere remains approximately constant, then the replacement of crustal material by sea-water at the top of the oceanic lithosphere acts in concordance with the replacement of mantle material by crustal material at the bottom of the lithosphere. At the top, lithosphere with a density ρ_L is replaced by water with a density ρ_w. At the bottom, mantle material with a density ρ_m is replaced by lithospheric material with a density ρ_L. Whereby in the case of erosion the mass of the column changes with an amount $\rho_L \Delta h$, the resultant change of mass in this case is equal to $(\rho_w - \rho_L)\Delta h + (\rho_L - \rho_m)\Delta h = -(\rho_m - \rho_w)\Delta h$, with Δh denoting the amount of subsidence. So the same expressions (3.22), (3.23) and (3.30) hold, except that ρ_m has to be replaced by $-(\rho_m - \rho_w)$.

Slab detachment and delamination

Several seismological studies give indications that there are places on Earth where a downgoing old oceanic lithospheric slab is presently in the process of detachment or has been detached in the past from the surface plate.

Spakman et al. (1988) have proposed slab detachment for the eastern Mediterranean area in their tomographic studies. When detachment takes place, the upper part of the ruptured slab becomes liberated from the downgoing part below and this results in the disappearing of the slab pull on it. As a consequence, the upper part reverses its descending tendency and buoys upwards. This process could in principle lead to large uplift rates at the surface of the elastically snapbacking lithosphere.

Δt (Myr)	minimum area (° × °)	uncompensated erosion rate (mm · yr^{-1})
2	77 × 77	1
1	45 × 45	2
0.5	30 × 30	4
0.2	19 × 19	10
0.1	13 × 13	20

Table 3.1. Minimum area to induce significant changes in J_2.

Chatelain et al. (1992) recently discuss the apparent relation between the gap in seismic activity beneath the New Hebrides and the pattern of uplift rates of the New Hebrides Islands. The uplift rates for parts of the overriding lithosphere are high, at some places reaching 5 mm/yr, while the uplift of the islands seems to have been going on for about 1 Myr. They attribute the largest part of the uplift of the New Hebrides arc to slab detachment of the subducting Australian lithosphere. According to them, seismic observations clearly point to a gap in the subducting profile, indicating that detachment has taken place or is still taking place at the moment. They show by a simple model that the measured uplift rates are indeed possible by the process of detachment.

There are several reasons why the process of slab detachment can be very effective in changing the moments and products of inertia. The elastic snapbacking of the upper lithospheric part of a slab undergoing detachment is obviously a process which takes place under non-isostatic conditions: the buoyancy strives to restore isostasy, counteracted by the stresses acting in the overriding plate and possibly by those induced in the rebounding and in the sinking detached slabs by the part of the subducting plate which has not been detached (otherwise isostasy would have been reached on timescales of those of post-glacial rebound, which is not compatible with the uplift going on for at least a few hundred thousands of years. Hence, the process is obviously controlled by the rheology of the subducting and overriding

plate instead of the mantle rheology). The density changes associated with it are large, at the free surface even the full lithospheric density when the region is subaerial.

If we consider the most simple model, in which the uplift is solely due to the buoyancing upper part of the slab under the assumption that the thickness of the lithosphere does not change, then at the surface air or water is replaced by lithospheric material of density ρ_L. As the bottom of the lithosphere rises with the same speed, lithospheric material is there replaced by mantle material with a density ρ_m. So the resulting change of the mass in a unit column is equal to $(\rho_L - \rho_w)\Delta h + (\rho_m - \rho_L)\Delta h = (\rho_m - \rho_w)\Delta h$ for submarine uplift, and $\rho_L \Delta h + (\rho_m - \rho_L)\Delta h = \rho_m \Delta h$ for subaerial uplift. Δh denotes the amount of uplift. Again, the same expressions (3.22), (3.23) and (3.30) hold with ρ_m replaced by $\rho_m - \rho_w$ in the case of submarine uplift.

Delamination of lithospheric mantle can be modeled in the same way. This process has been proposed as driving mechanism for the uplift in the Himayalan region (Bird, 1978) and for the Colorado Plateau (Bird, 1979).

Subhorizontal subduction and underplating

Apart from the deviations of isostasy and the resulting vertical movements which accompany lithospheric doubling (Vlaar, 1983), the process of consequent underplating can be effective in inducing uplift under non-isostatic conditions according to the following scenario: a plate which has obducted young oceanic lithosphere acquires gradually a low density layer at its bottom by magmatic differentiation processes acting in the reheated subhorizontally subducted oceanic lithosphere. This light material leads to an inversion of the density profile: the upper part of the lithosphere rests upon a gradually growing buoyant part. The upper part (usually continental lithosphere) will rise as a consequence, and the same arguments as with respect to deviations from isostasy apply as in the case of erosion: if the upper part of the lithosphere cannot accommodate itself rapidly enough, the uplift takes place under non-isostatic conditions.

There is a complication concerning the negative buoyancy of the lower lithospheric density layer from which the light material has been removed. We assume that the subsidence of this layer is negligible in magnitude compared to the uplift of the layer above it. With this assumption, the effective changes in density are limited to the upper part of the rising crust only, so ρ_m has to be replaced by ρ_L in (3.22), (3.23) and (3.30). The merit of this is that for our calculations it doesn't matter very much whether the uplift of e.g. the Tibetan Plateau is due to detachment of a slab or to magmatic processes related to lithospheric doubling (both mechanisms have been suggested in the past for being responsible for the uplift): apart from a

minor difference in the density, the same formulas apply with respect to the changes in rotation.

The minimum areas of table 3.1 were calculated under the assumption that there is a complete coupling between the lithosphere and the mantle. For a partial decoupling, the changes in mass distribution of the lithosphere would be more effective in changing the Earth's rotation, making the tabulated areas upper limits with regard to this (e.g. Dickman, 1979). There are indications that such a partial decoupling might exist: if it is assumed that the hot spot reference frame is fixed with respect to the deep mantle, then kinematic plate models indicate that the lithosphere globally rotates westward with respect to the mantle with a speed of up to a few centimeters per year around a pole situated in the south of the Indian Ocean (e.g. Ricard et al., 1991, and O'Connell et al., 1991).
To get an idea of the effects of such a partial decoupling: if the lithosphere should be completely decoupled from the mantle, then, using the values that Dickman mentions in his 1979 article for the principal moments of inertia of the lithosphere of $C_L \approx 1.8651 \times 10^{35}\ \mathrm{kg \cdot m^2}$ and $A_L \approx 1.8619 \times 10^{35}\ \mathrm{kg \cdot m^2}$, the polar shift would increase by a factor of $(C - A)/(C_L - A_L) \approx 820$, while the length of day and $\dot{J}_2$ would increase with a factor $C/C_L \approx 430$. Of course, these figures are large overestimates of the real values, as the lithosphere and mantle are certainly not totally uncoupled. In this respect it is interesting to note that the value of westward drift has about the same magnitude as the maximum rates of which the hotspots drift with respect to one another (Duncan and Richards, 1991). This is indicative for a rather strong coupling between mantle and lithosphere on a global scale. Even although lubricating layers might exist between the lithosphere and mantle over vast areas, lateral heterogeneities can provide a strong coupling between the moving plates and the mantle. These lateral heterogeneities (subduction zones, deep continental roots, etc.) provide a phrenological coupling between lithosphere and mantle. Although plates can shift with rather high velocities over the mantle, this coupling inhibits such a high velocity for the relative movement of the whole lithosphere with respect to the mantle to values of inter-hotspot drift.

Apart from the Himalayas and the Tibetan plateau, there are several other extensive regions in which large vertical movements have been reported, like New Zealand, the Baikal Rift Zone, the Russian Shield, the European Alps, the western part of the United States and Canada, and the South-American Andes. The tectonic activity in these regions is unrelated to post-glacial rebound.

Epeirogenic movements and denudation

Vertical movement rates and the areal extents in which they should be operative according to table 3.1 are by no means unrealistic. Large erosion rates and uplift rates, at some places even exceeding 20 mm/yr, are reported to take place at various regions distributed all over the globe.

Uplift rates, erosion rates and subsidence rates for the various tectonically active regions in the world appear to be rather dispersed throughout the literature, if they exist at all. They usually show significant variations for the same area between different authors, who often use diverse measurement techniques or estimation methods. In some cases the differences even exceed orders of magnitude.
To illustrate this, we below give a tentative compilation of uplift and subsidence rates for a number of tectonically active regions for which the mechanisms responsible for the vertical movements are believed to be unrelated or for the most part not related to post-glacial rebound. This list is far from complete, and is only intended to give a gross indication of what kind of rates are possible for some of the most importantly contributing continental areas. Truly world-wide more reliable data must await future satellite techniques and measurements. Smith et al. (1993) state that by combining GPS and VBLI data, accuracies of 3 mm/yr are presently already attainable for vertical movements, while in the near future accuracies of up to 1 mm/yr are envisioned to be possible.

New Zealand
Lensen (1975) finds that the highest uplift rates of about 10 mm/yr during the late Quaternary occur along the Alpine Fault. His figure 2f shows that the uplift rates diminish eastwards to become slightly negative (– 0.3 mm/yr) along the east coast of the South Island. These rates are derived from isotope and fission-track dating and from stratigraphic and geomorphological studies. According to Lensen, present-day precise leveling gives rates of up to 20 mm/yr in the geothermal region of Waiotapu.
Wellman (1979) presents an uplift map for the South Island of New Zealand in figure 1 of his article. This map is derived from various kinds of data. Wellman states that they are not likely to be less than 25% in error. The maximum uplift rates are found along the Southern Alps in the northwest with, according to Wellman's table 1, a maximum of 17 mm/yr. The same trend Lensen gives of uplift rates diminishing eastwards to become slightly negative along the east coast, can also be found in

Wellman's map.

The Baikal rift zone

Kolmogorov and Kolmogorova (1978) present results for recent vertical movements in the Baikal rift zone obtained from geodetic leveling measurements. They divide the region into three main morphostructures: the Siberian platform, the Baikal arched uplift and the Zabaikalye fold belt. Geodetic leveling measurements indicate that uplift rates within the Siberian platform do not exceed 4 mm/yr, but that these increase sharply nearer to Irkutsk where uplift rates of 8 mm/yr are measured. The rift zone itself and its mountain frame show the highest uplift rates: here they vary between 10 and 20 mm/yr. The deepest parts of the rift depressions show somewhat lower uplift rates: 6 – 8 mm/yr. The regions farther from the Baikal rift zone across the West Zabaikalye belt show a gradual decrease in uplift rate: from 12 mm/yr in the Hilok zone to 3 mm/yr in East Zabaikalye. The authors give as standard error in their uplift rates a value of 0 mm/yr in Krasnoyarsk up to ± 2.8 mm/yr in the eastern part of the region.

The Himalayas and the Tibetan Plateau

Mehta (1980) concludes that radioactive isotope and fission-track dating indicates that the Himalayas have been risen with rates of 0.7 – 0.8 mm/yr and states that geodetic surveys indicate that this is still the rate at which the Himalayas rise.

Kailasam (1980) reports an uplift rate obtained from geodetic leveling for the Shilling Plateau in north-eastern India of 2.5 cm during the period 1910 – 1977, resulting in a contemporaneous uplift rate of 0.4 mm/yr.

Arur and Rajal (1981) derive from geodetic triangulation and precision leveling observations an uplift rate of 5 – 25 mm/yr for the Shali Thrust near Shanan (Jogindar Nagar) in Himachal Pradesh for the time interval 1976 – 1978.

Zeitler (1985) presents in his table 4 uplift rates for the Himalaya ranges of northern Pakistan. He derived these rates from fission-track and isotope dating. The rates are generally below 1 mm/yr, except for those of the Quaternary. The increase in uplift rates during the last 10 Myr is illustrated in figure 13 of his article: the Nanga Parbat-Haramosh Massif experienced an accelerated uplift rate which can be modeled, according to Zeitler, with an exponential function: the uplift rate is equal to $5.0 \cdot \exp(-t/3)$, with t being the time before present in Myr, resulting in a present-day uplift rate of 5 mm/yr. From the fact that the uplift rates in northern Pakistan at least doubled during the late Tertiary, Zeitler concludes that this increase is not merely an isostatic response to unroofing, but must be ascribed largely to a further unspecified tectonic mechanism.

The Ponto-Caspian region
Blagovolin et al. (1975) report vertical movement rates derived from geodetic leveling for the Ponto (northern Turkey)-Caspian orogenic region. The general trend they give is that within this region the uplift rates increase from west to east from 2 – 4 mm/yr in the Stara Platina and Crimean mountains to 6 – 8 mm/yr in the western Caucasus, reaching uplift rates of more than 12 mm/yr in the axial zone of the central and eastern Caucasus. The Black Sea shores are subsiding slightly with rates of about – 1 mm/yr with peak values of around – 6 mm/yr, while the Caspian Sea western shore shows a variety of rates ranging from – 3.5 mm/yr subsidence to 4.5 mm/yr uplift. The most intense vertical movements are generally observed near the edges of some hills, where rates up to 30 mm/yr have been found.

The Russian Shield
Mattskova (1967) presents a map of recent vertical crustal movements in the western half of the European (formerly) USSR. Geodetic leveling measurements indicate that in this region the vertical rates vary from about – 6 mm/yr to 15 mm/yr. According to Mattskova, the absolute velocities were determined with a precision of about 1 mm/yr. Her map (figure 2 of her article) shows that various, relatively large parts of this region rise with rates exceeding 5 mm/yr, notably around Lvov, Mazurovka, Kupyansk, Rezekne and near Volgograd.

The Carpatho-Balkan region
Joó et al. (1981) give a map of recent crustal movements in the Carpatho-Balkan region. They report that the values inside this area are ranging from 4 mm/yr subsidence up to 6 mm/yr uplift. From the geodetic leveling network in this region they found that the chain of the Carpathians has a pronounced general uplift, while the Carpathian basin shows signs of uplift too. The subsidences are limited to relatively small zones, with more notable subsiding zones in Western Slovakia, a major part of the Yugoslav coast and some parts of the Bulgarian coast.

The European Alps
For the Swiss Alps, Kahle et al. (1980) and Geiger et al. (1986) present maps for crustal vertical movement averages, based on geodetic measurements from 1903 onwards, carried out by the Swiss Topographic Survey. They give the following values for a traverse from north to south: near Luzern, where the Molasse submerges beneath the Helvetic nappes, there is an uplift of 0.3 mm/yr, between Luzern and Andermatt uplift of 1 mm/yr till the Gotthard, where the uplift seems to diminish. Further south the uplift increases again and reaches a maximum of 1.4 mm/yr near Brescia. From there the uplift decreases gradually towards

Chiasso/Como, where a value of 0.8 mm/yr is observed. To the east and west of this geotraverse there are maxima of 1.7 mm/yr near Chur in the Rhein Valley and near Brig/Visp in the Rhône Valley.

The Rhenish Massif

Mälzer et al. (1983) present a map of vertical movements in the Rhenish Massif. They find from geodetic leveling that this massif is not uplifted as a rigid block, but that the present uplift is concentrated in limited areas. In general, west of the river Rhine the massif is predominantly either uplifting or stable, while east of the Rhine both subsidence and uplift occur. The largest uplift rates occur in the Nordeifel and Venn Sattel with values of up to 1.6 mm/yr. Uplift rates of up to 0.6 – 0.9 mm/yr are found north-east of the massif near Paderborn, in Bergisches Land north-east of the Lower Rhine Embayment, on both sides of the Rhine near Koblenz and in the Pfälzer Bergland (Palatinate mountains). In the central segment of the Rhine Graben uplift rates of 0.3 – 0.5 mm/yr are found. Large subsidence occurs in the west towards Bergisches Land, where between the Lüdenscheider Mulde and the Elsper Mulde a rapid change from uplift to subsidence up to – 0.6 mm/yr takes place, and in the northern part of the graben where the average rate of subsidence is also – 0.6 mm/yr. Near Mannheim and Frankfurt am Main the largest rates of subsidence are found: – 1.4 mm/yr.

Canada

Vanicek and Nagy (1981) present in their figure 4 a map of contemporary vertical crustal movements in Canada. The data were derived from geodetic leveling, water gauge and tide gauge measurements. Their map shows uplift being concentrated in the Yukon Territory and northern British Columbia, with maximum rates reaching 25 mm/yr in the Yukon region. Subsidence occurs especially in the Prairies with maximum rates of – 20 mm/yr. It is of great importance to note that these large vertical movements are not attributed to post-glacial rebound, but to various other tectonic mechanisms (such as thrusting of the American Rockies). The authors state that only towards the east of these areas the pattern of post-glacial rebound becomes evident.

The South-American Andes

Benjamin et al. (1987) find uplift rates for the Bolivian Andes derived from fission-track data of about 0.7 mm/yr, but remark that the present-day uplift rates may be higher.

Kroonenberg et al. (1990) present an analysis of existing data on the timing of uplift of the Columbian Andes. They mention the same kind of values as Benjamin

et al. give for the Bolivian Andes: fission-track data, for instance, indicate an uplift rate for the Sierra de Mérida of about 0.8 mm/yr between 5 and 2 Myr ago with possibly faster uplift rates thereafter.

The published uplift rates for mountainous areas and plateaus fall apart into two groups: rates which have been deduced from magnetostratigraphic, radioactive isotope and fission track mineral dating, and rates which have been determined by geodetic leveling and tide gauge measurements. Isotope dating applies to longer timescale rates (millions of years), while geodetic measurements applies to contemporary rates (up to hundreds of years). A marked difference between the two groups concerns the range of the determined values: isotope dating generally indicates uplift rates which do not exceed a few millimeters per year at most, while geodetic measurements indicate uplift rates which can even exceed a few centimeters per year in some tectonically active regions. This difference indicates that geologically short-term vertical movements can be an order of magnitude larger than the geologically long-term ones, implying that vertical movements with high uplift rates are rather episodic than continuous phenomena.
There is much debate on the reliability of the geodetically found high uplift rates – that is, exceeding 5 mm/yr – in relatively large areas, which are not attributable to post-glacial rebound.
Kaula (1980) states that vertical movements of internal cause should be less than 2 mm/yr almost everywhere and that leveling analyses which indicate greater rates not attributable to post-glacial rebound should be treated with skepticism. He acknowledges, however, that contemporary vertical movements can be an order of magnitude greater than those rates which apply to timescales of at least 100,000 years and mentions earthquakes and rapid erosion as possible causes.
Officer and Drake (1985) state that geological observations indicate that vertical movements of an episodic or oscillatory nature within intraplate regions can be in the range of 1 – 10 mm/yr, on a temporal scale of 10,000 – 100,000 years and a spatial scale of 100 – 1000 kilometers. They deduce this from recent movements, the Quaternary geologic record and the Phanerozoic sedimentary record. The rapid vertical movements are illustrated by work of Brown et al. (1980), who find from geodetic leveling that Florida has been risen at a rate of about 20 mm/yr with respect to Maine. It must be remarked that Officer and Drake do not attribute the values found for the east coast of North America to glacio-isostatic effects, but to continental shelf break off. Also Kalashnikova and Magnitsky (1980), who report vertical displacements reaching 5 – 10 mm/yr for platform regions in the European part of the Soviet Union, are cited in this respect. Kaula casts doubts on these high values, as tidemeters are reported to indicate differential vertical movements of less

than a few mm/yr between tide stations located at a number of the same points where the leveling data were obtained. He also commemorates that the large rates derived from the leveling data are an order of magnitude larger than those obtained from the leveling data of the Swiss Alps.

A striking general feature of the continental vertical movements is that there is an asymmetry between uplift and subsidence: there are more areas which are rising than areas which are subsiding, while the uplift rates are usually larger than the subsidence rates. Whether this is real or due to any kind of a selection effect in the data, remains an unanswered question. It is not imaginary, however, that we are living in a geological time in which the continents on the mean rise, just as there have been geological times in which plate tectonics was more vigorous.

Although a lot concerning data on uplift and subsidence rates is uncertain or lacking, it seems safe to conclude that large parts of the continental areas are experiencing vertical movements which are not attributable to post-glacial rebound, certainly if one bears in mind that the areas experiencing uplift or subsidence are likely to be more extended than indicated and that there are a number of areas for which the various rates are not listed or for which we did not find data.

Table 3.2 gives the induced polar shift and change in the second degree zonal gravitational harmonic on basis of the above compilation of vertical deformation rates for the various listed regions. The calculations were made under the assumption that the uplift or subsidence took place under non-isostatic conditions with no appreciable erosion or whereby the erosional products remained in the uplifted or subsided area. So (3.22), (3.23) and (3.30) were used, with ρ_m replaced by $-\rho_m$ in the case of subsidence. Table 3.3 gives the factors by which ρ_m has to be replaced in the different cases. The extent of the areas, as depicted in figure 3.2, and the mean vertical movement rates were determined by means of the maps (when available) and the listed uplift and subsidence rates in the cited literature.

The deformations listed in table 3.2 result in a polar shift of 2.7 cm $\cdot$ yr^{-1} in the direction $-101°$ east longitude, and a change in J_2 of $\dot{J}_2 = -2.9 \cdot 10^{-12}$ yr^{-1}.

For a comparison: the observed secular shift of the rotation axis for the past 100 years has been about 10 cm $\cdot$ yr^{-1} in the direction $-76°$ east longitude, while the observed change in J_2 for the past 10 years has been about $\dot{J}_2 = -3 \cdot 10^{-11}$ yr^{-1}.

A large part of the calculated changes in both J_2 and the position of the Earth's axis comes from the modeled uplift of the Himalayas and the Tibetan Plateau, the western part of Canada and the Baikal Rift zone. Important areas are also the Russian Shield, the Ponto-Caspian region zone and the South-American Andes.

region	east longitude (°)	co-latitude (°)	uplift rate (mm/yr)	polar shift (cm · yr^{-1})	direction (°E. L.)	$\dot{J}_2$ (10^{-12} yr^{-1})
New Hebrides	167 – 170	103.5 – 110.5	3	0.067	168.5	0.15
New Zealand	170 – 173	131 – 135	5	0.088	171.5	–0.059
	175 – 178	128 – 131	5	0.068	176.5	–0.025
Baikal Rift Zone	102 – 113	35 – 40	10	0.65	–72.5	–1.0
Himalayas and Tibetan Plateau	70 – 95	55 – 63	5	1.5	–97.5	0.60
Ponto-Caspian Region	41 – 49	46 – 50	5	0.24	–135.0	–0.14
Russian Shield	24 – 44	37 – 43	5	0.76	–146.0	–0.099
	24 – 36	34 – 37	2	0.08	–150.0	–0.14
Carpatho-Balkan	19 – 27	43 – 48	2	0.11	–157.0	–0.092
European Alps	6 – 11	42.5 – 44.5	1	0.014	–171.5	–0.014
Rhenish Massif	6 – 9	38.5 – 41	0.5	0.0047	–172.5	–0.0063
Canada	220 – 235	28 – 36	10	1.1	47.5	–2.5
	250 – 260	37 – 42	–10	0.62	–105.0	0.85
Colorado Plateau	247 – 253	50 – 56	0.5	0.028	–110	–0.042
South-American Andes	282 – 284	83 – 95	1	0.0017	103.0	0.080
	285 – 294	95 – 107	1	0.079	–70.5	0.32
	290 – 294	107 – 130	1	0.13	–68.0	0.086

Table 3.2. Changes in rotation by vertical deformation unrelated to post-glacial rebound of some tectonically active regions.

case	replace ρ_m in (3.22), (3.23) and (3.30) by
uncompensated erosion	$-\rho_L$
uncompensated underplating	ρ_L
subaerial uplift	ρ_m
subaerial subsidence	$-\rho_m$
submarine uplift	$\rho_m - \rho_w$
submarine subsidence	$-(\rho_m - \rho_w)$

Table 3.3. Replacement factors.

It is clear that the non-glacially induced tectonic movements can contribute considerably to the secular changes in the Earth's rotation, provided that the assumed model is realistic for all the regions listed in table 3.2 and that the vertical displacements take place under the assumed non-isostatic conditions. Our tentative calculations indicate that some 10% of the observed changes in J_2 and some 30% in magnitude of the polar wander (neglecting any shift of the equatorial bulge) can be attributed to non-glacially related tectonic mechanisms, but, as remarked before, these values might be substantially larger or smaller depending on the vertical movements rates, the departures of isostasy and the extent and amount of areas experiencing uplift, subsidence or erosion.

Are uplift and subsidence rates usually hard to determine, this only gets worse in the case of the determination of erosion rates. These rates are usually based upon a combination of gross assumptions on the prevailing erosion processes and a variety of measurements on circumstantial variables. Below, a few examples are given to illustrate this.
Adams (1980) finds that in the Southern Alps of New Zealand the contemporary uplift and erosion are approximately in balance, with values for crustal shortening of 700 ± 160 billion kg/yr and for tectonic uplift of 600 ± 100 billion kg/yr. The

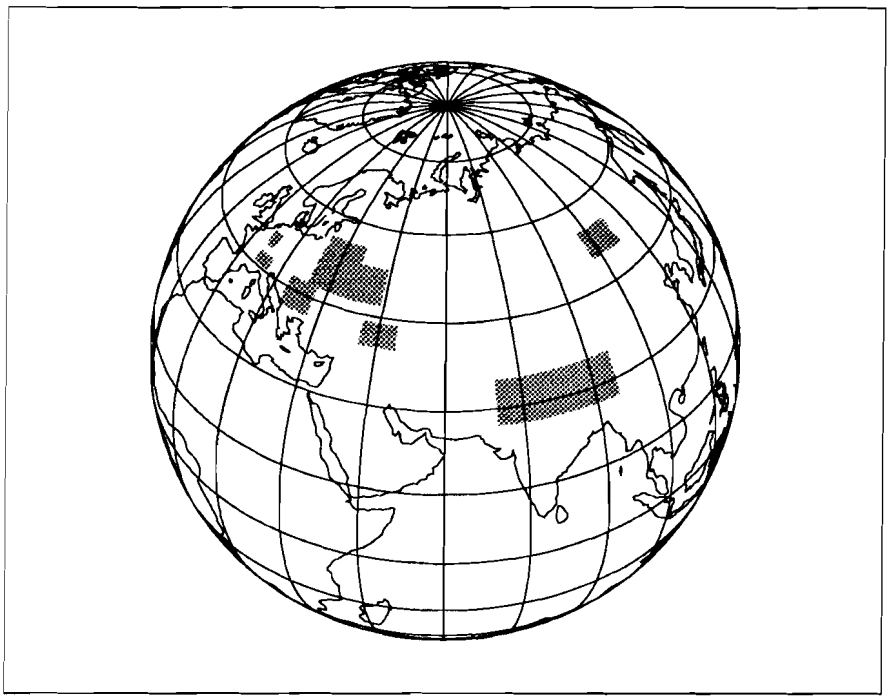

Figure 3.2a. Areas used in the simulations: Asia and Europe.

denudation is attributed to river erosion. The erosion rates are derived from water suspension and bed load analyses and are reported to exceed rates of 3.8 mm/yr at some places on the wet western side of the Southern Alps.

From geochronologic and thermobarometric data, Hubbard et al. (1991) deduce an average unroofing rate of the high Himalaya of eastern Nepal of 1.2 ± 0.6 mm/yr for the past 21 Myr. They acknowledge, however, that this value is surrounded with a lot of uncertainties. Apart from the pressure–temperature–time data derived from the collected rocks, these include uncertainties concerning the radiogenic heat production and the deep crustal structure.

Burbank and Beck (1991) derive denudation rates for the Cenozoic foreland basin

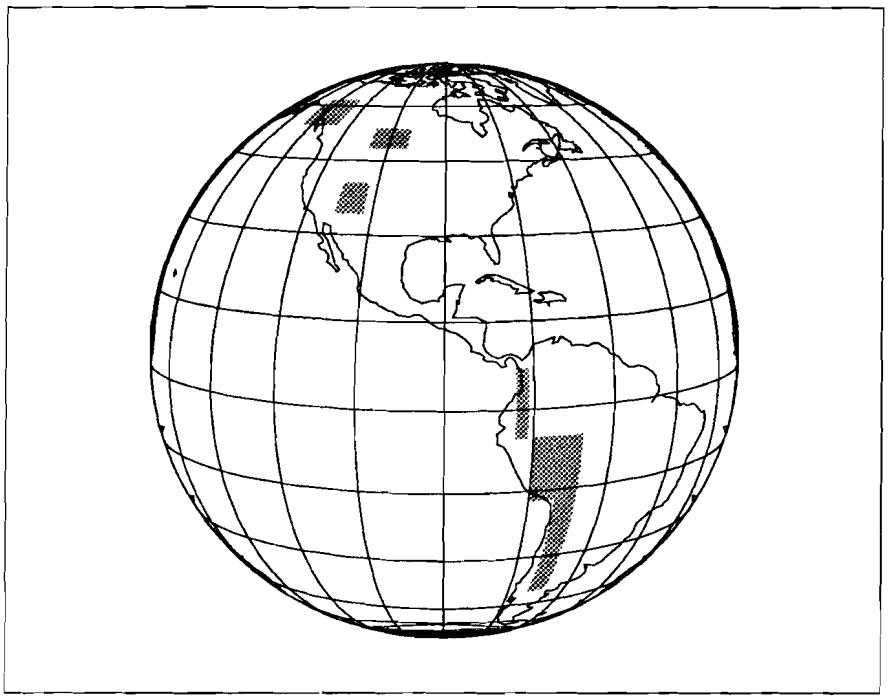

Figure 3.2b. Areas used in the simulations: North and South America.

of northern Pakistan from (fluvial) stratigraphic data. They deduce minimum rates of erosion of 1.5 – 15 mm/yr persisting for timescales as long as 1.6 Myr, and minimum rates of 10 – 15 mm/yr for timescales of 0.2 – 0.3 mm/yr. According to these authors, the erosion rates nearly kept pace with the latest Miocene to Pleistocene uplift events in this region.

Amano and Taira (1992) have studied sediments drilled from the Bengal Fan. They find two high-sedimentation episodes, from 10.9 to 7.5 Myr ago and from 0.9 Myr ago onwards. For the first period they report sedimentation rates of 0.1 – 0.2 mm/yr, while for the second period a rate of 0.2 mm/yr is established (cf. their figure 3). Making the assumption that the sedimentation patterns are not indicative of a change of the deposition area of the erosional products, they relate the patterns directly to phases of active tectonic uplift pulses of the Himalayas.

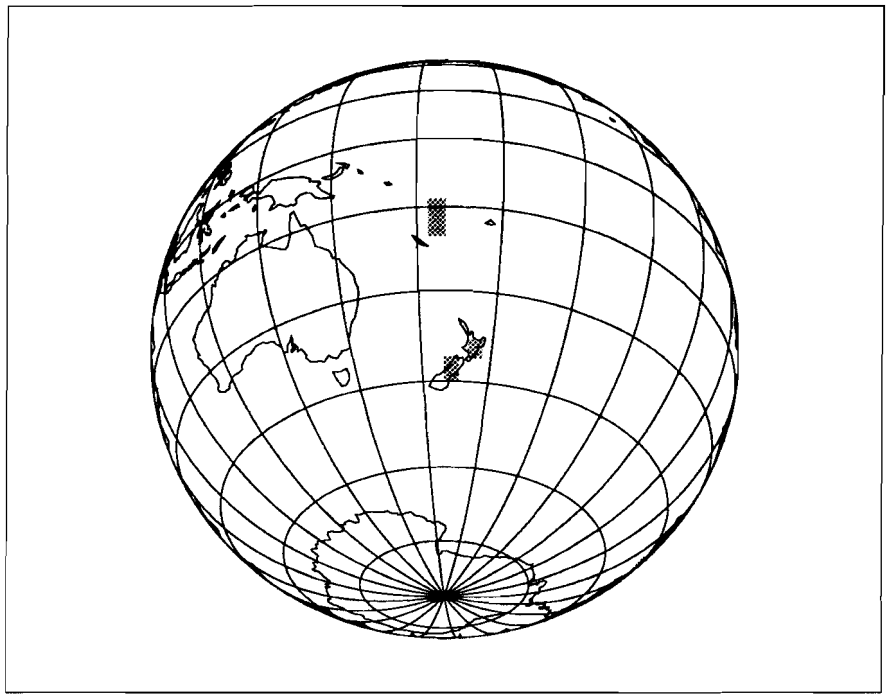

Figure 3.2c. Areas used in the simulations: New Zealand and New Hebrides.

In the examples given above, the erosion is found or assumed to be approximately equal to the uplift. Whether this is a general trend for all the young orogenic regions is unclear, however.

Displacements of the center of mass of the Earth

Mass displacements accompanying non-isostatic processes should not only lead to

changes in the eccentricity of the Earth (changes in J_2), but generally give rise to changes in the position of the center of mass (changes in the degree 1 Stokes coefficients of the gravitational potential field) also. Usually, it is assumed that the shifts of the center of mass are so small that they can be neglected, however. Together with the assumption that the mass of the Earth remains constant, changes in the gravitational potential field have therefore usually the degree 2 as lowest zonal coefficient in a spherical harmonic expansion of this field.
As the proposed vertical movements might be more or less stationary on time scales of hundreds of years up till several millions of years, this shift of the geoid might also be visible as an antipodal anti-symmetric rise and fall pattern in third (timescales of 1 to 10 million years) and higher order sea-level curves.
The shift is determined of the center of mass of the Earth by vertical tectonic movements using the uplift and subsidence data from table 3.2. Again, it is assumed that the uplift or subsidence takes place under non-isostatic conditions with no appreciable erosion or whereby the erosional products remain in the uplifted or subsided area.

If (x_0, y_0, z_0) denotes the position of the center of mass of the Earth, then in Cartesian coordinates (x, y, z)

$$x_0 = \frac{1}{M}\int_E \rho x dV \quad , \quad y_0 = \frac{1}{M}\int_E \rho y dV \quad , \quad z_0 = \frac{1}{M}\int_E \rho z dV \qquad (3.35)$$

in which $\rho = \rho(x, y, z)$ denotes the density, E the entire volume and $M = \int_E \rho dV$ the mass of the Earth.
If the Cartesian coordinate system is chosen such, that x and y are in the equatorial plane (x in the direction of the Greenwich meridian and y 90 degrees towards the east) and z is along the initial position of the rotational axis, then in a spherical coordinate system (r, θ, ϕ) with θ the degree of co-latitude and ϕ the degree of east longitude, (3.35) becomes

$$x_0 = \frac{1}{M}\int\int\int_E \rho(r, \theta, \phi) r^3 \sin^2\theta \cos\phi d\theta d\phi dr \qquad (3.36a)$$

$$y_0 = \frac{1}{M}\int\int\int_E \rho(r, \theta, \phi) r^3 \sin^2\theta \sin\phi d\theta d\phi dr \qquad (3.36b)$$

$$z_0 = \frac{1}{M} \int \int_E \int \rho(r, \theta, \phi) r^3 \sin\theta \cos\theta d\theta d\phi dr \tag{3.36c}$$

So, a change in the density distribution $\Delta\rho$ will generally result in a change of the position of the center of mass $\Delta(x_0, y_0, z_0)$ given by

$$\Delta x_0 = \frac{1}{M} \int \int_E \int \Delta\rho(r, \theta, \phi) r^3 \sin^2\theta \cos\phi d\theta d\phi dr \tag{3.37a}$$

$$\Delta y_0 = \frac{1}{M} \int \int_E \int \Delta\rho(r, \theta, \phi) r^3 \sin^2\theta \sin\phi d\theta d\phi dr \tag{3.37b}$$

$$\Delta z_0 = \frac{1}{M} \int \int_E \int \Delta\rho(r, \theta, \phi) r^3 \sin\theta \cos\theta d\theta d\phi dr \tag{3.37c}$$

These changes in the position of the center of mass can be related to changes in the degree 1 Stokes coefficients of the gravity field (3.24). From (3.25) it follows that $P_{10}(\cos\theta) = \cos\theta$ and $P_{11}(\cos\theta) = \sin\theta$. With this, the changes in the degree 1 coefficients ΔC_{10}, ΔC_{11} and ΔS_{11} are simply related to the displacements (3.37) as

$$\Delta C_{10} = \frac{\Delta z_0}{R} \quad , \quad \Delta C_{11} = \frac{\Delta x_0}{R} \quad \text{and} \quad \Delta S_{11} = \frac{\Delta y_0}{R} \tag{3.38}$$

For the uncompensated subaerial uplift model, in which the lithosphere with thickness L and its top at $r = R$ moves up by a height Δh, the displacement in the x-direction becomes

$$\Delta x_0 = \frac{1}{M} \int_{R-L}^{R-L+\Delta h} \int_{\phi_1}^{\phi_2} \int_{\theta_1}^{\theta_2} (\rho_m - \rho_L) r^3 \sin^2\theta \cos\phi d\theta d\phi dr$$
$$+ \frac{1}{M} \int_{R}^{R+\Delta h} \int_{\phi_1}^{\phi_2} \int_{\theta_1}^{\theta_2} \rho_L r^3 \sin^2\theta \cos\phi d\theta d\phi dr$$

in which ρ_m denotes the density of the mantle and ρ_L the density of the lithosphere. This leads to

$$\Delta x_0 = \frac{\rho_m - \rho_L}{M}\left(\frac{1}{4}(R - L + \Delta h)^4 - \frac{1}{4}(R - L)^4\right)(\sin\phi_2 - \sin\phi_1)\cdot$$
$$\cdot\left(\frac{1}{2}(\theta_2 - \theta_1) - \frac{1}{4}(\sin 2\theta_2 - \sin 2\theta_1)\right)$$
$$+ \frac{\rho_L}{M}\left(\frac{1}{4}(R + \Delta h)^4 - \frac{1}{4}R^4\right)(\sin\phi_2 - \sin\phi_1)\cdot$$
$$\cdot\left(\frac{1}{2}(\theta_2 - \theta_1) - \frac{1}{4}(\sin 2\theta_2 - \sin 2\theta_1)\right) \approx$$
$$\approx \frac{\rho_m \Delta h R^3}{4M}(\sin\phi_2 - \sin\phi_1)(2(\theta_2 - \theta_1) - (\sin 2\theta_2 - \sin 2\theta_1)) \tag{3.39}$$

In the same way Δy_0 and Δz_0 can be calculated, resulting in

$$\Delta y_0 \approx -\frac{\rho_m \Delta h R^3}{4M}(\cos\phi_2 - \cos\phi_1)(2(\theta_2 - \theta_1) - (\sin 2\theta_2 - \sin 2\theta_1)) \tag{3.40}$$

and

$$\Delta z_0 \approx -\frac{\rho_m \Delta h R^3}{4M}(\phi_2 - \phi_1)(\cos 2\theta_2 - \cos 2\theta_1) \tag{3.41}$$

The total displacement Δr_0 of the center of mass is thus given by

$$\Delta r_0 = \sqrt{(\Delta x_0)^2 + (\Delta y_0)^2 + (\Delta z_0)^2} \tag{3.42}$$

in the direction

$$\Phi = \arctan\left(\frac{\Delta y_0}{\Delta x_0}\right) \text{ east longitude} \tag{3.43a}$$

and

$$\Theta = \arccos\left(\frac{\Delta z_0}{\Delta r_0}\right) \text{ co-latitude} \tag{3.43b}$$

With Δx_0, Δy_0 and Δz_0 given by (3.39) – (3.41), this results in a total displacement of

$$\Delta r_0 \approx \frac{\rho_m \Delta h R^3}{4M}\left(2(1 - \cos(\phi_2 - \phi_1))\left[2(\theta_2 - \theta_1) - (\sin 2\theta_2 - \sin 2\theta_1)\right]^2\right.$$
$$\left. + (\phi_2 - \phi_1)^2(\cos 2\theta_2 - \cos 2\theta_1)^2\right)^{\frac{1}{2}} \tag{3.44}$$

in the direction

$$\Phi \approx -\arctan\left(\frac{\cos\phi_2 - \cos\phi_1}{\sin\phi_2 - \sin\phi_1}\right) \quad \text{east longitude} \tag{3.45}$$

and, if $\Delta z_0 \geq 0$, in the direction co-latitude

$$\Theta \approx \arccos\left(1 + 2(1 - \cos(\phi_2 - \phi_1))\left[\frac{2(\theta_2 - \theta_1) - (\sin 2\theta_2 - \sin 2\theta_1)}{(\phi_2 - \phi_1)(\cos 2\theta_2 - \cos 2\theta_1)}\right]^2\right)^{-\frac{1}{2}} \tag{3.46a}$$

or, if $\Delta z_0 \leq 0$, in the direction co-latitude

$$\Theta \approx -\arccos\left(1 + 2(1 - \cos(\phi_2 - \phi_1))\left[\frac{2(\theta_2 - \theta_1) - (\sin 2\theta_2 - \sin 2\theta_1)}{(\phi_2 - \phi_1)(\cos 2\theta_2 - \cos 2\theta_1)}\right]^2\right)^{-\frac{1}{2}} \tag{3.46b}$$

The factors by which ρ_m must be replaced in the expressions (3.39), (3.40), (3.41) and (3.44) in the various other possible cases of non-isostatic vertical movements are again given by table 3.3.

The contributions from the various regions given in table 3.4 result in a net shift of the center of mass of 0.070 mm/yr in the direction 81.4° east longitude and 34.7° co-latitude. The total changes in the degree 1 Stokes coefficients amount

$$\Delta C_{10} = 9.1 \times 10^{-12}\ \text{yr}^{-1}$$
$$\Delta C_{11} = 0.94 \times 10^{-12}\ \text{yr}^{-1}$$
$$\Delta S_{11} = 6.2 \times 10^{-12}\ \text{yr}^{-1}$$

For a comparison, Trupin et al. (1992) have determined the effects of recent sea-level variations and melting of glaciers, including the induced elastic yielding of the solid Earth, on the position of the center of mass. Their data on glaciers comprise the averaged yearly mass balances for 13 mountain glacier systems for the years 1965 – 1984.
From their figure 5(a) the shift of the center of mass induced by glacier melting, including the melt-water contribution to the rise in sea-level, can be deduced to be about 0.05 mm/yr in magnitude for the z-component, while for the x- and y-components the shift is negligible. So a net shift of about 0.05 mm/yr results for the glacier discharge effect.

region	east longitude (°)	co-latitude (°)	uplift rate (mm · yr^{-1})	shift (10^{-2} mm/yr)	direction (°E. L.)	direction (°co – lat.)
New Hebrides	167 – 170	103.5 – 110.5	3	0.26	168.5	107
New Zealand	170 – 173	131 – 135	5	0.19	171.5	133.0
	175 – 178	128 – 131	5	0.15	176.5	129.5
Baikal Rift Zone	102 – 113	35 – 40	10	1.4	107.5	37.5
Himalayas and Tibetan Plateau	70 – 95	55 – 63	5	3.7	82.5	58.9
Ponto-Caspian Region	41 – 49	46 – 50	5	0.51	45.0	48.0
Russian Shield	24 – 44	37 – 43	5	1.7	34.0	39.9
	24 – 36	34 – 37	2	0.18	30.0	35.5
Carpatho-Balkan	19 – 27	43 – 48	2	0.25	23.0	45.5
European Alps	6 – 11	42.5 – 44.5	1	0.030	8.5	43.5
Rhenish Massif	6 – 9	38.5 – 41	0.5	0.010	7.5	40.0
Canada	220 – 235	28 – 36	10	2.7	–132.5	32.1
	250 – 260	37 - 42	–10	1.4	75.0	140.5
Colorado Plateau	247 – 253	50 – 56	0.5	0.062	–110	53
South-American Andes	282 – 284	83 – 95	1	0.10	–77.0	89.0
	285 – 294	95 – 107	1	0.46	–70.5	101.0
	290 – 294	107 – 130	1	0.35	–68.0	118.0

Table 3.4. Changes in the position of the center of mass by vertical deformation unrelated to post-glacial rebound of some tectonically active regions.

The influence on the displacement of the center of mass due to the observed sea-level rise of 1.7 ± 0.5 mm/yr during the last 80 years can be deduced from their figure 5(b). The displacements along the three Cartesian coordinate axes amount in magnitude about 5 millimeter, 2.5 millimeter and 4.5 millimeter per 80 years, which results in a net shift of slightly less than 0.1 mm/yr.
Also the effects of the proposed polar ice sheet growth of Antarctica and Greenland on the shift of the center of mass have recently been determined. According to Trupin (1993), the shift of the center of mass in the z-direction would be -0.17 ± 0.2 mm/yr if the accumulation of the Antarctic ice sheet corresponds with a global sea-level drop of -0.6 mm/yr. Also in this case, the changes in the x- and y-direction would be negligible. The contribution from the ice-sheet growth on Greenland would be 0.04 ± 0.2 mm/yr in the z-direction, assuming a concomitant sea-level drop of -0.1 ± 0.4 mm/yr, and again negligible in the other two directions. Of course, the contributions of a possible ice sheet growth on Greenland and Antarctica at the same time partly cancel one another in the z-direction.
From these figures it is clear that non-isostatic vertical tectonic movements are capable of producing shifts of the center of mass which are comparable in magnitude to those induced by glacier melting, polar ice sheet growth and sea-level changes.

Antipodal symmetric and anti-symmetric geoid shifts

Shifts in the center of mass of the Earth with respect to the crust cause an antipodal anti-symmetric shift of the geoid, and consequently an antipodal anti-symmetric shift in sea-level: the sea-level is raised maximally in the direction where the center of the mass shifts to, while the sea-level falls maximally in the antipodal direction (cf. figure 3.3).
It is interesting to note that besides antipodal anti-symmetric global sea-level variations, recently also antipodal symmetric global sea-level variations have been proposed by Sabadini et al. (1990, 1991). They have modeled the effects on the sea-level of the adjustment of the equatorial bulge induced by the from paleomagnetic data determined true polar wander rates. They find that this adjustment induces antipodal symmetric sea-level changes of about $0.05 - 0.1$ mm/yr, being of the same order of magnitude as the antipodal anti-symmetric ones resulting from our

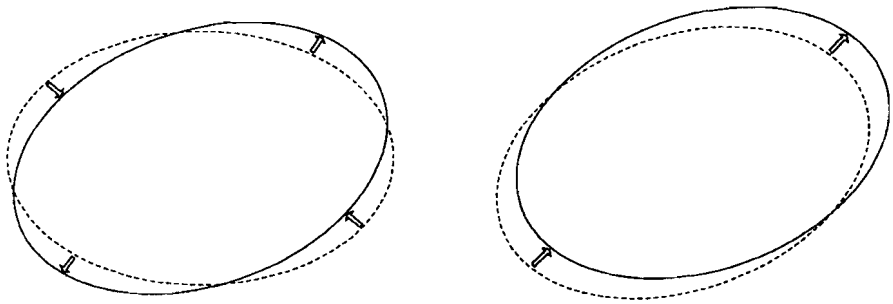

Figure 3.3. Antipodal patterns of eustatic sea-level variations.

modeling and resulting from present-day melting of glaciers and sea-level rise, as reported by Trupin et al.. The pattern of the induced sea-level variations by wandering of the Earth's rotation axis is depicted in figure 3.3: whereas shifts in the center of mass lead to a symmetric rise and fall pattern with one neutral line, polar wander leads to an anti-symmetric rise and fall pattern with two neutral lines which are along great circles and which are perpendicular to each other.
Together, polar wander and secular shifts of the center of mass of the Earth constitute two mechanisms which are capable of inducing large sea-level variations with a characteristic non-uniform global pattern on timescales of a few million years or shorter, irrespective of whether there is widespread glaciation during these times or not.

Conclusions

We have emphasized the fact that mass displacements by several tectonic processes taking place under non-isostatic conditions can induce significant changes in the Earth's rotation and in the geoid. In contrast to post-glacial rebound, where the forcings have disappeared some 10,000 years ago, the loads in our tectonic models are still operative. The mantle is rather forced by the movements of the lithosphere than forming the determining agents by which the processes take place. Whereas in models on post-glacial rebound mantle viscosities are assumed to be determinant, in our tectonic models lithospheric and crustal rheologies and intraplate-stresses are more important than the mantle rheologies. Moreover, one could speculate about whether the assumption of a lithosphere without internal deformations in the post-glacial rebound models is justified. Although some of the regions which are effective are positioned on the globe in such a way that they partly counteract each other's influence on polar wander – but this is also the case for the effects of post-glacial rebound –, it is clear that the contributions of these regions to changes in the rotation cannot be neglected.

Vertical tectonic movements have been shown to induce changes in the position of the center of mass of the Earth which have the same order of magnitude as those recently found from contemporary sea-level variations, melting of glaciers and polar ice sheet growth. Using tentative data for uplift and subsidence rates of a number of tectonically active regions, a shift of the center of mass of 0.7 millimeters per 10 years has been deduced.

As the uplift and subsidence of the modeled areas are likely to be ongoing for ten to hundred thousands of years, the induced shift of the geoid might be detectable as an antipodal anti-symmetric rise and fall pattern in eustatic sea-level over third and higher order sea-level cycle time scales, comparable in magnitude to the antipodal symmetric rise and fall pattern recently proposed to result from shifts of the equatorial bulge.

References

Adams, J., Contemporary uplift and erosion of the Southern Alps, New Zealand:

summary, *Geological Society of America Bulletin, Part I, 91*, 2-4, 1980.

Amano, K., and A. Taira, Two-phase uplift of Higher Himalayas since 17 Ma, *Geology, 20*, 391-394, 1992.

Arur, M.G., and B.S. Rajal, Study of crustal movements across Shali thrust in the area of Shanan (Joginder Nagar) in Himachal Pradesh, *Tectonophys., 71*, 154, 1981.

Barazangi, M., B.L. Isacks, J. Oliver, J. Dubois, and G. Pascal, Descent of lithosphere beneath New Hebrides, Tonga-Fiji and New Zealand: Evidence for detached slabs, *Nature, 242*, 98-101, 1973.

Basavaiah, N., B.P. Singh, and I.V. Radhakrishna Murthy, The Himalayan riddle of the free-air satellite gravity and a possible solution, *Phys. Earth Planet. Inter., 69*, 14-19, 1991.

Benjamin, M.T., N.M. Johnson, and C.W. Naeser, Recent rapid uplift in the Bolivian Andes: evidence from fission-track dating, *Geology, 15*, 680-683, 1987.

Besse, J., and V. Courtillot, Revised and synthetic apparent polar wander paths of the African, Eurasian, North American and Indian Plates, and true polar wander since 200 Ma, *J. Geophys. Res., 96*, 4029-4050, 1991.

Bird, P., Initiation of intracontinental subduction in the Himalaya, *J. Geophys. Res., 83*, 4975-4987, 1978.

Bird, P., Continental delamination and the Colorado Plateau, *J. Geophys. Res., 84*, 7561-7571, 1979.

Blagovolin, N.S., D.A. Lilienberg, and S.V. Pobedonostsev, Recent vertical crustal movements in the Ponto-Caspian orogenic region, *Tectonophys., 29*, 395-399, 1975.

Brown, L.D., R.E. Reilinger, and G.P. Citron, Recent crustal movements in the U.S.: Evidence from precise levelling, in *Rheology, Isostasy and Eustasy*, edited by N.-A. Mörner, p. 389-405, John Wiley, New York, 1980.

Burbank, D.W., and R.A. Beck, Rapid, long-term rates of denudation, *Geology, 19*, 1169-1172, 1991.

Butkov, E., *Mathematical Physics*, 735 pp., Addison-Wesley, Reading, Massachusetts, 1968.

Chatelain, J.-L., P. Molnar, R. Prevot, and B. Isacks, Detachment of part of the downgoing slab and uplift of the New Hebrides (Vanuatu) islands, *Geophys. Res. Lett., 19*, 1507-1510, 1992.

Cheng, M.K., R.J. Eanes, C.K. Shum, B.E. Schutz, and B.D. Tapley, Temporal variations in low degree zonal harmonics from Starlette orbit analysis, *Geophys. Res. Lett., 16*, 393-396, 1989.

Cloetingh, S.A.P.L., H. McQueen, and K. Lambeck, On a tectonic mechanism for regional sealevel variations, *Earth Planet. Sci. Lett., 75*, 157-166, 1985.

Dickman, S.R., Secular trend on the Earth's rotation pole: Consideration of motion of the latitude observations, *Geophys. J. R. astron. Soc., 51*, 229-244, 1977.

Dickman, S.R., Continental drift and true polar wandering, *Geophys. J. R. astron. Soc., 57*, 41-50, 1979.

Duncan, R.A., and M.A. Richards, Hotspots, mantle plumes, flood basalts, and true polar wander, *Rev. Geophys., 29*, 31-50, 1991.

Gasperini, P., D.A. Yuen, and R. Sabadini Effects of lateral viscosity variations on postglacial rebound: Implications for recent sea-level trends *Geophys. Res. Lett., 17*, 5-8, 1990.

Geiger, A., H.-G. Kahle, and E. Gubler, Recent crustal movements in the Alpine-Mediterranean region analyzed in the Swiss Alps, *Tectonophys., 130*, 289-298, 1986.

Hubbard, M., L. Royden, and K. Hodges, Constraints on unroofing rates in the high Himalaya, eastern Nepal, *Tectonics, 10*, 287-298, 1991.

Joó, I., E. Csáti, P. Jovanović, M. Popescu, V.I. Somov, H. Thurm, J. Thury, I.N. Totomanov, J. Vanko, and T. Wyrzykowski, Recent vertical crustal movements of the Carpatho-Balkan region, *Tectonophys., 71*, 41-52, 1981.

Kahle, H.-G., S. Müller, E. Klingele, R. Egloff, and E. Kissling, Recent dynamics, crustal structure and gravity in the Alps, in *Rheology, Isostasy and Eustasy*, edited by N.-A. Mörner, p. 377-388, John Wiley, New York, 1980.

Kaila, K.L., Structure and seismotectonics of the Himalaya-Pamir Hindukush region and the Indian plate boundary, in *Zagros, Hindu Kush, Himalaya Geodynamic Evolution, AGU Geodynamics Series Volume 3*, edited by H.K. Gupta and F.M. Delany, pp. 272-293, AGU, Washington D.C., 1981.

Kailasam, L.N., Late Cenozoic vertical movements in the Indian subcontinent and their relation to isostasy, in *Rheology, Isostasy and Eustasy*, edited by N.-A. Mörner, p. 407-418, John Wiley, New York, 1980.

Kalashnikova, I.V., and V.A. Magnitsky, Some regularities of recent vertical movements of the Earth's crust, in *Rheology, Isostasy and Eustasy*, edited by N.-A. Mörner, p. 371-375, John Wiley, New York, 1980.

Kaula, W.M., Problems in understanding vertical movements and Earth rheology, in *Rheology, Isostasy and Eustasy*, edited by N.-A. Mörner, p. 577-588, John Wiley, New York, 1980.

Kolmogorov, V.G., and P.P. Kolmogorova, Some results from studying recent crustal movements in the Baikal rift zone, *Tectonophys., 45*, 101-105, 1978.

Kroonenberg, S.B., J.G.M. Bakker, and A.M. van der Wiel, Late Cenozoic uplift and paleogeography of the Colombian Andes: constraints on the development of high-andean biota, *Geologie en Mijnbouw, 69*, 279-290, 1990.

Lambeck, K., *Geophysical Geodesy: The Slow Deformations of The Earth*, 718 pp.,

Oxford University Press, Oxford, 1988.

Lensen, G.J., Earth-deformation studies in New Zealand, *Tectonophys., 29,* 541-551, 1975.

Lucchitta, I., Late Cenozoic uplift of the Southwestern Colorado Plateau and adjacent lower Colorado River region, *Tectonophys., 61,* 63-95, 1979.

Lyon-Caen, H., and P. Molnar, Gravity anomalies, flexure of the Indian plate, and the structure, support and evolution fo the Himalaya and Ganga Basin, *Tectonics, 4,* 513-538, 1985.

Mälzer, H., G. Hein, and K. Zippelt, Height changes in the Rhenisch Massif: Determination and analysis, in *Plateau Uplift: The Rhenisch Shield - A Case History,* edited by K. Fuchs, K. von Gehlen, H. Mälzer, H. Murawski and A. Semmel, p. 164-176, Springer Verlag, Berlin, 1983.

Mattskova, V.A., A revised velocity map of recent vertical crustal movements in the western half of the European USSR, and some remarks on the period of these movements, in *Recent Crustal Movements,* edited by I.P. Gerasimov et al., p. 76-89, S. Monson, Jerusalem, 1967.

Mehta, P.K., Tectonic significance of the young mineral dates and the rates of cooling and uplift in the Himalaya, *Tectonophys., 62,* 205-217, 1980.

Nakiboglu, S.M., and K. Lambeck, Deglaciation effects on the rotation of the Earth, *Geophys. J. R. astron. Soc., 62,* 49-58, 1980 (corrigendum in Vol. 64, p. 559, 1981).

O'Connell, R.J., C.W. Gable, and B.H. Hager, Toroidal-poloidal partitioning of lithospheric plate motions, in *Glacial Isostasy, Sea-Level and Mantle Rheology, NATO ASI Series C, Vol. 334,* edited by R. Sabadini, K. Lambeck and E. Boschi, p. 535-551, Kluwer Academic Publishers, Dordrecht, The Netherlands, 1991.

Officer, C.B., and C.L. Drake, Epeirogeny on a short geologic time scale, *Tectonics, 4,* 603-612, 1985.

Ricard, Y., C. Doglioni, and R. Sabadini, Differential rotation between lithosphere and mantle: a consequence of lateral mantle viscosity variations, *J. Geophys. Res., 96,* 8407-8415, 1991.

Sabadini, R., and W.R. Peltier, Pleistocene deglaciation and the Earth's rotation: implications for mantle viscosity, *Geophys. J. R. astron. Soc., 66,* 553-578, 1981.

Sabadini, R., C. Doglioni, and D.A. Yuen, Eustatic sea level fluctuations induced by polar wander, *Nature, 345,* 708-710, 1990.

Sabadini, R., G. Spada, and Y. Ricard, Perturbations in the Earth's rotation induced by internal density anomalies: implications for sea-level fluctuations, in *Glacial Isostasy, Sea-Level and Mantle Rheology, NATO ASI Series C, Vol.*

334, edited by R. Sabadini, K. Lambeck and E. Boschi, p. 589-605, Kluwer Academic Publishers, Dordrecht, The Netherlands, 1991.

Smith, D.E., C. Ma, J.W. Robbins, P.J. Dunn, and M.H. Torrence, Combining VLBI and SLR for improved determination of vertical motion, *Annales Geophysicae, 11(1)*, C8, 1993.

Spakman, W., M.J.R. Wortel, and N.J. Vlaar, The Hellenic subduction zone: a tomographic image and its geodynamic implications, *Geophys. Res. Lett., 15*, 60-63, 1988.

Thompson, G.A., and M.L. Zoback, Regional geophysics of the Colorado Plateau, *Tectonophys., 61*, 149-181, 1979.

Trupin, A.S., Effect of polar ice on the Earth's rotation and gravitational potential, *Geophys. J. Int., 113*, 273-283, 1993.

Trupin, A.S., M.F. Meier, and J.M. Wahr, Effect of melting glaciers on the Earth's rotation and gravitational field: 1965-1984, *Geophys. J. Int., 108*, 1-15, 1992.

Unruh, J.R., The uplift of the Sierra Nevada and implications for late Cenozoic epeirogeny in the western Cordillera, *Geological Society of America Bulletin, 103*, 1395-1404, 1991.

Vanicek, P., and D. Nagy, On the compilation of the map of contemporary vertical crustal movements in Canada, *Tectonophys., 71*, 75-86, 1981.

Vlaar, N.J., Thermal anomalies and magmatism due to lithospheric doubling and shifting, *Earth Planet. Sci. Lett., 65*, 322 - 330, 1983.

Wellman, H.W., An uplift map for the South Island of New Zealand and a model for uplift of the Southern Alps, *Bull. R. Soc. N.Z., 18*, 13-20, 1979.

Zeitler, P.K., Cooling history of the NW Himalaya, Pakistan, *Tectonophys., 4*, 127-151, 1985.

CHAPTER 4

PRESENT-DAY CHANGES IN THE EARTH'S ROTATION BY TECTONIC MOVEMENTS, PART 2 †

Abstract

Whereas the present-day true polar wander and the secular non-tidal acceleration of the Earth have usually been attributed to post-glacial rebound, it was suggested in chapter 3 that non-glacially induced vertical tectonic movements taking place under non-isostatic conditions can also be effective in changing the Earth's rotation. In this chapter we present a case study in which we analyze the effects of some simple uplift histories of the Himalayas and the Tibetan Plateau on the rotational axis and on the second degree zonal harmonic of the geoid for timescales of up to a few million years. As the lithospheric forcings are assumed to remain operative, at least partly prohibiting mantle relaxation by intraplate stresses, a normal mode analysis in which mantle relaxation to the imposed loads is modeled can only supply us with a lower bound on the effects. The upper bound is given by assuming that essentially no relaxation is taking place at all. Both cases are presented for the effects of the uplift on the second degree zonal harmonic of the geoid. In our models, the mantle is divided into three layers - the transition zone sandwiched between the shallow upper mantle and the lower mantle - having linear Maxwell rheologies. Contrary to the readjustment of the mantle to the load, the readjustment of the equatorial bulge in our studies on polar wander is assumed to take place by pure mantle relaxation. We deal with the problem of incomplete mantle relaxation to the load in the models on the induced polar wander by analyzing two classes: one in which mantle relaxation is assumed to take place as response to both load and equatorial bulge readjustment, and the other in which it is assumed that one tenth

---

† This chapter is submitted for publication in modified form as: L.L.A. Vermeersen, R. Sabadini, G. Spada and N.J. Vlaar, Mountain building and Earth rotation, *Geophys. J. Int.*, 1993.

of the uplift of the studied region is not relaxed permanently.
Our modeling results show that full mantle relaxation to the imposed forcings would only result in significant contributions to changes in the second degree zonal geoid term for times shortly after a Heaviside type of uplift. For incomplete mantle relaxation maintained by an intraplate compressive stress field the contribution is significant for all times after the forcing commenced.
The polar wander is sensitive to the rate of relaxation of the modes M1 and M2 due to the discontinuities between the three mantle layers. The rate of readjustment is strongly sensitive on the viscosity of the transition zone whenever the lower mantle / shallow upper mantle viscosity ratio is small.

Introduction

During the last decade, contemporary secular changes in the rotation of the Earth have usually been attributed to post-glacial rebound and the present-day changes in the redistribution of ice and water over the surface of the planet. Attributing the astrometrically observed drift of the polar axis towards Canada and the satellite observed non-tidal secular decrease in rotation rate solely to (post-)glacial processes has been called into question recently by two studies.
Lefftz and Legros (1992a,b) have proposed that processes acting at or near the core - mantle boundary can induce a significant secular drift of the polar axis and a non-negligible secular change in the rate of rotation.
On the other hand, in chapter 3 it has been proposed that non-glacially induced tectonic movements are also capable of inducing a significant contribution to the observed changes. It was shown by a simple two-layer model that vertical lithospheric movements acting under non-isostatic conditions can be very effective in inducing both polar wander and non-tidal accelerations. In this model the effective density changes accompanying vertical movements are restricted to the upper part of the lithosphere, where air or water is replaced by crustal material or vice versa, and the lower part of the lithosphere, where lithospheric material is replaced by mantle material or vice versa. As examples of operative tectonic mechanisms responsible for observed large vertical movements acting under deviations from isostasy, they proposed mountain building and erosion in fold and thrust belts, lithospheric snap-backing resulting from detachment of subducting slabs and subsidence of oceanic

basins. The main reason why these mechanisms can be so effective is that compressive lithospheric stresses in combination with lithospheric and crustal rheologies prohibit the restoration of isostasy on timescales of post-glacial rebound. Rather than relaxing passively, as in models on post-glacial rebound, the mantle is envisioned to be subdue to the still acting lithospheric forces which maintain the deviations from isostasy on timescales exceeding those of post-glacial rebound. To illustrate the potency of the model, it was calculated in chapter 3 what the effects of the uplift of the Himalayas and Tibetan Plateau would be if the whole region is being uplifted by 5 millimeters per year. Values of 20 percent of the magnitude of the present-day true polar wander (the region is almost ideally situated for inducing changes in position of the rotation axis) and 4 percent of the magnitude of the non-tidal changes in the second degree zonal geoid term J_2 were found (but one must be aware of the fact that the region is not ideally situated for inducing changes in this value; should the region be located around the equator the influence would increase to about 15 percent).

The purpose of the present paper is to extend this pilot study in several respects by a normal mode analysis. In the models of chapter 3 it was assumed that the uplift, subsidence or erosion is totally uncompensated. Although the mechanisms proposed can be very effective in establishing such a situation, there will always be an unknown amount of relaxation (although less than in the existing models on post-glacial rebound), which diminishes the purported effects on the rotational and geoidal signatures.

As the lithospheric movements in the proposed models are rather forcing the mantle flow than the mantle relaxing passively with a high viscosity lithospheric layer on top of it and as there are internal changes in the lithospheric layer, a normal mode analysis of load relaxation is not the proper technique to study the full extent of this problem, however. A normal mode analysis for the load relaxation cannot deal with a lithosphere which is changing its internal properties laterally. A small change in geotherm or stress regime can alter the local (linear or non-linear) rheologies of crust and lithosphere drastically, but cannot be taken into account in the normal mode analysis. Also changes in depth of the Moho, which could even increase by a factor of 2, give problems. The most one can do is specifying the internal lithospheric loads and calculate how the mantle will relax to it, but this relaxation uses again the assumption that the lithosphere is laterally uniform with one specific value for the viscosity. Even apart from any regional stress field, the normal mode analysis should deal with the lithosphere being an active driving agent which changes as time proceeds and a passively relaxing medium at the same time. For the load relaxation this leads to an internal contradiction: the lithosphere is changing internally, while in the load relaxation it is assumed that the lithosphere is

not changing internally. Using a normal mode technique, one has to assume that the internal lithospheric changes are important for the load, but can be neglected for the relaxation.

Given this assumption, it is still useful to do a normal mode modeling for load relaxation in order to establish lower limits of the effects. The upper limits are given by assuming that essentially no relaxation to the imposed load takes place, which are the values obtained in chapter 3 for both the induced polar shift and the changes in J_2. In order to investigate the effects of mantle relaxation it is necessary to consider the temporal evolution of the vertical movements of the modeled region, that is the Himalayas and Tibetan Plateau. We have chosen for three uplift histories: a Heaviside type of uplift, linear uplift and exponential uplift.

The study made in chapter 3 also lacked an assessment of the induced shift of the equatorial bulge. The mass displacements induce a torque on the equatorial flattening which shifts the bulge by visco-elastic mantle flow. This induced process has only an effect on polar wander, not on changes in J_2. Contrary to being a poor modeling technique concerning load relaxation for our models, a normal mode analysis is a good technique in establishing the readjustment of the equatorial bulge in the calculations on polar wander. Here the technique is applied to global mantle readjustment instead of local or regional flows. Shifts of the equatorial bulge are not hampered by any local or regional lithospheric stress field, while the induced membrane stresses of up to a few tens of bars resulting from the shifting bulge are an order of magnitude smaller than the several hundreds of bars of the intraplate stress fields (Sabadini et al., 1982).

In our normal mode analysis the Earth is divided into five layers: an effectively elastic lithosphere, a visco-elastic shallow upper mantle, transition zone and lower mantle, and an inviscid core. The internal mantle boundaries are positioned at 420 and 670 kilometers depth. As rheological model we use a linear visco-elastic Maxwell model.

Sabadini and Peltier (1981) have reported that the difference between employing the non-linear Liouville equations and the linearized version of it remains beneath 10 percent for polar wander magnitudes of up to 15 degrees. As our calculated amounts of polar wander do not exceed this we use the linearized version of the Liouville equations. The timescales of up to a few million years we consider would also remain inside the 10^6 to 10^7 years of strongly time-dependent multiple phase upper mantle convection models – for which Moser et al. (1992) have recently questioned the use of visco-elastic normal mode models for longer timescales at all –, even apart from the question whether such convection models would adequately represent the true nature of the Earth's mantle.

Although there are a number of uncertainties concerning the vertical movements

and erosion rates and the relation between active lithospheric loadings and load relaxation, the timescales of up to a few million years on which the forcings we consider seem to be working open up new possibilities to study the visco-elastic properties of the transition zone. The M1 and M2 modes associated with the 420 and 670 km boundaries are the prevailing relaxation modes on these timescales.

Normal Mode Model

In the following the mathematical model is described for the response of the visco-elastic linear Maxwell Earth model to a delta function type of force. After having derived the Green functions, the response of the Earth to arbitrary loads in space and time is found by convolving these functions with the loads.
Neglecting inertial forces and assuming that the Earth is incompressible and hydrostatically pre-stressed, the linearized equation of motion can be written as

$$\nabla \cdot \sigma - \nabla(\rho g \vec{u} \cdot \hat{e}_r) - \rho \nabla \phi = 0 \tag{4.1}$$

with $\vec{u}$ the displacement vector, g the gravitational acceleration and σ the stress tensor.
The perturbed gravitational potential ϕ satisfies Poisson's equation for an incompressible medium

$$\nabla^2 \phi = 0 \tag{4.2}$$

For the Maxwell model, the Laplace transformed constitutive relation between the stress σ and the strain ε has the form of a Hookean elastic solid: for the incompressible case the rheological equation is (cf. Ranalli, p. 86)

$$\frac{d\varepsilon_{ij}}{dt} = \frac{1}{2\mu}\frac{d\sigma_{ij}}{dt} + \frac{\sigma_{ij}}{2\nu}$$

with ν being the kinematic viscosity, μ the shear modulus, and the strain ε being related to the displacement $\vec{u}$ by

$$\varepsilon_{ij} = \frac{1}{2}(\partial_j u_i + \partial_i u_j)$$

As an elastic case is mathematically easier to deal with than a visco-elastic case, this equation is transformed to the Laplace domain:

$$s\tilde{\varepsilon}_{ij}(s) = \frac{s\tilde{\sigma}_{ij}(s)}{2\mu} + \frac{\tilde{\sigma}_{ij}(s)}{2\nu}$$

or

$$\tilde{\sigma}_{ij}(s) = 2\tilde{\mu}(s)\tilde{\varepsilon}_{ij}(s) \tag{4.3}$$

with the Laplace transformed shear modulus

$$\tilde{\mu}(s) = \frac{\mu s}{s + \mu/\nu} \tag{4.4}$$

The so-called "Correspondence Principle" (e.g. Fung, 1965, sec. 15.3) states that by calculating the associated elastic solutions in the Laplace transformed domain the time dependent viscoelastic solutions can be found by Laplace inversion.
In a normal mode expansion, using spherical coordinates with rotational symmetry around the axis piercing through the delta function forcing, the quantities $\vec{u}$ and ϕ can be written as

$$\vec{\tilde{u}}(r,\theta,s) = \sum_{l=0}^{\infty}\left(\tilde{U}_l(r,s)P_l(\cos\theta)\hat{e}_r + \tilde{V}_l(r,s)\frac{\partial P_l(\cos\theta)}{\partial\theta}\hat{e}_\theta\right) \tag{4.5}$$

$$\tilde{\phi}(r,\theta,s) = \sum_{l=0}^{\infty}\tilde{\phi}_l(r,s)P_l(\cos\theta) \tag{4.6}$$

with θ the angular distance from the point source, and P_l the Legendre polynomial of zonal degree l, which can be derived from Rodrigues formula (e.g. Butkov, 1968, p. 347)

$$P_l(x) = \frac{1}{2^l l!}\frac{d^l}{dx^l}(x^2-1)^l \tag{4.7}$$

Substitution of (4.5) and (4.6) in the Laplace transformed equation of motion (4.1) and Poisson's equation (4.2), using the differential equation for the Legendre polynomials

$$\frac{d}{dx}\left((1-x^2)\frac{dP_l(x)}{dx}\right) = -l(l+1)P_l(x)$$

results in a set of three second order differential equations:

$$\tilde{\mu}(s)\left\{2\frac{d^2\tilde{U}_l}{dr^2} + \frac{4}{r}\frac{d\tilde{U}_l}{dr} - \frac{4\tilde{U}_l}{r^2} + \frac{l(l+1)}{r^2}\left(3\tilde{V}_l - \tilde{U}_l - r\frac{d\tilde{V}_l}{dr}\right)\right\} - \rho\frac{d}{dr}(g(r)\tilde{U}_l) - \rho\frac{d\tilde{\phi}_l}{dr} = 0$$

$$\tilde{\mu}(s)\left\{\frac{d}{dr}\left(\frac{d\tilde{V}_l}{dr} - \frac{\tilde{V}_l}{r} + \frac{\tilde{U}_l}{r}\right) + \frac{1}{r^2}\left(5\tilde{U}_l + 3r\frac{d\tilde{V}_l}{dr} - \tilde{V}_l - 2l(l+1)\tilde{V}_l\right)\right\} - \frac{\rho g(r)}{r}\tilde{U}_l - \frac{\rho\tilde{\phi}_l}{r} = 0$$

$$\frac{d^2\tilde{\phi}_l}{dr^2} + \frac{2}{r}\frac{d\tilde{\phi}_l}{dr} - \frac{l(l+1)}{r^2}\tilde{\phi}_l = 0$$

The gravity g in this set is related to the density ρ by the equation

$$\nabla \cdot \vec{g}(r) = -4\pi G\rho$$

in which G is the gravitational constant, or

$$\frac{dg}{dr} + \frac{2g}{r} = -4\pi G\rho$$

while the condition of incompressibility

$$\nabla \cdot \tilde{u}(r, \theta, s) = 0 \tag{4.8}$$

leads to

$$\frac{dU_l}{dr} + \frac{2}{r}U_l - \frac{l(l+1)}{r}V_l = 0$$

The set of three second order differential equations can be further reduced to a set of six first order differential equations.
Defining the normal stress as

$$\tilde{\sigma}_{rrl}(r, \theta, s) \equiv \tilde{\tau}_{rrl}(r, s)\, P_l(\cos\theta) \tag{4.9}$$

with (from (4.5) in (4.3))

$$\tilde{\tau}_{rrl} = 2\tilde{\mu}(s)\frac{d\tilde{U}_l}{dr} \tag{4.10}$$

and the lateral shear stress as

$$\tilde{\sigma}_{r\theta l}(r, \theta, s) \equiv \tilde{\tau}_{r\theta l}(r, s)\frac{\partial P_l(\cos\theta)}{\partial\theta} \tag{4.11}$$

with

$$\tilde{\tau}_{r\theta l} = \tilde{\mu}(s)\left(\frac{d\tilde{V}_l}{dr} - \frac{1}{r}\tilde{V}_l + \frac{1}{r}\tilde{U}_l\right) \tag{4.12}$$

this set reads

$$\frac{d\vec{\tilde{y}}_l(r, s)}{dr} = \tilde{A}_l(r, s)\vec{\tilde{y}}_l(r, s) \tag{4.13}$$

with $\vec{\tilde{y}}_l = (\tilde{U}_l, \tilde{V}_l, \tilde{\tau}_{rrl}, \tilde{\tau}_{r\theta l}, -\tilde{\phi}_l, \tilde{Q}_l)^T$, in which the quantity

$$\tilde{Q}_l = -\frac{d\tilde{\phi}_l}{dr} - \frac{l+1}{r}\tilde{\phi}_l + 4\pi G\rho\tilde{U}_l \tag{4.14}$$

is for obvious reasons sometimes nicknamed "the potential stress".
The 6×6 matrix $\tilde{\mathbf{A}}$ reads

$$\tilde{\mathbf{A}}_l(r,s) = \begin{pmatrix} 0 & 0 & \frac{1}{2\tilde{\mu}(s)} & 0 & 0 & 0 \\ -\frac{1}{r} & \frac{1}{r} & 0 & \frac{1}{\tilde{\mu}(s)} & 0 & 0 \\ \frac{4}{r}\left(\frac{\tilde{\mu}(s)}{r} - \rho g(r)\right) & -\frac{l(l+1)}{r}\left(\frac{2\tilde{\mu}(s)}{r} - \rho g(r)\right) & -\frac{2}{r} & \frac{l(l+1)}{r} & \frac{\rho(l+1)}{r} & -\rho \\ \frac{1}{r}\left(\rho g(r) - \frac{2\tilde{\mu}(s)}{r}\right) & \frac{2(l(l+1)-1)\tilde{\mu}(s)}{r^2} & 0 & -\frac{3}{r} & -\frac{\rho}{r} & 0 \\ -4\pi G\rho & 0 & 0 & 0 & -\frac{l+1}{r} & 1 \\ -\frac{4\pi G\rho(l+1)}{r} & \frac{4\pi G\rho l(l+1)}{r} & 0 & 0 & 0 & \frac{l-1}{r} \end{pmatrix}$$

For each of the N layers of the Earth model (each layer having material parameters which are constant inside it) the solution of this set can be written as

$$\vec{\tilde{y}}_l(r,s) = \tilde{\mathbf{Y}}_l(r,s)\vec{\tilde{C}}_l(s) \tag{4.15}$$

in which $\tilde{\mathbf{Y}}_l$ is the fundamental matrix and $\vec{\tilde{C}}_l$ the value of $\vec{\tilde{y}}_l$ at the various internal boundaries.
The fundamental matrix $\tilde{\mathbf{Y}}$ takes the form (cf. Spada et al., 1992)

$$\tilde{\mathbf{Y}}_l(r,s) = \begin{pmatrix} \frac{lr^{l+1}}{2(2l+3)} & r^{l-1} & 0 & \frac{(l+1)r^{-l-1}}{2(2l-1)} & r^{-l-2} & 0 \\ \frac{(l+3)r^{l+1}}{2(2l+3)(l+1)} & \frac{r^{l-1}}{l} & 0 & \frac{(2-l)r^{-l-1}}{2l(2l-1)} & -\frac{r^{-l-2}}{l+1} & 0 \\ \frac{l\rho g(r)r^{l+1}}{2(2l+3)} + \frac{(l^2-l-3)\tilde{\mu}(s)r^l}{2l+3} & \frac{\rho g(r)}{r^{-l+1}} + \frac{2(l-1)\tilde{\mu}(s)}{r^{-l+2}} & -\rho r^l & \frac{(l+1)\rho g(r)}{2(2l-1)r^l} + \frac{(-l^2-3l+1)\tilde{\mu}(s)}{(2l-1)r^{l+1}} & \frac{\rho g(r)}{r^{l+2}} - \frac{2(l+2)\tilde{\mu}(s)}{r^{l+3}} & -\frac{\rho}{r^{l+1}} \\ \frac{l(l+2)\tilde{\mu}(s)r^l}{(2l+3)(l+1)} & \frac{2(l-1)\tilde{\mu}(s)r^{l-2}}{l} & 0 & \frac{(l^2-1)\tilde{\mu}(s)}{l(2l-1)r^{l+1}} & \frac{2(l+2)\tilde{\mu}(s)}{(l+3)r^{l+3}} & 0 \\ 0 & 0 & -r^l & 0 & 0 & -\frac{1}{r^{l+1}} \\ \frac{2\pi G\rho l r^{l+1}}{2l+3} & 4\pi G\rho r^{l-1} & -\frac{2l+1}{r^{-l+1}} & \frac{2\pi G\rho(l+1)}{(2l-1)r^l} & \frac{4\pi G\rho}{r^{l+2}} & 0 \end{pmatrix}$$

The inverse of the fundamental matrix $\tilde{\mathbf{Y}}$ has the form

$$\tilde{\mathbf{Y}}_l^{-1}(r, s) = \tilde{\mathbf{D}}_l(r)\, \tilde{\bar{\mathbf{Y}}}_l(r, s)$$

with $\tilde{\mathbf{D}}$ being a diagonal matrix with

$$\mathrm{diag}(\tilde{\mathbf{D}}_l(r)) = \left(\frac{(l+1)r^{-l-1}}{2l+1}, \frac{l(l+1)r^{-l+1}}{2(2l+1)(2l-1)}, \frac{-r^{-l+1}}{2l+1}, \frac{lr^l}{2l+1}, \frac{l(l+1)r^{l+2}}{2(2l+1)(3l+2)}, \frac{-r^{l+1}}{2l+1} \right)$$

and

$$\tilde{\bar{\mathbf{Y}}}_l(r, s) = \begin{pmatrix} \frac{\rho g(r) r}{\mu(s)} - 2(l+2) & 2l(l+2) & -\frac{r}{\mu(s)} & \frac{lr}{\mu(s)} & \frac{\rho r}{\mu(s)} & 0 \\ -\frac{\rho g(r) r}{\mu(s)} + \frac{2(l^2+3l+1)}{l+1} & 2(l^2-1) & \frac{r}{\mu(s)} & \frac{(2-l)r}{\mu(s)} & -\frac{\rho r}{\mu(s)} & 0 \\ 4\pi G\rho & 0 & 0 & 0 & 0 & 1 \\ \frac{\rho g(r) r}{\mu(s)} + 2(l-1) & 2(l^2-1) & -\frac{r}{\mu(s)} & -\frac{(l+1)r}{\mu(s)} & \frac{\rho r}{\mu(s)} & 0 \\ -\frac{\rho g(r) r}{\mu(s)} - \frac{2(l^2-l-3)}{l} & -2l(l+2) & \frac{r}{\mu(s)} & \frac{(l+3)r}{\mu(s)} & -\frac{\rho r}{\mu(s)} & 0 \\ 4\pi G\rho r & 0 & 0 & 0 & 2l+1 & -r \end{pmatrix}$$

At the interface $r = r_i$, the top layer i, in which

$$\vec{\tilde{y}}_l^{(i)}(r_i, s) = \tilde{\mathbf{Y}}_l^{(i)}(r_i, s)\vec{\tilde{C}}_l^{(i)}(s) \tag{4.16}$$

can be linked to the layer i + 1 below it, with

$$\vec{\tilde{y}}_l^{(i+1)}(r_i, s) = \tilde{\mathbf{Y}}_l^{(i+1)}(r_i, s)\vec{\tilde{C}}_l^{(i+1)}(s) \tag{4.17}$$

by

$$\vec{\tilde{y}}_l^{(i)} = \vec{\tilde{y}}_l^{(i+1)} \tag{4.18}$$

Doing this for every internal boundary of a N layer model (layer 1 is the lithosphere, layers $2, 3, \ldots, N-1$ the mantle layers, and layer N the core), the solution

vector at the surface of the Earth at r = R can be related to the conditions $\vec{\tilde{C}}_l^{(N)}(s)$ at the core - mantle boundary r = r_c as

$$\vec{\tilde{y}}_l(R) = \prod_{i=1}^{N-1} \tilde{Y}_l^{(i)}(r_i, s)\, \tilde{Y}_l^{(i)^{-1}}(r_{i+1}, s)\, \tilde{Y}_l^{(N)}(r_c, s)\, \vec{\tilde{C}}_l^{(N)}(r_c, s) \tag{4.19}$$

The conditions at the solid-fluid core - mantle boundary can be found in Sabadini et al., 1982, while the s-independent solution vector $\vec{\tilde{y}}_l(R)$ is equal to the forcing, depending on whether one is considering surface mass loading or tidal loading: for a delta function mass load at the surface of the Earth this condition is

$$\vec{\tilde{y}}_l(R) = (0, 0, -\frac{1}{4\pi} g(R)(2l+1)/R^2, 0, 0, -G(2l+1)/R^2)^T \tag{4.20}$$

while for the tidal loading this condition reads (cf. Sabadini et al., 1982).

$$\vec{\tilde{y}}_l(R) = (0, 0, 0, 0, 0, -(2l+1)/R)^T \tag{4.21}$$

We refer to Spada et al. (1990, 1992a) how the roots $s = s_j$ $(j = 1, 2, \ldots, M)$ of (4.19) with (4.20) or (4.21) can be found by means of the algebraic software package *Mathematica*. The solution vector $\vec{\tilde{y}}_l(r, s)$ can thus be written as the sum of an elastic term and M viscous terms:

$$\vec{\tilde{y}}_l(r, s) = \vec{K}_l^e(r) + \sum_{j=1}^{M} \frac{\vec{K}_l^j(r)}{s - s_j} \tag{4.22}$$

in which the $\vec{K}_l(r)$ are the vector residues of the solution kernel vector $\vec{\tilde{y}}_l(r, s)$. This gives the radially dependent part of the Green functions for the six variables for each degree l. Multiplying the Green functions with the Laplace transformed forcing functions (which is the same as a convolution in the space - time domain) and performing an inverse Laplace transformation gives the sought-for expressions.
The perturbed potential (4.6) can be written as the sum of two terms: the direct contribution from the unit mass load at the surface (e.g. Lambeck, 1988, p. 99)

$$-\frac{G}{R} \sum_{l=0}^{\infty} P_l(\cos\theta)$$

and the induced contribution from the resulting deformation

$$-\frac{G}{R} \sum_{l=0}^{\infty} k_l P_l(\cos\theta)$$

in which k_l is the so-called Love number of degree l (e.g. Munk and MacDonald, 1960, p. 23).

So with (4.6) and

$$\frac{G}{R} = \frac{g(R)R}{M}$$

this results in

$$\tilde{\phi}_l = -(1 + k_l)\frac{g(R)R}{M}$$

or in terms of the Love number k_l

$$k_l = -1 - \frac{M}{g(R)R}\tilde{\phi}_l$$

Only the $l = 2$ terms are important in determining the changes in rotation. Using a Love number description, the expression for the perturbed potential (the fifth component of (4.22)) reads

$$k_2(s) = k_e + \sum_{i=1}^{M} \frac{k_i}{s - s_i} \tag{4.23}$$

in which k_e is the value of $k_2(s)$ in the limit $s \to -\infty$ (the elastic Love number). The Love numbers are dependent on which forcing one is considering, in contrast to the M relaxation times s_i, which are only dependent on the constitutive parameters of the Earth model. The Love numbers k_2 will apply to the case of tidal forcing, while the Love numbers k_2^L will apply to the load forcings.

For the five-layer model we are considering there are $M = 9$ effective roots (cf. Peltier, 1985): four transient modes T1, T2, T3 and T4 which have relaxation times near the Maxwell relaxation time; three modes M0, C0 and L0 which derive from the surface of the Earth, the core - mantle boundary and the mantle - lithosphere boundary respectively; and two modes M1 and M2 which are due to recovery of the two internal mantle boundaries at 420 and 670 kilometer depth to the applied forcings.

Uplift Histories

What has caused and is still causing the uplift of the Himalayas and the Tibetan Plateau, how large the uplift and erosion rates are and how great the deviations

from isostasy, were and remain hotly debated questions in the earth sciences. That the mountain building and plateau formation results from the collision between India and Asia some 40 to 50 million years ago is generally accepted, but as with respect to the nature of the mechanisms responsible for the uplift the opinions are diverse. Harrison et al. (1992) review a number of these models, ranging from thrust of the Indian lithosphere beneath the entire area to crustal shortening and associated thicking of the crust till it has acquired a roughly double-normal thickness. Apart from these mechanisms, the uplift of the Himalayas during the last few million years has recently been suggested to be due to isostatic rebound in response to enhanced erosion rates (Molnar and England, 1990, and Burbank, 1992a). The emergence of the Pleistocene ice ages with its accompanying worsening in climate conditions are held responsible for this. At the moment it is still debatable, however, whether such a change in climate works only in a unilateral direction, e.g. whether ice promotes denudation because of glacier movements or diminishes erosion by forming a protecting layer.

In our modeling we will assume that the tectonic mechanisms are still active and that they cause the majority of the uplift. As has been pointed out in chapter 3, erosion can also be an effective mechanism in inducing rotational changes, however, also in the case when the erosion keeps pace with the uplift rate so that the mean altitude of the region is not changing (although the effects are then a factor of about one sixth smaller as the effective mass changes are then only due to the lower layer of the two-layer model of chapter 3). Erosion can even enhance the induced changes by promoting the deviations from isostasy in the case of an overcompensated light crustal root, which seems to be the case for the Himalayas (Basavaiah et al., 1991).

As with respect to the temporal evolution of the uplift of the Himalayas and Tibetan Plateau:

A canonical value for the time of initiation of uplift is 20 to 25 million years ago, as paleomagnetic data indicate that continental underthrust of the Indian plate under the Eurasian plate along the Main Central Thrust commenced during the early Miocene (Klootwijk et al., 1985). The present-day mean altitude of the Himalayas and Tibetan Plateau is about 5 kilometers (Burbank, 1992b). Thus, if the uplift would have been linear, the net uplift rates (uplift rates – erosion rates) from the time the uplift was initiated till present would have been 0.2 to 0.4 mm/yr. There are strong geological indications, however, that the uplift did not proceed in such a smooth linear fashion from the Miocene onwards.

Zeitler (1985) presents uplift rates for the Himalaya ranges of northern Pakistan. He derived these rates from fission track and isotope dating. The rates remain generally below 1 mm/yr, except for the Quaternary. According to Zeitler, the Nanga

Parbat - Haramosh Massif experienced an accelerated uplift rate which can be modeled by an exponential function: the uplift rate is equal to $5.0 \cdot \exp(-t/3)$, with t being the time before present in Myr, resulting in a present-day uplift rate of 5 mm/yr. From the fact that the uplift rates in northern Pakistan at least doubled during the late Tertiary, Zeitler concludes that this increase is not merely an isostatic response to unroofing, but must be ascribed largely to a further unspecified tectonic mechanism.

Copeland and Harrison (1990) state that the uplift of the Himalayas and the Tibetan Plateau did not proceed uniformly as in linear uplift models, or has taken place mostly from Pliocene time onwards such as in the exponential uplift model of Zeitler. They deduce this from sedimentary samples drilled up during the Ocean Drilling Program Leg 116 in the Bay of Bengal. The sedimentation pattern is reported to be rather non-uniform, reflecting non-uniform erosion of the Himalayas which on its turn is assumed to be related directly to non-uniform uplift. This is further substantiated by a study of Amano and Taira (1992), who propose a two-phase uplift of the Higher Himalayas during early Miocene till Quaternary time. From sedimentary strata of the Bengal Fan drilled up during the same leg, they deduce that the Himalayas have undergone a surge of uplift between 10.9 and 7.5 million years ago and from 0.9 million years ago onwards. They claim that the enhanced deposition of the sediments during these time intervals is not the result from channel migration or drainage basin change within a part of the Bengal Fan, but reflects a true rise in uplift rate with concomitant increased rates of erosion.

Although a lot is uncertain concerning vertical motions and erosion rates during geological and recent times, we model the uplift of the Himalayas and Tibetan Plateau as if this region started to rise 5 million years ago. We have chosen to model three kinds of uplift histories with the condition that the total amount of uplift of the area after 5 million years have elapsed is equal to 5 kilometers (figure 4.1). Apart from a time history in which the uplift is proceeding in a smooth linear fashion and an exponential uplift history such as advocated by Zeitler, we study a Heaviside type of uplift to approximate the pulselike uplift behavior as advocated by Copeland and Harrison and by Amano and Taira. We believe that these three cases in combination can adequately represent any geological uplift history that one wants to model.

In the following the uplift of the Himalayas and Tibetan Plateau will be modeled for the case of an excess load, though it is more likely that the region is underlain by an excess low-density root. As shown in chapter 3, the transformation of the first case to the second is straightforward: the values of $\dot{J}_2$ change sign, while the polar wander has the same magnitude in the opposite direction.

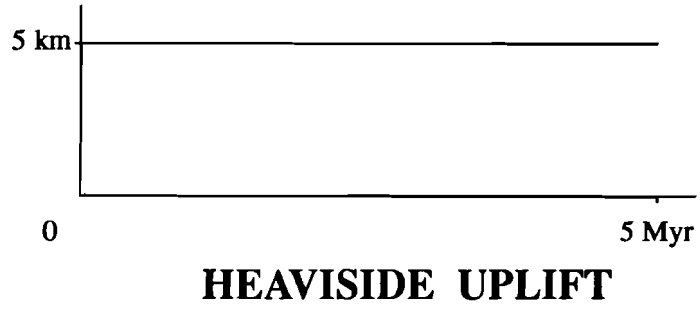

HEAVISIDE UPLIFT

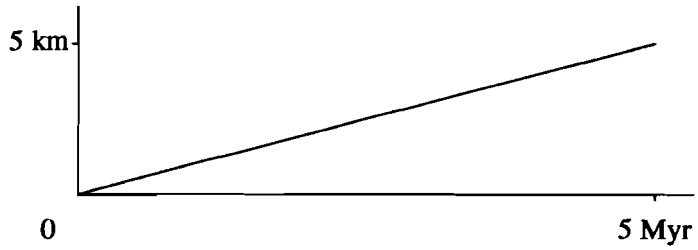

LINEAR UPLIFT

EXPONENTIAL UPLIFT

Figure 4.1. Uplift models used in the simulations.

Changes in J_2

In modeling the induced changes in the zonal degree 2 coefficient of the geoid, we approximate the load of the uplifting quadrilateral area shown in figure 4.2 by a delta function forcing positioned at the center of the region.

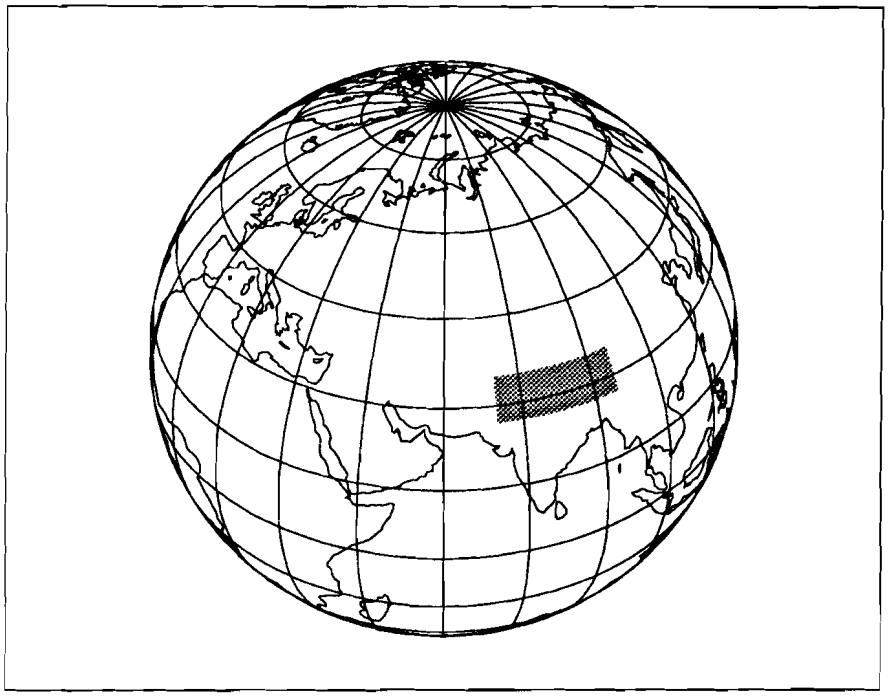

Figure 4.2. Cartoon of the modeled Himalaya / Tibetan Plateau area. The area extends from 70 degrees to 95 degrees eastern longitude and from 27 degrees to 35 degrees northern latitude.

The area extends from 70 to 95 degrees east longitude and from 27 to 35 degrees northern latitude. The whole region is assumed to be uplifted uniformly. As the region is rather small in extent, the errors that this approximation for determining the effects on the second degree zonal component introduces, are small.

The degree l spectral coefficient of the perturbed geoid due to a (spatial and temporal) delta function forcing on its surface is given in the Laplace domain by

$$\frac{1}{M_e}(1 + k_2^L(s))P_l(\cos\gamma)$$

with γ being the angular distance from the place on the globe where the delta function load is. Substituting (4.23), the total Green function becomes in the temporal domain

$$G(\gamma, t) = \sum_{l=0}^{\infty} G_l(t)P_l(\cos\gamma)$$

with

$$G_l(t) \equiv \frac{1}{M_e}\left((1 + k_e^L)\delta(t) + \sum_{j=1}^{M} k_j^L e^{s_j t} \right) \tag{4.24}$$

Surface density of finite spherical and delta surface loads

The surface density σ of a circular region with radius α can be written as (Longman, 1962)

$$\sigma = M_0 \qquad \text{for} \quad 0 < \theta < \alpha$$
$$\sigma = 0 \qquad \text{for} \quad \alpha < \theta < \pi$$

in which θ is the angular distance from the center of the region.
Expansion in Legendre series gives

$$\sigma = \sum_{n=0}^{\infty} \Gamma_n P_n(\cos\theta)$$

so

$$\Gamma_n = \frac{2n+1}{2} \int_{\cos\pi}^{\cos 0} \sigma P_n(\cos\theta) d\cos\theta =$$

$$= \frac{2n+1}{2} M_0 \int_{\cos\alpha}^{1} P_n(\cos\theta) d\cos\theta$$

Using the recurrence relation for Legendre polynomials

$$(2n+1)P_n(x) + \frac{dP_{n-1}(x)}{dx} - \frac{dP_{n+1}(x)}{dx} = 0 \quad \text{for} \quad n \geq 1$$

one obtains

$$\Gamma_n = \frac{1}{2} M_0 \left(P_{n-1}(\cos\alpha) - P_{n+1}(\cos\alpha) \right) \quad \text{for} \quad n \geq 1$$

and with $P_n(1) = 1$

$$\Gamma_0 = \frac{1}{2} M_0 (1 - \cos\alpha)$$

So

$$\sigma = \frac{1}{2} M_0 (1 - \cos\alpha) + \frac{1}{2} M_0 \sum_{n=1}^{\infty} \left(P_{n-1}(\cos\alpha) - P_{n+1}(\cos\alpha) \right) \cdot P_n(\cos\theta)$$

The total mass M_t of a circular disk with a surface density M_0 and a radius α is

$$M_t = 2\pi M_0 \int_0^{\alpha} R^2 \sin\theta d\theta = 2\pi R^2 (1 - \cos\alpha) M_0$$

in which R is the radius of the Earth.
So

$$M_0 = \frac{M_t}{2\pi R^2 (1 - \cos\alpha)}$$

With this and the recurrence relations (Butkov, 1968, p. 346)

$$P_{n-1}(x) = xP_n(x) + \frac{1 - x^2}{n} \frac{dP_n(x)}{dx} \quad \text{for} \quad n \geq 1$$

and

$$P_{n+1}(x) = xP_n(x) - \frac{1 - x^2}{n+1} \frac{dP_n(x)}{dx} \quad \text{for} \quad n \geq 0$$

the surface density of a spherical surface load becomes

$$\sigma = \frac{M_t}{4\pi R^2} \left(1 + \sum_{n=1}^{\infty} \frac{2n+1}{n(n+1)} (1 + \cos\alpha) \frac{\partial P_n(\cos\alpha)}{\partial \cos\alpha} P_n(\cos\theta) \right)$$

The surface density for a delta surface load can be obtained by taking the limit $\alpha \rightarrow 0$ and using the recurrence relation, resulting in

$$\sigma = \frac{M_t}{4\pi R^2} \sum_{n=0}^{\infty} (2n+1) P_n(\cos\theta)$$

(Note: see page 847 of Longman, 1962, for the problem of convergence of the series for every value of θ.)

The change in the geoid $\delta J(\theta, \phi, t)$ from a surface point load located at (θ_0, ϕ_0) follows from the convolution of this surface density and (4.24):

$$\delta J(\theta, \phi, t) = \frac{1}{M_e} \int dt' \int d\Omega' \, \sigma(\theta' - \theta_0, \phi' - \phi_0) \, f(t') \, G(\theta - \theta', \phi - \phi', t - t')$$

in which f(t) is the dimensionless uplift history of the region.
Briefly stated, this formula gives the geoid perturbation at (θ, ϕ) from the deformation at (θ', ϕ') resulting from the forcing at (θ_0, ϕ_0). Denoting ψ the angular distance between (θ', ϕ') and the source at (θ_0, ϕ_0), and Φ between (θ', ϕ') and (θ, ϕ), δJ can be written as

$$\delta J(\theta, \phi, t) = \frac{M_t}{M_e} \int dt' \int \frac{d\Omega'}{4\pi R^2} \sum_{n=0}^{\infty} (2n+1) P_n(\cos\psi) \, f(t') \sum_{l=0}^{\infty} G_l(t - t') \, P_l(\cos\Phi)$$

Application of the addition theorem (e.g. Arfken, 1970, p. 582) gives

$$P_n(\cos\psi) = \sum_{m=-n}^{n} \frac{(n-m)!}{(n+m)!} P_{nm}(\cos\theta') P_{nm}(\cos\theta_0) \cos m(\phi' - \phi_0)$$

and

$$P_l(\cos\Phi) = \sum_{l=-n}^{n} \frac{(l-m)!}{(l+m)!} P_{lm}(\cos\theta) P_{lm}(\cos\theta') \cos m(\phi - \phi')$$

in which P_{nm} are the associated Legendre functions.
Together with the orthogonality condition (Arfken, 1970, p. 562)

$$\int_0^{\pi} d\theta' \sin\theta' \, P_{nm}(\cos\theta') P_{lm}(\cos\theta') = \frac{2}{2l+1} \frac{(l+m)!}{(l-m)!} \delta_{ln}$$

this leads to

$$\delta J(\theta, \phi, t) = \frac{M_t}{M_e} \sum_{l=0}^{\infty} \int dt' f(t') G_l(t - t') \sum_{m=-l}^{l} \frac{4\pi}{2l+1} Y^*_{lm}(\theta_0, \phi_0) Y_{lm}(\theta, \phi)$$

in which the spherical harmonics Y_{lm} are defined here as (Arfken, 1970, p. 571)

$$Y_{lm}(\theta,\phi) \equiv \sqrt{\frac{2l+1}{4\pi}\frac{(l-m)!}{(l+m)!}}\, P_{lm}(\cos\theta)\, e^{im\phi}$$

The zonal harmonics $J_l(t)$ can be extracted from δJ by putting $m = 0$, resulting in

$$\delta J(\theta,t) = \frac{M_t}{M_e}\sum_{l=0}^{\infty}\int dt' f(t') G_l(t-t')\, P_l(\cos\theta_0)\, P_l(\cos\theta) =$$
$$= \sum_{l=0}^{\infty}\delta J_l(t)\, P_l(\cos\theta)$$

So the temporal change in the second degree zonal harmonic δJ_2 is equal to

$$\delta J_2(t) = \frac{M_t}{M_e}\int dt' f(t') J_2(t-t') P_2(\cos\theta_0) \qquad (4.25)$$

The second degree zonal harmonic follows from (4.7) as $P_2(\cos\theta_0) = \frac{3}{2}\cos^2\theta_0 - \frac{1}{2}$.

Heaviside uplift:

The uplift is assumed to be instantaneous and completed at time $t = -t_0$, i.e. the region is uplifted by 5 kilometers at 5 million years ago. This is a rather unrealistic situation, but it serves to study the effects of the relaxing modes. Besides this, Heaviside types of uplift with smaller amplitudes are geologically not unrealistic. So:

$$f(t') = H(t' + t_0) \qquad \text{for} \quad -t_0 \le t' \le t \qquad (4.26)$$

in which H is the Heaviside function.
The induced changes in the degree 2 zonal harmonic of the gravitational potential field by such a Heaviside function are given by ((4.24) and (4.26) in (4.25))

$$\delta J_2 = \frac{M_t}{M_e}\int_{-t_0}^{t} dt'\, H(t'+t_0)\left((1+k_e^L)\,\delta(t-t') + \sum_{j=1}^{M} k_j^L e^{s_j(t-t')}\right) P_2(\cos\theta_0)$$

which results with $\dot{J}_2 \equiv \frac{d\delta J_2}{dt}$ in

$$\dot{J}_2 = \frac{M_t}{M_e}\left((1+k_e^L)\,\delta(t+t_0) + \sum_{j=1}^{M} k_j^L\, e^{s_j(t+t_0)}\right) P_2(\cos\theta_0) \quad \text{for } t \ge -t_0 \qquad (4.27)$$

Figure 4.3 shows the results for a number of viscosity contrasts.

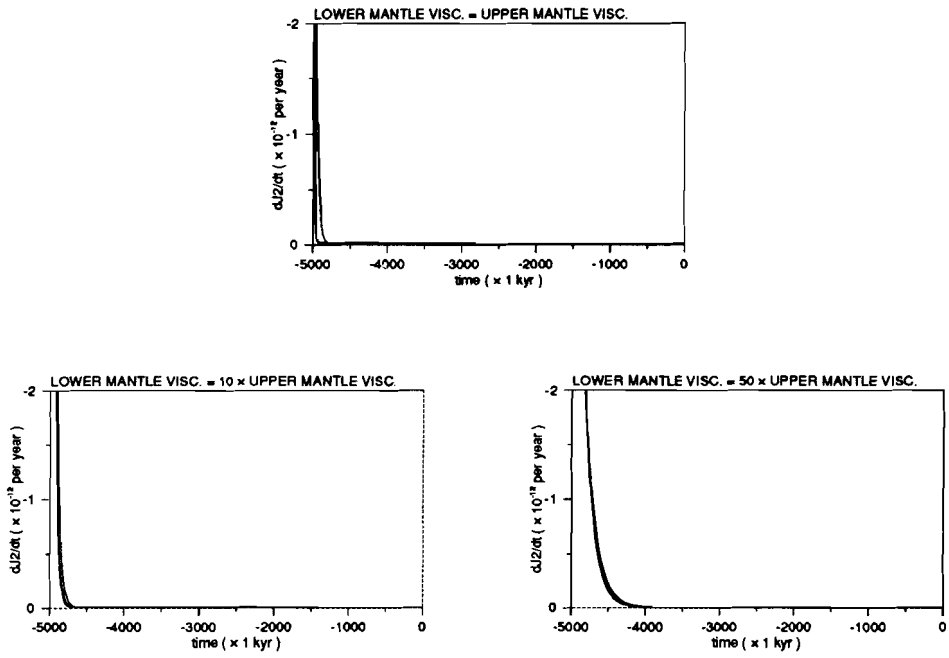

Figure 4.3. Changes in J_2 by full mantle relaxation; Heaviside case. The uplift of 5 kilometers takes place instantaneously 5 million years ago. The shallow upper mantle viscosity is held fixed at 10^{21} Pa · s, while the three panels show the cases for a viscosity of the lower mantle which is equal to, 10 times larger and 50 times larger than this value. Each panel contains four curves, representing the cases for a viscosity of the transition zone which is equal to, 5 times larger, 30 times larger and 100 times larger than the viscosity of the shallow upper mantle. In all cases the lowermost curve in each panel is for the equal viscosity case. The curves show less fast declining tendencies for exceedingly higher viscosity contrasts between the transition zone and the shallow upper mantle.

The standard rheological parameters for each layer and the depths of the boundaries can be found in table 4.1. Each of the three panels shows the changes in J_2 from the time of uplift (5 Myrs ago) to present for four values of the viscosity contrast between the transition zone and the shallow upper mantle, while the viscosity

contrast between the lower and shallow upper mantle is kept constant. The shallow upper mantle viscosity is held fixed at 10^{21} Pa · s in all the simulations.
What is not clear from these figures is that at the time of the instantaneous uplift the value of $\dot{J}_2$ is about 2.5×10^{-6} per year. After the moment at which the Heaviside uplift took place, the values of $\dot{J}_2$ immediately turn negative, declining exponentially afterwards. This temporal behavior is what one would have expected: the instantaneous uplift causes the Earth to become more elliptic, while after the instantaneous moment of uplift only the relaxation modes are operative which tend to make the Earth less flattened again in an exponentially decaying manner.
All three panels show that the absolute effects of the Heaviside uplift on changes in J_2 are only important shortly after the uplift took place. The relevant modes decay rapidly irrespective of the values for the viscosity contrasts, making a study after the roles played by the M1 and M2 modes which decay on timescales of millions of years not very useful.
It is interesting to note, however, that a Heaviside uplift of 5 millimeters taking place at present would induce a change in J_2 of 2.5×10^{-12} per year – being about one tenth of the satellite observed non-tidal value. After this initial moment, the value would turn immediately negative, starting to decay by the short timescale relaxation modes that also dominate post-glacial rebound. That is, if the lithosphere would not prohibit any relaxation of the mantle.

Linear uplift:

The modeled region starts rising with a constant rate at $t = -t_0$. At present, $t = 0$, the function f has the normalized value of $f(0) = 1$.
So:

$$f(t') = \frac{t'}{t_0} + 1 \qquad \text{for} \quad -t_0 \le t' \le t \tag{4.28}$$

The changes in the degree 2 zonal harmonic are given by ((4.28) and (4.26) in (4.25))

$$\delta J_2 = \frac{M_t}{M_e} \int_{-t_0}^{t} dt' \left(\frac{t'}{t_0} + 1 \right) \left((1 + k_e^L)\, \delta(t - t') + \sum_{j=1}^{M} k_j^L e^{s_j (t - t')} \right) P_2(\cos\theta_0)$$

resulting in

layer	outer radius (km)	density (kg/m^3)	rigidity ($\times 10^{10}$ N/m^2)
lithosphere	6371	4120	7.28
shallow upper mantle	6250	4120	9.54
transition zone	5951	4220	11.00
lower mantle	5701	4508	19.90
core	3480	10925	0.00

Table 4.1. Standard values of the physical parameters of the five-layer model.

$$\dot{J}_2 = \frac{M_t}{M_e}\left(\frac{1 + k_e^L}{t_0} - \sum_{j=1}^{M} \frac{k_j^L}{s_j t_0}\left[1 - e^{s_j(t + t_0)} \right] \right) P_2(\cos\theta_0) \qquad \text{for } t \geq -t_0 \qquad (4.29)$$

with $M_t = \dot{M}\, t_0$, whereby $\dot{M}$ is the mass that is uplifted per year. As M_t is equivalent to a mass of the area being uplifted by 5 kilometers and $t_0 = 5$ Myr, this implies that $\dot{M}$ is equivalent to a mass of the area being uplifted by 1 millimeter per year.

The simulations for a linear uplift model are shown in figure 4.4. Now the values for $\dot{J}_2$ remain negative for the whole 5 million years. The linear uplift causes the Earth to become more elliptical. After a relatively short time the relaxation of the mantle keeps track with the constant uplift, causing the ellipticity to increase with a constant rate. As well as in the case of the Heaviside uplift, the absolute values of the induced $\dot{J}_2$ remain two orders of magnitude too low for all modeled cases to have a significant influence on the present day rate of change of J_2.

Exponential uplift:

The region starts to rise exponentially at $t = -t_0$ with a characteristic rise time a.

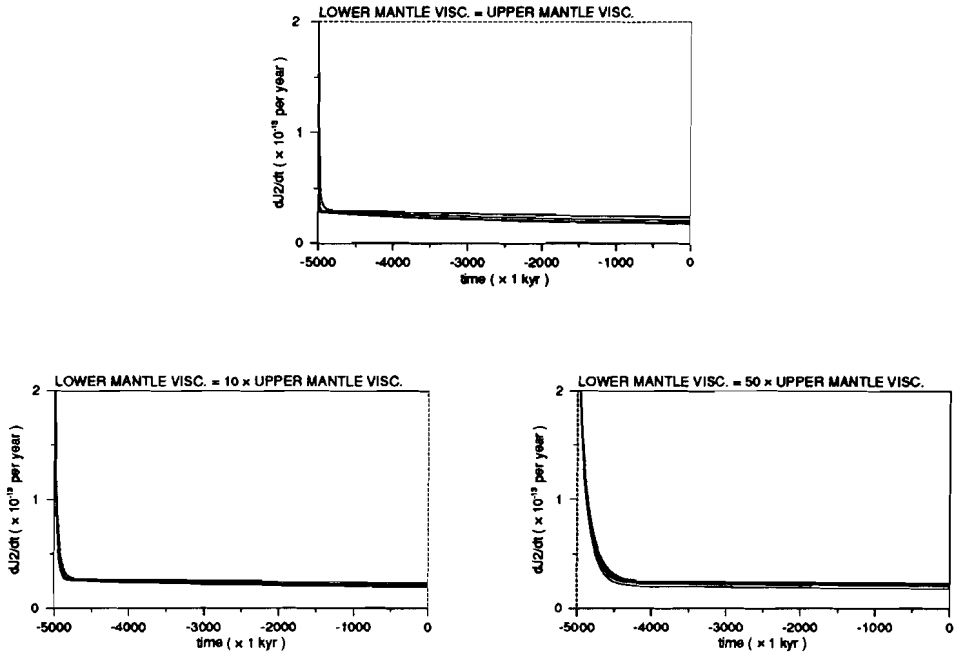

Figure 4.4. Changes in J_2 by full mantle relaxation; Linear case. The uplift starts to increase in a linear fashion 5 million years ago in such a way that at present an uplift of 5 kilometers is accomplished. The same remarks concerning the viscosity contrasts, the panels and the tendencies of the curves apply as for figure 4.3.

Together with the condition f(0) = 1, the function f takes the form

$$f(t') = \frac{e^{(t'+t_0)/a} - 1}{e^{t_0/a} - 1} \qquad \text{for} \quad -t_0 \le t' \le t \tag{4.30}$$

The changes in the degree 2 zonal harmonic are for this exponential rise given by ((4.30) and (4.26) in (4.25))

$$\delta J_2 = \frac{M_t}{M_e} \int_{-t_0}^{t} dt' \, \frac{e^{(t'+t_0)/a} - 1}{e^{t_0/a} - 1} \left((1 + k_e^L)\, \delta(t - t') + \sum_{j=1}^{M} k_j^L e^{s_j(t-t')} \right) P_2(\cos\theta_0)$$

resulting in

$$\dot{J}_2 = \frac{M_t}{M_e}\left(\frac{1+k_e^L}{a}\,\frac{e^{(t+t_0)/a}}{e^{t_0/a}-1} + \sum_{j=1}^{M} \frac{k_j^L}{e^{t_0/a}-1}\left[\frac{e^{(t+t_0)/a} - a s_j\, e^{s_j(t+t_0)}}{1-a s_j} - e^{s_j(t+t_0)} \right] \right) P_2(\cos\theta_0)$$

$$\text{for } t \geq -t_0 \quad (4.31)$$

with $M_t = \dot{M}(t=0) \cdot a \cdot (1 - e^{-t_0/a})$, with $\dot{M}(t=0)$ being the mass that is presently uplifted per year. For the constant a we have chosen the constant that is proposed by Zeitler: a = 3 million years. As M_t is again equivalent to a mass of the area being uplifted by 5 kilometers and $t_0 = 5$ Myr, $\dot{M}(t=0)$ is equal to a mass of the area being uplifted of $\frac{5/3}{1-e^{-5/3}} \approx 2$ millimeters per year at present.
Figure 4.5 shows the results of the simulations for this case. Also in this case, the absolute values of $\dot{J}_2$ are insignificant, although the tendencies the plots show are interesting in itself. After the uplift is initiated, the relaxation of the short time scale modes dominates the temporal behavior till at a certain point the exponential increase overcomes the relaxing modes. The turn-around point is especially sensitive to the viscosity contrast between the lower and shallow upper mantle, but also the viscosity contrast between the transition zone and the shallow upper mantle has a clear influence.

To summarize: if the mantle is purely relaxing passively, then on the timescales considered here (that is, exceeding those of post-glacial rebound), the values of $\dot{J}_2$ are orders of magnitude too low to be significant. However, as has been pointed out in chapter 3, the lithosphere will at least partly inhibit this mantle relaxation, so that the values for $\dot{J}_2$ of the figures 4.3, 4.4 and 4.5 must be interpreted as lower limits. The upper limits are given by assuming that there is no mantle rebound at all.
Another way to look at these results is the following: in the modeling we did not specify where the material which causes the uplift of the Himalayas and the Tibetan Plateau comes from. The places where the compensating material originates, are more likely to be wide-spread over the globe (with the majority most likely being beneath the oceans). These places are more likely to be subsiding under conditions where the mantle can relax passively, not prohibited by the lithospheric forcings in combination with intraplate stresses that are envisioned to be active in the Indian - South Asian collision zone. For these compensating regions, the normal mode modeling is more applicable than in the region experiencing uplift. So, the induced changes in J_2 by the Himalayan and Tibetan Plateau uplift will probably be closer to the upper values derived in chapter 3 than to the lower values derived here, while on the other hand the induced changes in J_2 by the mass-compensating regions will likely be very close to the values of the simulations depicted in the figures 4.3, 4.4 and 4.5. Of course, the upper values of chapter 3 can only be sus-

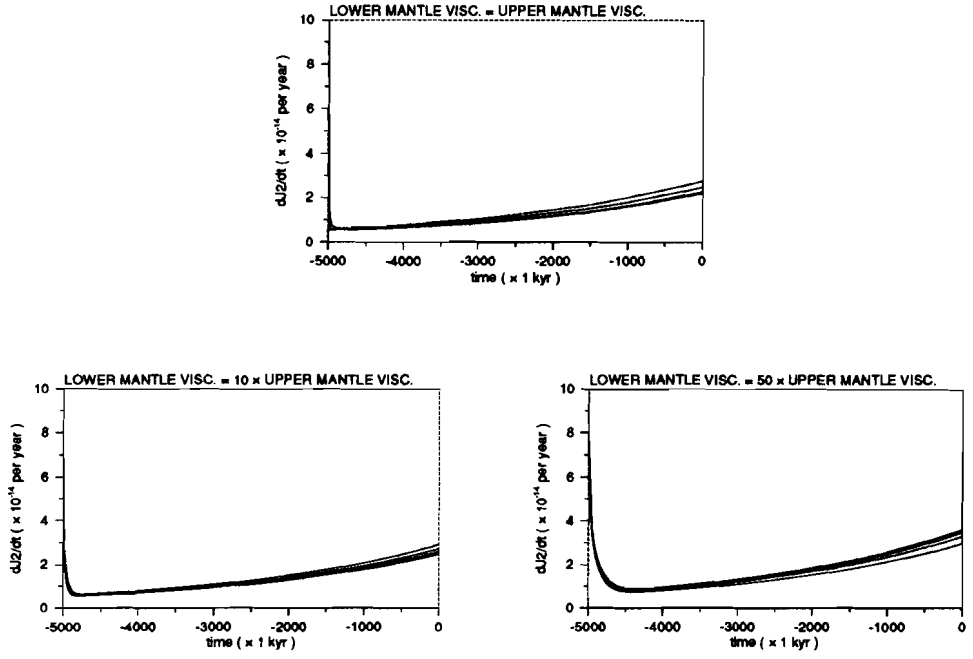

Figure 4.5. Changes in J_2 by full mantle relaxation; Exponential case. The uplift starts to increase exponentially 5 million years ago with a characteristic rise time of 3 million years till after 5 million years an uplift of 5 kilometers is established. Same viscosity contrast cases as in figures 4.3 and 4.4. In each panel the uppermost curve represents the case of highest viscosity contrast between the transition zone and the shallow upper mantle again; the lowermost curve a viscosity contrast of 1.

tained for limited periods in a Heaviside type of fashion, otherwise the Himalayas and Tibetan Plateau would not have a low-density root at all. Such a same kind of reasoning can be set up for the erosion models.

Polar Wander

In order to determine the effects of the adjustment of the equatorial bulge to the forcings, consider the following cartoon (cf. Lambeck, 1980, p. 39):

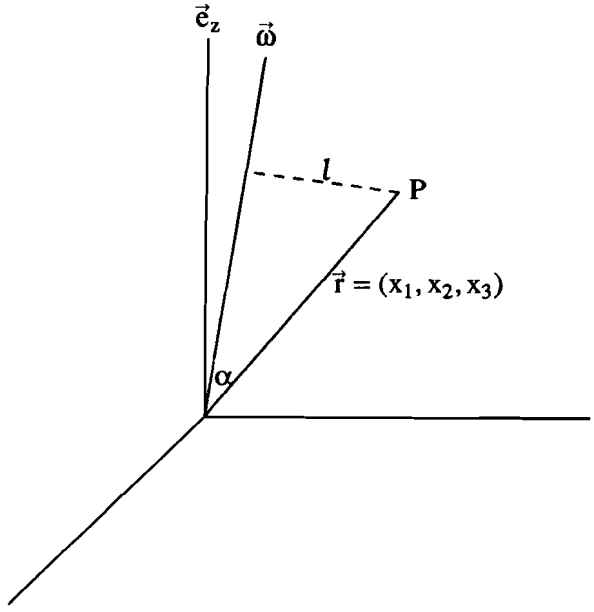

If α is the angle between the instantaneous rotation axis $\vec{\omega}$ and the line $\vec{r}$ from the center of mass of the Earth and a perturbation at point P, then

$$\vec{\omega} \cdot \vec{r} = |\vec{\omega}|\,|\vec{r}| \cos\alpha$$

with $\vec{\omega} \cdot \vec{r} = \sum_{i=1}^{3} \omega_i x_i$.

The distance l from P perpendicular to the axis of rotation follows now from

$$l^2 = r^2 - r^2 \cos^2\alpha = r^2 - \frac{(x_1 + x_2 + x_3)^2}{\omega^2}$$

with $r = |\vec{r}|$ and $\omega = |\vec{\omega}|$.

So the centrifugal potential U_c is given by

$$U_c = \frac{1}{2}\omega^2 l^2 = \frac{1}{2}\left(\omega^2 r^2 - (\omega_1 x_1 + \omega_2 x_2 + \omega_3 x_3)^2\right) =$$
$$= \frac{1}{2}\left(\omega^2 r^2 - \omega_1^2 x_1^2 - \omega_2^2 x_2^2 - \omega_3^2 x_3^2 - 2\omega_1\omega_2 x_1 x_2 - 2\omega_1\omega_3 x_1 x_3 - 2\omega_2\omega_3 x_2 x_3\right) =$$
$$= \frac{1}{2}\omega^2 r^2 - \frac{1}{2}\left(\frac{1}{3}\omega_1^2 r^2 - \frac{1}{3}\omega_1^2(x_2^2 + x_3^2 - 2x_1^2) + \frac{1}{3}\omega_2^2 r^2 - \frac{1}{3}\omega_2^2(x_1^2 + x_3^2 - 2x_2^2)\right.$$
$$\left. + \frac{1}{3}\omega_3^2 r^2 - \frac{1}{3}\omega_3^2(x_1^2 + x_2^2 - 2x_3^2)\right) =$$
$$= \frac{1}{3}\omega^2 r^2 + \frac{1}{6}\omega_1^2(x_2^2 + x_3^2 - 2x_1^2) + \frac{1}{6}\omega_2^2(x_1^2 + x_3^2 - 2x_2^2)$$
$$+ \frac{1}{6}\omega_3^2(x_1^2 + x_2^2 - 2x_3^2) - \omega_1\omega_2 x_1 x_2 - \omega_1\omega_3 x_1 x_3 - \omega_2\omega_3 x_2 x_3 =$$
$$= \frac{1}{3}\omega^2 r^2 + \Delta U_c$$

with $\frac{1}{3}\omega^2 r^2$ the purely radial part of U_c, and ΔU_c the part which describes the equatorial flattening. This latter part can be written in spherical coordinates as

$$\Delta U_c = \frac{1}{6}\omega_1^2 r^2(\sin^2\theta\sin^2\phi + \cos^2\theta - 2\sin^2\theta\cos^2\phi)$$
$$+ \frac{1}{6}\omega_2^2 r^2(\sin^2\theta\cos^2\phi + \cos^2\theta - 2\sin^2\theta\sin^2\phi)$$
$$+ \frac{1}{6}\omega_3^2 r^2(\sin^2\theta - 2\cos^2\theta)$$
$$- \omega_1\omega_2 r^2\sin^2\theta\sin\phi\cos\phi - \omega_1\omega_3 r^2\sin\theta\cos\theta\cos\phi$$
$$- \omega_2\omega_3 r^2\sin\theta\cos\theta\sin\phi$$

and this can be rewritten as

$$\Delta U_c = \frac{1}{6}r^2(\omega_1^2 + \omega_2^2 - 2\omega_3^2)P_{20}(\cos\theta)$$
$$- \frac{1}{3}r^2(\omega_1\omega_3\cos\phi + \omega_2\omega_3\sin\phi)P_{21}(\cos\theta)$$
$$+ \frac{1}{12}r^2((\omega_2^2 - \omega_1^2)\cos 2\phi - 2\omega_1\omega_2\sin 2\phi)P_{22}(\cos\theta)$$

with the second degree associated Legendre polynomials P_{2m} according to (3.25) given by

$$P_{20}(\cos\theta) = \frac{3}{2}\cos^2\theta - \frac{1}{2}$$
$$P_{21}(\cos\theta) = 3\sin\theta\cos\theta$$
$$P_{22}(\cos\theta) = 3\sin^2\theta$$

The potential that deforms the equatorial bulge is now simply given by

$$\Delta U_c' = k_2 \Delta U_c \qquad \text{for } r = R$$

The general expression for the degree 2 spherical harmonic gravitational potential field is for $r \geq R$ given by (3.24) as

$$\Delta U_2 = \frac{GM}{r}\left(\frac{R}{r}\right)^2 \sum_{m=0}^{2} (C_{2m} \cos m\phi + S_{2m} \sin m\phi)\, P_{2m}(\cos\theta)$$

which becomes for $r = R$ equal to

$$\Delta U_2 = \frac{GM}{r} \sum_{m=0}^{2} (C_{2m} \cos m\phi + S_{2m} \sin m\phi)\, P_{2m}(\cos\theta)$$

The coefficients C_{2m} and S_{2m} are given by (3.26) as

$$C_{2m} = \frac{2 - \delta_{0m}}{MR^2} \frac{(2-m)!}{(2+m)!} \int_E \rho r^2 P_{2m}(\cos\theta) \cos m\phi \, dV$$

$$S_{2m} = \frac{2 - \delta_{0m}}{MR^2} \frac{(2-m)!}{(2+m)!} \int_E \rho r^2 P_{2m}(\cos\theta) \sin m\phi \, dV$$

so

$$C_{20} = \frac{k_2 R^3}{6GM} (\omega_1^2 + \omega_2^2 - 2\omega_3^2)$$

$$C_{21} = -\frac{k_2 R^3}{3GM} \omega_1 \omega_3 \qquad S_{21} = -\frac{k_2 R^3}{3GM} \omega_2 \omega_3$$

$$C_{22} = \frac{k_2 R^3}{12GM} (\omega_2^2 - \omega_1^2) \qquad S_{22} = -\frac{k_2 R^3}{6GM} \omega_1 \omega_2$$

These coefficients can be expressed in the moments and products of inertia with the result

$$C_{20} = \frac{1}{2MR^2} (\Delta I_{xx} + \Delta I_{yy} - 2\Delta I_{zz})$$

$$C_{21} = -\frac{\Delta I_{xz}}{MR^2} \qquad S_{21} = -\frac{\Delta I_{yz}}{MR^2}$$

$$C_{22} = \frac{\Delta I_{xx} - \Delta I_{yy}}{4MR^2} \qquad S_{22} = -\frac{\Delta I_{xy}}{2MR^2}$$

So the changes in the products of inertia ΔI_{xz} and ΔI_{yz} can be expressed in a linear approximation, using (2.8), as

$$\Delta I_{xz} = -MR^2C_{21} = \frac{k_2R^5}{3G}\omega_1\Omega_3 \approx \frac{k_2R^5\omega^2}{3G}m_1(1+m_3)$$

$$\Delta I_{yz} = -MR^2S_{21} = \frac{k_2R^5}{3G}\omega_2\Omega_3 \approx \frac{k_2R^5\omega^2}{3G}m_2(1+m_3)$$

and, as $m_3 \ll 1$, the complex forcing function Φ_R for rotational deformation becomes

$$\Phi_R = \frac{\Delta I_{xz}}{C-A} + i\frac{\Delta I_{yz}}{C-A} \approx \frac{k_2}{k_0}\mathbf{m}$$

with $\mathbf{m} = m_1 + i\,m_2$, and

$$k_0 \equiv \frac{3G(C-A)}{R^5\Omega^2}$$

the so-called secular Love number.

The linearized Liouville equation for polar wander which includes both loading and tidal forcings thus becomes (cf. (2.18))

$$i\frac{\dot{\mathbf{m}}}{\sigma_r} + \mathbf{m} = \Phi \tag{4.32}$$

with the forcing function Φ consisting of two parts: $\Phi = \Phi_L + \Phi_R$, with Φ_L the part describing the direct geodynamic forcing and Φ_R the induced rotational deformation. Again, m_1 and m_2 are the direction cosines of the rotation axis in the x- and y-direction respectively. The x-direction is chosen to be in the equatorial plane from the center of the Earth towards the Greenwich meridian, the y-direction towards 90 degrees East longitude. The z-direction is along the initial mean position of the rotation axis. It is assumed that the origin of the geographic coordinate system (x, y, z) coincides with the center of mass of the Earth. σ_r is the Chandler wobble frequency for a rigid Earth, given (2.14).

The deformation of the equatorial bulge can be expressed in Love numbers as $\Phi_R = \frac{k_2}{k_0}\mathbf{m}$, so (4.32) becomes

$$i\frac{\dot{\mathbf{m}}}{\sigma_r} + (1 - \frac{k_2}{k_0})\mathbf{m} = \Phi_L \tag{4.33}$$

Laplace transformation and substituting (4.23) leads to

$$\left[i\frac{s}{\sigma_r} + 1 - \frac{1}{k_f}\left(k_e + \sum_{i=1}^{M}\frac{k_i}{s-s_i}\right)\right]\tilde{\mathbf{m}}(s) = \tilde{\Phi}_L(s) \tag{4.34}$$

with $k_f = k_2(s=0)$ being the tidal fluid Love number.

With the tidal elastic Love number

$$k_e = k_f + \sum_{i=1}^{M} \frac{k_i}{s_i} \tag{4.35}$$

(cf. (4.23)), and

$$\frac{k_i}{s_i} + \frac{k_i}{s - s_i} = \frac{k_i s}{s_i(s - s_i)}$$

(4.34) becomes

$$s\left(1 + i\frac{\sigma_r}{k_f}\sum_{i=1}^{M}\frac{k_i}{s_i(s - s_i)}\right)\tilde{m}(s) = -i\sigma_r\,\tilde{\Phi}_L(s)$$

So

$$s\left(1 + \sum_{i=1}^{M}\frac{x_i}{s - s_i}\right)\tilde{m}(s) = -i\sigma_r\tilde{\Phi}_L(s) \tag{4.36}$$

with

$$x_i \equiv i\frac{\sigma_r k_i}{k_f s_i} \tag{4.37}$$

Now

$$1 + \sum_{i=1}^{M}\frac{x_i}{s - s_i} = \frac{\prod_{j=1}^{M}(s - s_j)}{\prod_{j=1}^{M}(s - s_j)} + \sum_{i=1}^{M} x_i\frac{\prod_{j\neq i}^{M}(s - s_j)}{\prod_{j=1}^{M}(s - s_j)} \tag{4.38}$$

where $\prod_{j\neq i}^{M}$ means $\prod_{j=1}^{M}$ without the term $j = i$.

The right-hand side of (4.38)

$$\frac{\prod_{j=1}^{M}(s - s_j) + \sum_{i=1}^{M} x_i \prod_{j\neq i}^{M}(s - s_j)}{\prod_{j=1}^{M}(s - s_j)}$$

can be transformed into

$$\frac{\sum_{i=0}^{M} \alpha_i s^i}{\prod_{j=1}^{M} (s - s_j)}$$

(whereby it immediately follows that $\alpha_M = 1$), and consequently (4.38) can be put as

$$1 + \prod_{i=1}^{M} \frac{\mathbf{x}_i}{s - s_i} = \frac{\sum_{j=1}^{M} (s - \mathbf{a}_j)}{\prod_{j=1}^{M} (s - s_j)} \tag{4.39}$$

with $\mathbf{a}_i$ being the M complex roots of the equation $\sum_{i=0}^{M} \alpha_i s^i = 0$.

(4.39) in (4.36) gives

$$s \frac{\prod_{j=1}^{M} (s - \mathbf{a}_j)}{\prod_{j=1}^{M} (s - s_j)} \tilde{m}(s) = -i\sigma_r \tilde{\Phi}_L(s)$$

and so

$$\tilde{m}(s) = -i\sigma_r \frac{\prod_{j=1}^{M} (s - s_j)}{s \prod_{j=1}^{M} (s - \mathbf{a}_j)} \tilde{\Phi}_L(s)$$

$$= -i\sigma_r \left(\frac{\mathbf{A}_0}{s} + \sum_{j=1}^{M} \frac{\mathbf{A}_j}{s - \mathbf{a}_j} \right) \tilde{\Phi}_L(s) \tag{4.40}$$

In this expression, the terms $\mathbf{a}_j$ are the inverse relaxation times from the tidal problem for the M modes, having the strength given by the residues $\mathbf{A}_j$. The residue $\mathbf{A}_0$ gives the strength of the secular term.

We now consider two classes: in the first the mantle is both relaxing to the load and to the tidal forcing; in the second the mantle is only relaxing to the tidal forcing, but not to the load.

The Laplace transformed forcing function $\tilde{\Phi}_L(s)$ for the situation in which there is only mantle relaxation due to the changed tidal potential (no mantle relaxation due to the load) reads for the uplift case

$$\tilde{\Phi}_L(s) = G(\Delta h, \theta, \phi)\, \tilde{f}(s) \tag{4.41}$$

with, for the load specified as an uplifting quadrilateral block (cf. (2.17) with (3.23) and (3.24))

$$G(\Delta h, \theta, \phi) = -\frac{\rho_m \Delta h R^4}{3(C-A)} (\sin^3\theta_2 - \sin^3\theta_1) \cdot \cdot \left(\sin\phi_2 - \sin\phi_1 \, , -(\cos\phi_2 - \cos\phi_1) \right) \tag{4.42}$$

in which C and A are the equatorial and polar principal moment of inertia respectively with $C - A \approx 2.63 \times 10^{35}\ kg \cdot m^2$, ρ_m is the density of the shallow upper mantle (cf. table 4.1) and Δh the height over which the region extending from co-latitude $\theta_1 = 55^\circ$ to $\theta_2 = 63^\circ$ and from eastern longitude $\phi_1 = 70^\circ$ to $\phi_2 = 95^\circ$ is uplifted.

The Laplace transformed forcing function for fully operating mantle relaxation (to load and tidal potential) as response to uplift is given from (4.41) and (4.23) by

$$\tilde{\Phi}_L(s) = G(\Delta h, \theta, \phi) \left(1 + k_e^L + \sum_{j=1}^{M} \frac{k_j^L}{s - s_j} \right) \tilde{f}(s) \tag{4.43}$$

in which k_e^L is the elastic part and k_j^L the visco-elastic part of the loading Love number, and $\tilde{f}(s)$ denotes the Laplace transformed temporal part of the forcing function. (Note: in (4.43) the density ρ_m is to be replace by ρ_L upon implementing (4.42)).

So for the case in which the mantle relaxes to the induced change in tidal potential, but not to the load, (4.41) in (4.40) gives

$$\tilde{m}(s) = -i\sigma_r G(\Delta h, \theta, \phi) \left(\frac{A_0}{s} + \sum_{i=1}^{M} \frac{A_i}{s - a_i} \right) \tilde{f}(s) \tag{4.44}$$

while for fully operating mantle relaxation (4.43) in (4.40) gives

$$\tilde{m}(s) = -i\sigma_r G(\Delta h, \theta, \phi) \left(\frac{A_0}{s} + \sum_{i=1}^{M} \frac{A_i}{s - a_i} \right) \left(1 + k_e^L + \sum_{j=1}^{M} \frac{k_j^L}{s - s_j} \right) \tilde{f}(s) \tag{4.45}$$

with

$$\left(\frac{A_0}{s}+\sum_{i=1}^{M}\frac{A_i}{s-a_i}\right)\left(1+k_e^L+\sum_{j=1}^{M}\frac{k_j^L}{s-s_j}\right)=\frac{A_0(1+k_e^L)}{s}+\sum_{i=1}^{M}\frac{A_0k_i^L}{s(s-s_i)}$$
$$+\sum_{i=1}^{M}\frac{A_i(1+k_e^L)}{s-a_i}$$
$$+\sum_{i=1}^{M}\sum_{j=1}^{M}\frac{A_i\,k_j^L}{(s-a_i)\,(s-s_j)}=$$
$$=\frac{A_0^*}{s}+\sum_{i=1}^{M}\frac{\beta_i}{s-s_i}+\sum_{i=1}^{M}\frac{\gamma_i}{s-a_i} \tag{4.46}$$

in which

$$\beta_i=A_0\frac{k_i^L}{s_i}+\sum_{j=1}^{M}\frac{A_jk_i^L}{s_i-a_j} \tag{4.47}$$

$$\gamma_i=A_i(1+k_e^L)-\sum_{j=1}^{M}\frac{A_ik_j^L}{s_j-a_i} \tag{4.48}$$

and

$$A_0^*=A_0(1+k_f^L) \tag{4.49}$$

in which

$$k_f^L=k_e^L-\sum_{i=1}^{M}\frac{k_i^L}{s_i} \tag{4.50}$$

is the loading fluid Love number.
So for the case of mantle relaxation to load and tidal potential (4.46) in (4.45) leads to

$$\tilde{m}(s)=-i\sigma_rG(\Delta h,\theta,\phi)\left(\frac{A_0^*}{s}+\sum_{i=1}^{M}\frac{\beta_i}{s-s_i}+\sum_{i=1}^{M}\frac{\gamma_i}{s-a_i}\right)\tilde{f}(s) \tag{4.51}$$

The three cases for the temporal evolution of the uplift will be considered again: uplift in a very short time interval which can be approximated by a Heaviside function, linear uplift and exponential uplift.

Heaviside uplift

If the uplift can be regarded as started and being completed instantaneously at t = 0, then the function f(t) has the form f(t) = H(t), with H(t) being the Heaviside function.

The Laplace transformed function reads

$$\tilde{f}(s) = \frac{1}{s} \tag{4.52}$$

Substituting (4.52) in (4.44) gives the expression for $\tilde{m}(s)$ for the case in which the mantle only relaxes to the tidal potential:

$$\tilde{m}(s) = -i\sigma_r G(\Delta h, \theta, \phi)\left(\frac{A_0}{s^2} - \frac{1}{s}\sum_{i=1}^{M}\frac{A_i}{a_i} + \sum_{i=1}^{M}\frac{A_i/a_i}{s-a_i} \right) \tag{4.53}$$

Inverse Laplace transformation finally gives

$$m(t) = -i\sigma_r G(\Delta h, \theta, \phi)\left(A_0 t + \sum_{i=1}^{M}\frac{A_i}{a_i}\left(e^{a_i t} - 1\right) \right) \quad \text{for } t \geq 0 \tag{4.54}$$

Figure 4.6 shows the results of the calculations with the same rheological parameters as were used in the modeling on $\dot{J}_2$. We have assumed that one tenth of the Heaviside uplift of 5 kilometers, again assumed to take place 5 million years ago, is permanent, i.e. not relaxed by mantle relaxation due to the intraplate stress field. That this is far from being a ridiculous large number can be illustrated by the work of Basavaiah et al. (1991). They calculated that the free-air gravity anomaly over the Himalayas is better explained by a root which has a 30 percent isostatic overcompensation than a root which would lead to the area being in isostatic equilibrium. This is in agreement with cited studies in their article on Bouguer gravity anomalies and seismic observations of the extreme great depth of the Moho in this region.

The three panels show the temporal development of the magnitude of the polar wander $m = \sqrt{m_1^2 + m_2^2}$ as a function of the viscosity contrast between the lower and shallow upper mantle. In each of the panels the situation is depicted as a function of the viscosity contrast between the transition zone and the shallow upper mantle. It is clear from the third panel that for high viscosity contrasts between the lower and shallow upper mantle, the polar wander is small irrespective of the viscosity contrast between the transition zone and the shallow upper mantle. This is in agreement with what Spada et al. (1992b) have found from analyzing the effects of long-term changes in subduction on the rotational axis. For small viscosity contrasts between the lower and shallow upper mantle, however, the viscosity of the transition zone has a strong influence on the induced amount of polar wander. The

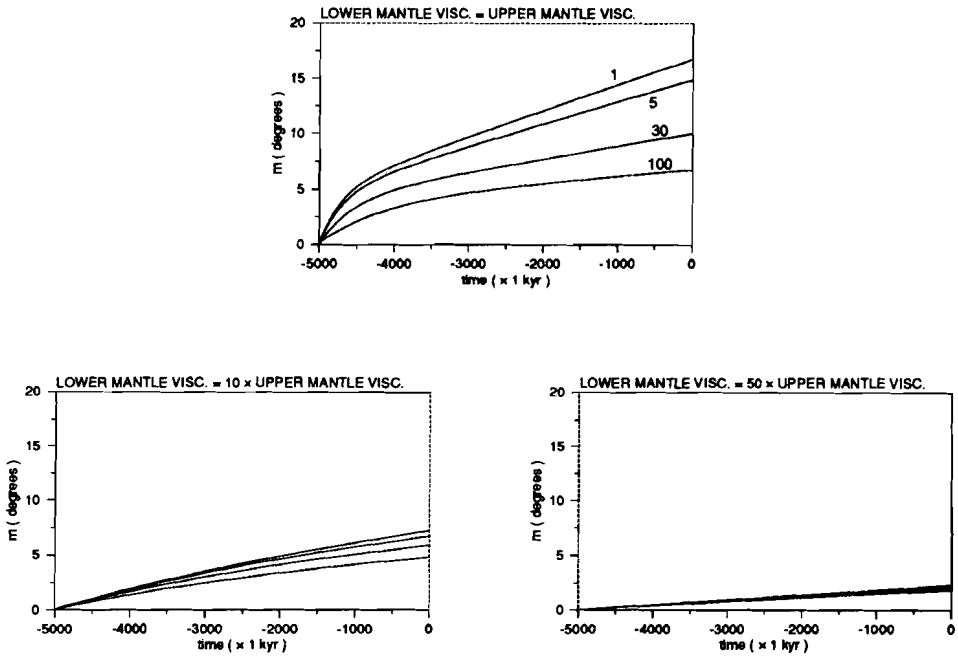

Figure 4.6. Polar wander by tidal relaxation only; Heaviside case. Only tidal relaxation is operative. The uplift of 500 meters is instantaneous 5 million years ago and is assumed to keep the mantle from relaxing to the load. The magnitude $m = \sqrt{m_1^2 + m_2^2}$ *of the induced polar wander is plotted as function of time before present. The viscosity of the shallow upper mantle is again held fixed at* 10^{21} *Pa · s for all cases. The four numbers for each curve in the first panel denote the values of the viscosity contrasts between the transition zone and the shallow upper mantle. The relative position of the four curves in the other two panels is the same.*

first panels shows that if the lower mantle would have the same viscosity as the shallow upper mantle, the induced polar wander would be about 3 times as large in the case of the mantle having a uniform viscosity than in the case of the transition zone having a 30 times as high viscosity than the rest of the mantle. This panel in particular clearly shows where the transition point between the long term relaxation

modes M1 and M2 becoming more important than the short term relaxation modes is situated. The polar wander rates are greatest during the first few hundreds of thousands of years and become constant thereafter, completely determined by the three long-term modes.

For the case of the mantle also relaxing to the load, the polar wander is given from (4.52) in (4.45) in the Laplace domain as:

$$\tilde{m}(s) = -i\sigma_r G(\Delta h, \theta, \phi)\left(\frac{A_0^*}{s^2} - \frac{1}{s}\sum_{i=1}^{M}\left(\frac{\beta_i}{s_i} + \frac{\gamma_i}{a_i}\right) + \sum_{i=1}^{M}\left(\frac{\beta_i/s_i}{s-s_i} + \frac{\gamma_i/a_i}{s-a_i}\right)\right) \qquad (4.55)$$

which has the inverse Laplace transform

$$m(t) = -i\sigma_r G(\Delta h, \theta, \phi)\left(A_0^* t + \sum_{i=1}^{M}\frac{\beta_i}{s_i}\left(e^{s_i t} - 1\right) + \frac{\gamma_i}{a_i}\left(e^{a_i t} - 1\right)\right)$$

$$\text{for } t \geq 0 \qquad (4.56)$$

Figure 4.7 shows the temporal development of this fully operating mantle relaxation case. Here, the uplift is assumed to amount the full 5 kilometers again. Apart from the absolute magnitudes, the form of the four cases in each of the three panels do not differ very much from the former cases in which no mantle relaxation to the load was assumed to take place. In the third panel the excitation of the Chandler wobble is clearly visible, but the main difference is that the polar wander is relatively much smaller after the first few hundreds of thousands of years have elapsed than in the cases of figure 4.6. This is simply due to the fact that the centrifugal forces in the cases of a permanent deviation from isostasy are a few orders of magnitude greater than those in the cases where isostasy has been attained, even when the initial uplift was 10 times as large as in the no-mantle-relaxation-to-the-load cases.

These conclusions justify a scrutinization of the role played by the different relaxation modes in the readjustment of the tidal bulge. It is clear that, if the lower to shallow upper mantle viscosity ratios are not too large (about 10 or less), the amount of polar wander becomes very sensitive to the properties of the transition zone.
The contributions of the long-timescale relaxation modes M1 and M2 on the induced amount of polar wander is sketched in figure 4.8.
In all four cases the M1 mode, which is related to the relaxation of the 670 km discontinuity, has more strength than the M2 mode. Only for times exceeding 5 million years the M2 mode has more strength (modeling results show that this will be

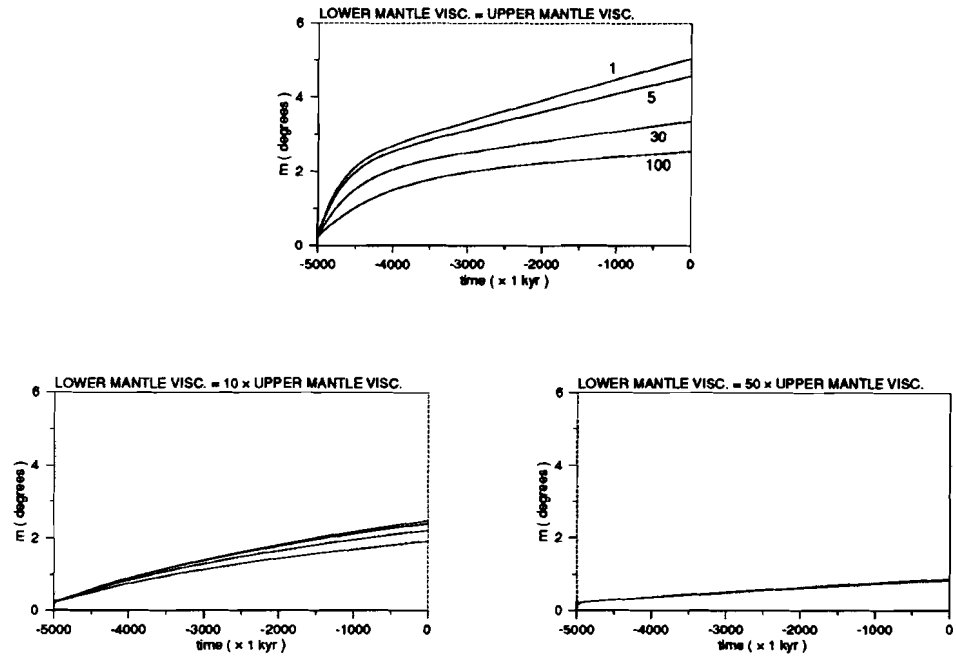

Figure 4.7. Polar wander by full mantle relaxation; Heaviside case. Both load and tidal relaxation are operative. The uplift of 5 kilometers takes place instantaneously 5 million years ago. The same remarks concerning the viscosity contrasts apply as in figure 4.6.

the case for 5.8 Myrs after the triggering of the Heaviside function for the uniform mantle case of the first panel). The reason for this is due to the long timescales on which the M2 relaxes. It strikes from all four panels that the M2 mode shows no sign of diminishing in strength: its temporal behavior is almost linear. Figure 4.9 shows that the relaxation time of the M2 mode is one to two orders of magnitude larger than the M1 mode for all modeled values of the viscosity contrasts. This explains why the trend of the contribution of the M2 mode in figure 4.8 seems linear: 5 million years are short compared to the M2 relaxation times which exceed 100 million years.

That the amount of polar wander is not very sensitive to changes in density contrast

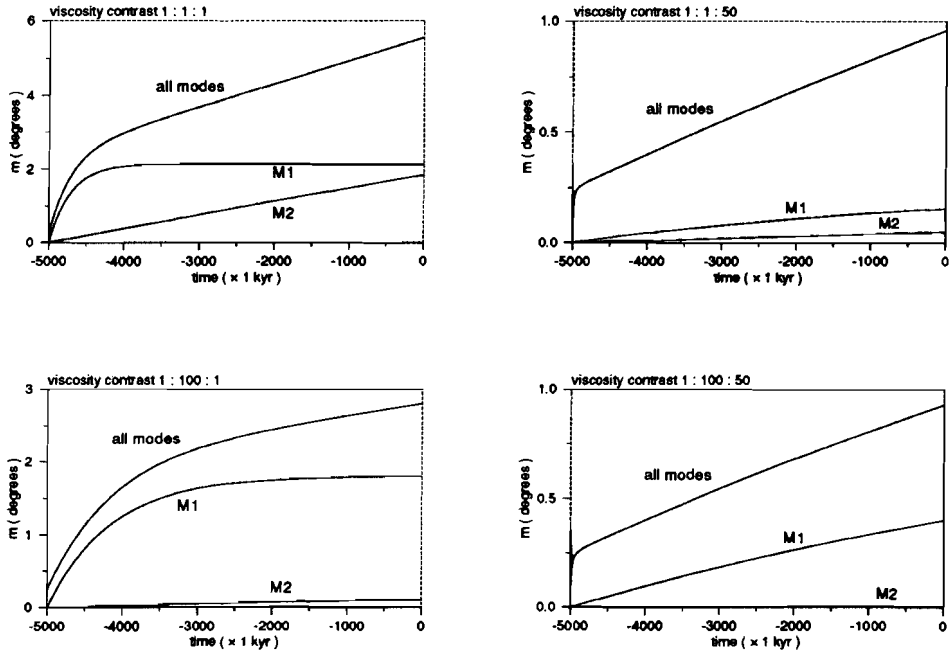

Figure 4.8. Relative importance of the M1 and M2 modes. The viscosities on top of the four panels indicate the viscosity of shallow upper mantle : transition zone : lower mantle in units of 10^{21} $Pa \cdot s$. The curves denoted "all modes" depict the total amount of induced polar wander by the Heaviside uplift case in which there is both load and tidal relaxation (see figure 4.7). The curves denoted "M1" and "M2" give the contributions from the M1 and M2 mode relaxations respectively. The four panels of this figure depict the evolution of the total polar wander and the contributions from M1 and M2 as function of four different mantle viscosity stratifications.

between the shallow upper mantle and the transition zone, or between the lower mantle and the transition zone, is shown in figure 4.10. One of the Heaviside uplift cases of figure 4.7 is chosen: the viscosity contrast between the transition zone and the shallow upper mantle is held fixed at 5, while that between the lower and the shallow upper mantle is 10.
In the first panel of figure 4.10 the polar wander is plotted for three values of the

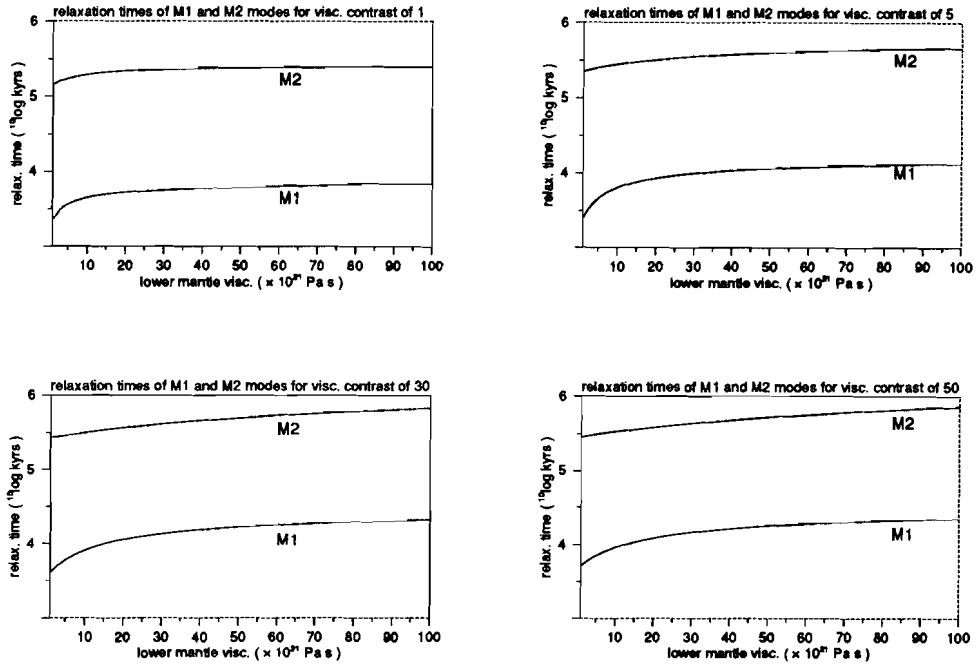

Figure 4.9. Relaxation timescales of the M1 and M2 modes. The relaxation times are logarithmically plotted as a function of the lower mantle viscosity. The viscosity contrast referred to at the top of each panel is the viscosity contrast between the transition zone and the shallow upper mantle.

density of the lithosphere and shallow upper mantle: 4000 kg · m^{-3}, 4120 kg · m^{-3} (the standard value) and 4200 kg · m^{-3}. In the second panel the same is done for the values of the lower mantle: 4400 kg · m^{-3}, 4508 kg · m^{-3} (the standard value) and 4600 kg · m^{-3}.

It is obvious from these curves and from comparison with figure 4.7 that changing the density contrast effects the curves far less than changing the viscosity contrasts. Figures 4.11 and 4.12 show the temporal development of the loading and tidal Love number as a function of the viscosity stratification of the mantle. From comparison of the three panels of each figure it appears that the viscosity contrast between the transition zone and the shallow upper mantle is far less important than the viscosity

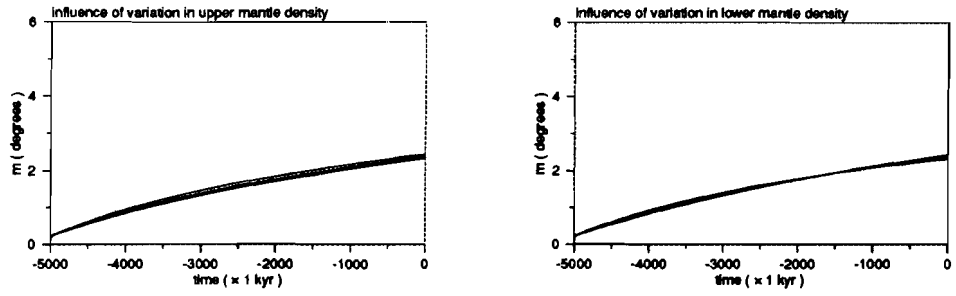

Figure 4.10. Effects of variations in density contrast of the boundaries. The induced polar wander for the Heaviside uplift case in which both load and tidal relaxation are operative is depicted. The viscosity contrast between the transition zone and the shallow upper mantle is 5, between the lower and shallow upper mantle 10. The top panel shows the effects of varying the lithospheric/shallow upper mantle densities. The three curves show the cases for values of 4000, 4100 and 4200 kg · m^{-3}, with the top curve being the case of the lowest value for the lithospheric/shallow upper mantle density. The lower panel does the same for variations in the lower mantle density. Values of 4400, 4508 and 4600 kg · m^{-3} are chosen, with the top curve for the first few million years after uplift onset representing the case of the highest value for the lower mantle density. As is vaguely visible, the order of top and bottom curves changes after some time.

contrast between the lower and shallow upper mantle. The differences between the various values of the transition zone viscosity are hardly visible.

Linear uplift

For a linear rate of uplift, which is supposed to start at t = 0, f(t) can be written as $f(t) = t/t_0$ if the timespan till present amounts t_0 under the condition that at present f must be equal to one. The Laplace transformed function for this linear uplift reads

$$\tilde{f}(s) = \frac{1}{t_0 s^2} \tag{4.57}$$

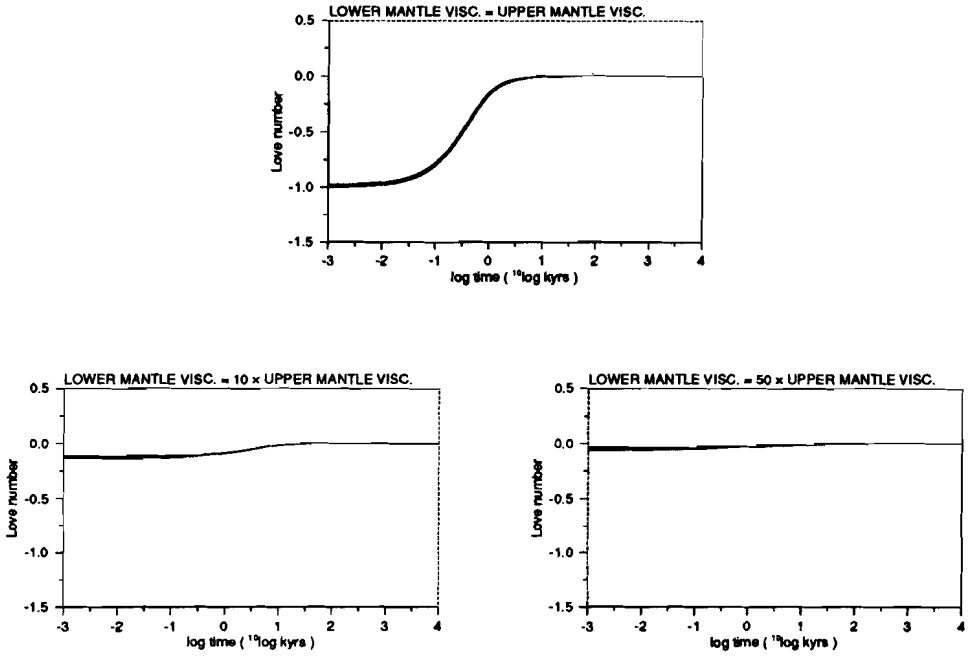

Figure 4.11. Temporal development of the loading Love number. For each of the three panels four cases are plotted, having viscosity contrasts between the transition zone and the shallow upper mantle of 1, 5, 30 and 100. The differences between the curves in each panel are negligible. The top curve in each panel is for the largest viscosity contrast between the transition zone and the shallow upper mantle, the bottom curve for the case of a viscosity contrast of 1.

For the case of the mantle only relaxing to the change in tidal potential, (4.57) in (4.44) results in

$$\tilde{m}(s) = -i\sigma_r \frac{G(\Delta h, \theta, \phi)}{t_0} \left(\frac{A_0}{s^3} - \frac{1}{s^2} \sum_{i=1}^{M} \frac{A_i}{a_i} - \frac{1}{s} \sum_{i=1}^{M} \frac{A_i}{a_i^2} + \sum_{i=1}^{M} \frac{A_i/a_i^2}{s - a_i} \right)$$

Inverse Laplace transformation gives

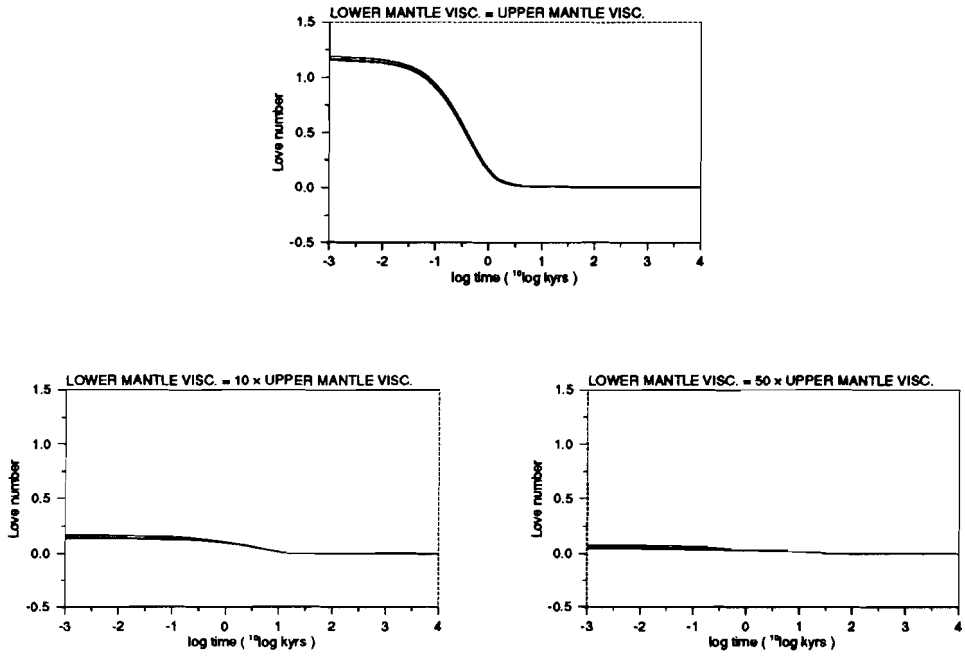

Figure 4.12. Temporal development of the tidal Love number. The plots are for the same cases of the viscosity contrasts as in figure 4.11. The top curve in each panel is for a viscosity contrast between the transition zone and the shallow upper mantle of 1, the bottom curve for the case of a viscosity contrast of 100.

$$m(t) = -i\sigma_r \frac{G(\Delta h, \theta, \phi)}{t_0} \left(\frac{1}{2} A_0 t^2 - \sum_{i=1}^{M} \frac{A_i}{a_i} t + \sum_{i=1}^{M} \frac{A_i}{a_i^2} \left(e^{a_i t} - 1 \right) \right)$$

$$\text{for } t \geq 0 \quad (4.58)$$

The results as a function of the viscosity contrasts are shown in figure 4.13. The polar wander rates at present with this linear model can be up to about 30 cm/yr (case of uniform mantle viscosity) which is about three times the observed value. For a lower mantle viscosity which is 10 times higher than the value for the shallow upper mantle, this rate would be much smaller, but for a value of the viscosity of the transition zone equal to that of the shallow upper mantle the rate of secular drift

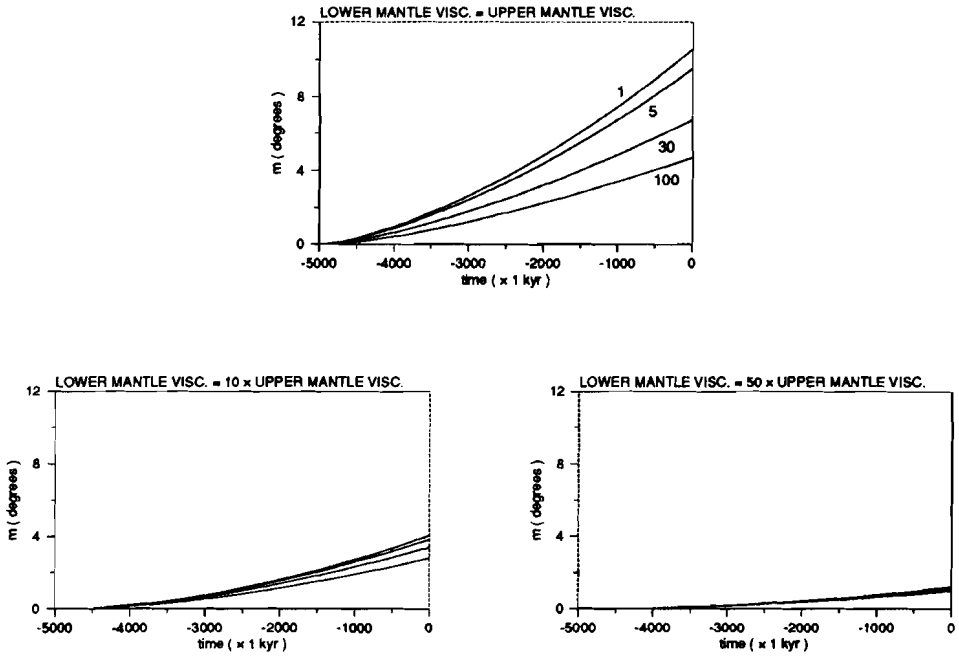

Figure 4.13. Polar wander by tidal relaxation only; Linear case. It is assumed that no mantle relaxation takes place to the loading. The modeled region of figure 1 starts to uplift linearly at 5 million years ago with an uncompensated uplift rate of 0.1 mm/yr. The same cases for the viscosity contrasts are modeled as in figure 4.6.

would still amount some 10 cm/yr, which is about the value of the contemporaneous rate. As a value of the lower mantle viscosity between one to ten times the value for the shallow upper mantle viscosity is quite a reasonable figure (e.g. Hager, 1991, by reviewing the results of studies on several geophysical signatures comes to a value of the lower mantle viscosity of 6×10^{21} Pa · s), the results depicted in the panels of figure 4.13 only strengthens the claim that vertical tectonic movements unrelated to post-glacial rebound can be very effective in contributing a considerable amount to the present-day polar wander.

For the case of the mantle also relaxing to the load, (4.52) in (4.45) gives

$$\tilde{m}(s) = -i\sigma_r \frac{G(\Delta h, \theta, \phi)}{t_0} \left(\frac{A_0^*}{s^3} - \frac{1}{s^2} \sum_{i=1}^{M} \left(\frac{\beta_i}{s_i} + \frac{\gamma_i}{a_i} \right) - \frac{1}{s} \sum_{i=1}^{M} \left(\frac{\beta_i}{s_i^2} + \frac{\gamma_i}{a_i^2} \right) + \sum_{i=1}^{M} \left(\frac{\beta_i/s_i^2}{s - s_i} + \frac{\gamma_i/a_i^2}{s - a_i} \right) \right)$$

which has the inverse Laplace transform

$$m(t) = -i\sigma_r \frac{G(\Delta h, \theta, \phi)}{t_0} \left(\frac{1}{2} A_0^* t^2 - \sum_{i=1}^{M} \left(\frac{\beta_i}{s_i} + \frac{\gamma_i}{a_i} \right) t + \sum_{i=1}^{M} \frac{\beta_i}{s_i^2} \left(e^{s_i t} - 1 \right) + \sum_{i=1}^{M} \frac{\gamma_i}{a_i^2} \left(e^{a_i t} - 1 \right) \right) \quad \text{for } t \geq 0 \qquad (4.59)$$

Figure 4.14 shows the results of the simulations. As was the case with the Heaviside-types of uplift, the tendencies of these linear uplift models with full mantle relaxation to the load are the same as those of figure 4.13. The absolute values of the polar wander are of course less than the corresponding no-mantle relaxation cases, even more when one takes into account that the uplift rates of figure 4.13 are ten times smaller.

Exponential uplift

An exponential rate of uplift can be represented by

$$f(t) = \frac{e^{t/t_0} - 1}{e - 1}$$

The uplift is supposed to start at $t = 0$. The normalization factor $e - 1$ makes the function f equal to one after a timespan t_0 has elapsed.

The Laplace transformed function for such an exponential time evolution reads

$$\tilde{f}(s) = \frac{1}{e - 1} \left(\frac{1}{s - 1/t_0} - \frac{1}{s} \right) \qquad (4.60)$$

The case of the mantle only relaxing to the change in tidal potential and not to the load, (4.60) in (4.44) gives

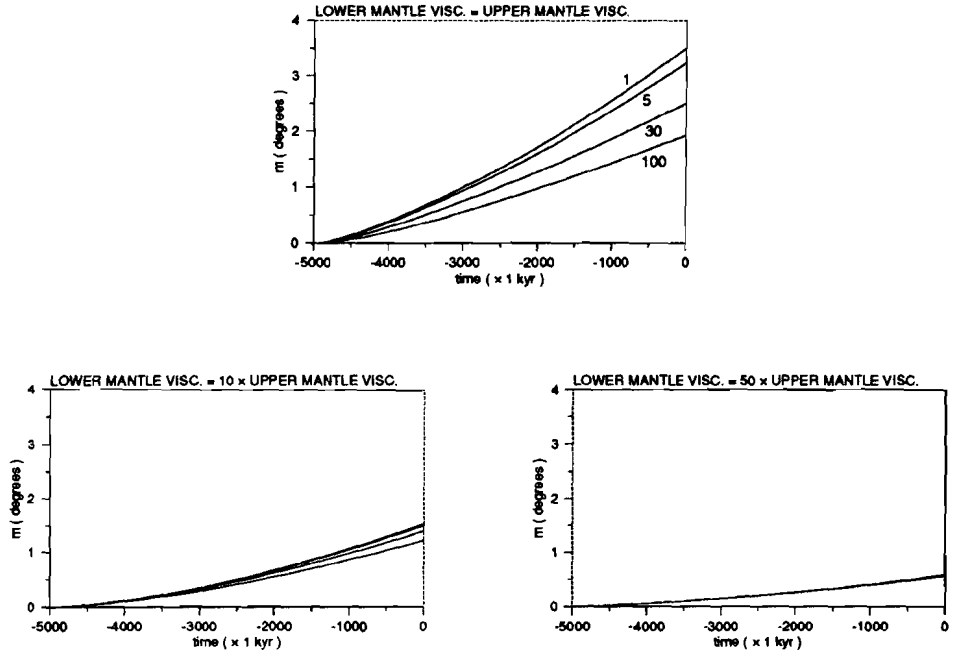

Figure 4.14. Polar wander by full mantle relaxation; Linear case. Both load and tidal relaxation act. The region is uplifted linearly, starting 5 million years ago, with an uplift rate of 1 mm/yr.

$$\tilde{m}(s) = -i\sigma_r G(\Delta h, \theta, \phi)\left(-\frac{A_0}{s^2} - \frac{A_0 t_0}{s} - \frac{A_0 t_0}{1/t_0 - s} + \frac{1}{s}\sum_{i=1}^{M}\frac{A_i}{a_i} - \sum_{i=1}^{M}\frac{A_i/a_i}{s-a_i} - \sum_{i=1}^{M}\frac{A_i/(1/t_0 - a_i)}{s-a_i} - \frac{1}{1/t_0 - s}\sum_{i=1}^{M}\frac{A_i}{1/t_0 - a_i}\right)$$

resulting in

$$m(t) = -i\sigma_r G(\Delta h, \theta, \phi)\left(-A_0 t + A_0 t_0\left(e^{t/t_0} - 1\right) - \sum_{i=1}^{M}\frac{A_i}{a_i}\left(e^{a_i t} - 1\right)\right.$$

$$+ \sum_{i=1}^{M} \frac{A_i}{1/t_0 - a_i} \left(e^{t/t_0} - e^{a_i t} \right) \Bigg) \quad \text{for } t \geq 0 \qquad (4.61)$$

Figure 4.15 portrays the induced amount of polar wander as a function of the viscosity stratification of the mantle. The same tendencies and about the same magnitudes are found in these cases for the present polar wander rates as in the corresponding linear cases of figure 4.13.

Both mantle relaxation to load and tidal potential gives ((4.60) in (4.45))

$$\begin{aligned} \tilde{m}(s) = - i\sigma_r G(\Delta h, \theta, \phi) \Bigg(& - \frac{A_0^*}{s^2} - \frac{A_0^* t_0}{s} - \frac{A_0^* t_0}{1/t_0 - s} + \frac{1}{s} \sum_{i=1}^{M} \left(\frac{\beta_i}{s_i} + \frac{\gamma_i}{a_i} \right) \\ & - \sum_{i=1}^{M} \left(\frac{\beta_i / s_i}{s - s_i} + \frac{\gamma_i / a_i}{s - a_i} \right) \\ & - \sum_{i=1}^{M} \left(\frac{\beta_i / (1/t_0 - s_i)}{s - s_i} + \frac{\gamma_i / (1/t_0 - a_i)}{s - a_i} \right) \\ & - \frac{1}{1/t_0 - s} \sum_{i=1}^{M} \left(\frac{\beta_i}{1/t_0 - s_i} + \frac{\gamma_i}{s - a_i} \right) \Bigg) \end{aligned}$$

which results after inverse Laplace transformation in

$$\begin{aligned} m(t) = - i\sigma_r G(\Delta h, \theta, \phi) \Bigg(& - A_0^* t + A_0^* t_0 \left(e^{t/t_0} - 1 \right) - \sum_{i=1}^{M} \frac{\beta_i}{s_i} \left(e^{s_i t} - 1 \right) \\ & - \sum_{i=1}^{M} \frac{\gamma_i}{a_i} \left(e^{a_i t} - 1 \right) + \sum_{i=1}^{M} \frac{\beta_i}{1/t_0 - s_i} \left(e^{t/t_0} - e^{s_i t} \right) \\ & + \sum_{i=1}^{M} \frac{\gamma_i}{1/t_0 - a_i} \left(e^{t/t_0} - e^{a_i t} \right) \Bigg) \quad \text{for } t \geq 0 \qquad (4.62) \end{aligned}$$

The results are depicted in figure 4.16. Apart from the somewhat more exponential behavior of the curves, the plots are very similar to those of the linear uplift case of figure 4.14.

The polar wander plots for the three modeled uplift histories have a few characteristics in common. Irrespective of the question whether there is mantle relaxation to the load or not, the polar wander remains very small for the cases in which the viscosity ratio between the lower and shallow upper mantle is large, i.e. for values larger than about 10. The viscosity of the transition zone is not important then. For viscosity ratios between the lower and shallow upper mantle which are smaller than about 10, the induced polar wander is, apart from the time history of the uplift and

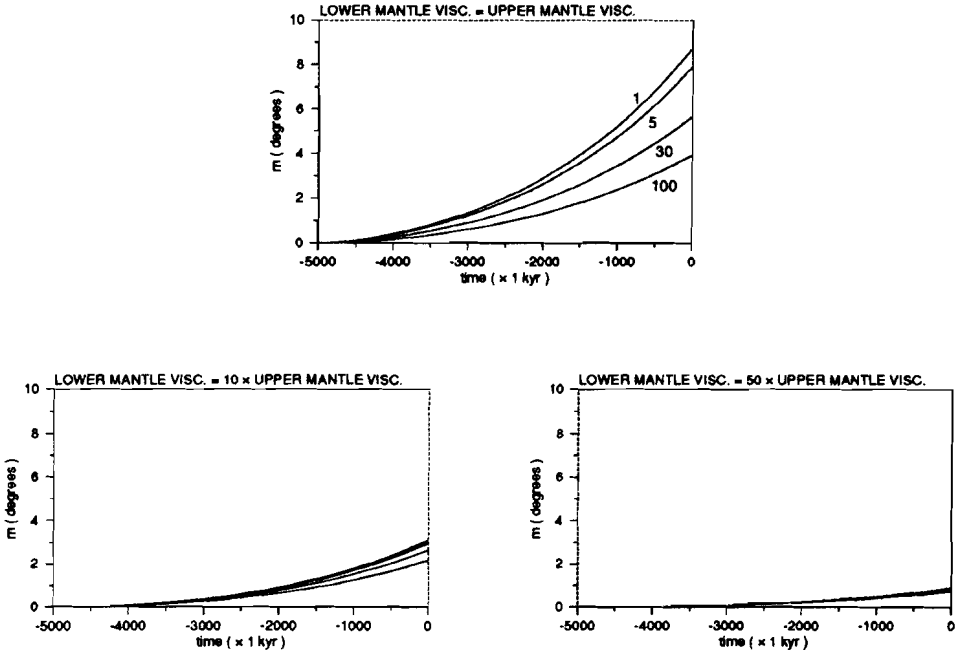

Figure 4.15. Polar wander by tidal relaxation only; Exponential case. There is no mantle relaxation to the load. The uplift starts exponentially 5 million years ago with an exponential rise time of 3 million years. The uplift is normalized such as to result in a total uncompensated uplift of 500 meters at present.

the amount of mantle relaxation to the load, very sensitive to the viscosity of the transition zone. Given the uplift history and the amount of mantle compensation to the load, the difference in the polar wander achieved after 5 million years can be as large as 300 percent, depending on the transition zone viscosity being between 10^{21} Pa · s and 10^{23} Pa · s.

Most important, however, is that induced rates of polar wander have the right order of magnitude for both the linear and exponential uplift cases. We are aware, however, that there are more areas in the world which experience high rates of vertical movement and which are most likely associated with deviations from Airy or Pratt isostasy, even apart from the contributions due to post-glacial rebound, recent ice -

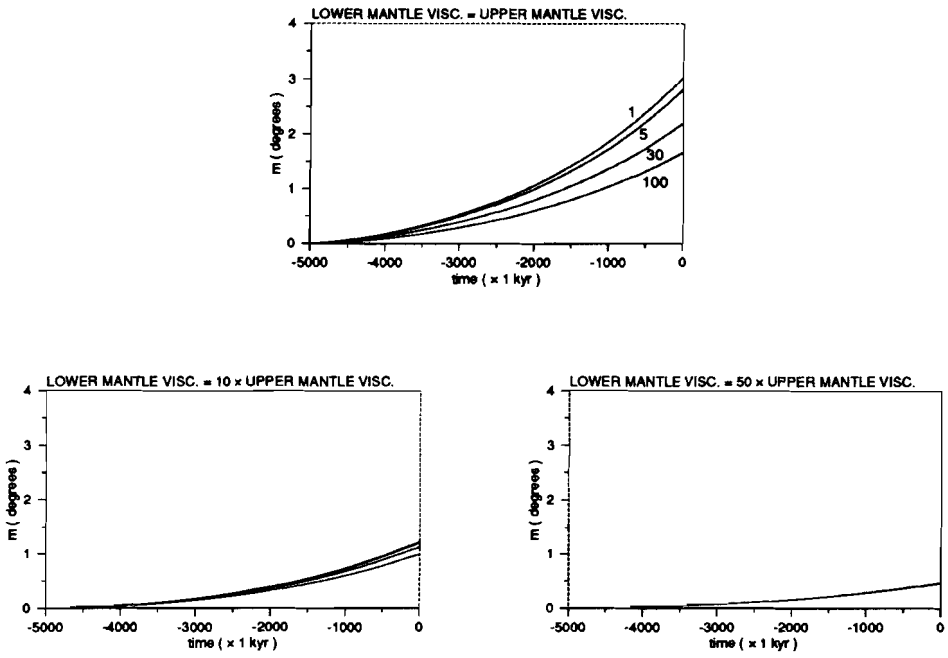

Figure 4.16. Polar wander by full mantle relaxation; Exponential case. Both load and tidal mantle relaxation are operative. The region is uplifted exponentially with an exponential rise time of 3 million years, resulting in a total uplift of 5 kilometers at present.

water redistributions and probably events taking place at the core - mantle boundary.

Comparison of the three uplift histories shows that the differences between a linear and exponential uplift evolution are not large. The Heaviside uplift history induces a marked different polar wander history, but, as noted already, this is not a very realistic case. The case of a number of Heaviside uplift histories partitioned over the past few million years would be more realistic. It then becomes important to consider when the changes in uplift took place: if the (change in) uplift happened recently, the small timescale relaxation modes (if not to the load, then certainly to the tidal forcing) are determining the shift of the rotation axis over the globe, just as

they do in the post-glacial rebound case. On the longer timescales of a few hundreds of thousands of years to a few millions of years, the effects of all the small timescale uplift histories tend to result into a linear or exponential uplift history, being strongly dependent on the rheological properties of the transition zone in the case of small viscosity contrasts between the lower and shallow upper mantle. So, the results of the modelings shown in the linear and exponential uplift cases would only give mean values in such a case, around which higher and lower shifts of the rotation axis of shorter duration (on timescales of post-glacial rebound) are likely.

Conclusions

The relation between non-glacially induced tectonic movements and changes in rotation is a difficult one to establish. Apart from the uncertainties in the rheological mantle stratification of our planet – which is assumed to be the major unknown in post-glacial rebound modeling –, the vertical movement and erosion rates of various regions, and the deviations from isostasy maintained by compressive intraplate stresses and (continental) lithospheric rheologies present extra uncertainties in establishing the relation.

In this study we have extended the original two-layer model proposed in chapter 3 in the realm of a normal mode linear visco-elastic model. Such a model certainly has its shortcomings, unable as it is to deal with the varying lateral lithospheric heterogeneities that are of paramount importance in maintaining an effective forcing. But it also has its advantages: the adjustment of the equatorial bulge to the forcings can very well be studied with such a widely-used analytical modeling technique.

Given the restrictions using a normal mode model, the best which we can do concerning load relaxation is to assume that a certain amount of lithospheric uplift is unrelaxed by mantle relaxation. The simulations then show a polar wander which for reasonable uplift rates and mantle stratifications has the right order of magnitude to induce significant contributions in the contemporaneously observed value. For a lower to shallow upper mantle viscosity contrast which is not too large (i.e., smaller than about 10) the induced polar wander is sensitive to the value of the viscosity of the transition zone.

This study has also outlined another important issue. The uplift of the Himalayas is only possible when there are compensating regions which experience subsidence.

The chances for these latter regions to relax by mantle relaxation on timescales of post-glacial rebound are much higher than the modeled area of the Himalayas. This gives an asymmetry in effectiveness which is clearly emerging from the studies on $\dot{J}_2$: the uplifted region with its actively maintained deviations from isostasy give effective contributions, as was shown in chapter 3; the compensating regions with its rebounding mantle unprohibited by the lithosphere on top, not. This implies that it is not necessary to consider Earth models which have mass conservation implicit. Finally, in this study we only considered one region which experiences uplift under non-isostatic conditions, although this one region is a very active and potentially the most important one. It was not our aim in this article to give an exhaustive treatment of all the possible regions in the world which undergo active lithospheric vertical movements accompanied by deviations from isostasy. Rather we wanted to present a case study of only one. Future truly comprehensive studies on the mechanisms behind the shift in the rotation axis will not only have to include these other areas, but also post-glacial rebound, the recent ice - water redistributions and perhaps a number of other mechanisms like the recently proposed changes at the core - mantle boundary.

Acknowledgments

This research has been supported by the Twinning Project of the European Economical Community.

References

Amano, K., and A. Taira, Two-phase uplift of Higher Himalayas since 17 Ma, *Geology, 20*, 391-394, 1992.

Arfken, G., *Mathematical Methods for Physicists*, 815 pp., Academic Press, New York, 1970.

Basavaiah, N., B.P. Singh, and I.V. Radhakrishna Murthy, The Himalayan riddle of the free-air satellite gravity and a possible solution, *Phys. Earth Planet. Inter., 69*, 14-19, 1991.

Burbank, D.W., Causes of recent Himalayan uplift deduced from deposited patterns in the Ganges basin, *Nature, 357*, 680-683, 1992a.

Burbank, D.W., Characteristic size of relief, *Nature, 359*, 483-484, 1992b.

Butkov, E., *Mathematical Physics*, 735 pp., Addison-Wesley, Reading, Massachusetts, 1968.

Copeland, P., and T.M. Harrison, Episodic rapid uplift in the Himalaya revealed by $^{40}Ar/^{39}Ar$ analysis of detrital K-feldspar and muscovite, Bengal fan, *Geology, 18*, 354-357, 1990.

Fung, Y.C., *Foundations of Solid Mechanics*, 525 pp., Prentice-Hall, Englewood Cliffs, New Jersey, 1965.

Hager, B.H., Mantle viscosity: A comparison of models from Postglacial rebound and from the geoid, plate driving forces, and advected heat flux, in *Glacial Isostasy, Sea-Level and Mantle Rheology, NATO ASI Series C, Vol. 334*, edited by R. Sabadini, K. Lambeck and E. Boschi, p. 493-513, Kluwer Academic Publishers, Dordrecht, The Netherlands, 1991.

Harrison, T.M., P. Copeland, W.S.F. Kidd, and A. Yin, Raising Tibet, *Science, 255*, 1663-1670, 1992.

Klootwijk, C.T., P.J. Conaghan, and C.McA. Powell, The Himalayan Arc: large-scale continental subduction, oroclinical bending and back-arc spreading, *Earth Planet. Sci. Lett., 75*, 167-183, 1985.

Lambeck, K., *The Earth's Variable Rotation: Geophysical Causes and Consequences*, 449 pp., Cambridge University Press, New York, 1980.

Lambeck, K., *Geophysical Geodesy. The Slow Deformations of The Earth*, 718 pp., Oxford University Press, Oxford, 1988.

Lefftz, M. and H. Legros, Some remarks about the rotations of a viscous planet and its homogeneous liquid core: linear theory, *Geophys. J. Int., 108*, 705-724, 1992a.

Lefftz, M. and H. Legros, Influence of viscoelastic coupling on the axial rotation of the Earth and its fluid core, *Geophys. J. Int., 108*, 725-734, 1992b.

Longman, I.M., A Green's function for determining the deformation of the Earth under surface mass loads; 1. Theory, *J. Geophys. Res., 67*, 845-850, 1962.

Molnar, P., and P. England, Late Cenozoic uplift of mountain ranges and global climate change: chicken or egg?, *Nature, 346*, 29-34, 1990.

Moser, J., D.A. Yuen, and C. Matyska, Polar motions excited by a convecting viscous mantle, *Geophys. Res. Lett., 19*, 2251-2254, 1992.

Munk, W.H., and G.J.F. MacDonald, *The Rotation of the Earth: A Geophysical*

Discussion, 323 pp., Cambridge University Press, Cambridge, England, 1960.

Peltier, W.R., The impulse response of a Maxwell Earth, *Rev. Geophys. Space Phys.*, *12*, 649-669, 1974.

Peltier, W.R., The LAGEOS constraint on deep mantle viscosity: results from a new normal mode method for the inversion of viscoelastic relaxation spectra, *J. Geophys. Res.*, *90*, 9411-9421, 1985.

Sabadini, R., and W.R. Peltier, Pleistocene deglaciation and the Earth's rotation: implications for mantle viscosity, *Geophys. J. R. astron. Soc.*, *66*, 553-578, 1981.

Sabadini, R., D.A. Yuen, and E. Boschi, Polar wandering and the forced responses of a rotating, multilayered viscoelastic planet, *J. Geophys. Res.*, *87*, 2885-2903, 1982.

Sabadini, R., D.A. Yuen, and P. Gasperini, Mantle rheology and satellite signatures from present-day glacial forcings, *J. Geophys. Res.*, *93*, 437-447, 1988.

Spada, G., D.A. Yuen, R. Sabadini, P.J. Morin, and P. Gasperini, A computer-aided, algebraic approach to the post-glacial rebound problem, *Mathematica J.*, *1*, 65-69, 1990.

Spada, G., R. Sabadini, D.A. Yuen, and Y. Ricard, Effects on post-glacial rebound from the hard rheology in the transition zone, *Geophys. J. Int.*, *109*, 683-700, 1992a.

Spada, G., Y. Ricard, and R. Sabadini, Excitation of true polar wander by subduction, *Nature*, *360*, 452-454, 1992b.

Zeitler, P.K., Cooling history of the NW Himalaya, Pakistan, *Tectonophys.*, *4*, 127-151, 1985.

CHAPTER 5

LONG-TERM CHANGES IN ROTATION BY CHANGES IN OCEANIC SPREADING RATES AND SUBDUCTION

Abstract

Recently, Goldreich and Toomre's visco-elastic model of true polar wander driven by continental drift has been extended to a visco-elastic model of those induced by mass movements in the mantle. In some of these models, the true polar wander induced by an internal mass redistribution due to changes in subduction and its induced surface and internal boundary deflections in a radially stratified, visco-elastic mantle is determined. Relating changes in the Earth's rotation solely to changes in subduction could lead to incomplete results, however, if the cold slabs are inserted into the mantle without considering the forcing functions of the hot material that emerges at the surface to complete the circulation. Also hot upwellings from the deep mantle, like the hypothetical mantle plumes, could give non-negligible contributions. These forcing functions are naturally included in true polar wander calculations derived from recent mantle convection simulations, but at present they lack the forcing functions of accompanying lithospheric phenomena, sea-level changes etc., and generally do not model the adjustment of the equatorial bulge to the changed mass distributions. In fact, these models only determine the axis of maximum moment of inertia which does not necessarily coincide with the rotation axis for all times.

In this chapter the rotational effects of the increased spreading rate of a mid-ocean ridge accompanying enhanced rates of subduction are studied by a simple model. Only the forcing functions are considered in order to compare the effectiveness of this process in relation to subduction. A full treatment of the induced true polar wander should include the effects of the induced shifts of the equatorial bulge, like has been done in chapter 4. Given the uncertainties in the forcing functions, this is beyond the scope of this chapter, however. The results indicate that the induced changes in the products of inertia might become comparable to those resulting from

the subduction of the slab if the increases of the sea-level are dynamically supported by the deeper mantle regions. Only a few percent of these changes are due to the lithosphere, while the bulk amount comes from the non-isostatic increase in sea-level. The isostatic condition by which the bathymetry is calculated only pertains to a certain period: there is no relation between the isostatic conditions at different times, making an increase in sea-level - being the same above the ridge as above a lithosphere column elsewhere - not isostatically compensated. Such a compensation could be established by uplift of the continents, shifting mantle material from underneath the oceanic areas towards the continental areas. Another possibility is that the compensation is to be sought in the deeper mantle, making the bathymetry dynamically supported by the convection pattern. In the former case the changes in the products of inertia due to the increase in bathymetry become negligible, in the latter case not.

Introduction

During the last 200 Myr there appears to have been a considerable amount of true polar wander that can not be related to changes in ice volumes, as these shifts sometimes occurred during warm periods. Andrews (1985) derives from paleomagnetic data that during the last 180 Myr a true polar wander has occurred of $22^\circ \pm 10^\circ$. According to Andrews, the relative motion between the geomagnetic poles and the hotspot reference frame was especially large (on the order of 80 - 100 mm/yr) during the periods 180-160 Myr ago, 115-85 Myr ago, 65-50 Myr ago, and at present. Besse and Courtillot (1991) find that the true polar wander during the last 200 Myr can be divided into 5 periods: the identify relatively large excursions from 200 to 180 Myr ago, from 110 to 50 Myr ago and from 10 Myr ago to present, while during the intervening times the true polar wander has been much less. They come to the conclusion that the true polar wander during the last 200 Myr must have been more than 20°. If it is assumed that the Earth's magnetic axis roughly coincides with the rotation axis over long periods, then it is obvious that solid Earth displacements in mantle and lithosphere must be responsible for this shift, which occurred in a period of enhanced continental drift. Radial displacements associated with departures from isostasy, which were shown to be extremely effective in changing the moments and products of inertia in chapter 3, may have occurred in

times of enhanced plate activity such as in the Cretaceous.

After Goldreich and Toomre (1969) had publiced their model of true polar wander induced by the wandering continents, several studies have been performed to apply and extend this idea in a tectonophysical and mantle convection modeling context. In their model, Goldreich and Toomre proposed that the non-hydrostatic part of the equatorial flattening is simply due to lateral adjustment of the equatorial bulge to an extremum of the non-hydrostatic part of the moments of inertia, instead of being a fossil relict of times in which the Earth was rotating faster. This latter mechanism gave severe problems with respect to the viscosity of the mantle. From studies on post-glacial rebound, mantle viscosities were found to be of the order of 10^{21} Pa · s, while an explanation of the excess equatorial flattening by a fossil bulge model resulted in mantle viscosities being orders of magnitude larger. Lateral movements of the equatorial bulge – like a water wave traveling over the ocean – in response to secular changes in the mass distribution of the planet, could solve this problem. If near-surface mass displacements took place, like plate movements which they represented by a colony of beetles crawling slowly over the Earth's surface, the equatorial bulge could adjust itself by viscous flow with viscosities compatible with those derived from post-glacial rebound. If the non-hydrostatic mass redistribution commenced gradually and if there was not a switch to the non-hydrostatic part of the moment of inertia around the rotation axis becoming larger than the non-hydrostatic part of the moment of inertia around one of the two coordinate axes perpendicular to it, the rotation axis was envisaged to follow the movement of the axis of the maximum non-hydrostatic moment of inertia steadily.

Whereas Goldreich and Toomre envisioned the moving continents as the driving mechanism, Ricard et al. (1992, 1993) and Spada et al. (1992) have recently proposed that especially internal mantle processes, away from internal and external boundaries, are effective in driving true polar wander. They assume that the changes in rotation are solely attributable to the evolution of subducting cold slabs and its induced dynamical deflections of the surface and internal boundaries. The slabs are inserted in a radially stratified mantle, and consequently the temporal displacements of the rotation axis are determined by modeling the mantle as a linear visco-elastic medium with a Maxwell rheology. The effects of the induced ascending currents are not taken into account, only the average inertia tensor is kept constant by subtracting one third of the trace of this tensor from the diagonal elements (otherwise the Earth would spin up by the downward displacement of cold material). In their models, the lithosphere is taken as effective elastic. Strong lateral variations (the lithosphere beneath a mid-oceanic ridge is essentially zero, while underneath continental areas like the western part of Russia lithospheric phenomena are observed reaching depths of up to 400 km or about 2/3 of the upper mantle thick-

ness) are neither taken into account.
Whereas the studies by Ricard et al. and Spada et al. lack an assessment of actively rising mantle material, Jurdy (1983) has calculated what the effect is on the moments of inertia and thereby on polar wander of a redistribution of the hotspot swells and subduction zones in the Cretaceous compared to the present situation. She assumes in her paper that the main driving constituents of true polar wander are associated with geoid highs. She bases herself on a study made by Crough and Jurdy (1980), in which was shown that these geoid highs are not only associated with subduction zones, but also with hotspots: the distribution of the geoid highs that are assumed to be related with the hotspots mimic the characteristic pattern in which the surface of a tennis ball is divided into two parts. Jurdy finds that if both effects have the same strength the pole is 8° away from the paleomagnetically measured one, but if hotspots have a weighting of 2/3 and subduction zones 1/3 this number reduces to 1°. These weighting functions seem to be rather arbitrary however. She gives not a physical explanation for this particular choice.
Recent determinations of true polar wander rates from mantle convection models (Moser et al., 1992 and Tackley et al., 1992) also take as a natural consequence of the way of modeling the upwelling of hot material into account as a forcing function, but they lack the effects of all kinds of lithospheric processes.
In order to study the effects of rising hot material, in this chapter the effects of an increased spreading rate of mid-ocean sea-floor production and the accompanying rise in sea-level on the Earth's rotation are determined. A simple half-space cooling model is used for this purpose. Although this is a widely used model to determine the long-term changes in sea-level, Hager (1980) has pointed out that the relation between sea-level variations and increases in spreading rates or volume of mid-ocean ridges might be more complex as also the rates at which slabs subduct increases (the total surface area of the continents is approximately constant). This latter increase causes, according to him, an increased local cooling which might even result in a decrease of eustatic sea-level in some cases. On the other hand, this subducted material will on the average be much younger during times of increase mid-ocean ridge spreading rates, and thereby subducting under small deflection angles (Vlaar and Wortel, 1976), preventing the formation of deep ocean trenches.
As the main purpose of this chapter is to study the possible effectiveness of the complement of the changes in subduction and to show that this complement can have a non-negligible strength which must be taken into account when one wants to model the true polar wander during the last few hundreds of millions of year, the effects of a rise of the sea-floor by increased mid-ocean spreading rates will be considered without the proposed effects of the vertical movements of the continents or the eventual cooling by the subducting plates taken into account. Future studies

will have to deal with these effects, however.

Increase in spreading activity

Whenever the spreading rate of a mid-oceanic ridge changes, a redistribution of mass is associated with it, inflicting a change in the position of the polar axis. Assuming that there is an increase in the spreading rate of a ridge, two contributions can be distinguished: the lithospheric column at a fixed distance from the spreading ridge will be raised, thereby inducing an increase in sea-level.
If the increase in spreading rate happens on a geological fast time scale over the whole spreading area, so that this increase can be modeled as a delta function in time, the oceanic lithosphere will temporarily have a thickness that is discordant with its increased spreading rate. The lithosphere starts to rise until after some time (several tens of millions of years) it has accommodated to the new situation. The concomitant rise of the sea-level will thus be rather secular than episodic in comparison with the change in spreading rate.
In order to study the effects of a changed spreading activity upon the position of the polar axis and the rotation rate of the Earth, a hypothetical model is scrutinized in which the pole of spreading coincides with the North Pole and the spreading ridge is situated along the Greenwich Meridian. The spreading area is assumed to be symmetrically distributed around the ridge. The lithospheric columns are assumed to be always in Pratt isostatic equilibrium. Only the effects after the bathymetry has accommodated to the new spreading rate, so that the moments of inertia have settled to stationary values, are calculated. This model can serve as the standard model from which models for arbitrarily positioned spreading areas with associated spreading poles can be derived by means of transformations by Eulerian angles.
A model that has proven to adequately describe the form and physical state of a spreading ridge is the cooling half-space model (cf. Turcotte and Schubert, 1982). In this model, the temperature T of a cooling oceanic lithosphere, traveling away from the spreading ridge, can be expressed as

$$T(x, y) = T_0 + (T_m - T_0)\,\mathrm{erf}\left(\frac{y}{2\sqrt{\kappa x/u}}\right) \tag{5.1}$$

in which x denotes the distance from the spreading ridge, y the depth with respect

to the upper boundary of the lithosphere (the boundary between the lithosphere and the ocean), T_0 is the temperature of the water, T_m the temperature of the mantle, u the spreading rate (so x/u gives the time it has taken for the lithospheric column at x to travel away from the spreading ridge) and κ the thermal diffusivity. The quantity $\sqrt{\kappa x/u}$ is the thermal diffusivity distance. The error function is defined as

$$\mathrm{erf}(z) = \frac{2}{\sqrt{\pi}} \int_0^z \exp(-\chi^2) d\chi \tag{5.2}$$

The density ρ_L of the lithospheric material as a function of x and y can readily be found by applying the expression for thermal expansion (cf. (3.2))

$$\rho_L(x, y) - \rho_m = -\alpha\rho_m(T(x, y) - T_m) \tag{5.3}$$

in which ρ_m is the density of the mantle material and α the thermal expansivity.
The thickness of the lithospheric column can be found by choosing the temperature of the lower boundary of the lithosphere with respect to the temperature of the mantle. Usually, this is taken to be $T/T_m = 0.9$.
By comparing the lithospheric column at the spreading ridge with a lithospheric column elsewhere, the depth of the ocean (the bathymetry) can be derived by application of the condition of isostasy. Figure 5.1 shows on the left side a column with depth L with respect to the ocean ic surface at the position of the ridge. This column is assumed to have a uniform density ρ_m. Also a column away from the spreading ridge is depicted in the left-side figure, consisting of water with a uniform density ρ_w with a depth w, above the lithosphere extending to a depth L – w. From the isostatic condition it can be derived, that

$$w = \frac{2\alpha\rho_m(T_m - T_0)}{\rho_m - \rho_w} \cdot \sqrt{\frac{\kappa x}{\pi u}} \tag{5.4}$$

The right side of figure 5.1 gives the situation after increased spreading. The same symbols are used as in the case before increased spreading, apart from an additional asterisk. If λ is the factor of the increased spreading rate, it is clear that

$$L^* = L/\sqrt{\lambda} \quad \text{and} \quad w^* = w/\sqrt{\lambda} \tag{5.5}$$

The parameter h stands for the increased sea-level with respect to the sea-level before the increased spreading set in. The same isostasy condition applies to this situation, as the increase of sea-level is the same above the spreading ridge as above a column elsewhere. Note, however, that the isostatic conditions before and after the increased spreading are disjoint: there is no comparison between a lithospheric column before and after the enhanced spreading rate.

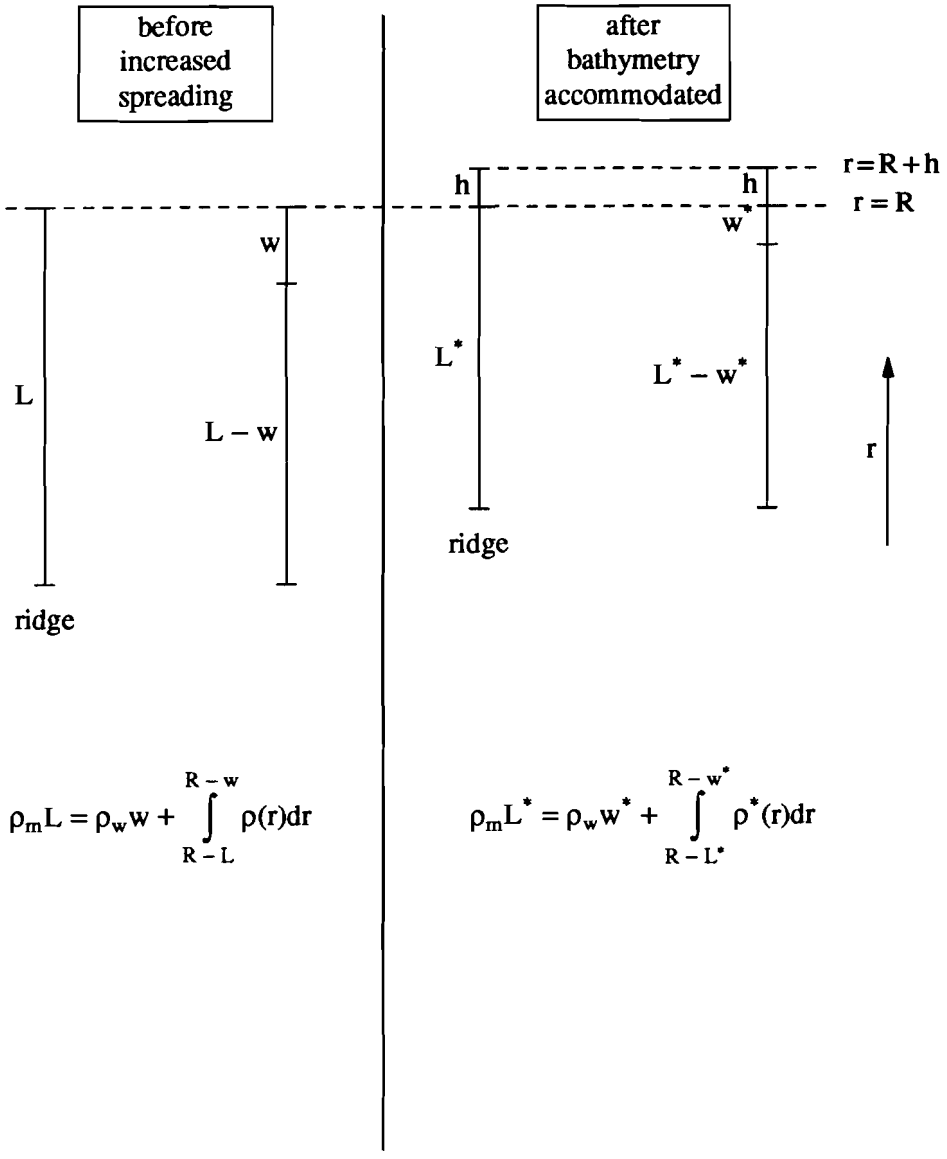

Figure 5.1. Isostatic columns before and after increased spreading rates.

In the calculations, the depth dependence of the various parameters will be expressed as a function of r, in which $r = 0$ gives the position of the center of the Earth and $r = R$ gives the position of the sea-level before increased spreading. So y is to be replaced by $R - r$.
The lateral dependence will be expressed as a function of ϕ, which denotes the angle with respect to the spreading pole. Now, if u_0 is the (maximum) rate of spreading at 90° from the spreading pole, the velocity u can be written as $u = u_0 \sin\theta$ if the spreading pole is placed on the North Pole, with θ being the co-latitude. In this case, x is equal to $R\phi \sin\theta$, making x/u independent of θ.
The correlation of this model of the oceanic lithosphere with observations is generally good up to ages of about 70 Myr. For ages larger than this the form of the lithosphere seems to be best described by a smooth decaying exponential function. The approximation, made in the forthcoming modeling, that the lithospheric thickness and the bathymetry do not change significantly after 70 Myr and before subduction eventually sets in, is a reasonable one.
Three regimes can be distinguished, as illustrated in the cartoons of figure 5.2. ϕ denotes the angle away from the spreading ridge, ψ is the angle away from the ridge at which the outer edge of the oceanic region is situated (this angle is assumed to be the same before and after the increased spreading) and ψ_0 is the angle away from the ridge where the parabolically shaped lithosphere turns into a linear one before increased spreading. The value of this angle is equal to $\lambda\psi_0$ after the increased spreading has begun.
In the first regime, the outer edge of the spreading area at $\phi = \psi$ lies closer to the spreading ridge than the point $\phi = \psi_0$, where the parabolic shape of the lithosphere changes into a linear one before spreading. As it assumed that spreading rates increase, also the shape of the entire oceanic lithosphere after the increased spreading activity began will be parabolic.
In the second regime, the outer edge of the spreading area lies beyond the point where the parabolic shape of the lithosphere changes into a linear fashion before spreading. So originally the lithosphere will be parabolically shaped till $\phi = \psi_0$, but will not change its form anymore, spreading purely horizontally, in the region $\psi_0 \leq \phi \leq \psi$. After the increased spreading has set in, this situation is changed however. The outer edge of the spreading area where the linear shape changes into a parabolic one is now situated at an angle $\phi = \lambda\psi_0$ away from the ridge. So for $\psi_0 \leq \phi \leq \psi$, the linear shape transforms into a parabolic one.
Finally, the outer edge of the spreading area in the third regime lies beyond the point $\phi = \lambda\psi_0$, where the lithospheric shape after the increased spreading rate has commenced changes from parabolic to linear. At the angle $\phi = \lambda\psi_0$, the lithospheric shape after increased spreading changes from parabolic into linear. It is

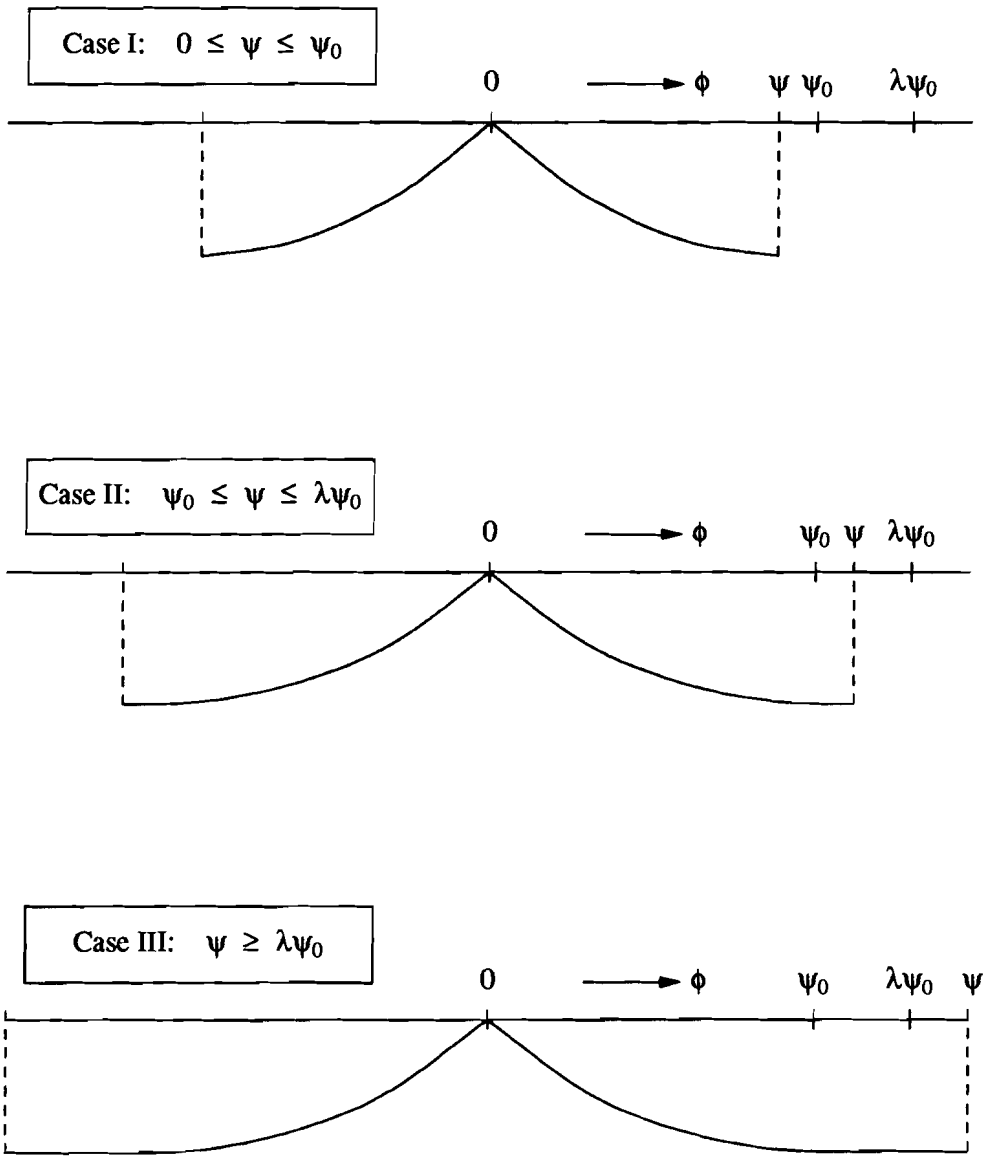

Figure 5.2. Cartoon showing the three spreading area regimes.

assumed that the depth at which the lower and the upper boundary of the lithosphere are situated before and after increased spreading are the same for angles $\lambda\psi_0 \leq \phi \leq \psi$. So there is no net lithospheric mass redistribution for angles $\phi \geq \lambda\psi_0$. Of course, if the ocean extends beyond $\phi = \lambda\psi_0$, there will be an ocean mass redistribution in this area by the increase of the sea-level.

With the various assumptions and simplifications made, the effects of an increased spreading rate and associated rise of the sea-level on the position of the polar axis can be calculated for the three cases. In the calculations, x, y and z form a fixed cartesian coordinate system, with x and y in the equatorial plane (x in the direction of the Greenwich Meridian and y 90 degrees East Longitude) and z along the rotational axis.

Case I : $\psi \leq \psi_0$

The density difference $\Delta\rho$ as a function of r and ϕ between the situation after the bathymetry accommodated itself to the higher spreading rate and the situation before the increased spreading was turned on, is given by

$$R \leq r \leq R + h: \qquad \Delta\rho = \rho_w \tag{5.6a}$$

$$R - w \leq r \leq R - w^*: \qquad \Delta\rho = \rho_L^*(r,\phi) - \rho_w \tag{5.6b}$$

$$R - L^* \leq r \leq R - w: \qquad \Delta\rho = \rho_L^*(r,\phi) - \rho_L(r,\phi) \tag{5.6c}$$

$$R - L \leq r \leq R - L^*: \qquad \Delta\rho = \rho_m - \rho_L(r,\phi) \tag{5.6d}$$

with, using (5.3),

$$\rho_L(r,\phi) = \rho_m \left\{ 1 - \alpha(T_m - T_0)\left(\mathrm{erf}\left(\frac{R-r}{c_0\sqrt{\phi}} \right) - 1 \right) \right\} \tag{5.7}$$

and

$$\rho_L^*(r,\phi) = \rho_m \left\{ 1 - \alpha(T_m - T_0)\left(\mathrm{erf}\left(\frac{\sqrt{\lambda}(R-r)}{c_0\sqrt{\phi}} \right) - 1 \right) \right\} \tag{5.8}$$

with c_0 defined as

$$c_0 \equiv 2\sqrt{\kappa R/u_0} \tag{5.9}$$

So with (5.7) and (5.8), (5.6) becomes

$$R \le r \le R + h: \qquad \Delta\rho = \rho_w \tag{5.10a}$$

$$R - w \le r \le R - w^*: \quad \Delta\rho = \rho_m - \rho_w + \alpha\rho_m(T_m - T_0)\left(1 - \operatorname{erf}\left(\frac{\sqrt{\lambda}(R-r)}{c_0\sqrt{\phi}}\right)\right) \tag{5.10b}$$

$$R - L^* \le r \le R - w: \quad \Delta\rho = \alpha\rho_m(T_m - T_0)\left(-\operatorname{erf}\left(\frac{\sqrt{\lambda}(R-r)}{c_0\sqrt{\phi}}\right) + \operatorname{erf}\left(\frac{R-r}{c_0\sqrt{\phi}}\right)\right) \tag{5.10c}$$

$$R - L \le r \le R - L^*: \qquad \Delta\rho = \alpha\rho_m(T_m - T_0)\left(\operatorname{erf}\left(\frac{R-r}{c_0\sqrt{\phi}}\right) - 1\right) \tag{5.10d}$$

The total change of the product of inertia I_{xz} is given by

$$\Delta I_{xz} = (\Delta I_{xz})_{litho} + (\Delta I_{xz})_{water} \tag{5.11}$$

in which *litho* denotes the lithospheric contribution and *water* denotes the contribution from the increase in sea-level, while

$$\Delta I_{yz} = 0 \tag{5.12}$$

as the spreading ridge is symmetric with respect to the xz-plane.
The lithospheric contribution can now be calculated, using the expressions (5.10) for the various density differences. By using (2.22) it follows that

$$(\Delta I_{xz})_{litho} = -\int \Delta\rho x z \, dV =$$

$$= -\int_{\theta_1}^{\theta_2} d\theta \sin^2\theta \cos\theta \int_0^{\psi} d\phi \cos\phi \left\{ \int_{R-w}^{R-w^*} dr\, r^4 \left(\rho_m - \rho_w + \alpha\rho_m(T_m - T_0) \right.\right.$$

$$\left.\left. - \alpha\rho_m(T_m - T_0) \operatorname{erf}\left(\frac{\sqrt{\lambda}(R-r)}{c_0\sqrt{\phi}}\right)\right) + \int_{R-L^*}^{R-w} dr\, r^4 \alpha\rho_m(T_m - T_0)\left(- \operatorname{erf}\left(\frac{\sqrt{\lambda}(R-r)}{c_0\sqrt{\phi}}\right)\right.\right.$$

$$+\operatorname{erf}\left(\frac{R-r}{c_0\sqrt{\phi}}\right)\Bigg)+\int_{R-L}^{R-L^*} dr\, r^4\alpha\rho_m(T_m-T_0)\left(\operatorname{erf}\left(\frac{R-r}{c_0\sqrt{\phi}}\right)-1\right)\Bigg\}$$

$$+\int_{\theta_1}^{\theta_2} d\theta\,\sin^2\theta\cos\theta\int_0^{-\psi} d\phi\,\cos\phi\left\{\int_{R-w}^{R-w^*} dr\, r^4\left(\rho_m-\rho_w+\alpha\rho_m(T_m-T_0)\right.\right.$$

$$\left.-\alpha\rho_m(T_m-T_0)\operatorname{erf}\left(\frac{\sqrt{\lambda}(R-r)}{c_0\sqrt{-\phi}}\right)\right)+\int_{R-L^*}^{R-w} dr\, r^4\alpha\rho_m(T_m-T_0)\left(-\operatorname{erf}\left(\frac{\sqrt{\lambda}(R-r)}{c_0\sqrt{-\phi}}\right)\right.$$

$$\left.\left.+\operatorname{erf}\left(\frac{R-r}{c_0\sqrt{-\phi}}\right)\right)+\int_{R-L}^{R-L^*} dr\, r^4\alpha\rho_m(T_m-T_0)\left(\operatorname{erf}\left(\frac{R-r}{c_0\sqrt{-\phi}}\right)-1\right)\right\}\approx$$

$$\approx-\frac{1}{3}(\sin^3\theta_2-\sin^3\theta_1)\int_0^{\psi} d\phi\,\cos\phi\left\{(\rho_m-\rho_w)w-\alpha\rho_m(T_m-T_0)(L-w)\right.$$

$$+\alpha\rho_m(T_m-T_0)\int_w^L dr\,\operatorname{erf}\left(\frac{r}{c_0\sqrt{\phi}}\right)-\left((\rho_m-\rho_w)w^*-\alpha\rho_m(T_m-T_0)(L^*-w^*)\right.$$

$$\left.\left.+\alpha\rho_m(T_m-T_0)\int_{w^*}^{L^*} dr\,\operatorname{erf}\left(\frac{\sqrt{\lambda}r}{c_0\sqrt{\phi}}\right)\right)\right\}\cdot R^4$$

$$-\frac{1}{3}(\sin^3\theta_2-\sin^3\theta_1)\int_0^{\psi} d\phi\,\cos\phi\left\{2\alpha\rho_m(T_m-T_0)(1-\frac{1}{\lambda})L^2\right.$$

$$-2(\rho_m-\rho_w+\alpha\rho_m(T_m-T_0))(1-\frac{1}{\lambda})w^2+4\alpha\rho_m(T_m-T_0)\int_{w^*}^{L^*} dr\,r\,\operatorname{erf}\left(\frac{\sqrt{\lambda}r}{c_0\sqrt{\phi}}\right)$$

$$\left.-4\alpha\rho_m(T_m-T_0)\int_w^L dr\,r\,\operatorname{erf}\left(\frac{r}{c_0\sqrt{\phi}}\right)\right\}\cdot R^3$$

$$+\frac{1}{3}(\sin^3\theta_2-\sin^3\theta_1)\int_0^{-\psi}d\phi\cos\phi\left\{\left((\rho_m-\rho_w)w-\alpha\rho_m(T_m-T_0)(L-w)\right.\right.$$

$$\left.+\alpha\rho_m(T_m-T_0)\int_w^L dr\,\mathrm{erf}\left(\frac{r}{c_0\sqrt{-\phi}}\right)\right)-\left((\rho_m-\rho_w)w^*-\alpha\rho_m(T_m-T_0)(L^*-w^*)\right.$$

$$\left.\left.+\alpha\rho_m(T_m-T_0)\int_{w^*}^{L^*}dr\,\mathrm{erf}\left(\frac{\sqrt{\lambda}r}{c_0\sqrt{-\phi}}\right)\right)\right\}\cdot R^4$$

$$+\frac{1}{3}(\sin^3\theta_2-\sin^3\theta_1)\int_0^{-\psi}d\phi\cos\phi\left\{2\alpha\rho_m(T_m-T_0)(1-\frac{1}{\lambda})L^2\right.$$

$$-2(\rho_m-\rho_w+\alpha\rho_m(T_m-T_0))(1-\frac{1}{\lambda})w^2+4\alpha\rho_m(T_m-T_0)\int_{w^*}^{L^*}dr\,r\,\mathrm{erf}\left(\frac{\sqrt{\lambda}r}{c_0\sqrt{-\phi}}\right)$$

$$\left.-4\alpha\rho_m(T_m-T_0)\int_w^L dr\,r\,\mathrm{erf}\left(\frac{r}{c_0\sqrt{-\phi}}\right)\right\}\cdot R^3 \qquad (5.13)$$

Isostasy cancels the terms which are proportional to the fourth power of the radius **R**:

$$\rho_m L=\rho_w w+\int_{R-L}^{R-w}dr\,\rho_L(r,\phi)=\rho_w w+\int_{R-L}^{R-w}dr\rho_m(1+\alpha(T_m-T_0))$$

$$-\int_{R-L}^{R-w}dr\,\alpha\rho_m(T_m-T_0)\,\mathrm{erf}\left(\frac{R-r}{c_0\sqrt{\phi}}\right)=$$

$$=\rho_w w+\rho_m(1+\alpha(T_m-T_0))(L-w)-\alpha\rho_m(T_m-T_0)\int_w^L dr\,\mathrm{erf}\left(\frac{r}{c_0\sqrt{\phi}}\right)$$

leading to

$$(\rho_m-\rho_w)w-\alpha\rho_m(T_m-T_0)(L-w)+\alpha\rho_m(T_m-T_0)\int_w^L dr\,\mathrm{erf}\left(\frac{r}{c_0\sqrt{\phi}}\right)=0 \qquad (5.14)$$

In the same way

$$(\rho_m-\rho_w)w^*-\alpha\rho_m(T_m-T_0)(L^*-w^*)+\alpha\rho_m(T_m-T_0)\int_{w^*}^{L^*}dr\,\mathrm{erf}\left(\frac{\sqrt{\lambda}r}{c_0\sqrt{\phi}}\right)=0 \qquad (5.15)$$

So with (5.5), (5.14) and (5.15), (5.13) results in

$$(\Delta I_{xz})_{litho}\approx-\frac{1}{3}(1-\frac{1}{\lambda})(\sin^3\theta_2-\sin^3\theta_1)\int_0^{\Psi}d\phi\,\cos\phi\left\{-2(\rho_m-\rho_w)w^2\right.$$

$$\left.+2\alpha\rho_m(T_m-T_0)\left((L^2-w^2)-2c_0\,\phi\int_{w/(c_0\sqrt{\phi})}^{L/(c_0\sqrt{\phi})}dr\,r\,\mathrm{erf}(r)\right)\right\}\cdot R^3$$

$$+\frac{1}{3}(1-\frac{1}{\lambda})(\sin^3\theta_2-\sin^3\theta_1)\int_0^{-\Psi}d\phi\,\cos\phi\left\{-2(\rho_m-\rho_w)w^2\right.$$

$$\left.+2\alpha\rho_m(T_m-T_0)\left((L^2-w^2)-2c_0\,\phi\int_{w/(c_0\sqrt{-\phi})}^{L/(c_0\sqrt{-\phi})}dr\,r\,\mathrm{erf}(r)\right)\right\}\cdot R^3$$

As

$$\int dr\,r\,\mathrm{erf}(r)=\frac{2r^2-1}{4}\,\mathrm{erf}(r)+\frac{r}{2\sqrt{\pi}}\exp(-r^2)$$

this results in

$$(\Delta I_{xz})_{litho}\approx-\frac{1}{3}(1-\frac{1}{\lambda})(\sin^3\theta_2-\sin^3\theta_1)\int_0^{\Psi}d\phi\,\cos\phi\left\{-2(\rho_m-\rho_w)w^2\right.$$

$$+2\alpha\rho_m(T_m-T_0)(L^2-w^2)$$

$$\left.+\alpha\rho_m(T_m-T_0)\left(-2L^2\mathrm{erf}\left(\frac{L}{c_0\sqrt{\phi}}\right)+c_0^2\phi\,\mathrm{erf}\left(\frac{L}{c_0\sqrt{\phi}}\right)+2w^2\mathrm{erf}\left(\frac{w}{c_0\sqrt{\phi}}\right)\right.\right.$$

$$- c_0^2\phi\,\mathrm{erf}\left(\frac{w}{c_0\sqrt{\phi}}\right) - \frac{2}{\sqrt{\pi}}\,c_0\sqrt{\phi}\,L\exp\left(-\frac{L^2}{c_0^2\phi}\right) + \frac{2}{\sqrt{\pi}}\,c_0\sqrt{\phi}\,w\exp\left(-\frac{w^2}{c_0^2\phi}\right)\Bigg)\Bigg\}\cdot R^3$$

$$+ \tfrac{1}{3}\left(1-\frac{1}{\lambda}\right)(\sin^3\theta_2 - \sin^3\theta_1)\int_0^{-\psi} d\phi\,\cos\phi\left\{-2(\rho_m-\rho_w)w^2\right.$$

$$+ 2\alpha\rho_m(T_m - T_0)(L^2 - w^2)$$

$$+ \alpha\rho_m(T_m - T_0)\left(-2L^2\,\mathrm{erf}\left(\frac{L}{c_0\sqrt{-\phi}}\right) - c_0^2\phi\,\mathrm{erf}\left(\frac{L}{c_0\sqrt{-\phi}}\right) + 2w^2\,\mathrm{erf}\left(\frac{w}{c_0\sqrt{-\phi}}\right)\right.$$

$$\left.+ c_0^2\phi\,\mathrm{erf}\left(\frac{w}{c_0\sqrt{-\phi}}\right)\right)$$

$$\left.- \frac{2}{\sqrt{\pi}}\,c_0\sqrt{-\phi}\,L\exp\left(\frac{L^2}{c_0^2\phi}\right) + \frac{2}{\sqrt{\pi}}\,c_0\sqrt{-\phi}\,w\exp\left(\frac{w^2}{c_0^2\phi}\right)\Bigg)\right\}\cdot R^3$$

Substituting, according to (5.4),

$$w = c_1\sqrt{\phi} \qquad \text{and} \qquad L = c_2\sqrt{\phi} \tag{5.16}$$

with (c_0 given by (5.9))

$$c_1 = \frac{\alpha\rho_m(T_m - T_0)}{\sqrt{\pi}(\rho_m - \rho_w)}\cdot c_0 \tag{5.17}$$

and, assuming that the bottom of the lithosphere is situated at $T - T_0 = 0.9(T_m - T_0)$,

$$c_2 = \mathrm{erf}^{-1}(0.9)\cdot c_0 \tag{5.18}$$

gives

$$(\Delta I_{xz})_{\mathrm{litho}} \approx -\tfrac{1}{3}\left(1-\frac{1}{\lambda}\right)(\sin^3\theta_2 - \sin^3\theta_1)\left\{\int_0^{\psi} d\phi\,\phi\,\cos\phi + \int_0^{-\psi} d\phi\,\phi\,\cos\phi\right\}\cdot$$

$$\cdot\left\{-2(\rho_m-\rho_w)c_1^2 + 2\alpha\rho_m(T_m - T_0)(c_2^2 - c_1^2) + \alpha\rho_m(T_m - T_0)\left(-2c_2^2\,\mathrm{erf}\left(\frac{c_2}{c_0}\right)\right.\right.$$

$$+ c_0^2 \operatorname{erf}\left(\frac{c_2}{c_0}\right) + 2c_1^2 \operatorname{erf}\left(\frac{c_1}{c_0}\right) - c_0^2 \operatorname{erf}\left(\frac{c_1}{c_0}\right)$$

$$- \frac{2}{\sqrt{\pi}} c_0 c_2 \exp\left(-\frac{c_2^2}{c_0^2}\right) + \frac{2}{\sqrt{\pi}} c_0 c_1 \exp\left(-\frac{c_1^2}{c_0^2}\right)\Bigg\} \cdot R^3 =$$

$$= -B\left(1 - \frac{1}{\lambda}\right)(\sin^3\theta_2 - \sin^3\theta_1)(\psi \sin\psi + \cos\psi - 1) \cdot R^3 \qquad (5.19)$$

with

$$B \equiv \frac{2}{3}\Bigg\{-2(\rho_m - \rho_w)c_1^2 + \alpha\rho_m(T_m - T_0)\Bigg(2(c_2^2 - c_1^2) - (2c_2^2 - c_0^2)\operatorname{erf}\left(\frac{c_2}{c_0}\right)$$

$$+ (2c_1^2 - c_0^2)\operatorname{erf}\left(\frac{c_1}{c_0}\right)\Bigg) - \frac{2c_0}{\sqrt{\pi}}\left(c_2 \exp\left(-\frac{c_2^2}{c_0^2}\right) - c_1 \exp\left(-\frac{c_1^2}{c_0^2}\right)\right)\Bigg\} =$$

$$= \frac{2}{3}(\rho_m - \rho_w)\Bigg\{-2c_1^2 + \sqrt{\pi}\frac{c_1}{c_0}\Bigg(2(c_2^2 - c_1^2) - (2c_2^2 - c_0^2)\operatorname{erf}\left(\frac{c_2}{c_0}\right)$$

$$+ (2c_1^2 - c_0^2)\operatorname{erf}\left(\frac{c_1}{c_0}\right)\Bigg) - 2c_1\left(c_2 \exp\left(-\frac{c_2^2}{c_0^2}\right) - c_1 \exp\left(-\frac{c_1^2}{c_0^2}\right)\right)\Bigg\} \qquad (5.20)$$

The increase of the eustatic sea-level gives a contribution

$$(\Delta I_{xz})_{water} = -\int \rho_w xz\,dV =$$

$$= -\rho_w \int_{\theta_1}^{\theta_2} d\theta \int_{-\psi}^{\psi} d\phi \int_{R}^{R+h} dr\, r^4 \sin^2\theta \cos\theta \cos\phi =$$

$$= -\frac{2}{3}\rho_w(\sin^3\theta_2 - \sin^3\theta_1)\sin\psi \cdot \frac{1}{5}\left((R+h)^5 - R^5\right) \approx$$

$$\approx -\frac{2}{3}\rho_w(\sin^3\theta_2 - \sin^3\theta_1)\sin\psi\,(hR^4 + 2h^2R^3) \qquad (5.21)$$

with the increase in sea-level h to be determined from conservation of oceanic water, assuming that the amount of continental flooding is negligible. If V_{oc}^{pre} denotes the volume of the oceanic basin before the increased mid-oceanic spreading rate commenced and V_{oc}^{post} after the bathymetry has accommodated itself to the increased spreading rate, then

$$V_{oc}^{pre} = V_{oc}^{post} \tag{5.22}$$

with

$$V_{oc}^{pre} = 2 \int_{\theta_1}^{\theta_2} d\theta \int_0^{\psi} d\phi \int_{R-w}^{R} dr\, r^2 \sin\theta = 2(-\cos\theta_2 + \cos\theta_1) \int_0^{\psi} d\phi \int_{R-w}^{R} dr\, r^2$$

$$V_{oc}^{post} = 2 \int_{\theta_1}^{\theta_2} d\theta \int_0^{\psi} d\phi \int_{R-w^*}^{R+h} dr\, r^2 \sin\theta = 2(-\cos\theta_2 + \cos\theta_1) \int_0^{\psi} d\phi \int_{R-w^*}^{R+h} dr\, r^2$$

Now, with (5.16),

$$\int_{R-w}^{R} dr\, r^2 = \frac{1}{3}R^3 - \frac{1}{3}(R-w)^3 \approx w \cdot R^2 = c_1\sqrt{\phi} \cdot R^2$$

and, with (5.5),

$$\int_{R-w^*}^{R+h} dr\, r^2 = \frac{1}{3}(R+h)^3 - \frac{1}{3}(R-w^*)^3 \approx (h+w^*) \cdot R^2 = (h + \frac{w}{\sqrt{\lambda}}) \cdot R^2 =$$

$$= (h + \frac{c_1}{\sqrt{\lambda}}\sqrt{\phi}) \cdot R^2$$

So (5.22) amounts to

$$\int_0^{\psi} d\phi\, c_1\sqrt{\phi} \approx \int_0^{\psi} d\phi\, (h + \frac{c_1}{\sqrt{\lambda}}\sqrt{\phi})$$

or

$$h \approx c_1(1 - \frac{1}{\sqrt{\lambda}}) \frac{\int_0^{\psi} d\phi\sqrt{\phi}}{\int_0^{\psi} d\phi} = \frac{2}{3} c_1(1 - \frac{1}{\sqrt{\lambda}})\sqrt{\psi} \tag{5.23}$$

The question now arises whether the R^4-effect of the sea-level rise on polar wander is isostatically compensated. Such an isostatic compensation is probably established by flow of mantle material from below the oceanic region towards the surrounding continent. As a consequence, the sea-level which was increased by the raised bathymetry will decrease, while the continental areas will rise. On the other hand, as the process by which the bathymetry is raised is related to a large convective circulation in which deep mantle regions are likely to take part (the subducting slabs at least reach the 670 kilometer discontinuity), such an isostatic compensation might well not take place as deeper mantle regions might supply the dynamical support.
Neglecting the isostatic compensation between oceanic and continental areas, the increased sea-level gives a contribution to the shift of the polar axis which is proportional to the fourth power of the radius. From substituting (5.23) in (5.21) it follows that

$$(\Delta I_{xz})_{water} \approx -\frac{2}{3}\rho_w(\sin^3\theta_2 - \sin^3\theta_1)\sin\psi \cdot hR^4$$

$$\approx -\frac{4}{9}\rho_w c_1(1 - \frac{1}{\sqrt{\lambda}})(\sin^3\theta_2 - \sin^3\theta_1)\sqrt{\psi}\sin\psi \cdot R^4 \qquad (5.24)$$

So for $\psi \leq \psi_0$, according to (2.21) and (2.22) the total amount of polar shift for a rigid Earth is given in radians by

$$\left(\frac{\Delta I_{xz}}{C-A}, \frac{\Delta I_{yz}}{C-A}\right)$$

with, from (5.19) and (5.24) in (5.11),

$$\Delta I_{xz} \approx -\frac{4}{9}\rho_w c_1(1 - \frac{1}{\sqrt{\lambda}})(\sin^3\theta_2 - \sin^3\theta_1)\sqrt{\psi}\sin\psi \cdot R^4$$

$$-B(1 - \frac{1}{\lambda})(\sin^3\theta_2 - \sin^3\theta_1)(\psi\sin\psi + \cos\psi - 1) \cdot R^3 \qquad (5.25)$$

and, according to (5.12),

$$\Delta I_{yz} = 0$$

The contribution proportional to the third power in the radius of $(\Delta I_{xz})_{water}$ is negligible with respect to $(\Delta I_{xz})_{litho}$, but this term on its turn is not necessarily negligible with respect to the contribution proportional to the fourth power in the radius of $(\Delta I_{xz})_{water}$.

The increase in spreading rate also changes the length of day. This amount is to be determined from (2.23), with

$$\Delta I_{zz} = (\Delta I_{zz})_{\text{litho}} + (\Delta I_{zz})_{\text{water}} \tag{5.26}$$

The lithospheric contribution to the change in the inertia component is given by (see (2.24))

$$(\Delta I_{zz})_{\text{litho}} = \int \Delta\rho(x^2 + y^2)dV$$

$$= \int_{\theta_1}^{\theta_2} d\theta \sin^3\theta \int_0^{\psi} d\phi \left\{ \int_{R-w}^{R-w^*} dr\, r^4 \left(\rho_m - \rho_w + \alpha\rho_m(T_m - T_0) \right.\right.$$

$$\left. - \alpha\rho_m(T_m - T_0)\,\text{erf}\left(\frac{\sqrt{\lambda}(R-r)}{c_0\sqrt{\phi}} \right) \right) + \int_{R-L^*}^{R-w} dr\, r^4 \alpha\rho_m(T_m - T_0) \left(- \text{erf}\left(\frac{\sqrt{\lambda}(R-r)}{c_0\sqrt{\phi}} \right) \right.$$

$$\left. \left. + \text{erf}\left(\frac{R-r}{c_0\sqrt{\phi}} \right) \right) + \int_{R-L}^{R-L^*} dr\, r^4 \alpha\rho_m(T_m - T_0) \left(\text{erf}\left(\frac{R-r}{c_0\sqrt{\phi}} \right) - 1 \right) \right\}$$

$$- \int_{\theta_1}^{\theta_2} d\theta \sin^3\theta \int_0^{-\psi} d\phi \left\{ \int_{R-w}^{R-w^*} dr r^4 \left(\rho_m - \rho_w + \alpha\rho_m(T_m - T_0) \right.\right.$$

$$\left. - \alpha\rho_m(T_m - T_0)\,\text{erf}\left(\frac{\sqrt{\lambda}(R-r)}{c_0\sqrt{-\phi}} \right) \right) + \int_{R-L^*}^{R-w} dr\, r^4 \alpha\rho_m(T_m - T_0) \left(- \text{erf}\left(\frac{\sqrt{\lambda}(R-r)}{c_0\sqrt{-\phi}} \right) \right.$$

$$\left. \left. + \text{erf}\left(\frac{R-r}{c_0\sqrt{-\phi}} \right) \right) + \int_{R-L}^{R-L^*} dr\, r^4 \alpha\rho_m(T_m - T_0) \left(\text{erf}\left(\frac{R-r}{c_0\sqrt{-\phi}} \right) - 1 \right) \right\} \tag{5.27}$$

It can be readily verified from the derivation of the amount of polar shift that (5.27) results in

$$(\Delta I_{zz})_{\text{litho}} \simeq -\frac{1}{2} B\left(1 - \frac{1}{\lambda}\right)\left(3(\cos\theta_2 - \cos\theta_1) - (\cos^3\theta_2 - \cos^3\theta_1) \right).$$

$$\cdot \left\{ \int_0^{\psi} d\phi\, \phi + \int_0^{-\psi} d\phi\, \phi \right\} \cdot R^3 =$$

$$= -\frac{1}{2} B(1 - \frac{1}{\lambda}) \Big(3(\cos\theta_2 - \cos\theta_1) - (\cos^3\theta_2 - \cos^3\theta_1) \Big) \psi^2 \cdot R^3 \quad (5.28)$$

The sea-level rise contributes

$$(\Delta I_{zz})_{water} = \int \rho_w (x^2 + y^2)\, dV =$$

$$= \rho_w \int_{\theta_1}^{\theta_2} d\theta \int_{-\psi}^{\psi} d\phi \int_{R}^{R+h} dr\, r^4 \sin^3\theta \approx$$

$$\approx -\frac{2}{3} \rho_w \Big(3(\cos\theta_2 - \cos\theta_1) - (\cos^3\theta_2 - \cos^3\theta_1) \Big) \psi\, (hR^4 + 2h^2R^3) \quad (5.29)$$

Neglecting isostatic compensation for the increased sea-level gives from (5.23) in (5.29)

$$(\Delta I_{zz})_{water} \approx -\frac{4}{9} \rho_w c_1 (1 - \frac{1}{\sqrt{\lambda}}) \Big(3(\cos\theta_2 - \cos\theta_1) - (\cos^3\theta_2 - \cos^3\theta_1) \Big) \psi^{3/2} \cdot R^4$$

So for $\psi \le \psi_0$, the increase in the length of day is approximately given by

$$-\frac{4\rho_w c_1}{9C} (1 - \frac{1}{\sqrt{\lambda}}) \Big(3(\cos\theta_2 - \cos\theta_1) - (\cos^3\theta_2 - \cos^3\theta_1) \Big) \psi^{3/2} \cdot R^4 \cdot 86164 \text{ s}$$

$$-\frac{B}{2C} (1 - \frac{1}{\lambda}) \Big(3(\cos\theta_2 - \cos\theta_1) - (\cos^3\theta_2 - \cos^3\theta_1) \Big) \psi^2 \cdot R^3 \cdot 86164 \text{ s} \quad (5.30)$$

Case II : $\psi_0 \le \psi \le \lambda\psi_0$

The density difference $\Delta\rho(r, \phi)$ is given by

$$R \le r \le R + h: \qquad \Delta\rho = \rho_w \quad (5.31a)$$

$$R - w \le r \le R - w^*: \qquad \Delta\rho = \rho_L^*(r, \phi) - \rho_w \quad (5.31b)$$

$$R - L^* \le r \le R - w: \qquad \Delta\rho = \rho_L^*(r, \phi) - \rho_L(r) \quad (5.31c)$$

$$R - L \le r \le R - L^*: \qquad \Delta\rho = \rho_m - \rho_L(r) \quad (5.31d)$$

with, using (5.3),

$$\rho_L(r) = \rho_m \left\{ 1 - \alpha(T_m - T_0)\left(\operatorname{erf}\left(\frac{R - r}{c_0\sqrt{\psi_0}} \right) - 1 \right) \right\} \tag{5.32}$$

and

$$\rho_L^*(r,\phi) = \rho_m \left\{ 1 - \alpha(T_m - T_0)\left(\operatorname{erf}\left(\frac{\sqrt{\lambda}(R - r)}{c_0\sqrt{\phi}} \right) - 1 \right) \right\} \tag{5.33}$$

So with (5.32) and (5.33), (5.31) becomes

$$R \le r \le R + h: \qquad \Delta\rho = \rho_w \tag{5.34a}$$

$$R - w \le r \le R - w^*: \quad \Delta\rho = \rho_m - \rho_w + \alpha\rho_m(T_m - T_0)\left(1 - \operatorname{erf}\left(\frac{\sqrt{\lambda}(R - r)}{c_0\sqrt{\phi}} \right) \right) \tag{5.34b}$$

$$R - L^* \le r \le R - w: \quad \Delta\rho = \alpha\rho_m(T_m - T_0)\left(-\operatorname{erf}\left(\frac{\sqrt{\lambda}(R - r)}{c_0\sqrt{\psi_0}} \right) + \operatorname{erf}\left(\frac{R - r}{c_0\sqrt{\phi}} \right) \right) \tag{5.34c}$$

$$R - L \le r \le R - L^*: \qquad \Delta\rho = \alpha\rho_m(T_m - T_0)\left(\operatorname{erf}\left(\frac{R - r}{c_0\sqrt{\psi_0}} \right) - 1 \right) \tag{5.35d}$$

(5.11) and (5.12) give again the total changes in the products of inertia.
For $0 \le \phi \le \psi_0$, the lithospheric contribution to the change in the moment of inertia results from (5.19) as

$$(\Delta I_{xz})_{litho} = -B\left(1 - \frac{1}{\lambda}\right)(\sin^3\theta_2 - \sin^3\theta_1)(\psi_0 \sin\psi_0 + \cos\psi_0 - 1) \cdot R^3 \tag{5.36}$$

while for $\psi_0 \le \phi \le \lambda\psi_0$

$$(\Delta I_{xz})_{litho} = -\int \Delta\rho xz dV =$$

$$= -\int_{\theta_1}^{\theta_2} d\theta \sin^2\theta \cos\theta \int_{\psi_0}^{\psi} d\phi \cos\phi \left\{ \int_{R-w}^{R-w^*} dr\, r^4 \left(\rho_m - \rho_w + \alpha\rho_m(T_m - T_0) \right. \right.$$

$$- \alpha\rho_m(T_m - T_0)\,\mathrm{erf}\left(\frac{\sqrt{\lambda}(R-r)}{c_0\sqrt{\phi}}\right)\Bigg) + \int_{R-L^*}^{R-w} dr\, r^4 \alpha\rho_m(T_m - T_0)\Bigg(-\mathrm{erf}\left(\frac{\sqrt{\lambda}(R-r)}{c_0\sqrt{\phi}}\right)$$

$$+ \mathrm{erf}\left(\frac{R-r}{c_0\sqrt{\psi_0}}\right)\Bigg) + \int_{R-L}^{R-L^*} dr\, r^4 \alpha\rho_m(T_m - T_0)\left(\mathrm{erf}\left(\frac{R-r}{c_0\sqrt{\psi_0}}\right) - 1\right)\Bigg\}$$

$$+ \int_{\theta_1}^{\theta_2} d\theta \sin^2\theta\cos\theta \int_{-\psi_0}^{-\psi} d\phi \cos\phi \Bigg\{ \int_{R-w}^{R-w^*} dr\, r^4 \Big(\rho_m - \rho_w + \alpha\rho_m(T_m - T_0)$$

$$- \alpha\rho_m(T_m - T_0)\,\mathrm{erf}\left(\frac{\sqrt{\lambda}(R-r)}{c_0\sqrt{-\phi}}\right)\Bigg) + \int_{R-L^*}^{R-w} dr\, r^4 \alpha\rho_m(T_m - T_0)\Bigg(-\mathrm{erf}\left(\frac{\sqrt{\lambda}(R-r)}{c_0\sqrt{-\phi}}\right)$$

$$+ \mathrm{erf}\left(\frac{R-r}{c_0\sqrt{\psi_0}}\right)\Bigg) + \int_{R-L}^{R-L^*} dr\, r^4 \alpha\rho_m(T_m - T_0)\left(\mathrm{erf}\left(\frac{R-r}{c_0\sqrt{\psi_0}}\right) - 1\right)\Bigg\}$$

$$\approx -\frac{1}{3}(\sin^3\theta_2 - \sin^3\theta_1) \int_{-\psi_0}^{\psi} d\phi \cos\phi \Bigg\{\Bigg((\rho_m - \rho_w)w - \alpha\rho_m(T_m - T_0)(L - w)$$

$$+ \alpha\rho_m(T_m - T_0) \int_w^L dr\, \mathrm{erf}\left(\frac{r}{c_0\sqrt{\psi_0}}\right) - \Bigg((\rho_m - \rho_w)w^* - \alpha\rho_m(T_m - T_0)(L^* - w^*)$$

$$+ \alpha\rho_m(T_m - T_0) \int_{w^*}^{L^*} dr\, \mathrm{erf}\left(\frac{\sqrt{\lambda}r}{c_0\sqrt{\phi}}\right)\Bigg)\Bigg\} \cdot R^4$$

$$- \frac{1}{3}(\sin^3\theta_2 - \sin^3\theta_1) \int_{\psi_0}^{\psi} d\phi \cos\phi \Bigg\{2\alpha\rho_m(T_m - T_0)\left(1 - \frac{1}{\lambda}\right)L^2$$

$$- 2(\rho_m - \rho_w + \alpha\rho_m(T_m - T_0))\left(1 - \frac{1}{\lambda}\right)w^2 + 4\alpha\rho_m(T_m - T_0) \int_{w^*}^{L^*} dr\, r\, \mathrm{erf}\left(\frac{\sqrt{\lambda}r}{c_0\sqrt{\phi}}\right)$$

$$- 4\alpha\rho_m(T_m - T_0)\int_w^L dr\, r\, \mathrm{erf}\left(\frac{r}{c_0\sqrt{\psi_0}}\right)\Bigg\} \cdot R^3$$

$$+ \frac{1}{3}(\sin^3\theta_2 - \sin^3\theta_1)\int_{-\psi_0}^{-\psi} d\phi\, \cos\phi \Bigg\{\Bigg((\rho_m - \rho_w)w - \alpha\rho_m(T_m - T_0)(L - w)$$

$$+ \alpha\rho_m(T_m - T_0)\int_w^L dr\, \mathrm{erf}\left(\frac{r}{c_0\sqrt{\psi_0}}\right)\Bigg) - \Bigg((\rho_m - \rho_w)w^* - \alpha\rho_m(T_m - T_0)(L^* - w^*)$$

$$+ \alpha\rho_m(T_m - T_0)\int_{w^*}^{L^*} dr\, \mathrm{erf}\left(\frac{\sqrt{\lambda}r}{c_0\sqrt{-\phi}}\right)\Bigg)\Bigg\} \cdot R^4$$

$$+ \frac{1}{3}(\sin^3\theta_2 - \sin^3\theta_1)\int_{-\psi_0}^{-\psi} d\phi\, \cos\phi \Bigg\{2\alpha\rho_m(T_m - T_0)(1 - \frac{1}{\lambda})L^2$$

$$- 2(\rho_m - \rho_w + \alpha\rho_m(T_m - T_0))(1 - \frac{1}{\lambda})w^2 + 4\alpha\rho_m(T_m - T_0)\int_{w^*}^{L^*} dr\, r\, \mathrm{erf}\left(\frac{\sqrt{\lambda}r}{c_0\sqrt{-\phi}}\right)$$

$$- 4\alpha\rho_m(T_m - T_0)\int_w^L dr\, r\, \mathrm{erf}\left(\frac{r}{c_0\sqrt{\psi_0}}\right)\Bigg\} \cdot R^3 \qquad (5.37)$$

Again, isostasy cancels the terms which are proportional to the fourth power of the radius R:

$$\rho_m L = \rho_w w + \int_{R-L}^{R-w} dr\, \rho_L(r) = \rho_w w + \int_{R-L}^{R-w} dr\, \rho_m(1 + \alpha(T_m - T_0))$$

$$- \int_{R-L}^{R-w} dr\alpha\rho_m(T_m - T_0)\, \mathrm{erf}\left(\frac{R - r}{c_0\sqrt{\psi_0}}\right)$$

$$= \rho_w w + \rho_m(1 + \alpha(T_m - T_0))(L - w) - \alpha\rho_m(T_m - T_0)\int_w^L dr\, \mathrm{erf}\left(\frac{r}{c_0\sqrt{\psi_0}}\right)$$

leading to

$$(\rho_m - \rho_w)w - \alpha\rho_m(T_m - T_0)(L - w) + \alpha\rho_m(T_m - T_0)\int_w^L dr\,\mathrm{erf}\left(\frac{r}{c_0\sqrt{\psi_0}}\right) = 0 \qquad (5.38)$$

The same expression (5.15) for the situation after the increased spreading applies in this case.

So with

$$w = c_1\sqrt{\psi_0} \quad \text{and} \quad L = c_2\sqrt{\psi_0} \qquad (5.39)$$

and, using (5.5),

$$w^* = \frac{c_1}{\sqrt{\lambda}}\sqrt{\phi} \quad \text{and} \quad L^* = \frac{c_2}{\sqrt{\lambda}}\sqrt{\phi} \qquad (5.40)$$

(5.15) and (5.38) in (5.37) result in

$$(\Delta I_{xz})_{litho} \approx -B(1 - \frac{1}{\lambda})(\sin^3\theta_2 - \sin^3\theta_1)\psi_0(\sin\psi - \sin\psi_0)\cdot R^3$$

$$- D\,\frac{1}{\lambda}(\sin^3\theta_2 - \sin^3\theta_1)\,((\psi - \psi_0)\sin\psi + \cos\psi - \cos\psi_0)\cdot R^3 \qquad (5.41)$$

with

$$D = B - \frac{4}{3}(\rho_m - \rho_w)\left(-c_1^2 + \sqrt{\pi}\,\frac{c_1}{c_0}(c_2^2 - c_1^2)\right) \qquad (5.42)$$

and B given by (5.20).

The increase of the eustatic sea-level gives a contribution

$$(\Delta I_{xz})_{water} \approx -\frac{2}{3}\rho_w(\sin^3\theta_2 - \sin^3\theta_1)\sin\psi\,(hR^4 + 2h^2R^3) \qquad (5.43)$$

in which the increase in sea-level h follows from (5.22), with

$$V_{oc}^{pre} = \int_{\theta_1}^{\theta_2} d\theta \int_{-\psi}^{\psi} d\phi \int_{R-w}^{R} dr\, r^2 \sin\theta =$$

$$= 2(-\cos\theta_2 + \cos\theta_1)\left\{\int_0^{\psi_0} d\phi + \int_{\psi_0}^{\psi} d\phi\right\}\int_{R-w}^{R} dr\, r^2 \qquad (5.44)$$

$$V_{oc}^{post} = \int_{\theta_1}^{\theta_2} d\theta \int_{-\psi}^{\psi} d\phi \int_{R-w^*}^{R+h} dr\, r^2 \sin\theta =$$

$$= 2(-\cos\theta_2 + \cos\theta_1) \int_{0}^{\psi} d\phi \int_{R-w^*}^{R+h} dr\, r^2 \tag{5.45}$$

Now, with (5.16) and (5.39),

$$\int_{R-w}^{R} dr\, r^2 = \frac{1}{3}R^3 - \frac{1}{3}(R-w)^3 \approx w \cdot R^2 = c_1\sqrt{\phi} \cdot R^2 \quad \text{for } 0 \le \phi \le \psi_0$$

$$\int_{R-w}^{R} dr\, r^2 \approx c_1\sqrt{\psi_0} \cdot R^2 \quad \text{for } \psi_0 \le \phi \le \psi$$

and, with (5.40),

$$\int_{R-w^*}^{R+h} dr\, r^2 = \frac{1}{3}(R+h)^3 - \frac{1}{3}(R-w^*)^3 \approx (h+w^*) \cdot R^2 =$$

$$= (h + \frac{c_1}{\sqrt{\lambda}}\sqrt{\phi}) \cdot R^2$$

So (5.22) amounts to

$$\int_{0}^{\psi_0} d\phi c_1\sqrt{\phi} + \int_{\psi_0}^{\psi} d\phi c_1\sqrt{\psi_0} \approx \int_{0}^{\psi} d\phi (h + \frac{c_1}{\sqrt{\lambda}}\sqrt{\phi})$$

or

$$h \approx c_1 \frac{\int_{0}^{\psi_0} d\phi\sqrt{\phi} + \int_{\psi_0}^{\psi} d\phi\sqrt{\psi_0} - \frac{1}{\sqrt{\lambda}} \int_{0}^{\psi} d\phi\sqrt{\phi}}{\int_{0}^{\psi} d\phi} = \frac{1}{3}c_1\left(3\sqrt{\psi_0} - \frac{\psi_0^{3/2}}{\psi} - \frac{2}{\sqrt{\lambda}}\sqrt{\psi}\right) \tag{5.46}$$

If isostatic compensation of the increased sea-level is neglected again, then from substituting (5.46) in (5.43) it follows that

$$(\Delta I_{xz})_{water} \approx -\frac{2}{3}\rho_w(\sin^3\theta_2 - \sin^3\theta_1)\sin\psi \cdot hR^4 \approx$$

$$\approx -\frac{2}{9}\rho_w c_1(\sin^3\theta_2 - \sin^3\theta_1)\left(3\sqrt{\psi_0} - \frac{\psi_0^{3/2}}{\psi} - \frac{2}{\sqrt{\lambda}}\sqrt{\psi}\right)\sin\psi \cdot R^4 \qquad (5.47)$$

So for $\psi_0 \le \psi \le \lambda\psi_0$, the total shift of the rotation axis is given in radians by

$$\left(\frac{\Delta I_{xz}}{C-A}, \frac{\Delta I_{yz}}{C-A}\right)$$

with, from (5.42) and (5.47) in (5.11),

$$\Delta I_{xz} \approx -\frac{2}{9}\rho_w c_1(\sin^3\theta_2 - \sin^3\theta_1)\left(3\sqrt{\psi_0} - \frac{\psi_0^{3/2}}{\psi} - \frac{2}{\sqrt{\lambda}}\sqrt{\psi}\right)\sin\psi \cdot R^4$$

$$-B(1-\frac{1}{\lambda})(\sin^3\theta_2 - \sin^3\theta_1)(\psi_0 \sin\psi + \cos\psi_0 - 1)\cdot R^3$$

$$-D\,\frac{1}{\lambda}(\sin^3\theta_2 - \sin^3\theta_1)\,((\psi-\psi_0)\sin\psi + \cos\psi - \cos\psi_0)\cdot R^3 \qquad (5.48)$$

and, according to (5.12),

$$\Delta I_{yz} = 0$$

Analogous as in the case $\psi \le \psi_0$, the increase in the length of day can be easily derived by considering the derivation of the shift of the rotation axis. The lithospheric contribution to the change in the inertia component is given by

$$(\Delta I_{zz})_{litho} = \int \Delta\rho(x^2+y^2)dV \approx$$

$$\approx -\frac{1}{2}B(1-\frac{1}{\lambda})\Big(3(\cos\theta_2 - \cos\theta_1) - (\cos^3\theta_2 - \cos^3\theta_1)\Big)\psi_0^2 \cdot R^3$$

$$-\frac{1}{2}(D-B)\,(1-\frac{1}{\lambda})\Big(3(\cos\theta_2 - \cos\theta_1) - (\cos^3\theta_2 - \cos^3\theta_1)\Big)\cdot$$

$$\cdot\,\psi_0\left\{\int_{\psi_0}^{\psi} d\phi - \int_{-\psi_0}^{-\psi} d\phi\right\}\cdot R^3$$

$$-\frac{1}{2}\,D\left(3(\cos\theta_2-\cos\theta_1)-(\cos^3\theta_2-\cos^3\theta_1)\right)\cdot$$

$$\cdot\left\{\frac{1}{\lambda}\int_{\psi_0}^{\psi}d\phi\,\phi+\frac{1}{\lambda}\int_{-\psi_0}^{-\psi}d\phi\,\phi-\psi_0\int_{\psi_0}^{\psi}d\phi+\psi_0\int_{-\psi_0}^{-\psi}d\phi\right\}\cdot R^3=$$

$$=\frac{1}{2}\,B(1-\frac{1}{\lambda})\left(3(\cos\theta_2-\cos\theta_1)-(\cos^3\theta_2-\cos^3\theta_1)\right)\psi_0\,(2\psi-3\psi_0)\cdot R^3$$

$$-\frac{1}{2}\,D\,\frac{1}{\lambda}\left(3(\cos\theta_2-\cos\theta_1)-(\cos^3\theta_2-\cos^3\theta_1)\right)(\psi-\psi_0)^2\cdot R^3 \qquad (5.49)$$

The contribution from the increased sea-level (no isostatic compensation) amounts, substituting (5.46),

$$(\Delta I_{zz})_{water}=\int\rho_w(x^2+y^2)dV\approx$$

$$\approx-\frac{2}{3}\,\rho_w\left(3(\cos\theta_2-\cos\theta_1)-(\cos^3\theta_2-\cos^3\theta_1)\right)\psi\cdot hR^4\approx$$

$$\approx-\frac{2}{9}\,\rho_w c_1\left(3(\cos\theta_2-\cos\theta_1)-(\cos^3\theta_2-\cos^3\theta_1)\right)\cdot$$

$$\cdot\left(3\sqrt{\psi_0}\,\psi-\psi_0^{3/2}-\frac{2}{\sqrt{\lambda}}\,\psi^{3/2}\right)\cdot R^4 \qquad (5.50)$$

So for $\psi_0\le\psi\le\lambda\psi_0$, the increase in the length of day is approximately given by

$$-\frac{2\rho_w c_1}{9C}\left(3(\cos\theta_2-\cos\theta_1)-(\cos^3\theta_2-\cos^3\theta_1)\right)\cdot$$

$$\cdot\left(3\sqrt{\psi_0}\,\psi-\psi_0^{3/2}-\frac{2}{\sqrt{\lambda}}\,\psi^{3/2}\right)\cdot R^4\cdot 86164\ s$$

$$+\frac{B}{2C}(1-\frac{1}{\lambda})\left(3(\cos\theta_2-\cos\theta_1)-(\cos^3\theta_2-\cos^3\theta_1)\right)\psi_0\,(2\psi-3\psi_0)\cdot R^3\cdot 86164\ s$$

$$-\frac{D}{2C}\,\frac{1}{\lambda}\left(3(\cos\theta_2-\cos\theta_1)-(\cos^3\theta_2-\cos^3\theta_1)\right)(\psi-\psi_0)^2\cdot R^3\cdot 86164\ s \qquad (5.51)$$

Case III : $\psi \geq \lambda\psi_0$

In the case $\psi \geq \lambda\psi_0$, the volume of the ocean basin before the increased spreading is given by (5.44), while the volume of the ocean basin after the increased spreading reads

$$V_{oc}^{post} = \int_{\theta_1}^{\theta_2} d\theta \int_{-\psi}^{\psi} d\phi \int_{R-w^*}^{R+h} dr\, r^2 \sin\theta =$$

$$= 2(-\cos\theta_2 + \cos\theta_1)\left\{ \int_{0}^{\lambda\psi_0} d\phi + \int_{\lambda\psi_0}^{\psi} d\phi \right\} \int_{R-w^*}^{R+h} dr\, r^2 \qquad (5.52)$$

with, using (5.16) and (5.39),

$$\int_{R-w}^{R} dr\, r^2 = \frac{1}{3}R^3 - \frac{1}{3}(R-w)^3 \approx w \cdot R^2 = c_1\sqrt{\phi} \cdot R^2 \quad \text{for } 0 \leq \phi \leq \psi_0$$

$$\int_{R-w}^{R} dr\, r^2 \approx c_1\sqrt{\psi_0} \cdot R^2 \quad \text{for } \psi_0 \leq \phi \leq \psi$$

and, with (5.40),

$$\int_{R-w^*}^{R+h} dr\, r^2 = \frac{1}{3}(R+h)^3 - \frac{1}{3}(R-w^*)^3 \approx (h+w^*) \cdot R^2 =$$

$$= (h + \frac{c_1}{\sqrt{\lambda}}\sqrt{\phi}) \cdot R^2 \quad \text{for } 0 \leq \phi \leq \lambda\psi_0$$

$$\int_{R-w^*}^{R+h} dr\, r^2 \approx (h + c_1\sqrt{\psi_0}) \cdot R^2 \quad \text{for } \lambda\psi_0 \leq \phi \leq \psi$$

Condition (5.22) then gives

$$\int_{0}^{\psi_0} d\phi c_1\sqrt{\phi} + \int_{\psi_0}^{\psi} d\phi c_1\sqrt{\psi_0} \approx \int_{0}^{\lambda\psi_0} d\phi(h + \frac{c_1}{\sqrt{\lambda}}\sqrt{\phi}) + \int_{\lambda\psi_0}^{\psi} d\phi(h + c_1\sqrt{\psi_0})$$

or

$$h \approx c_1 \frac{\int_0^{\psi_0} d\phi\sqrt{\phi} + \int_{\psi_0}^{\psi} d\phi\sqrt{\psi_0} - \frac{1}{\sqrt{\lambda}} \int_0^{\lambda\psi_0} d\phi\sqrt{\phi} - \int_{\lambda\psi_0}^{\psi} d\phi\sqrt{\psi_0}}{\int_0^{\psi} d\phi} = \frac{1}{3} c_1(\lambda - 1) \frac{\psi_0^{3/2}}{\psi} \quad (5.53)$$

So in the case $\psi \geq \lambda\psi_0$, the total amount of polar shift is given in radians by

$$\left(\frac{\Delta I_{xz}}{C - A}, \frac{\Delta I_{yz}}{C - A} \right)$$

with, from (5.41), (5.43) and (5.53) in (5.11),

$$\Delta I_{xz} \approx -\frac{2}{9} \rho_w c_1(\lambda - 1)(\sin^3\theta_2 - \sin^3\theta_1) \frac{\psi_0^{3/2}}{\psi} \sin\psi \cdot R^4$$

$$- B(1 - \frac{1}{\lambda})(\sin^3\theta_2 - \sin^3\theta_1)(\psi_0 \sin(\lambda\psi_0) + \cos\psi_0 - 1) \cdot R^3$$

$$- D \frac{1}{\lambda} (\sin^3\theta_2 - \sin^3\theta_1) \left((\lambda - 1)\psi_0 \sin(\lambda\psi_0) + \cos(\lambda\psi_0) - \cos\psi_0 \right) \cdot R^3 \quad (5.54)$$

and, according to (5.12),

$$\Delta I_{yz} = 0$$

The increase in the moment of inertia component ΔI_{zz} is given by (5.26), with

$$(\Delta I_{zz})_{water} \approx -\frac{2}{3} \rho_w c_1 \left(3(\cos\theta_2 - \cos\theta_1) - (\cos^3\theta_2 - \cos^3\theta_1) \right) \psi \cdot hR^4 \approx$$

$$\approx -\frac{2}{9} \rho_w c_1(\lambda - 1) \left(3(\cos\theta_2 - \cos\theta_1) - (\cos^3\theta_2 - \cos^3\theta_1) \right) \psi_0^{3/2} \cdot R^4 \quad (5.55)$$

provided no isostatic compensation of the increased sea-level is taken into account, and

$$(\Delta I_{zz})_{litho} \approx \left(\frac{B}{2} \frac{(\lambda - 1)(2\lambda - 3)}{\lambda} - \frac{D}{2} \frac{(\lambda - 1)^2}{\lambda} \right) \cdot$$

$$\cdot \left(3(\cos\theta_2 - \cos\theta_1) - (\cos^3\theta_2 - \cos^3\theta_1) \right) \psi_0^2 \cdot R^3 \quad (5.56)$$

The increase in the length of day for the case $\psi \geq \lambda\psi_0$ thus becomes approximately

$$-\frac{2\rho_w c_1}{9C}(\lambda-1)\Big(3(\cos\theta_2-\cos\theta_1)-(\cos^3\theta_2-\cos^3\theta_1)\Big)\psi_0^{3/2}\cdot R^4\cdot 86164\ \mathrm{s}$$

$$+\left(\frac{B}{2C}\,\frac{(\lambda-1)(2\lambda-3)}{\lambda}-\frac{D}{2C}\,\frac{(\lambda-1)^2}{\lambda}\right)\cdot$$

$$\cdot\Big(3(\cos\theta_2-\cos\theta_1)-(\cos^3\theta_2-\cos^3\theta_1)\Big)\psi_0^2\cdot R^3\cdot 86164\ \mathrm{s} \qquad (5.57)$$

To study the resultant shift of the rotation axis, increase in the length of the day and the rise of the sea-level as a function of the various parameters of the spreading ridge, we consider a standard spreading area (figure 5.3). This standard area has its spreading ridge from the equator to 70° degrees Northern Latitude along the Greenwich Meridian. The initial spreading velocity is taken to be 1 centimeter per year, while the rate of spreading velocity increase is set to 2. The standard spreading area extends to 45° longitude on both sides of the ridge.
In figures 5.4 – 5.8, the dependence on each of the five parameters mentioned above is sketched. Each of these five figures shows the dependence of the polar shift, the total non-tidal variation in the second degree gravitational potential harmonic and the eustatic sea-level rise on one of the parameters with the other four held fixed to their standard value.
The following values for the constants appearing in the formulas have been used in the computations:

$$\alpha = 3.2\cdot 10^{-5}\ \mathrm{K}^{-1}$$

$$\kappa = 0.8\ \mathrm{mm}^2\ \mathrm{s}^{-1}$$

$$T_m - T_0 = 1300\ \mathrm{K}$$

$$R = 6370\ \mathrm{km}$$

$$\rho_m = 3.3\cdot 10^3\ \mathrm{kg}\cdot\mathrm{m}^{-3}$$

$$\rho_w = 1.0\cdot 10^3\ \mathrm{kg}\cdot\mathrm{m}^{-3}$$

$$A = 8.0131\cdot 10^{37}\ \mathrm{kg}\cdot\mathrm{m}^2$$

$$C = 8.0394\cdot 10^{37}\ \mathrm{kg}\cdot\mathrm{m}^2$$

$$M = 6\cdot 10^{24}\ \mathrm{kg}$$

Almost the whole amount of polar shift is due to the non-isostatic increase of the sea-level. This is reflected in the figures by the close correlation between the

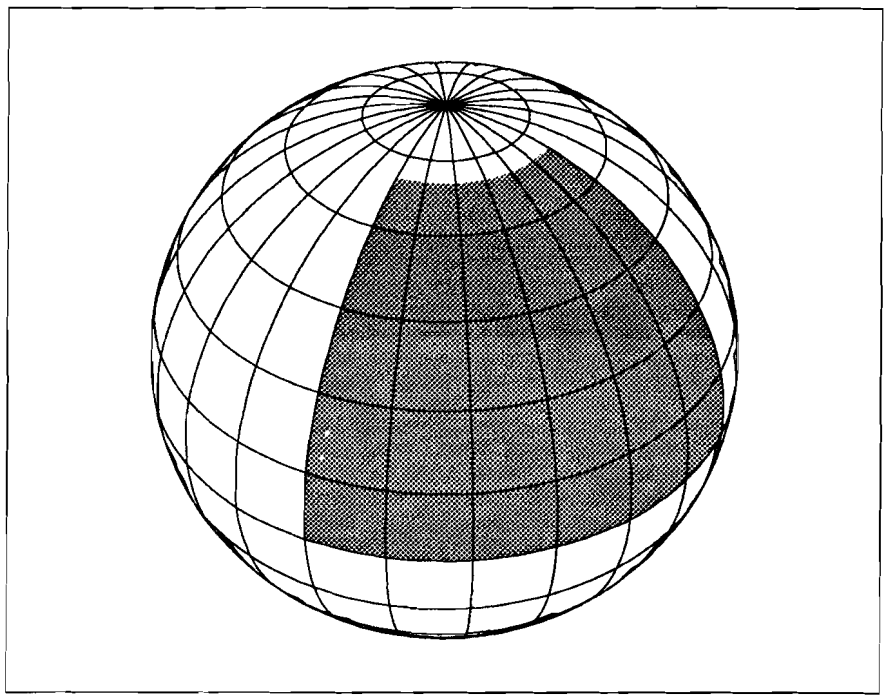

Figure 5.3. Standard spreading area used in the simulations.

rotational signatures and the sea-level rise. The lithosphere contributes no more than a few percent, again a clear manifestation that isostatic processes do not induce large quantities of polar wander.

The eustatic sea-level rises are too large for the real Earth, as the ocean surface area in the calculations is too small. Also flooding of the continental freeboard has not been taken into account. To extend the ocean surface area to about 70 percent of the total surface area, while still trying to obtain a maximum amount of shift, requires the addition of a spreading ridge at the antipodal position of the spreading ridge on the Greenwich Meridian.

A simple calculation can show that in the case of the sea-level rise being dynamically supported by deeper mantle regions, the induced shifts in the rotation axis induced by this process are of the same order as the shifts induced by changes in

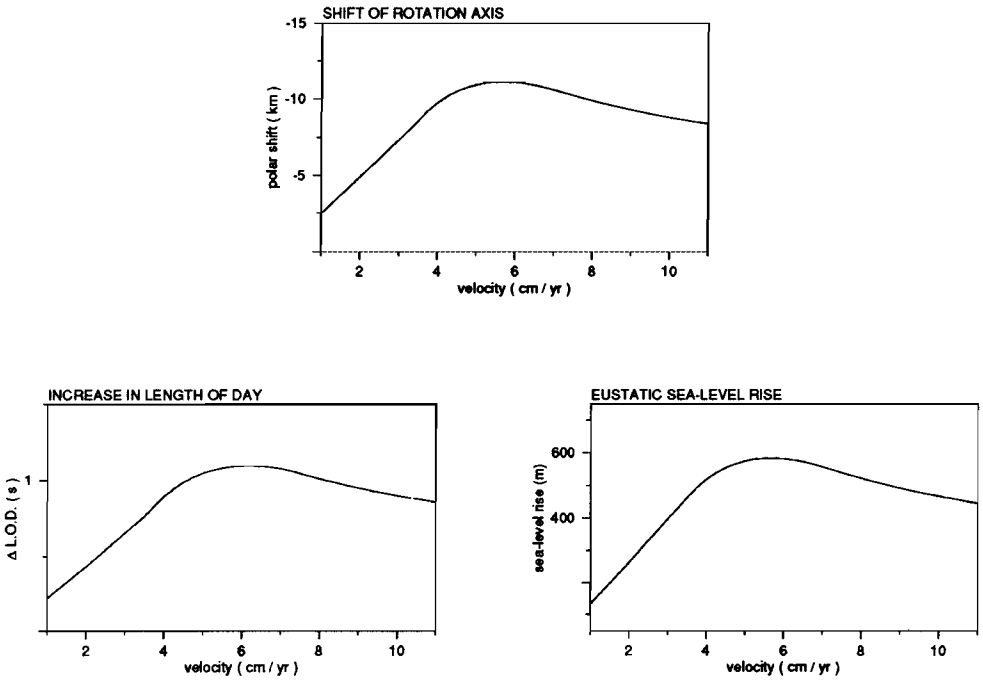

Figure 5.4. Total induced shift of the rotation axis, increase in the length of day and eustatic sea-level rise: dependence on initial rate of spreading.

subduction.

A change in the geometry or velocity of a subducting slab, or the initiation of subduction changing a passive continental margin into an active one, is generally accompanied by a change in density as the subducting oceanic lithosphere is cooler than the surrounding mantle. The largest density contrasts induced by thermal contraction are to be found near the Earth's surface. The temperature differences between slab and mantle become progressively smaller as the slab sinks deeper into the mantle and heats up. However, the surrounding mantle is cooled at the same time, so that the total mass difference per unit of depth might be considered as constant. This assumption is only valid, however, when it is assumed that the mantle around the slab does not restore its cooling by convection in the time it takes the slab to reach the 670 kilometer discontinuity.

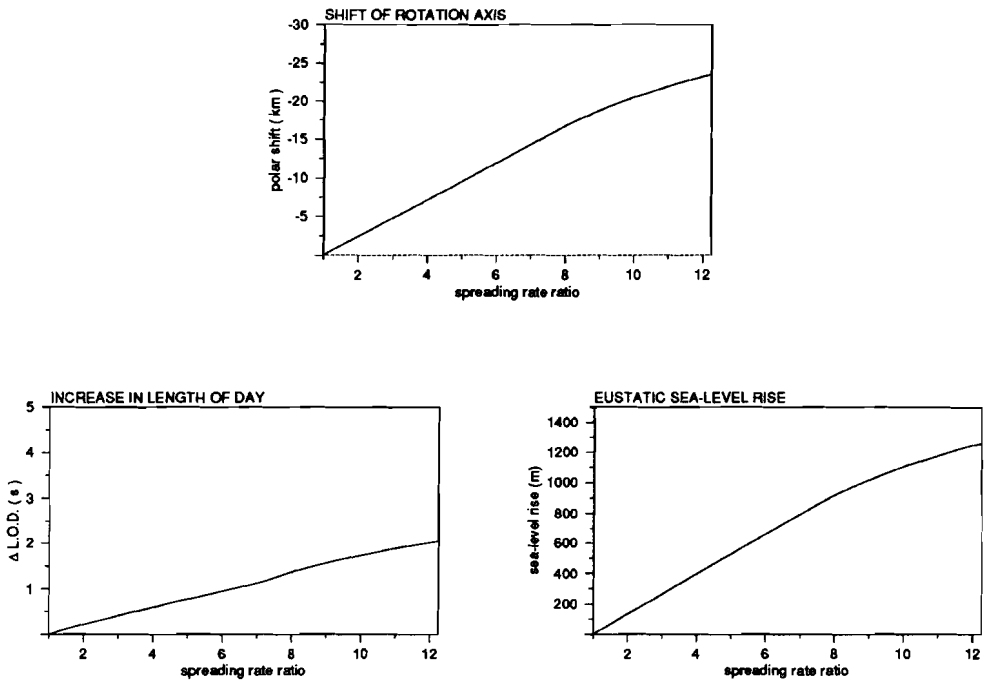

Figure 5.5. Dependence on spreading rate increase.

A further approximation in determining the density contrast between the slab and the mantle is to assume that the density differences are only due to thermal contraction, neglecting phase changes. Density changes from phase changes can be important, however, e.g. the eclogite top layer of the slab has a larger density than the basaltic layers and also the olive - spinel phase change at 400 kilometers depth gives rise to a deviating density contrast from a simple thermal contraction model. Assuming an initial temperature difference between slab and mantle of 300 K, this would result (according to (3.2)) in a density difference of about 30 $kg \cdot m^{-3}$. In order to model the effects on the changes in the products of inertia, the thickness of the subducting oceanic lithosphere is taken to be 100 kilometers, while the subduction zone is supposed to be along the Greenwich Meridian. Assuming that the total width of the slab remains approximately constant and that the slab, extending from the equator to 70° northern latitude, has reached the 670 kilometer discontinuity

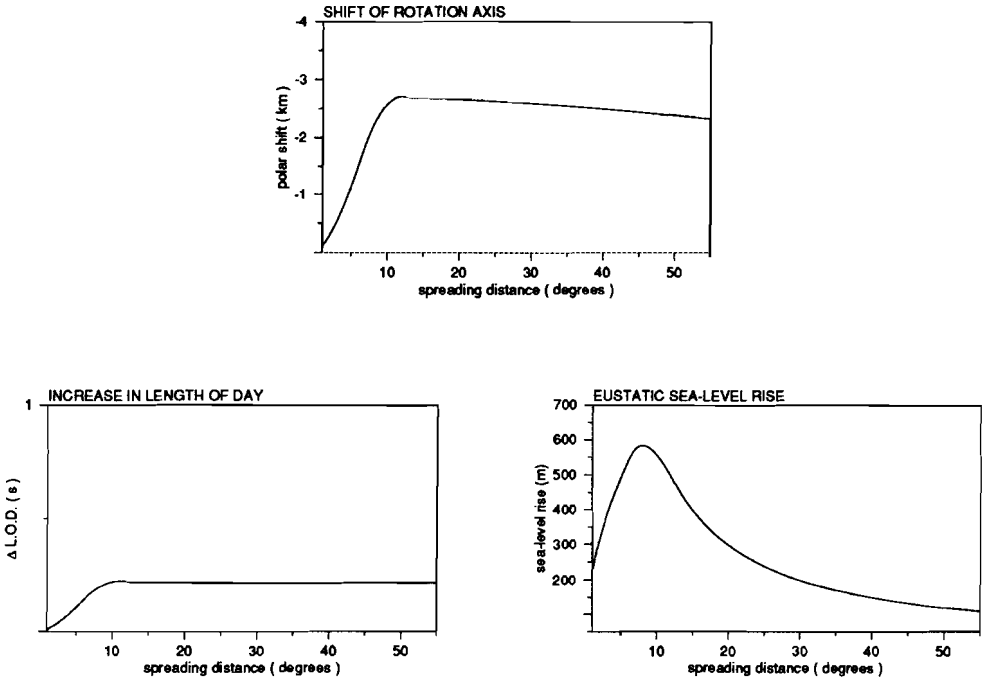

Figure 5.6. Dependence on spreading area distance.

with a dip of 90°, the total difference in I_{xz} between the situation before subduction and at the moment the slab has reached the boundary between the upper and lower mantle is according to (3.19) equal to

$$\Delta I_{xz} \approx -\frac{1}{3}\Delta\rho\,\Delta h\,R^4\sin\phi\,(1-\sin^3\theta) \tag{5.58}$$

with

$$\Delta\rho = 50\ \text{kg}\cdot\text{m}^{-3}$$

$$\Delta h = 670\ \text{km}$$

$$R = 6371\ \text{km}$$

$$\phi \approx 1^\circ$$

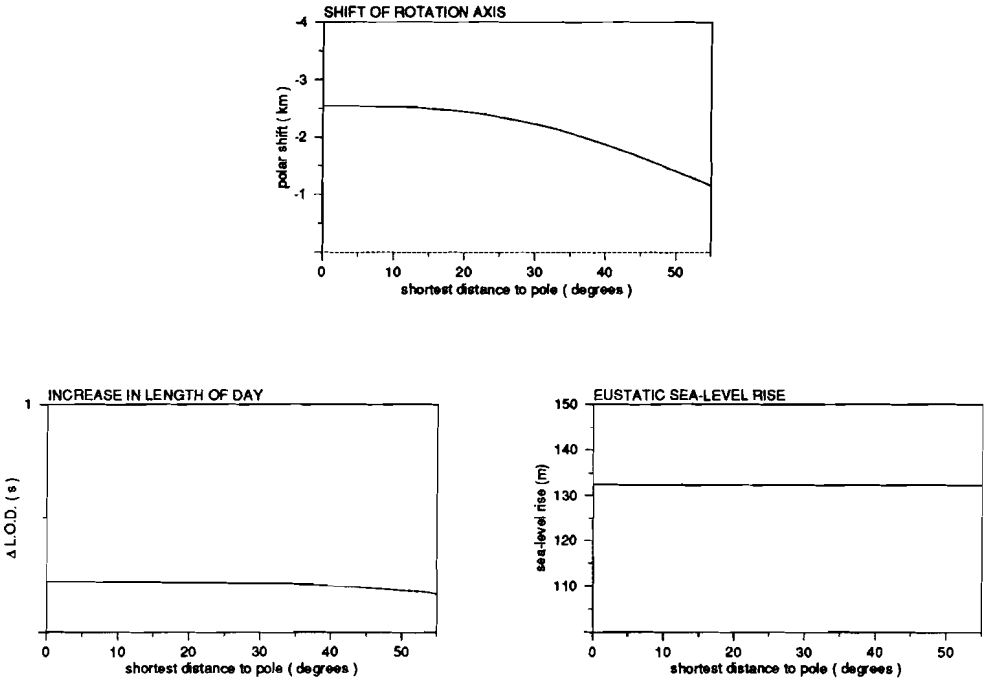

Figure 5.7. Dependence on shortest distance spreading area to pole.

$$\theta = 20^{\circ}$$

resulting in $\Delta I_{xz} \approx 10^{32}$ kg · m^2, which gives (cf. (2.19)) a shift of the rotation axis of about 2.5 kilometers. Comparing this value with the shifts depicted in the figures shows that they are of the same order of magnitude for most cases. The effects could be a few factors higher compared to the increased sea-level cases if phase changes are included, but it is clear that incorporation of these effects can not lead to orders of magnitude larger values.

As with respect to the values found for the changes in the length of day in the figures 5.5 – 5.8: these are not indicative for inducing significant changes on geological timescales. From the figures 5.5 – 5.8 it seems save to take 1 second per 10 million years as an upper limit for the change in the length of day, as the realistic

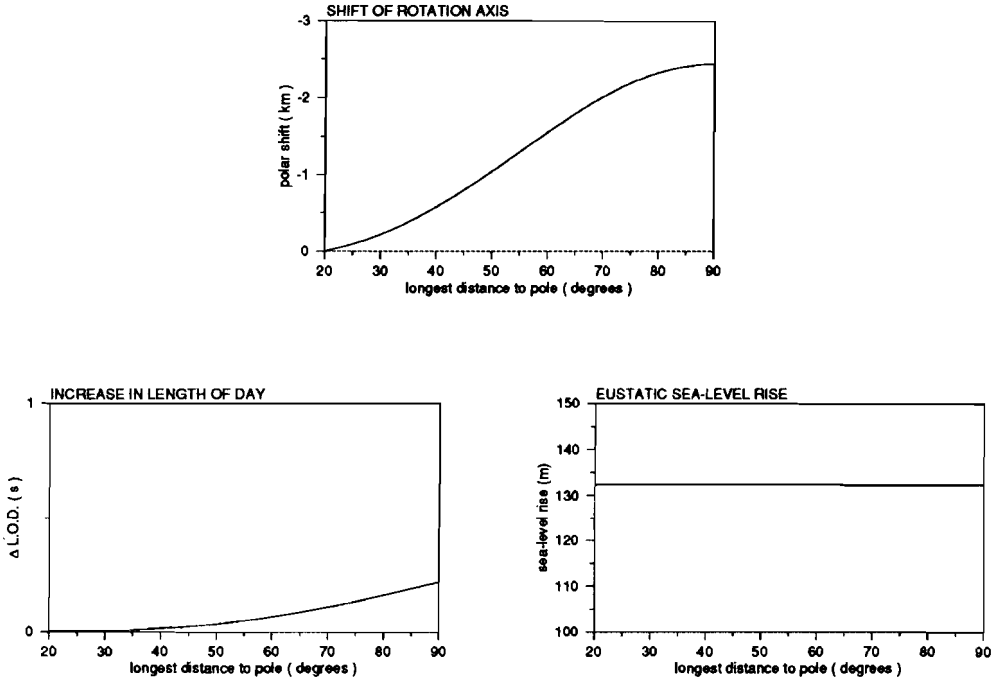

Figure 5.8. Dependence on longest distance spreading area to pole.

cases induce a total change which is less than 1 second and as the increase in bathymetry will most likely only have been completed after several tens of millions of years have elapsed. The present-day tidal decelleration results in a lengthening of the day of about 2 milliseconds per 100 years (chapter 2). If this tidal decelleration would have been constant throughout the Phanerozoic, this would result in a tidally induced lengthening of the day of about 200 seconds per 10 million years, two orders of magnitude larger than the upper limit from the models presented in this chapter.

The tidal decelleration seems to have been steady throughout the Phanerozoic indeed. Whereas the position of the rotation pole during the last few hundred million years is supposed to be derivable from paleomagnetic records, the changes in the length of the day can be derived from the grow patterns of marine organisms (e.g. Lambeck, 1980, p. 360). Fossil corals, bi-valves and stromatolites (these

latter are structures which have been formed by the interplay between micro-organisms and sedimentary processes) from hundreds of million years ago show that the organisms responsible for its formation were sensible for three astronomical cycles: the diurnal rotation of the Earth, the rotation of the Moon around the Earth, and the rotation of the Earth around the Sun. This sensibility is still observable in various organisms living today. Growth of a shale takes sometimes place especially during daytime. If it gets dark, the growth rate is reduced and sometimes different biological and chemical processes become active so that the shales show a clear day - night pattern. The same can happen as a function of the phase of the Moon and of the seasons. When two or three of these rhythmic cycles are present, e.g. the diurnal and the yearly, the number of days of the year during the period the fossil was formed can be determined by counting the number of day - night patterns. In practice, the 'paleontological clocks' turn out not to be very precise, however, due to a number of complicating factors like changes in food supply, environment, etc. Still, it has been reported from such observations that the Devonian year (some 400 million years ago) must have had some 400 days. Such an increase of about 35 days over 400 million years is compatible with the contemporary increase in the length of day due to tidal interaction between the Moon and the Earth: a lengthening of the day with a rate of 2 milliseconds per 100 years results in a shortening of a day 400 million years ago with 2 hours and 12 minutes, or an increase of the number of days in a year 400 million years ago of 33.4 days, indicating that the deceleration of the Earth must have been rather steady during the last 400 million years.

Conclusions

By a simple cooling half-space model it has been shown in this chapter that if the sea-level rise accompanying enhanced rates of subduction is dynamically supported by deeper mantle regions, the sea-level rise can have a non-negligible influence on long-term true polar wander. In general, this result indicates that it is not correct to consider only the sinking material and to determine the induced dynamic topographies, neglecting rising material to complete the cycle. It is important in this case to note that the situation here is markably different from the classic model of sinking a sphere through a fluid in one respect: the sphere is the driving agent in such a

case, and one does not have to consider compensating rising material in order to determine the dynamic topography as the total mass of the fluid material is conserved. In the case of a subducting slab, however, the Earth's mantle is making its own sinking material - in fact extracting it from the mantle. In such a case the total mass of the fluid is not conserved and one has to consider the missing mass as a forcing function. It is debatable whether this rising material from the deep mantle shows up at the surface at the mid-ocean ridges, hotspots or perhaps even elsewhere. The purpose of the model calculations in this chapter was not to outline the exact nature of this backflowing material, however, but to illustrate the importance of considering the return flows and accompanying changes in sea-level as forcing functions as well.

The long-term changes in sea-level (or subduction) have an orders of magnitude less influence on the changes of the length of the day compared to tidal decelleration. As a consequence, measured secular deviations from a decelleration rate of about 2 milliseconds per 100 years can only be due to geologically fast phenomena, like post-glacial rebound or the tectonic processes discussed in chapter 3.

References

Andrews, J.A., True polar wander: An analysis of Cenozoic and Mesozoic paleomagnetic poles, *J. Geophys. Res., 90,* 7737-7750, 1985.

Besse, J., and V. Courtillot, Revised and synthetic apparent polar wander paths of the African, Eurasian, North American and Indian Plates, and true polar wander since 200 Ma, *J. Geophys. Res., 96,* 4029-4050, 1991.

Crough, S.T., and D.M. Jurdy, Subducted lithosphere, hotspots, and the geoid, *Earth Planet. Sci. Lett., 48,* 15-22, 1980.

Goldreich, P., and A. Toomre, Some remarks on polar wandering, *J. Geophys. Res., 74,* 2555-2567, 1969.

Hager, B.H., Eustatic sea level and spreading rate are not simply related, *EOS Trans. AGU, 61,* 374, 1980.

Jurdy, D.M., Early Tertiary subduction zones and hot spots, *J. Geophys. Res., 88,* 6395-6402, 1983.

Lambeck, K., *The Earth's Variable Rotation: Geophysical Causes and Consequences,* 449 pp., Cambridge University Press, New York, 1980.

Moser, J., D.A. Yuen, and C. Matyska, Polar motions excited by a convecting viscous mantle, *Geophys. Res. Lett., 19,* 2251-2254, 1992.

Ricard, Y., R. Sabadini, and G. Spada, Isostatic deformations and polar wander induced by redistribution of mass with the Earth, *J. Geophys. Res., 97,* 14223-14236, 1992.

Ricard, Y., Spada, G., and R. Sabadini, Polar wandering of a dynamic earth, *Geophys. J. Int., 113,* 284-298, 1993.

Spada, G., Y. Ricard, and R. Sabadini, Excitation of true polar wander by subduction, *Nature, 360,* 452-454, 1992.

Tackley, P.J., Stevenson. D.J., and G.A. Glatzmaier, 3D spherical mantle convection simulations at high Rayleigh number: Time dependence and true polar wander, *EOS Trans. AGU, 73(43),* 576, 1992.

Turcotte, D.L., and G. Schubert, *Geodynamics. Applications of Continuum Physics to Geological Problems,* 450 pp., John Wiley & Sons Inc., 1982.

Vlaar, N.J., and M.J.R. Wortel, Lithospheric aging, instability and subduction, *Tectonophys., 32,* 331-351, 1976.

Daar zijn op de weg onzer verbeelding
afgronden die we niet durven peilen.
Wij worden ze instinktmatig gewaar,
schrikken terug, sluiten de ogen en...
ik weet niet verder.

Woutertje Pieterse - Multatuli

CHAPTER 6

THE GRAVITO-ELASTODYNAMICS OF A PRE-STRESSED ELASTIC EARTH †

Abstract

The notion that the self-gravitation problem of a perfectly elastic solid body involves small strains from a reference state with arbitrary large initial stresses is reconfirmed and extended. It is shown that the Lagrangian, from which the equations of motion, the boundary conditions and Poisson's equation can be derived in Eulerian or Lagrangian coordinates by the Variational Principle, can be written in a general form which incorporates the various stress measures (Piola-Kirchhoff, Cauchy). Especially for an Eulerian description it is shown that the derived equations of motion and boundary conditions lead to a complete set of mutually orthogonal seismic normal modes.

The Lagrangian which Geller (1988) gives is re-evaluated. It appears that in his considerations Geller neglected finite pre-stresses and only accounted for gravitational contributions. This, in general, is not correct. Though the static equilibrium equation has no unique solution for the initial stress components, this does not imply that in physical situations there would not be a specified initial pre-stress. Geller's statement that the asymmetric stress tensor Woodhouse & Dahlen (1978) employ in their Lagrangian necessarily leads to non-conservation of angular momentum is not valid. This stress tensor is a first Piola-Kirchhoff stress tensor, which is a so-called two-point tensor, associating two vector fields defined in different coordinate systems.

---

† This chapter was originally published as: L.L.A. Vermeersen and N.J. Vlaar, The gravito-elastodynamics of a pre-stressed elastic earth, *Geophys. J. Int., 104,* 555-563, 1991. © 1991 by The Royal Astronomical Society. Published by Blackwell Scientific Publications.

See also: L.L.A. Vermeersen and N.J. Vlaar, Reply to "Comment on 'The gravito-elastodynamics of a pre-stressed elastic earth' by L.L.A. Vermeersen and N.J. Vlaar" by R.J. Geller, *Geophys. J. Int., 106,* 505, 1991.

Introduction

There is a controversy in geophysics about the correct elastodynamical description of an arbitrary self-gravitating solid body. The problem concentrates around the introduction of an initial stress tensor in the gravito-elastodynamical equations, and particularly the deviatoric part of such a pre-stress tensor. Though this problem is largely an academic one in seismology (the initial state of stress of the Earth is predominantly isotropic), Geller (1988) renewed the interest in it by re-evaluating results obtained by Dahlen (1972), Woodhouse & Dahlen (1978) and Valette (1986), who treated the problem in Lagrangian coordinates. Whereas Saito (1971) stated that they were not, Dahlen (1972) has shown that in these coordinates the linear operators are Hermitian. Saito instead treated the problem in Eulerian coordinates, whereas Dahlen used a Lagrangian coordinate system. Although it is physically implicit that if in one coordinate system the equations lead to self-adjointness this must also be true in another, none of these authors explicitly checked or were able to check mathematically the self-adjointness of the linear operators in an Eulerian approach.

The principal difference in the equations of motion and in the Lagrangians, from which the equations of motion can be derived by the Variational Principle, given by these authors and Geller is the absence of terms with initial stress components in the work of the latter; only divergences of these components show up in his equations. This is a consequence of the introduction of an 'Incremental Gravitational Force Density', which accounts for differences in the gravitational force after an infinitesimal displacement of the considered unit volume, but not for differences in the initial static stress field. Geller motivates this by stating that the initial stress tensor cannot uniquely be determined in a self-gravitating body such as the Earth.

Moreover, Geller states that the theory developed by Woodhouse, Dahlen and Valette is in conflict with the basic principles of physics. The latter authors extended the theory originally developed by Biot (1965), who considered small elasto-gravitational disturbances away from an arbitrary initial static stress field. The asymmetric Piola-Kirchhoff stress tensor which Woodhouse and Dahlen employ is especially criticized by Geller. Valette however uses a symmetric Piola-Kirchhoff stress tensor and points to the fact that the asymmetric first Piola-Kirchhoff stress tensor is hybrid, relating a force defined on a deformed volume element to a surface element of the corresponding undeformed volume element.

Initial finite stresses and the finite strain problem

The deformation of an elastic solid continuum can generally be described as the linear combination of a solid body translation and rotation and a pure deformation of an infinitesimal volume element in its interior. Inside a hydrostatic pressure supported body the rotation doesn't change the energy. This is not the case however in solid bodies where there are deviations from hydrostaticity. The rotational component of the displacement inside such a body generally gives rise to different energy contributions as the existing deviatoric pre-stress components inside the volume element are changed with respect to their environment. This was first realized by Biot in the 1930's. In his work he distinguishes rotations and deformations of the coordinate axes - purely geometrical changes ought not to give rise to energy changes - from material rotations and deformations. Dahlen, Woodhouse and Valette use this concept in their articles on gravito-elastodynamics with finite initial stresses.

Geller's article differs from Biot's work in that he only considers gravitational force differences after an infinitesimal displacement of a unit volume element. He states that the introduction of an initial stress tensor is necessary for describing a pre-stressed Earth and points to the fact that the components of such a symmetric tensor $\sigma_{ij}^{(0)}$, obtained from the static equilibrium equation

$$\sigma_{ij,j}^{(0)} = -\rho^{(0)}\psi_{,i}^{(0)} \tag{6.1}$$

with $\rho^{(0)}$ the initial density and $\psi^{(0)}$ the initial gravitational potential, cannot uniquely be determined. If the terms on the right-hand side of (6.1) are known, the three equations (6.1) give three unique solutions $\sigma_{ij,j}^{(0)}$ and as there are six independent components $\sigma_{ij}^{(0)}$ one can indeed always add solutions σ_{ij}^{*} with $\sigma_{ij,j}^{*} = 0$ to (6.1), so that $\sigma_{ij}^{(0)} + \sigma_{ij}^{*}$ satisfies (6.1) as well.

Though (6.1) does not lead to uniquely specified initial stress values, the Earth is clearly pre-stressed. In principle these stresses can be measured or modeled, irrespective of whether these pre-stresses can be related to elastic or inelastic strains, which may be finite. Determining these pre-stresses in practice may be difficult, or even virtually impossible, but this does not imply that these pre-stresses should not be there inside the Earth, having a specific value. In physical situations like this, differential equations like (6.1) should be supplemented with initial conditions, boundary conditions and continuity conditions until the initial values and the boundary values have been specified. Backus (1967) e.g. gives an exhaustive catalogue of all possible equilibrium stress fields in the mantle.

This means that the self-gravitation problem has to consider infinitesimal strains away from a steady-state situation which has arbitrarily large initial stresses. Consequently a clear distinction between Eulerian and Lagrangian coordinates with accompanying stress measures must be made. In the Appendix the various measures of stress are briefly reviewed.

The hydrostatic case

According to Geller, the Lagrangian for the general adiabatic, non-rotating case with the no-slip condition prevailing in the interior of the body consists of four contributions:

$$L^G = T - H_1 - H_2 - I \tag{6.2}$$

where

$$T = \frac{1}{2}\omega^2 \int dV u_i \rho^{(0)} u_i \quad \text{is the kinetic energy} \tag{6.3}$$

$$H_1 = \frac{1}{2}\int dV u_{i,j} C_{ijkl} u_{k,l} \quad \text{is the elastic potential energy} \tag{6.4}$$

$$H_2 = -\frac{1}{2}\int dV u_i (IGFD)_i \quad \text{is the gravitational potential energy, and} \tag{6.5}$$

$$I = \frac{1}{2}\int dV \left\{ \frac{1}{4\pi G}\psi^{(1)}_{,i}\psi^{(1)}_{,i} - \rho^{(0)} u_i \psi^{(1)}_{,i} \right\} \tag{6.6}$$

Note that in the derivation of the correct implementation of Poisson's equation into the Lagrangian the surface term $\int_{\partial V} dS\, n_i \delta\psi^{(1)}_{,i}\left[\frac{2\alpha}{4\pi G}\psi^{(1)}_{,i} - (\alpha-1)\rho^{(0)}u_i\right]^+$ ought to be included in Geller's equation (28), because at that point it is not clear that $\alpha = -1$. The term $I = 0$ is added to the Lagrangian so that variation of L^G with respect to $\psi^{(1)}$ gives Poisson's equation. The elastic constants C_{ijkl} in H_2 obey the symmetry relations $C_{ijkl} = C_{jikl} = C_{ijlk} = C_{klij}$. The 'Incremental Gravitational Force Density' in H_2 is given by

$$(\mathrm{IGFD})_i = \rho^{(0)}\left\{u_{j,i}\psi^{(0)}_{,j} + u_j\psi^{(0)}_{,ij} - u_{j,j}\psi^{(0)}_{,i} + \psi^{(1)}_{,i}\right\} \tag{6.7}$$

This IGFD is the difference between the gravitational force acting on a unit volume element after and before a small displacement $\vec{u}$ from equilibrium. Geller extensively demonstrates that this first-order quantity is independent of the coordinate system used. The terms $\rho^{(0)}\psi^{(1)}_{,i} + \rho^{(0)}u_j\psi^{(0)}_{,ij}$ denote the incremental gravitational force of the volume element and the redistribution of the body as a whole respectively. Geller remarks that these two terms comprise Biot's 'Incremental Gravitational Force Density'. He states that this IGFD is incorrect because it is the difference between the gravitational force density after the displacement per unit deformed volume and that in the initial state per unit undeformed volume. In Geller's IGFD the difference is taken between gravitational force densities which are both reckoned per unit undeformed (or deformed) volume.
Geller recognizes however that in Woodhouse & Dahlen's Lagrangian (their equation (26)), which can be written as

$$2L^{\mathrm{PK}(1)} = \omega^2\int \mathrm{d}V u_i\rho^{(0)}u_i - \int \mathrm{d}V u_{j,i}\Lambda_{ijkl}u_{l,k} + \int \mathrm{d}V u_i\rho^{(0)}\left\{\psi^{(1)}_{,i} + u_j\psi^{(0)}_{,ij}\right\}$$

$$+ \int \mathrm{d}V\left\{\frac{1}{4\pi G}\psi^{(1)}_{,i}\psi^{(1)}_{,i} - \rho^{(0)}u_i\psi^{(1)}_{,i}\right\} \tag{6.8}$$

with

$$\Lambda_{ijkl} = C_{ijkl} + \frac{1}{2}\left\{\sigma^{(0)}_{ij}\delta_{kl} + \sigma^{(0)}_{kl}\delta_{ij} + \sigma^{(0)}_{ik}\delta_{jl} - \sigma^{(0)}_{jk}\delta_{il} - \sigma^{(0)}_{il}\delta_{jk} - \sigma^{(0)}_{jl}\delta_{ik}\right\} \tag{6.9}$$

the remaining terms $\rho^{(0)}u_{j,i}\psi^{(0)}_{,j} - \rho^{(0)}u_{j,j}\psi^{(0)}_{,i}$ that make Biot's IGFD (which is equal to Woodhouse & Dahlen's one) equal to his IGFD are present in the elastic-gravitational energy integral $\int \mathrm{d}V u_{j,i}\Lambda_{ijkl}u_{l,k}$ in the hydrostatic case: substituting $\sigma^{(0)}_{ij} = -p_0\delta_{ij}$ into (6.9) gives

$$\Lambda_{ijkl} = C_{ijkl} - p_0(\delta_{ij}\delta_{kl} - \delta_{il}\delta_{jk}) \tag{6.10}$$

Note that in Dahlen's equation (34) the last term $\frac{1}{2}T^0_{jl}\delta_{ik}$ must have a minus sign. This typographical error was corrected in Dahlen & Smith (1975). Woodhouse & Dahlen's equation (11) is correct. Substituting (6.10) in (6.8) gives (6.2) if one takes (6.1) into account. Geller qualifies this result as 'fortuitous'. Instead of Geller's stress tensor $C_{ijkl}u_{k,l}$, Dahlen uses the stress tensor $T^{\mathrm{PK}(1)}_{ij} = \Lambda_{ijkl}u_{l,k}$, which

reads in the hydrostatic case $T_{ij}^{PK(1)} = C_{ijkl}u_{k,l} - p_0(u_{k,k}\delta_{ij} - u_{i,j})$ (Dahlen's equation (37)). The two extra terms in Dahlen's (first Piola-Kirchhoff pseudo-)stress tensor express the hydrostatic pressure acting on the deformed volume element in terms of the undeformed volume element.
According to Geller, in the case of a general initial stress it is impossible to derive equation (6.5) from (6.8) and (6.9). This conclusion is an artifact of the improper deletion of terms in (6.9) by Geller, based on the incorrect statement that Woodhouse & Dahlen's asymmetric pseudo-stress tensor is physically unadmissible (cf. Appendix), as will be shown in the next section.

The general case

In the hydrostatic case Geller's Lagrangian L^G (equation (6.2)) becomes equal to Woodhouse & Dahlen's Lagrangian $L^{PK(1)}$ (equation (6.8)). In the case of a general initial stress field the elastic-gravitational energy integral in (6.8) can be rewritten with (6.9) as (in the equations in this section no explicit indication is given whether volume elements dV, surface elements dS and their normals $\hat{n}$ are defined in the deformed or undeformed state):

$$\int dV u_{j,i}\Lambda_{ijkl}u_{l,k} = \int dV u_{j,i}C_{ijkl}u_{l,k} + \frac{1}{2}\int dV u_{j,i}\Big\{\sigma_{ij}^{(0)}\delta_{kl} + \sigma_{kl}^{(0)}\delta_{ij} + \sigma_{ik}^{(0)}\delta_{jl}$$

$$- \sigma_{jk}^{(0)}\delta_{il} - \sigma_{il}^{(0)}\delta_{jk} - \sigma_{jl}^{(0)}\delta_{ik}\Big\}u_{l,k} =$$

$$= \int dV u_{j,i}C_{ijkl}u_{l,k} - \frac{1}{2}\int dV u_{j,i}\sigma_{ij}^{(0)}u_{k,k} - \frac{1}{2}\int dV u_{i,i}\sigma_{kl}^{(0)}u_{l,k} - \frac{1}{2}\int dV u_{j,i}\sigma_{ik}^{(0)}u_{j,k}$$
$$+ \frac{1}{2}\int dV u_{j,i}\sigma_{jk}^{(0)}u_{i,k} + \frac{1}{2}\int dV u_{j,i}\sigma_{il}^{(0)}u_{l,j} + \frac{1}{2}\int dV u_{j,i}\sigma_{jl}^{(0)}u_{l,i} =$$
$$= \int dV u_{i,j}C_{ijkl}u_{k,l} - \int dV u_{i,j}\sigma_{ij}^{(0)}u_{k,k} - \frac{1}{2}\int dV u_{j,i}\sigma_{ik}^{(0)}u_{j,k} + \int dV u_{j,i}\sigma_{jk}^{(0)}u_{i,k}$$
$$+ \frac{1}{2}\int dV u_{j,i}\sigma_{jk}^{(0)}u_{k,i} =$$

$$= \int dV_{i,j} C_{ijkl} u_{k,l} - \int dSn_j u_i \left\{ \sigma^{(0)}_{ij} u_{k,k} - \sigma^{(0)}_{jk} u_{k,i} \right\} + \int dV u_i \left\{ \sigma^{(0)}_{ij,j} u_{k,k} + \sigma^{(0)}_{ij} u_{k,jk} \right.$$

$$\left. - \sigma^{(0)}_{jk,j} u_{k,i} - \sigma^{(0)}_{jk} u_{j,ik} \right\} - \frac{1}{2} \int dV u_{i,j} \left\{ \sigma^{(0)}_{jk} u_{i,k} - \sigma^{(0)}_{ik} u_{k,j} \right\} \tag{6.11}$$

In the derivation of (6.11) dummy indices have been interchanged. The surface integral is equal to zero because of the boundary condition $\sigma^{(0)}_{ij} n_j = 0$ (on the undeformed boundary).

Substituting (6.11) in (6.8), taking into account (6.1), gives

$$2L^{PK(1)} = \omega^2 \int dV u_i \rho^{(0)} u_i - \int dV u_{i,j} C_{ijkl} u_{k,l}$$

$$+ \int dV u_i \rho^{(0)} \left\{ \psi^{(1)}_{,i} + u_j \psi^{(0)}_{,ij} - u_{k,k} \psi^{(0)}_{,i} + u_{k,i} \psi^{(0)}_{,k} \right\}$$

$$+ \int dV u_i \left\{ \sigma^{(0)}_{ij} u_{k,jk} - \sigma^{(0)}_{jk} u_{k,ij} \right\} - \frac{1}{2} \int dV u_{i,j} \left\{ \sigma^{(0)}_{jk} u_{i,k} - \sigma^{(0)}_{ik} u_{k,j} \right\} =$$

$$= (6.2) + \int dV u_i \left\{ \sigma^{(0)}_{ij} u_{k,jk} - \sigma^{(0)}_{jk} u_{j,ik} \right\}$$

$$- \frac{1}{2} \int dV u_{i,j} \left\{ \sigma^{(0)}_{jk} u_{i,k} - \sigma^{(0)}_{ik} u_{k,j} \right\} \tag{6.12}$$

Equation (6.12) shows that Woodhouse & Dahlen's Lagrangian is equal to Geller's Lagrangian plus some extra terms. It is easily verified that these extra volume integrals are zero in the hydrostatic case $\sigma^{(0)}_{ij} = -p_0 \delta_{ij}$. In the general case the extra terms describe the energy contributions of the changes in the initial non-hydrostatic stress field.

The main reason why Geller is not able to derive the expression for his gravitational potential energy (6.5) from Woodhouse & Dahlen's truncated Lagrangian in the general case, is that he does not allow terms with bare initial stresses instead of divergences of them.

Geller's relation (58b) can be written as

$$\int dV u_{i,j} \left\{ \sigma^{(0)}_{kl} \delta_{ij} - \sigma^{(0)}_{il} \delta_{jk} \right\} u_{k,l} = \int dSn_l \left\{ u_{i,i} \sigma^{(0)}_{kl} u_k - u_{i,j} \sigma^{(0)}_{il} u_j \right\} - \int dV u_{i,il} \sigma^{(0)}_{kl} u_k$$

$$- \int dV u_{i,i} \sigma^{(0)}_{kl,l} u_k + \int dV u_{i,jl} \sigma^{(0)}_{il} u_j + \int dV u_{i,j} \sigma^{(0)}_{il,l} u_j =$$

$$= \int dV u_i \rho^{(0)} \left\{ \psi^{(0)}_{,i} u_{k,k} - \psi^{(0)}_{j} u_{j,i} \right\} - \int dV u_i \left\{ \sigma^{(0)}_{ij} u_{k,jk} - \sigma^{(0)}_{jk} u_{j,ik} \right\} \qquad (6.13)$$

Again, dummy indices have been interchanged and the surface integral is equal to zero because of the boundary condition $\sigma^{(0)}_{ij} n_j = 0$. With (6.1) equation (6.13) reads

$$\int dV u_{i,j} \left\{ \sigma^{(0)}_{kl} \delta_{ij} - \sigma^{(0)}_{il} \delta_{jk} \right\} u_{k,l} = \int dV u_i \rho^{(0)} \left\{ u_{k,k} \psi^{(0)}_{,i} - u_{j,i} \psi^{(0)}_{j} \right\}$$

$$- \int dV u_i \left\{ \sigma^{(0)}_{ij} u_{k,jk} - \sigma^{(0)}_{jk} u_{j,ik} \right\} \qquad (6.14)$$

From (6.14) it can be seen that Geller's equations (58b) and (58c) together give the correct expression for the IGFD-term in his Lagrangian, plus an integral which is zero in the hydrostatic case.
Instead of putting his equation (58b) in (58c) he 'corrects' (58c) by just replacing Biot's IGFD with his IGFD, which is remarkable because this is intrinsically inconsistent with the way he treated Woodhouse & Dahlen's Lagrangian in the hydrostatic case. His conclusion that (58b) "represents a kind of 'double counting'" and so ought to be deleted is an artificial consequence of this.
As there is nothing wrong with the asymmetric character of a first Piola-Kirchhoff stress tensor, deleting the terms describing the rotation of the initial stress field in (6.9), because they make Woodhouse & Dahlen's stress tensor asymmetric, is not correct.

As Woodhouse & Dahlen relate actual forces with pseudo surface elements by the first Piola-Kirchhoff stress tensor and because they use an Eulerian rather than a Lagrangian description of the perturbation of the gravitational potential, their description of gravito-elastodynamics is not a pure Lagrangian one. In the first part of his article Valette derives the equation of motion in Lagrangian coordinates, using the second Piola-Kirchhoff stress tensor (cf. Appendix). The result, his equation (14), can be Fourier transformed and rewritten as

$$\omega^2 \rho^{(0)} u_i + T^{PK(2)}_{ij,j} + (\sigma^{(0)}_{jk} u_{i,k})_{,j} + \rho^{(0)} u_j \psi^{(0)}_{,ij} + \rho^{(0)} \psi^{(1)}_{,i} = 0 \qquad (6.15)$$

with

$$T^{PK(2)}_{ij} = C^{*}_{ijkl} u_{l,k} \qquad (6.16)$$

In order to obtain a purely Lagrangian description also the Eulerian defined variation in the gravitational potential $\psi^{(1)}$ must be translated into the Lagrangian de-

fined variation in the gravitational potential $\psi^{*(1)} = \psi^{(1)} + u_j\psi^{(0)}_{,j}$. Substitution in (6.15) gives the equation of motion in a purely Lagrangian form:

$$\omega^2\rho^{(0)}u_i + T^{PK(2)}_{ij,j} + (\sigma^{(0)}_{jk}u_{i,k})_{,j} - \rho^{(0)}u_{j,i}\psi^{(0)}_{,j} + \rho^{(0)}\psi^{(1)}_{,i} = 0$$

Again, rotation of the body as a whole and complex notation is neglected. In this rewriting use has been made of Valette's equations (13a) and (19). The latter one reads: $(\vec{g} - \vec{g}_0)_i = u_j\psi^{(0)}_{,ij} + \psi^{(1)}_{,i}$, so $\rho^{(0)}(\vec{g} - \vec{g}_0)$ is Biot's IGFD.
The Lagrangian which gives (6.15) upon varying with respect to $\vec{u}$ is

$$2L^{PK(2)} = \omega^2 \int dV u_i\rho^{(0)}u_i - \int dV u_{j,i}C^*_{ijkl}u_{l,k} + \int dV\left\{-\frac{1}{4\pi G}\psi^{(1)}_{,i}\psi^{(1)}_{,i} + 2\rho^{(0)}u_i\psi^{(1)}_{,i}\right\}$$
$$+ \int dV u_i\rho^{(0)}\psi^{(0)}_{,ij}u_j - \int dV u_{i,j}\sigma^{(0)}_{jk}u_{i,k} \qquad (6.17)$$

This Lagrangian gives Poisson's equation upon varying with respect to $\psi^{(1)}$. Variation with respect to $\vec{u}$ gives

$$\delta L^{PK(2)} = 0 = \int dV\delta u_i\omega^2\rho^{(0)}u_i - \int dS n_j\delta u_i C^*_{ijkl}u_{l,k} + \int dV\delta u_i(C^*_{ijkl}u_{l,k})_{,j}$$
$$+ \int dV\delta u_i\rho^{(0)}\psi^{(1)}_{,i} + \int dV\delta u_i\rho^{(0)}\psi^{(0)}_{,ij}u_j$$
$$- \int dS n_j\delta u_i\sigma^{(0)}_{jk}u_{i,k} + \int dV\delta u_i(\sigma^{(0)}_{jk}u_{i,k})_{,j} \qquad (6.18)$$

The Lagrangian equation of motion (6.15) can be extracted from the volume integrals in (6.18), while the surface integrals deliver the boundary condition

$$\left[C^*_{ijkl}u_{l,k} + u_{i,k}\sigma^{(0)}_{jk}\right]n_j = 0$$

As $\sigma^{(0)}_{ij}n_j = 0$ this becomes

$$T^{PK(2)}_{ij}\,n_j = 0 \qquad (6.19)$$

on the undeformed boundary. This agrees with Valette's equation (34).
Replacing the second Piola-Kirchhoff stress tensor (6.16) in (6.17) by the first Piola-Kirchhoff stress tensor by means of equation (6.A6) gives expression (6.8), Woodhouse & Dahlen's Lagrangian.
Dahlen has shown that the bilinear form of the Lagrangian (6.8) is Hermitian. It is easily verified that the bilinear form of the Lagrangian (6.25) is Hermitian too, because (cf. equation (6.A6))

$$\int dV u_{j,i}\sigma^{(0)}_{ik}v_{j,k} = \int dV v_{j,i}\sigma^{(0)}_{ik}u_{j,k}$$

where the displacements $\vec{u}$ and $\vec{v}$ both satisfy (6.16) and (6.19).

The equation of motion in an Eulerian coordinate system can also be derived from the Lagrangian (6.18) by replacing the second Piola-Kirchhoff stress tensor by the Cauchy stress tensor. Substituting (6.A7) in (6.17) gives

$$2L^C = \omega^2 \int dV u_i \rho^{(0)} u_i - \int dV u_{j,i} T_{ij}^C + \int dV \left\{ -\frac{1}{4\pi G} \psi_{,i}^{(1)} \psi_{,i}^{(1)} + 2\rho^{(0)} u_i \psi_{,i}^{(1)} \right\}$$

$$- \int dV u_{j,i} \sigma_{ij}^{(0)} u_{k,k} + \int dV u_{j,i} \sigma_{jk}^{(0)} u_{i,k} + \int dV u_i \rho^{(0)} \psi_{,ij}^{(0)} u_j \qquad (6.20)$$

The Cauchy stress tensor T_{ij}^C can be expressed in a Lagrangian coordinate system in terms of the elastic constants d_{ijkl}

$$T_{ij}^C = d_{ijkl} u_{l,k} \qquad (6.21)$$

With (6.A7) and (6.16) it follows that

$$d_{ijkl} = C_{ijkl}^* - \sigma_{ij}^{(0)} \delta_{kl} + \sigma_{ik}^{(0)} \delta_{jl} + \sigma_{jk}^{(0)} \delta_{il} \qquad (6.22)$$

Equations (6.21) and (6.22) are Valette's equations (15b) and (16) respectively. Note that Valette's elastic coefficients d_{ijkl} are Dahlen's coefficients Γ_{ijkl}.
Varying (6.20) with respect to $\vec{u}$, using (6.21) and (6.22), gives

$$\begin{aligned}
\delta L^C = 0 = & \int dV \delta u_i \omega^2 \rho^{(0)} u_i - \frac{1}{2} \int dS n_i \delta u_j d_{ijkl} u_{l,k} + \frac{1}{2} \int dV \delta u_j (d_{ijkl} u_{l,k})_{,i} \\
& - \frac{1}{2} \int dS n_k \delta u_l d_{ijkl} u_{j,i} + \frac{1}{2} \int dV \delta u_l (d_{ijkl} u_{j,i})_{,k} - \frac{1}{2} \int dS n_i \delta u_j \sigma_{ij}^{(0)} u_{k,k} \\
& + \frac{1}{2} \int dV \delta u_j (\sigma_{ij}^{(0)} u_{k,k})_{,i} - \frac{1}{2} \int dS n_k \delta u_k \sigma_{ij}^{(0)} u_{j,i} + \frac{1}{2} \int dV \delta u_k (\sigma_{ij}^{(0)} u_{j,i})_{,k} \\
& + \frac{1}{2} \int dS n_i \delta u_j \sigma_{jk}^{(0)} u_{i,k} - \frac{1}{2} \int dV \delta u_j (\sigma_{jk}^{(0)} u_{i,k})_{,i} + \frac{1}{2} \int dS n_k \delta u_i \sigma_{jk}^{(0)} u_{j,i} \\
& - \frac{1}{2} \int dV \delta u_i (\sigma_{jk}^{(0)} u_{j,i})_{,k} + \int dV \delta u_i \rho^{(0)} \psi_{,i}^{(1)} + \int dV \delta u_i \rho^{(0)} \psi_{,ij}^{(0)} u_j
\end{aligned}$$

with

$$- \frac{1}{2} \int dS n_k \delta u_l d_{ijkl} u_{j,i} + \frac{1}{2} \int dV \delta u_l (d_{ijkl} u_{j,i})_{,k} =$$

$$
\begin{aligned}
&= -\frac{1}{2}\int dSn_i \delta u_j T^C_{ij} - \frac{1}{2}\int dSn_i \delta u_j \sigma^{(0)}_{ij} u_{k,k} \\
&\quad + \int dSn_i \delta u_i \sigma^{(0)}_{kl} u_{l,k} + \frac{1}{2}\int dSn_i \delta u_j \sigma^{(0)}_{jk} u_{i,k} \\
&\quad - \frac{1}{2}\int dSn_i \delta u_j \sigma^{(0)}_{il} u_{l,j} + \frac{1}{2}\int dV \delta u_i T^C_{ij,j} \\
&\quad + \frac{1}{2}\int dV \delta u_j (\sigma^{(0)}_{ij} u_{k,k})_{,i} - \frac{1}{2}\int dV \delta u_i (\sigma^{(0)}_{kl} u_{l,k})_{,j} \\
&\quad - \frac{1}{2}\int dV \delta u_j (\sigma^{(0)}_{jk} u_{i,k})_{,i} + \frac{1}{2}\int dV \delta u_j (\sigma^{(0)}_{il} u_{l,j})_{,j}
\end{aligned}
$$

so

$$
\begin{aligned}
\delta L^C = 0 = &\int dV \delta u_i \omega^2 \rho^{(0)} u_i - \int dSn_j \delta u_i T^C_{ij} + \int dV \delta u_i T^C_{ij,j} - \int dSn_j \delta u_i \sigma^{(0)}_{ij} u_{k,k} \\
&+ \int dV \delta u_i (\sigma^{(0)}_{ij} u_{k,k})_{,j} + \int dSn_j \delta u_i \sigma^{(0)}_{ik} u_{j,k} - \int dV \delta u_i (\sigma^{(0)}_{ik} u_{j,k})_{,j} \\
&+ \int dV \delta u_i \rho^{(0)} \psi^{(1)}_{,i} + \int dV \delta u_i \rho^{(0)} \psi^{(0)}_{,ij} u_j
\end{aligned} \tag{6.23}
$$

The surface integrals together give the boundary condition on the deformed boundary

$$
\left[T^C_{ij} + u_{k,k} \sigma^{(0)}_{ij} - u_{j,k} \sigma^{(0)}_{ik} \right] n_j = 0 \tag{6.24}
$$

The volume integrals give the equation of motion

$$
\omega^2 \rho^{(0)} u_i + T^C_{ij,j} + (\sigma^{(0)}_{ij} u_{k,k})_{,j} - (\sigma^{(0)}_{ik} u_{j,k})_{,j} + \rho^{(0)} \psi^{(0)}_{,ij} u_j + \rho^{(0)} \psi^{(1)}_{,i} = 0 \tag{6.25}
$$

This equation of motion can be rewritten in a purely Eulerian form by making use of equation (6.1) and noting that $(\rho^{(0)} u_j)_{,j} \psi^{(0)}_{,i} = (\rho^{(0)} u_j \psi^{(0)}_{,i})_{,j} - \rho^{(0)} u_j \psi^{(0)}_{,ij}$

$$
\omega^2 \rho^{(0)} u_i + T^{C_E}_{ij,j} - (\rho^{(0)} u_j)_{,j} \psi^{(0)}_{,i} + \rho^{(0)} \psi^{(1)}_{,i} = 0 \tag{6.26}
$$

with $T^{C_E}_{ij} = T^C_{ij} - u_k \sigma^{(0)}_{ij,k}$ the Cauchy stress tensor in Eulerian coordinates. Note that this stress tensor is not linearly related to a displacement gradient. Equation (6.26) is equal to the Fourier transformed version of Valette's equation (25) and to the Fourier transformed version of Dahlen's equation (7). The boundary condition (6.24) on the deformed boundary can be rewritten as

$$
\left[T^{C_E}_{ij} + (u_k \sigma^{(0)}_{ij})_{,k} - u_{j,k} \sigma^{(0)}_{ik} \right] n_j = 0 \tag{6.27}
$$

Normal modes

Whereas Saito (1971) claimed that the equations describing the gravito-elastodynamics of a pre-stressed Earth are not self-adjoint, Dahlen (1972) has shown that the Lagrangian equation of motion with associated boundary conditions lead to the necessary Hermitian property. In his calculations Dahlen used the first Piola-Kirchhoff stress tensor. Though on physical grounds it is implicit that if in one coordinate frame using a certain stress tensor there is self-adjointness, then there must be self-adjointness in any other coordinate frame using any other stress tensor too, it was never explicitly verified mathematically in the literature, as far as we know, for an Eulerian coordinate frame. In this paragraph it is shown that the Eulerian equation of motion (6.26), together with the boundary condition (6.27), leads to a complete set of orthogonally seismic normal modes. In our calculations we use the second Piola-Kirchhoff stress tensor.

The terms in the Eulerian equation of motion can be written as a bilinear operator

$$L(u_i, \psi^{(1)}) = \omega^2 \rho^{(0)} u_i + T^{C_E}_{ij,j} - (\rho^{(0)} u_j)_{,j} \psi^{(0)}_{,i} + \rho^{(0)} \psi^{(1)}_{,i} = 0 \qquad (6.28)$$

with the boundary condition for the stress tensors on the deformed boundary

$$\left[T^{C_E}_{ij} + (u_k \sigma^{(0)}_{ij})_{,k} - u_{j,k} \sigma^{(0)}_{ik} \right] n_j = 0 \qquad (6.29)$$

The Cauchy stress tensor in (6.20) can be replaced by the second Piola-Kirchoff stress tensor $T^{PK(2)}_{ij} = C^*_{ijkl} u_{l,k}$ by means of (6.21) and (6.22)

$$\begin{aligned} T^{C_E}_{ij} &= T^{C}_{ij} - u_k \sigma^{(0)}_{ij,k} = d_{ijkl} u_{l,k} - u_k \sigma^{(0)}_{ij,k} = \\ &= C^*_{ijkl} u_{l,k} - \sigma^{(0)}_{ij} u_{k,k} + \sigma^{(0)}_{ik} u_{j,k} + \sigma^{(0)}_{jk} u_{i,k} - u_k \sigma^{(0)}_{ij,k} \end{aligned} \qquad (6.30)$$

so that the boundary conditions for the stress tensors are given on the undeformed boundary

$$T^{PK(2)}_{ij} n_j = 0 \qquad \text{and} \qquad \sigma^{(0)}_{ij} n_j = 0 \qquad (6.31)$$

The elastic constants C^*_{ijkl} have the symmetry relations

$$C^*_{ijkl} = C^*_{jikl} = C^*_{klij} = C^*_{ijlk} \qquad (6.32)$$

so that there are generally 21 independent constants C^*_{ijkl}.
In order to fulfill the Hermitian property, it has to be shown that

$$\int_V dV' v_i L(u_i, \psi^{(1)}) - \int_V dV' u_i L(v_i, \phi^{(1)}) = 0 \tag{6.33}$$

for solutions $(\vec{u}, \psi^{(1)})$ and $(\vec{v}, \phi^{(1)})$ of (6.28) and (6.31) in order for the operator L to be self-adjoint.

From equation (6.28) it follows that ($\vec{u}$ periodic with cyclic frequency ω_1 and $\vec{v}$ periodic with cyclic frequency ω_2)

$$v_i L(u_i, \psi^{(1)}) - u_i L(v_i, \phi^{(1)}) =$$

$$= (\omega_1^2 - \omega_2^2)\rho^{(0)} u_i v_i + C^*_{ijkl}(v_i u_{l,jk} - u_i v_{l,jk}) \tag{6.34}$$

$$+ v_i(-\sigma^{(0)}_{ij} u_{k,k} + \sigma^{(0)}_{ik} u_{j,k} + \sigma^{(0)}_{jk} u_{i,k} - u_k \sigma^{(0)}_{ij,k})_{,j} \tag{6.35}$$

$$- u_i(-\sigma^{(0)}_{ij} v_{k,k} + \sigma^{(0)}_{ik} v_{j,k} + \sigma^{(0)}_{jk} v_{i,k} - v_k \sigma^{(0)}_{ij,k})_{,j} \tag{6.36}$$

$$- v_i(\rho^{(0)} u_j)_{,j} \psi^{(0)}_{,i} + u_i(\rho^{(0)} v_j)_{,j} \psi^{(0)}_{,i} \tag{6.37}$$

$$+ v_i \rho^{(1)} \psi^{(0)}_{,i} - u_i \rho^{(0)} \phi^{(1)}_{,i} \tag{6.38}$$

The terms in (6.35) can be written as

$$-v_i \sigma^{(0)}_{ij,j} u_{k,k} - v_i \sigma^{(0)}_{ij} u_{k,jk} + v_i \sigma^{(0)}_{ik,j} u_{j,k} + v_i \sigma^{(0)}_{ik} u_{j,jk} + v_i(\sigma^{(0)}_{jk} u_{i,k})_{,j} - v_i u_{k,j} \sigma^{(0)}_{ij,k} - v_i u_k \sigma^{(0)}_{ij,jk}$$

By interchanging dummy indices j and k this can be written as

$$- v_i \sigma^{(0)}_{ij,j} u_{k,k} + v_i(\sigma^{(0)}_{jk} u_{i,k})_{,j} - v_i u_k \sigma^{(0)}_{ij,jk}$$

Substituting equation (6.1) finally gives

$$v_i \rho^{(0)} \psi^{(0)}_{,i} u_{k,k} + v_i(\sigma^{(0)}_{jk} u_{i,k})_{,j} + v_i u_k(\rho^{(0)} \psi^{(0)}_{,i})_{,k} =$$

$$= v_i \rho^{(0)} \psi^{(0)}_{,i} u_{k,k} + v_i(\sigma^{(0)}_{jk} u_{i,k})_{,j} + v_i u_k \rho^{(0)}_{,k} \psi^{(0)}_{,i} + v_i u_k \rho^{(0)} \psi^{(0)}_{,ik} \tag{6.39}$$

And so (6.36) can be written as

$$- u_i \rho^{(0)} \psi^{(0)}_{,i} v_{k,k} - u_i(\sigma^{(0)}_{jk} v_{i,k})_{,j} - u_i v_k \rho^{(0)}_{,k} \psi^{(0)}_{,i} - u_i v_k \rho^{(0)} \psi^{(0)}_{,ik} \tag{6.40}$$

The terms in (6.37) can be written as

$$- v_i \rho^{(0)}_{,j} u_j \psi^{(0)}_{,i} - v_i \rho^{(0)} u_{j,j} \psi^{(0)}_{,i} + u_i \rho^{(0)}_{,j} v_j \psi^{(0)}_{,i} + u_i \rho^{(0)} v_{j,j} \psi^{(0)}_{,i} \tag{6.41}$$

Taking (6.39), (6.40) and (6.41) together, changing dummy indices i,j and k, it is obvious that (6.35) + (6.36) + (6.37) can be written as

$$v_i(\sigma^{(0)}_{jk} u_{i,k})_{,j} - u_i(\sigma^{(0)}_{jk} v_{i,k})_{,j} = (v_i \sigma^{(0)}_{jk} u_{i,k})_{,j} - (u_i \sigma^{(0)}_{jk} v_{i,k})_{,j} \tag{6.42}$$

Integrating (6.35), (6.42) and (6.38) over the entire space $E = (E - V) + V$, with V the deformed volume of the Earth and S the deformed surface (V_0 and S_0 denote

the undeformed volume and surface of the Earth respectively) gives

$$(\omega_1^2 - \omega_2^2)\int_V dV'\rho^{(0)}u_i v_i + \int_{V_0} dV' C^*_{ijkl}(v_i u_{l,jk} - u_i v_{l,jk})$$
$$+ \int_{V_0} dV'\left\{(v_i\sigma^{(0)}_{jk}u_{i,k})_{,j} - (u_i\sigma^{(0)}_{jk}v_{i,k})_{,j}\right\} + \int_E dV'\left\{v_i\rho^{(0)}\psi^{(1)}_{,i} - u_i\rho^{(0)}\phi^{(1)}_{,i}\right\} \quad (6.43)$$

Poisson's equation, $\psi^{(1)}_{,ii} - 4\pi G(\rho^{(0)}u_i)_{,i} = 0$, can be used to transform the last integral of (6.43)

$$u_i\rho^{(0)}\phi^{(1)}_{,i} = (u_i\rho^{(0)}\phi^{(1)})_{,i} - (u_i\rho^{(0)})_{,i}\phi^{(1)} =$$
$$= (u_i\rho^{(0)}\phi^{(1)})_{,i} - \frac{1}{4\pi G}\psi^{(1)}_{,ii}\phi^{(1)} =$$
$$= \left\{u_i\rho^{(0)}\phi^{(1)} - \frac{1}{4\pi G}\psi^{(1)}_{,i}\phi^{(1)}\right\}_{,i} + \frac{1}{4\pi G}\psi^{(1)}_{,i}\phi^{(1)}_{,i}$$

and so

$$v_i\rho^{(0)}\psi^{(0)}_{,i} = \left\{v_i\rho^{(0)}\psi^{(1)} - \frac{1}{4\pi G}\phi^{(1)}_{,i}\psi^{(1)}\right\}_{,i} + \frac{1}{4\pi G}\phi^{(1)}_{,i}\psi^{(1)}_{,i}$$

so

$$\int_E dV'\left\{v_i\rho^{(0)}\psi^{(1)}_{,i} - u_i\rho^{(0)}\phi^{(1)}_{,i}\right\} =$$
$$= \int_E dV'\left\{(\rho^{(0)}v_i - \frac{1}{4\pi G}\phi^{(1)}_{,i})\psi^{(1)} - (\rho^{(0)}u_i - \frac{1}{4\pi G}\psi^{(1)}_{,i})\phi^{(1)}\right\}_{,i} =$$
$$= \int_S dS' n_i\left[(\rho^{(0)}v_i - \frac{1}{4\pi G}\phi^{(1)}_{,i})\psi^{(1)} - (\rho^{(0)}u_i - \frac{1}{4\pi G}\psi^{(1)}_{,i})\phi^{(1)}\right]^+_- = 0$$

because of the continuity conditions:

$$\psi^{(1)}\,,\ \phi^{(1)} \quad \text{continuous}$$

and

$$\rho^{(0)}u_i - \frac{1}{4\pi G}\psi^{(1)}_{,i}\ ,\ \rho^{(0)}v_i - \frac{1}{4\pi G}\phi^{(1)}_{,i} \quad \text{continuous}$$

The third integral of (6.43) can also be rewritten in a surface integral using Gauss'

theorem

$$\int_{V_0} dV' \left\{ v_i \sigma_{jk}^{(0)} u_{i,k} - u_i \sigma_{jk}^{(0)} v_{i,k} \right\}_j = \int_{S_0} dS' n_j \sigma_{jk}^{(0)} (v_i u_{i,k} - u_i v_{i,k}) = 0$$

because of the boundary condition $\sigma_{jk}^{(0)} n_j = 0$.
The second integral of (6.43) can be expressed as

$$\int_{V_0} dV' C_{ijkl}^* (v_i u_{l,jk} - u_i v_{l,jk}) =$$

$$= \int_{S_0} dS' n_j C_{ijkl}^* (v_i u_{l,k} - u_i v_{l,k}) - \int_{V_0} dV' C_{ijkl}^* (v_{i,j} u_{l,k} - u_{i,j} v_{l,k}) = 0$$

The surface integral is equal to zero because of the boundary conditions $C_{ijkl}^* u_{l,k} n_j = 0$ and $C_{ijkl}^* v_{l,k} n_j = 0$.
The volume integral is equal to zero because of the symmetry relation $C_{ijkl}^* = C_{lkji}^*$.
So ultimately only the first integral of (6.43), $(\omega_1^2 - \omega_2^2) \int_V dV' \rho^{(0)} u_i v_i$, remains. If $\omega_1 = \omega_2$, the term becomes equal to zero; if $\omega_1 \neq \omega_2$, the term becomes equal to zero if $\vec{u} \cdot \vec{v} = 0$. This amounts to mutual orthogonality.

Unified scheme

The various descriptions for the gravito-elastodynamics of a perfectly elastic, non-rotating Earth model with a general initial stress field can be unified to one single expression: a Lagrangian first derived by Dahlen in the early seventies, from which the equation of motion and the boundary conditions can be derived by the Variational Principle, given by

$$L = T - H_1 - H_2 - I$$

where

$$T = \frac{1}{2} \omega^2 \int dV u_i \rho^{(0)} u_i \quad \text{is the kinetic energy}$$

$$H_1 = \frac{1}{2} \int dV u_{i,j} T_{ij} \quad \text{is the elastic} - \text{gravitational potential energy}$$

$$H_2 = -\frac{1}{2}\int dV u_i \rho^{(0)}\left\{u_j \psi^{(0)}_{,ij} + \psi^{(0)}_{,i}\right\}$$ is the gravitational potential energy (Biot's IGFD),

and

$$I = \frac{1}{2}\int dV \left\{\frac{1}{4\pi G}\psi^{(1)}_{,i}\psi^{(1)}_{,i} - \rho^{(0)}u_i\psi^{(1)}_{,i}\right\}$$

Variation with respect to $\psi^{(1)}$ gives Poisson's equation

$$\psi^{(1)}_{,ii} = 4\pi G(\rho^{(0)}u_i)_{,i}$$

Variation with respect to u_i gives, dependent of the choice of stress measure and coordinate frame, the equation of motion from the volume integrals and the boundary conditions from the surface integrals.

Significant combinations are as follows.

A. $T_{ij} = T^{PK(1)}_{ij}$, Lagrangian coordinate frame [Dahlen 1972; Woodhouse & Dahlen 1978]

equation of motion:

$$\omega^2\rho^{(0)}u_i + T^{PK(1)}_{ij,j} + \rho^{(0)}u_j\psi^{(0)}_{,ij} + \rho^{(0)}\psi^{(1)}_{,i} = 0$$

boundary conditions:

$$T^{PK(1)}_{ij}n_j = 0 \quad \text{and} \quad \sigma^{(0)}_{ij}n_j = 0 \qquad \text{(undeformed boundary)}$$

B. $T_{ij} = T^{PK(2)}_{ij} + u_{j,k}\sigma^{(0)}_{ik}$, Lagrangian coordinate frame [Valette 1986]

equation of motion:

$$\omega^2\rho^{(0)}u_i + T^{PK(2)}_{ij,j} + (\sigma^{(0)}_{jk}u_{i,k})_{,j} + \rho^{(0)}u_j\psi^{(0)}_{,ij} + \rho^{(0)}\psi^{(1)}_{,i} = 0$$

boundary conditions:

$$T^{PK(2)}_{ij}n_j = 0 \quad \text{and} \quad \sigma^{(0)}_{ij}n_j = 0 \qquad \text{(undeformed boundary)}$$

C. $T_{ij} = T^{C}_{ij} - u_{k,k}\sigma^{(0)}_{ij} + u_{i,k}\sigma^{(0)}_{jk}$, Lagrangian coordinate frame

equation of motion:

$$\omega^2\rho^{(0)}u_i + T^C_{ij,j} + (\sigma^{(0)}_{ij}u_{k,k})_{,j} - (\sigma^{(0)}_{ik}u_{j,k})_{,j} + \rho^{(0)}u_j\psi^{(0)}_{,ij} + \rho^{(0)}\psi^{(1)}_{,i} = 0$$

boundary condition:

$$\left[T^C_{ij} + u_{k,k}\sigma^{(0)}_{ij} - u_{j,k}\sigma^{(0)}_{ik}\right]n_j = 0 \qquad \text{(deformed boundary)}$$

D. $T_{ij} = T^{C_E}_{ij} + u_k\sigma^{(0)}_{ij,k} - u_{k,k}\sigma^{(0)}_{ij} + u_{i,k}\sigma^{(0)}_{jk}$, Eulerian coordinate frame

equation of motion:

$$\omega^2\rho^{(0)}u_i + T^{C_E}_{ij,j} - (\rho^{(0)}u_j)_{,j}\psi^{(0)}_{,i} + \rho^{(0)}\psi^{(1)}_{,i} = 0$$

boundary condition:

$$\left[T^{C_E}_{ij} + (u_k\sigma^{(0)}_{ij})_{,k} - u_{j,k}\sigma^{(0)}_{ik}\right]n_j = 0 \qquad \text{(deformed boundary)}$$

These various Lagrangians, equations of motion and boundary conditions reduce to Geller's Lagrangian, equation of motion and boundary condition in the hydrostatic case.

Conclusions

We have extended the basic equations describing a perfectly elastic, non-rotating, self-gravitating Earth model to incorporate various finite initial stress measures and coordinate frames by means of a single Lagrangian, which has the form originally derived by Dahlen. From this Lagrangian the equations of motion, boundary conditions and Poisson's equation can be derived by means of the Variational Principle. It is explicitly checked that the derived equations in Eulerian coordinates lead to a complete set of seismic free normal modes (as was done for Lagrangian coordinates by Dahlen).

We have shown that in the general laterally heterogeneous case both Woodhouse & Dahlen's and Valette's descriptions of gravito-elastodynamics are correct. Geller essentially only rederived the Lagrangian for the elastodynamics of a self-gravitating body with an isotropic initial stress field. As he incorrectly discards the concept of a finite initial stress tensor as necessary for describing the self-

gravitation problem, he did not have to make a choice of which coordinate system to use. To put it in another way: he had to make his equations coordinate-independent. That's why his IGFD differs from Biot's one. The two additional terms that make Geller's IGFD coordinate independent are contained however in the elastic-gravitational potential energy integral of Woodhouse & Dahlen's Lagrangian. It is shown that Geller's Lagrangian is equal to Woodhouse & Dahlen's Lagrangian in the case of an isotropic initial stress field, but that the latter contains the extra terms in the case of a general initial stress field. Geller's criticism about the first Piola-Kirchhoff stress tensor being asymmetric has been shown to be unjustified.

References

Backus, G.E., Converting vector and tensor equations to scalar equations in spherical coordinates, *Geophys. J. R. astron. Soc., 13*, 71-101, 1976.

Biot, M.A., *Mechanics of Incremental Deformations*, 504 pp., John Wiley, New York, 1965.

Dahlen, F.A., Elastic dislocation theory for a self-gravitating, elastic configuration with an initial stress field, *Geophys. J. R. astron. Soc., 28*, 357-383, 1972.

Dahlen, F.A. and M.L. Smith, The influence of rotation on the free oscillations of the Earth, *Phil. Trans. R. Soc. London, A279*, 583-624, 1975

Geller, R.J., Elastodynamics in a laterally heterogeneous, self-gravitating body, *Geophys. J. R. astron. Soc., 94*, 271-283, 1988

Malvern, L.E., *Introduction to The Mechanics of A Continuous Medium*, 713 pp., Prentice-Hall, Englewood Cliffs, NJ, 1969.

Saito, M., Theory for the elastic-gravitational oscillation of a laterally heterogeneous Earth, *J. Phys. Earth, 19*, 259-270, 1971.

Valette, B., About the influence of pre-stress upon adiabatic perturbations of the Earth, *Geophys. J. R. astron. Soc., 85*, 179-208, 1986.

Woodhouse, J.H. and F.A. Dahlen, The effect of a general aspherical perturbation on the free oscillations of the Earth, *Geophys. J. R. astron. Soc., 53*, 335-354, 1978.

Appendix: Measures of stress

If a material is finitely pre-stressed, one must make a clear distinction between the various measures of stress that are associated with choosing between an Eulerian or spatial description and a Lagrangian or material description.

A force $\vec{dF}$ acting on a surface element dS of a deformed volume element dV is related to the normal $\hat{n}$ of dS as

$$dF_j = n_i T^{\Gamma}_{ij} dS \tag{6.A1}$$

The tensor T^{Γ}_{ij} is called the Cauchy tensor, which can be split into an initial part and an incremental part

$$T^{\Gamma}_{ij} = \sigma^{(0)}_{ij} + T^{C}_{ij}$$

(note that in the initial state, respectively taking the limit $\vec{u} \to 0$ of the deformed state, the stress tensor reduces to the initial stress tensor $\sigma^{(0)}_{ij}$ and $dF_j = N_i \sigma^{(0)}_{ij} dS_0 = 0$ on the external boundary of dV). Dahlen (1972) demonstrated that the incremental part of the Cauchy stress tensor can be expressed in terms of strains and rotations of the finite initial stress components $\sigma^{(0)}_{ij}$. For example, he derived this tensor in Lagrangian coordinates, which can be rewritten as

$$T^{C}_{ij} = C_{ijkl} u_{k,l} + \frac{1}{2} u_{k,l} \sigma^{(0)}_{kl} \delta_{ij} - \frac{1}{2} u_{k,k} \sigma^{(0)}_{ij} + \frac{1}{2} (u_{i,k} - u_{k,i}) \sigma^{(0)}_{jk} - \frac{1}{2} (u_{k,j} - u_{j,k}) \sigma^{(0)}_{ik}$$

where $\vec{u}$ is a small displacement from the initial state and C_{ijkl} are the elastic constants, with the symmetry relations $C_{ijkl} = C_{jikl} = C_{ijlk} = C_{klij}$.
The deformed surface element dS with normal $\hat{n}$ can be transformed into the undeformed surface element dS_0 with normal $\hat{N}$ and one can express the force $\vec{dF}$ acting on the deformed surface in terms of the undeformed surface

$$dF_j = N_i T^{\Pi(1)}_{ij} dS_0 \tag{6.A2}$$

The tensor $T^{\Pi(1)}_{ij}$ is called the first Piola-Kirchhoff stress tensor or Lagrangian stress tensor. This tensor can also be split into an initial part and an incremental part

$$T^{\Pi(1)}_{ij} = \sigma^{(0)}_{ij} + T^{PK(1)}_{ij}$$

The first Piola-Kirchhoff stress tensor relates an actual force defined in the deformed state with a surface element defined in the undeformed state. It is this tensor which Woodhouse & Dahlen employ in their equations.

It is also possible to use the transpose of the tensor as the definition of the first Piola Kirchhoff stress tensor ($dF_i = T_{ij}^{\Pi(1)} n_j dS$). The convention we adopt in this appendix is the same as the one used by Malvern (1969).
As expressions (6.A1) and (6.A2) are equal it is possible to express the first Piola-Kirchhoff stress tensor in terms of the Cauchy stress tensor.
If X_i and x_i denote the coordinates in the undeformed and in the deformed state respectively, both with respect to a common origin O (figure 6.1)

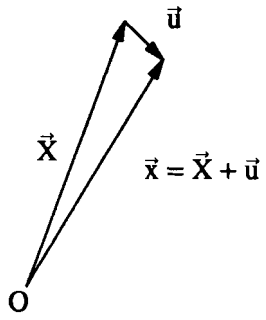

Figure 6.1. Coordinates in the deformed and undeformed states.

and the infinitesimal surface elements have edges $d\vec{X}$ and $\delta\vec{X}$ in the undeformed and $d\vec{x}$ and $\delta\vec{x}$ in the deformed state, then

$$N_i dS_0 = \varepsilon_{ijk} dX_j \delta X_k$$
$$n_l dS = \varepsilon_{lmn} dx_m \delta x_n$$

with ε_{ijk} the Levi-Civita tensor.
$N_i dS_0$ can be expressed in the deformed coordinates as

$$N_i dS_0 = \varepsilon_{ijk} \frac{\partial X_j}{\partial x_m} \frac{\partial X_k}{\partial x_n} dx_m \delta x_n$$

Multiplying both sides with $\frac{\partial X_i}{\partial x_l}$ gives

$$\frac{\partial X_i}{\partial x_l} N_i dS_0 = \varepsilon_{ijk} \frac{\partial X_i}{\partial x_l} \frac{\partial X_j}{\partial x_m} \frac{\partial X_k}{\partial x_n} dx_m \delta x_n =$$

$$= \varepsilon_{lmn} \det\left(\frac{\partial X_r}{\partial x_s}\right) dx_m \delta x_n$$

If ρ_0 and ρ denote the density in the undeformed state and in the deformed state respectively, this becomes

$$\frac{\partial X_i}{\partial x_l} N_i dS_0 = \frac{\rho}{\rho_0} \varepsilon_{lmn} dx_m \delta x_n =$$
$$= \frac{\rho}{\rho_0} n_l dS$$

so

$$n_l dS = \frac{\rho_0}{\rho} \frac{\partial X_i}{\partial x_l} N_i dS_0$$

Furthermore,

$$\frac{\rho_0}{\rho} = \frac{dV}{dV_0} \approx 1 + u_{l,l}$$

and hence

$$n_l dS \approx (1 + u_{l,l})\left(\frac{\partial x_i}{\partial x_l} - \frac{\partial u_i}{\partial x_l}\right) N_i dS_0 =$$
$$= (1 + u_{l,l})(\delta_{il} - u_{i,l}) N_i dS_0$$

Equating (6.A1) and (6.A2) gives

$$T_{ij}^{\Pi(1)} \approx (1 + u_{l,l})(\delta_{ik} - u_{i,k}) T_{k_j}^{\Gamma} \approx T_{ij}^{\Gamma} + u_{l,l} T_{ij}^{\Gamma} - u_{i,k} T_{k_j}^{\Gamma}$$

which in first order leads to

$$T_{ij}^{PK(1)} = T_{ij}^{C} + u_{k,k} \sigma_{ij}^{(0)} - u_{i,k} \sigma_{jk}^{(0)} \tag{6.A3}$$

It follows from (6.A3) that the first Piola-Kirchhoff stress tensor is generally not symmetric. This is no violation of any physical principle however, as this so-called 'two-point' tensor (cf. Malvern) associates an actual force on the deformed surface (by the column of the tensor) with a normal on a surface element of the undeformed volume (by the row of the tensor). In order to investigate whether or not fundamental principles of physics are at stake one must carefully distinguish this.
To obtain a purely Lagrangian description of the gravito-elastodynamical problem, the force $\vec{dF}$ acting on a surface element of the deformed volume must be transformed into a force $\vec{dF}^*$ acting on a surface element of the undeformed volume

$$dF_j^* = \frac{\partial X_j}{\partial x_k} dF_k = \left(\frac{\partial x_j}{\partial x_k} - \frac{\partial u_j}{\partial x_k} \right) dF_k =$$
$$= (\delta_{jk} - u_{j,k}) dF_k \tag{6.A4}$$

The (pseudo-)force $\vec{dF}^*$ can be written as

$$dF_j^* = N_i T_{ij}^{\Pi(2)} dS_0 \tag{6.A5}$$

The tensor $T_{ij}^{\Pi(2)}$ is called the second Piola-Kirchhoff stress tensor, which can be split into an initial part and an incremental part again

$$T_{ij}^{\Pi(2)} = \sigma_{ij}^{(0)} + T_{ij}^{PK(2)}$$

It deserves the term 'Lagrangian stress tensor' more than the first one (though it is not named so), because it relates two vector fields which are both defined on the undeformed volume element. The second Piola-Kirchhoff stress tensor can be expressed in terms of the first. From the equations (6.A2), (6.A4) and (6.A5) it follows that

$$T_{ij}^{\Pi(2)} = (\delta_{jk} - u_{j,k}) T_{ik}^{\Pi(1)} = T_{ij}^{\Pi(1)} - u_{j,k} T_{ik}^{\Pi(1)}$$

hence in first order:

$$T_{ij}^{PK(2)} = T_{ij}^{PK(1)} - u_{j,k} \sigma_{ik}^{(0)} \tag{6.A6}$$

Substituting (6.A3) in (6.A6) gives the relation in first order between the second Piola-Kirchhoff stress tensor and the Cauchy stress tensor

$$T_{ij}^{PK(2)} = T_{ij}^{C} + u_{k,k} \sigma_{ij}^{(0)} - u_{i,k} \sigma_{jk}^{(0)} - u_{j,k} \sigma_{ik}^{(0)} \tag{6.A7}$$

Equation (6.A7) shows that the second Piola-Kirchhoff stress tensor is symmetric whenever the Cauchy stress tensor is symmetric. It is this stress tensor which Valette uses in his description of gravito-elastodynamics.
All the various descriptions become equal to each other if the initial strains are infinitesimal.

SAMENVATTING (SUMMARY IN DUTCH)

De rotatie van de Aarde is niet regelmatig. Zowel de denkbeeldige as waarom de Aarde draait als de snelheid waarmee zij haar dagelijkse omwenteling volbrengt vertonen veranderingen in de loop der tijd. Uit astronomische waarnemingen is bekend dat de rotatie-as van de Aarde zich gedurende de afgelopen 90 jaar van de geografische Noordpool richting Canada heeft verplaatst met een snelheid van zo'n 10 centimeter per jaar. Verder heeft men uit nauwkeurige bepalingen van de baan van satellieten met behulp van lasers kunnen afleiden dat gedurende de afgelopen 15 jaar de afplatting van de Aarde sterker is verminderd dan op grond van de afremming van de rotatie van de Aarde door getijdenwerking met de Maan kan worden verklaard. Algemeen wordt verondersteld dat deze beide veranderingen in de rotatie van de Aarde toe te schrijven zijn aan post-glaciale opheffing (het huidige oprijzen van de bodem op die plaatsen waar zo'n 10.000 jaar geleden enorme ijsmassa's lagen, zoals in Canada en Scandinavië) en aan recente veranderingen in de verdeling van ijs en water over het aardoppervlak (zoals het afsmelten van gletsjers en de zeespiegelstijging door het broeikaseffect).
In dit proefschrift wordt aangetoond dat allerlei tektonische processen die niets met herverdeling van ijs en water van doen hebben ook een bijdrage leveren aan de waargenomen poolvlucht en verminderde afplatting. Voorbeelden van deze tektonische processen zijn gebergtevorming en erosie, het losscheuren *(detachment)* van de oceaanbodem op plaatsen waar deze langzaam de diepere gedeelten van de Aarde induikt en het verzakken *(foundering)* van oceaanbekkens door compressie. Deze processen zijn effectief indien ze snelle verticale bewegingen induceren onder niet-isostatische condities. Een combinatie van actieve krachten en compressieve spanningsvelden in een sterke lithosfeer kan er daarbij voor zorgen dat het herstel van de isostatische conditie heel wat langer duurt dan de tijdschalen waarop post-glaciale opheffing plaatsvindt. De effectiviteit van deze processen wordt geïllustreerd aan de hand van modellen van het oprijzen van de Himalaya en het Tibetaans Plateau. Sommige van de modellen geven zelfs als resultaat poolvluchtsnelheden te zien die dezelfde grootte hebben als de waargenomen poolvlucht. Toekomstige modellen waarmee men gegevens wil afleiden uit de relatie tussen herverdeling van water en ijs over onze planeet en veranderingen in rotatie zullen rekening moeten houden met deze tektonische componenten.

In hoofdstuk 2 wordt een globaal overzicht gegeven van de veranderingen in positie van de poolas en in rotatiesnelheid van de Aarde. Uit een beknopt historisch overzicht blijkt dat modellen waarin poolvlucht wordt toegeschreven aan herverde-

ling van ijs en water en aan deformaties in het inwendige van de Aarde elkaar regelmatig hebben afgewisseld tot het eind van de jaren 70. De negatieve resultaten van een studie naar de effectiviteit van continentale drift als aandrijvingsmechanisme van poolvlucht leidden er toen toe dat vanaf het begin van de jaren 80 postglaciale opheffing als de veroorzaker van de huidige seculiere rotatieveranderingen werd beschouwd, later aangevuld met contemporaine veranderingen in de verdeling van ijs en water. De veronderstelling dat de continentale en oceanische kolommen zich in isostatisch evenwicht bevinden blijkt de meest kritische aanname te zijn geweest in de modellen naar de invloed van continentale drift op rotatie.
Indien een lithosferische kolom snelle verticale bewegingen ondergaat, waarbij de kolom niet in isostatisch evenwicht verkeert of uit isostatisch evenwicht geraakt, dan blijkt uit de modellen van hoofdstuk 3 dat een dergelijke kolom een effectieve bijdrage kan leveren aan de waargenomen rotatieveranderingen. Zo volgt uit een van de modellen dat de bijdrage van een dertiental tektonisch actieve gebieden aan de huidige afname van de dynamische afplatting van de Aarde zo'n 10% van de niet door getijdenwerking veroorzaakte gemeten waarde bedraagt. Snelle niet-isostatische verticale bewegingen kunnen naast rotatieveranderingen ook verschuivingen van het massamiddelpunt van de Aarde t.o.v. het aardoppervlak induceren. De modellen van hoofdstuk 3 duiden op snelheden van iets minder dan 1 millimeter per 10 jaar. Aangezien de tektonische processen werkzaam kunnen zijn over perioden van vele honderdduizenden jaren en daar met een verschuiving van het massamiddelpunt een antipodaal antisymmetrische verschuiving van de zeespiegel is geassocieerd, zou dit mechanisme een mogelijke verklaring kunnen bieden voor waargenomen zeespiegelvariaties op deze tijdschalen.
Bij het bepalen van de poolvlucht is het noodzakelijk rekening te houden met de verplaatsing van de equatoriale uitstulping. De poolverschuiving zoals die in hoofdstuk 3 is bepaald veronderstelt dat de aarde rigide is met betrekking tot dit geïnduceerde effect. Doordat de Aarde kan deformeren, zal een krachtkoppel wat uitgeoefend wordt op de equatoriale uitstulping de afplatting als een golf over het aardoppervlak trachten te verschuiven. De mate van verschuiving hangt, naast het krachtkoppel, af van de snelheid waarmee de aardmantel kan vervloeien. De poolvlucht volgt zo uit een vrij ingewikkeld samenspel tussen de tektonische processen die het krachtkoppel veroorzaken en de relaxatie van de equatoriale uitstulping. In hoofdstuk 4 wordt dit bestudeerd voor de vorming van de Himalaya en het Tibetaans Plateau met een aardmodel waarbij de mantel is opgedeeld in drie lagen: de transitiezone ligt ingeklemd tussen de ondiepe bovenmantel en de ondermantel. Als rheologisch model wordt een linear visco-elastisch Maxwellmodel genomen. Alhoewel de ondiepe bovenmantel snel kan vervloeien, reduceert het gravitatieveld van de afplatting van de meer visceuze diepere lagen de verschuiving van de equa-

toriale uitstulping sterk. Het zijn deze diepere lagen die voor de stabiliteit van de aardrotatie zorgen. Uit de simulaties blijkt dat een lineare opheffing van het gebied die leidt tot een 10% afwijking van isostasie een poolvlucht van dezelfde grootte induceert als wordt waargenomen, aangenomen dat de ondermantel een 10 maal hogere viscositeit heeft dan de ondiepe bovenmantel.
In hoofdstuk 5 worden de rotatieveranderingen op geologische tijdschalen bestudeerd. Deze worden veelal relateerd aan veranderingen in subductie van oceanische lithosfeer in de mantel. In dit hoofdstuk wordt de invloed van de ermee gepaard gaande verticale verplaatsingen van de zeebodem en zeespiegelvariaties op poolvlucht en lengte van de dag bestudeerd. Het blijkt dat, indien de zeespiegelvariaties dynamisch ondersteund worden door diepere mantelheterogeniteiten, deze een aandrijfmechanisme van dezelfde orde van grootte kunnen vormen voor poolvlucht als subductie. De invloed van deze lange-termijn processen op de lengte van de dag is verwaarloosbaar ten opzichte van de verlenging van de dag door getijdenwerking van de Aarde met de Maan.

Hoofdstuk 6 heeft geen direct verband met de eerste vijf hoofdstukken van dit proefschrift. In dit hoofdstuk wordt in de vorm van een variatieprincipe een algemene formulering gegeven voor de gravito-elastodynamica. Met name de rol die eindige deviatorische voorspanningen spelen in een zelf-graviterend medium (zijnde een medium waarbij de door deformaties geïnduceerde veranderingen in het gravitatieveld niet verwaarloosbaar zijn) heeft in het verleden aanleiding gegeven tot uiteenlopende en soms onverenigbare opvattingen over de correcte bewegingsvergelijkingen en randvoorwaarden. Voorbeelden van toepassingen van deze theorie zijn te vinden in studies naar de invloed van aardbevingen op de vrije precessie van de Aarde (de zogenaamde *Chandler wobble)* en de invloed van spanningsvelden in het inwendige van de Aarde op de voortplanting van seismische golven.
In hoofdstuk 6 wordt beargumenteerd dat de in het algemene geval asymmetrische Piolo-Kirchhoffspanningstensor van de eerste soort niet onverenigbaar is met basale fysische principes. Tevens wordt aangetoond dat een Euleriaanse beschrijvingswijze leidt tot een hermitisch compleet stelsel van normaalmodes. Deze beide aspecten waren door sommige auteurs in twijfel getrokken. De diverse beschrijvingswijzen voor de gravito-elastodynamica, zoals die in de loop der jaren door diverse onderzoekers zijn opgesteld, worden in dit hoofdstuk geünificeerd in een Lagrangiaan. Door het variatieprincipe toe te passen kunnen hieruit de bewegingsvergelijkingen en randvoorwaarden voor verschillende coördinaatsystemen en typen spanningstensoren eenvoudig worden afgeleid.

DANKBETUIGING / ACKNOWLEDGMENTS

Mijn dank gaat in de eerste plaats uit naar mijn ouders en broer, die mij steeds gedurende mijn studie onvoorwaardelijk hebben gesteund en bemoedigd. Helaas heeft mijn vader de voltooiing van dit proefschrift niet meer mogen meemaken.
Professor Vlaar ben ik uitermate erkentelijk dat hij mij heeft aangesteld als assistent in opleiding, en voor het vertrouwen wat hij sindsdien in mij is blijven houden. Ik heb grote waardering voor zijn niet aflatende inzet voor de geofysica en zijn brede kennis van de aardwetenschappen. In dit proefschrift zijn veel van zijn ideeën terug te vinden. Daarnaast ben ik hem en zijn vrouw dankbaar voor hun gastvrijheid in het Amersfoortse.
Velen hebben in direkte of indirekte zin een bijdrage geleverd aan dit proefschrift. Ik ben hen allen zeer erkentelijk. The members of the reviewing committee, Profs. De Jong, Lambeck, Sabadini, Snieder and Vlaar, are thanked for their constructive remarks on the original manuscript. Rob Govers and Jay Pulliam are thanked for their comments on the first two chapters.
De medewerkers en studenten van de vakgroep geofysica hebben mij vier uiterst aangename jaren bezorgd, waar ik met plezier op terug zie. Mijn eerste kamergenoten op het instituut, Peter van Keken en Saskia Goes, hebben er voor gezorgd dat ik mij als vreemde eend in de bijt snel thuis voelde. Aan Peter heb ik gedurende de afgelopen vier jaar niet alleen binnen, maar ook buiten de muren van het instituut een uitstekende collega gehad.
De groep van Prof. Rinus Wortel heeft een diepgaande invloed uitgeoefend op mijn beeld van de Aarde. Met Rob Govers heb ik heel wat tektonofysische aspecten besproken, met name in de vroege ochtenduren van de winter 91/92. Maarten Remkes, Paul Meijer en Marc de Jonge hebben ieder op hun manier mijn belangstelling voor tektonofysica en geologie opgewekt en levendig gehouden, ook al zijn de begrippen *voorspanning* en *Piola-Kirchhoffspanningstensor* tijdens onze conversaties op een gegeven moment taboe geworden. Ik zal de ochtenden rond de koffietafel met hen missen.
Mijn interesse voor de geologie is verder uitgebouwd tijdens de Normandië-excursie van 1991, die ik op instigatie van mijn promotor heb meegemaakt onder leiding van Cees van den Ende. Dat aan de ene kant de studenten mij als een van hen beschouwden en dat aan de andere kant de staf mij soms vroeg de geologische zaken in een geofysische context te plaatsen, heeft ertoe bijgedragen dat ik aan deze excursie erg goede herinneringen bewaar.
In Prof. Roberto Sabadini I have met one of the finest scientists I know to cooperate with. Giorgio Spada was always helpful in assisting me with implementing his and

Roberto's computer codes. I am very grateful to have received the opportunity to work with both Roberto and Giorgio. Their knowledge on rotation dynamics was indispensable for the models of chapter 4.
I thank the whole Bologna department community for their hospitality. Especially Maria-Elina Belardinelli, Warner Marzocchi and Laura Pezzoli have introduced me to the cultural and social aspects of Italy and have made my stays in Bologna extra colorful.
Carolina Lithgow and Silvia Pondrelli have been a great support to me through some crucial periods during the past four years.
Tenslotte wil ik Abir Abdul Aziz en Ulli Hansen bedanken voor de prettige wijzen waarop ze, zij het met zeer uiteenlopende motieven, op onvoorspelbare tijdstippen mijn werk kwamen onderbreken. Hoewel de rest van de afdeling soms minder te spreken was over het kabaal waarmee dat weleens gepaard ging, heeft het uitsluitend een positieve uitwerking op mijn arbeidsprestaties gehad.

During my PhD study I received grants from NATO, the Italian Istituto Nazionale di Geofisica, the Dutch national science organization NWO, Royal Dutch Shell, the European Geophysical Society and the American Geophysical Union.
I especially acknowledge the grants from the Twinning Project of the European Communities and the Dipartimento di Fisica - Settore Geofisica di Università di Bologna for my stays in Bologna.

CURRICULUM VITAE

De auteur van dit proefschrift is geboren op 25 augustus 1961 in Clinge, Zeeuwsch-Vlaanderen. Na aan de Clemens Mavo te Hulst het Mavo-4 diploma te hebben behaald in 1977, werden met succes de Havo en het Atheneum doorlopen aan de Jansenius Scholengemeenschap te Hulst. In 1980 werd het VWO diploma Atheneum-β uitgereikt.
In september van dat jaar werd gestart met de studie theoretische sterrenkunde aan de faculteit Natuur- en Sterrenkunde van de Universiteit Utrecht. Het kandidaatsexamen werd met goed gevolg afgelegd in 1984. Op 19 januari 1987 werd het doctoraaldiploma theoretische sterrenkunde, met bijvakken theoretische natuurkunde en mathematische fysica, behaald. Het afstudeeronderzoek werd verricht aan extragalactische straalstromen onder begeleiding van Dr A.A. Achterberg van de werkgroep Hoge-energie en Plasma -astrofysica.
Van 1 april 1989 tot 1 april 1993 was de auteur werkzaam als assistent in opleiding aan de faculteit Aardwetenschappen van de Universiteit Utrecht, waarna van 1 mei tot 1 december 1993 een aanstelling als toegevoegd docent bij de vakgroep Theoretische Geofysica volgde.
Vanaf 1 januari 1994 hoopt de auteur zijn werkzaamheden voort te zetten aan de faculteit natuurkunde van de universiteit van Bologna, Italië.

Astrometric observations indicate that during the past 90 years the rotation axis piercing through Arctica has drifted towards Canada with a velocity of about 10 centimeters per year. Laser ranging observations to satellites during the past 15 years show a residual non-tidal decrease in ellipticity of the Earth. Both these observations are commonly attributed to post-glacial rebound and contemporary changes in the distribution of water and ice over the Earth's surface, such as melting of mountain glaciers and sea-level rise by the greenhouse effect.

In this thesis it is proposed that various non-glacial tectonic processes are also contributing to these changes in rotation. Tectonic processes are effective whenever they induce fast vertical movements under non-isostatic conditions. Examples of tectonic mechanisms where these conditions can be met are mountain building, plateau uplift, fast subsidence of oceanic basins and detachment of subducting slabs. The effectiveness of the proposed tectonic mechanisms is shown by a case study of the uplift of the Himalayas and Tibetan Plateau. Depending on the uplift history, radial viscosity profile in the Earth's mantle and deviations from isostasy, some of the models result in displacement rates of the rotation axis which have the same magnitude as the measured present-day rate.

In the last part of this thesis a general formulation is given for the gravito-elastodynamics for a self-gravitating body that is arbitrarily pre-stressed. This formulation unifies different descriptions presented earlier in the geophysical literature and discards descriptions based on the claim that the concept of pre-stress has no physical meaning.

ISBN 90-71577-65-1